UNIVERSIDADE ESTADUAL DE CAMPINAS
FACULDADE DE ENGENHARIA MECÂNICA
E INSTITUTO DE GEOCIÊNCIAS

SHAHRAM DANAEI

FAST-TRACK 4D SEISMIC DATA ASSIMILATION USING PROXY FOR SEISMIC FORWARD MODELING

ASSIMILAÇÃO DE DADOS SÍSMICOS 4D COMO FAST-TRACK USANDO *PROXY* PARA MODELAGEM DIRETA SÍSMICA

CAMPINAS
[2023]

SHAHRAM DANAEI

FAST-TRACK 4D SEISMIC DATA ASSIMILATION USING PROXY FOR SEISMIC FORWARD MODELING

ASSIMILAÇÃO DE DADOS SÍSMICOS 4D COMO FAST-TRACK USANDO *PROXY* PARA MODELAGEM DIRETA SÍSMICA

Tese de Doutorado apresentada à Faculdade de Engenharia Mecânica e Instituto de Geociências da Universidade Estadual de Campinas como parte dos requisitos exigidos para obtenção do título de Doutor em Ciências e Engenharia de Petróleo, na área de Reservatórios e Gestão.

Orientador: Prof. Dra. Alessandra Davolio Gomes

Coorientador: Prof. Dr. Denis Jose Schiozer

Este exemplar corresponde à versão final da Tese defendida pelo aluno Shahram Danaei e orientada pelo Prof. Dra. Alessandra Davolio Gomes.

Assinatura do Orientador

CAMPINAS

[2023]

Ficha catalográfica
Universidade Estadual de Campinas
Biblioteca da Área de Engenharia e Arquitetura
Rose Meire da Silva - CRB 8/5974

D194f

Danaei, Shahram, 1986-
Fast-track 4D seismic data assimilation using proxy for seismic forward modeling / Shahram Danaei. – Campinas, SP : [s.n.], 2023.

Orientador: Alessandra Davolio.
Coorientador: Denis José Schiozer.
Tese (doutorado) – Universidade Estadual de Campinas, Faculdade de Engenharia Mecânica.

1. Reservatorios (Simulação). 2. Geofísica. I. Davolio, Alessandra, 1980-. II. Schiozer, Denis José, 1963-. III. Universidade Estadual de Campinas. Faculdade de Engenharia Mecânica. IV. Título.

Informações Complementares

Título em outro idioma: Assimilacao de dados sismicos 4D como fast-track usando proxy para modelagem direta sismica
Palavras-chave em inglês:
Reservoirs (Simulation)
Petroleum engineering
Área de concentração: Reservatórios e Gestão
Titulação: Doutor em Ciências e Engenharia de Petróleo
Banca examinadora:
Alessandra Davolio [Orientador]
Alexandre Anoze Emerick
Celio Maschio
Guilherme Daniel Avansi
Marcos Sebastiao
Data de defesa: 22-03-2023
Programa de Pós-Graduação: Ciências e Engenharia de Petróleo

Identificação e informações acadêmicas do(a) aluno(a)
- ORCID do autor: https://orcid.org/0009-0008-4601-237X
- Currículo Lattes do autor: http://lattes.cnpq.br/6148487336012272

UNIVERSIDADE ESTADUAL DE CAMPINAS
FACULDADE DE ENGENHARIA MECÂNICA
E INSTITUTO DE GEOCIÊNCIAS

TESE DE DOUTORADO

FAST-TRACK 4D SEISMIC DATA ASSIMILATION USING PROXY FOR SEISMIC FORWARD MODELING

Autor: Shahram Danaei
Orientador: Prof. Dra. Alessandra Davolio Gomes
Coorientador: Prof. Dr. Denis Jose Schiozer

A Banca Examinadora composta pelos membros abaixo aprovou esta Tese:

Prof. Dra Alessandra Davolio Gomes, Presidente
DEP / FEM / CEPETRO / UNICAMP

Dr. Célio Maschio Membro Interno
CEPETRO / UNICAMP

Dr. Guilherme Daniel Avansi Membro Interno
CEPETRO / UNICAMP

Dr. Marcos Sebastião dos Santos Membro Externo
PETROBRAS

Dr. Alexandre Anoze Emerick Membro Externo
PETROBRAS

A Ata de Defesa com as respectivas assinaturas dos membros encontra-se no SIGA/Sistema de Fluxo de Dissertação/Tese e na Secretaria do Programa da Unidade.

Campinas, 22 de Março de 2023.

DEDICATION

This work is wholeheartedly dedicated to my family especially my mother and father for their full and unconditional support and love.

ACKNOWLEDGMENTS

First and foremost, I would like to express my deepest gratitude to my supervisor Prof. Dra. Alessandra Davolio for her guidance, support, and kindness. Dra. Alessandra followed my work very well, guided me to the right direction during my study, and linked me to the right specialists for consultation. Prof. Dra Alessndra, I am thankful and appreciate it.

I also would like to express my gratitude to Prof. Dr. Denis Schiozer who gave me the opportunity to be part of the Research Group in Reservoir Simulation and Management (UNISIM) and to study at the State University of Campinas (UNICAMP). As a person with backgrounds mainly in Geophysics, UNISIM helped me to learn the Petroleum engineering topics. During my study, I was able to connect the dots and made a bridge between Geophysics and Petroleum engineering. Prof. Dr. Denis, I am thankful and appreciate the opportunity.

I would like to thank Gilson Moura Silva Neto (from Petrobras) who helped me alot during my study. I learned alot from him and every conversation with him was like a technical session for me. Gilson, I am thankful for the time, patience, and conversations.

In addition, my special thanks go to my friends at UNICAMP especially I would like to thank Masoud Maleki, Kourosh Mahjour, and Bahram Lavi. Talking to them in the Persian language was a refreshment for me and helped me alot. Masoud and Koroush, thanks for all the advices and chit-chat. Moreover, I would like to thank Mr. Branco and Mrs. Frida and Amora for their non-stop support, motivation and help during my stay in Brazil.

Finally, I would like to thank all of my fellow researchers at the Department of Energy of the school of Mechanical Engineering (DE-FEM) and all the team members of our research group for time-laspe seismic study (S4D-UNISIM) or I call it “S4D-Squad” for their support and kindness. S4D-Squad, I am grateful for the supports.

RESUMO

Os dados sísmicos 4D contêm informações relacionadas às mudanças dinâmicas dos reservatórios de óleo e gás, como mudanças de pressão e saturação. Essas informações são frequentemente combinadas com os dados de produção para atualizar os modelos de simulação de reservatórios. O processo de atualização de modelos com os dados observados é denominado assimilação de dados. Ao usar dados sísmicos 4D, este processo tradicionalmente usa uma modelagem direta de dados sísmicos 4D com duas etapas conectadas executadas em sequência com 2 modelos: petro-elástico (PEM) e sísmico. Cada uma dessas etapas possui particularidades que tornam o processo de assimilação desafiador. O PEM é incerto, especialmente para alguns casos como reservatórios carbonáticos. A modelagem sísmica é tipicamente demorada, o que aumenta o tempo de resposta do uso de informações sísmicas 4D para atualizar os modelos de simulação especialmente nos casos mais recentes com monitoramento permanente. Este trabalho pretende abordar essas duas questões e propor modelos proxy como possíveis formas de substituir a tradicional modelagem direta de dados sísmicos 4D. O trabalho compreende quatro abordagens usando modelos *proxy* para substituir a modelagem direta. A primeira abordagem propõe uma *proxy* para o PEM e assimila os dados sísmicos 4D em conjunto com os dados de produção. A segunda abordagem melhora a *proxy* para o PEM (proposto no primeiro artigo) ao adicionar a porosidade do reservatório em sua formulação; nesta também propomos maneiras de considerar o erro da *proxy* no processo de assimilação de dados. A terceira abordagem oferece uma *proxy* para substituir as duas etapas conectadas (PEM mais modelo sísmico) usando modelos de aprendizado de máquina. Por fim, no quarto artigo, fizemos um estudo para avaliar o impacto do conjunto de treinamento no algoritmo de rede neural profunda usado na *proxy* para modelagem direta sísmica 4D.

As implementações dos dois modelos *proxy* para o PEM na assimilação de dados forneceram resultados satisfatórios comparados à aplicação do PEM. As funções objetivo de dados sísmicos 4D e de produção mostraram respostas semelhantes para as implementações proxy e PEM. Em termos de quantificação de incerteza e previsão de produção, adicionar porosidade à formulação proxy e contabilizar o erro do modelo proxy forneceram respostas semelhantes ao PEM. Portanto, as duas primeiras abordagens mostraram ser uma boa solução para substituir o PEM nos procedimentos de assimilação de dados, tornando-o mais simples e rápido. Na terceira abordagem, os modelos de aprendizado de máquina foram desenvolvidos como uma substituição à abordagem passo a passo tradicional (PEM mais modelo sísmico). A comparação dos resultados dos modelos de aprendizado de máquina e da abordagem tradicional mostrou que os modelos proxy são capazes de gerar sinais sísmicos 4D semelhantes aos da abordagem tradicional (modelagem direta). Os modelos de aprendizado de máquina automatizam a modelagem sísmica direta completa (modelagem PEM e sísmica), evitando passos custoso como transferência de escala e conversão de profundidade a tempo dos dados. No quarto artigo, um algoritmo de rede neural profunda é avaliado para investigar as melhores práticas de treinamento para o desenvolvimento de proxy. Esta proxy permite que os engenheiros realizem a assimilação de dados no domínio da amplitude sísmica, o que pode ser uma grande vantagem em termos do uso rápido desta informação. Este tipo de ferramenta tem grande valor especialmente para reservatórios com monitoramento permanente, onde a assimilação rápida de dados sísmicos 4D é altamente necessária.

Palavras-Chave: Dados sísmicos 4D; Assimilação de dados; Modelagem direta; Modelo proxy.

ABSTRACT

Time-lapse seismic data (4D seismic) has information related to the dynamic changes in the oil and gas reservoirs such as saturation-pressure changes. This information is often combined with the production data to update reservoir simulation models. The process of model updating with observed data is called data assimilation. When using 4D seismic data, this process traditionally involves with a 4D seismic forward model with two consecutive steps. The first step is a petro-elastic model (PEM) and the second is a seismic model. Each step of the traditional 4D seismic forward has some particularities making the assimilation process challenging. The PEM is uncertain and it might not be easy to develop a reliable one for some cases. The seismic modelling is time-consuming, increasing the turnaround time of using 4D seismic information to update the simulation models. This work addresses these issues and proposes proxy models to replace the traditional 4D seismic forward modelling. The work comprises four research papers to address the gap in the literature and to use proxy models to replace the traditional approach. The first paper proposes a proxy for the PEM and assimilates 4D seismic data jointly with the production data. The second paper improves the proxy for the PEM (proposed in the first paper) by adding reservoir porosity in the proxy formulation. Moreover, as the proxy approximates the PEM, its application has a model error. The second paper introduces ways to account for the proxy model error in the data assimilation process. The third paper offers a proxy to replace the two connected steps (PEM plus seismic model). Machine learning models are developed and proposed as an alternative to the traditional PEM plus seismic model. Finally, in the fourth paper, we evaluate a deep neural network algorithm as a proxy for 4D seismic forward modeling. The training phase of model development is analyzed and investigated.

The implementations of two proxy models for PEM in the data assimilation provide satisfactory data match quality when compared to the PEM application. Both production and 4D seismic data objective functions show similar responses for the proxy and PEM implementations. Regarding uncertainty quantification and production forecast, adding porosity to the proxy formulation and accounting for the proxy model error provide a similar response to the PEM results. Therefore, the first two approaches showed to be good solutions to replace the PEM in the data assimilation procedures, making it simpler and faster. In the third approach, machine learning models are developed to replace the complete seismic forward modeling (PEM plus seismic model). Comparing the results from the machine learning models and the traditional approach shows that the proxy models can generate 4D seismic signals similar to those from the traditional approach but in a much cheaper procedure. Machine learning models automate the PEM and seismic modeling task and reduce cycle time of the 4D seismic forward modeling. Moreover, they avoid scale transformation and depth-to-time conversion of the traditional 4D seismic forward modeling. The fourth paper evaluates a deep neural network algorithm to investigate the best training practices for proxy development. The proxy models enable petroleum engineers to perform joint data assimilation in the amplitude domain while accelerating the data assimilation process. All these benefits make the proxy model valuable especially for permanent reservoir monitoring systems where fast 4D seismic data assimilation is highly demanded.

Key Word: 4D seismic data; Data assimilation; Forward modeling; Proxy model

List of Figures

List of Tables

Table of Contents

1 Introduction

Time-lapse (4D) seismic data is a sophisticated geophysical data for reservoir surveillance whose significance is acknowledged by the oil and gas industry. The data consists of timely different 3D seismic surveys acquired over the same reservoir during its productive life. Production activities induce changes in the reservoir such as saturation-pressure changes. 4D seismic data analysis relies on this fact and might reveal these changes. Reservoir density and stiffness alter with these changes, affecting seismic parameters such as primary and secondary waves. Analysing timely changes in the seismic parameters (4D seismic data analysis) could be useful for understanding reservoir behaviour. For example, this analysis could provide important insights into fluid flow patterns and pressure distribution in the reservoir (Pathak et al., 2018) or the analysis helps in placing infill wells in the optimum locations (Gee et al., 2017). Overall, there are good examples of using 4D seismic data for reservoir monitoring and management activities as shown in Buksh et al. (2015) and Mateeva et al. (2015).

The general sentiment of the 4D seismic data analysis intends to use the information qualitatively by applying different 4D seismic attributes. Reservoir fluid movements could be depicted visually and might explain how the reservoir behaves with the applied production strategies. The analysis of this data qualitatively can establish causal factors and carries useful information about each 4D seismic signal. The qualitative interpretation could also reveal facts behind 4D signals regarding dynamic reservoir changes such as saturation-pressure changes. This interpretation is commonly used to monitor reservoir fluid movements and generally utilizes different seismic attributes, geological information, rock-physics relations, and reservoir simulation model. For example, Danaei et al. (2018) used different 4D seismic attributes to interpret qualitatively 4D signals in a field located in Southeast Asia. The authors analysed different 4D seismic attributes and their interpretation revealed hidden channels in the reservoir and also answered questions related to the early breakthrough for some producers. Maleki et al. (2021) presented another example of the 4D seismic qualitative interpretation. The authors used various 4D seismic attributes, rock-physics relations, and reservoir simulation models for qualitative interpretation. A cohesive 4D seismic qualitative interpretation has proven useful for detecting reservoir model deficiencies (Maleki et al., 2018a, 2021).

Besides qualitative interpretation which is helpful, 4D seismic data could be used quantitatively to estimate saturation-pressure changes or to update reservoir simulation models. For example, Landrø (2001) estimated saturation-pressure changes from 4D seismic data or

Lang and Grana (2019) recently proposed an approach to estimate these parameters. To update reservoir simulation models, 4D seismic data could be used simultaneously with production data to calibrate the reservoir models. For instance, a joint 4D seismic and production data assimilation is shown in Emerick (2016) and Luo et al. (2017). Quantitative use of the production and 4D seismic data poses some problems as the seismic and engineering data have different characteristics and are related to different scientific disciplines. This requires close collaboration among geologists, geophysicists, and petroleum engineers.

One of the problems in the quantitative applications is the 4D seismic forward modelling to generate simulated 4D signals in the same domain with the observed data. There are different domains to generate synthetic 4D seismic signals; one possible domain is elastic attributes such as time-lapse acoustic impedance or Poisson's ratio. Here, the forward model only includes a petro-elastic model (PEM) linking reservoir properties such as lithology, porosity, initial reservoir pressure, and temperature to synthetic seismic parameters like a compressional wave (P-wave), shear wave (S-wave), and density. The other domain to integrate 4D seismic data could be amplitude or its attribute domain. Here, the forward model not only includes the PEM but also a seismic model to simulate wave propagation inside the oil and gas reservoir. This forward modelling is a combination of a PEM and a seismic model (usually 1D convolution). Figure 1-1 shows 4D seismic forward modeling in a typical joint assimilation of production and 4D seismic data. As shown in the figure, the elastic domain for 4D seismic data assimilation needs a single step of PEM and the amplitude domain needs back-to-back PEM and seismic modeling. The forward model for the elastic domain (PEM) and the one for the amplitude domain (PEM and seismic model) bring multifaceted problems in the 4D seismic data integration. The traditional 4D seismic forward model approach has a PEM which typically is composed of some equations to relate rock and fluid properties. The seismic model usually is the 1D convolutional model which convolves a wavelet to the reflection coefficients (the contrast of the reflection between two layers) to simulate the seismic data. The 1D convolution is a relatively simple mathematical process, but to compute it, we need to perform time-consuming steps such as scale transference (from a stratigraphic grid to a regular seismic grid) and depth to time conversion. Therefore, running this procedure thousands of times is very challenging and fast-track approaches are desired. This work aims to address these problems, fill gaps in the literature, and offer solutions for these problems.

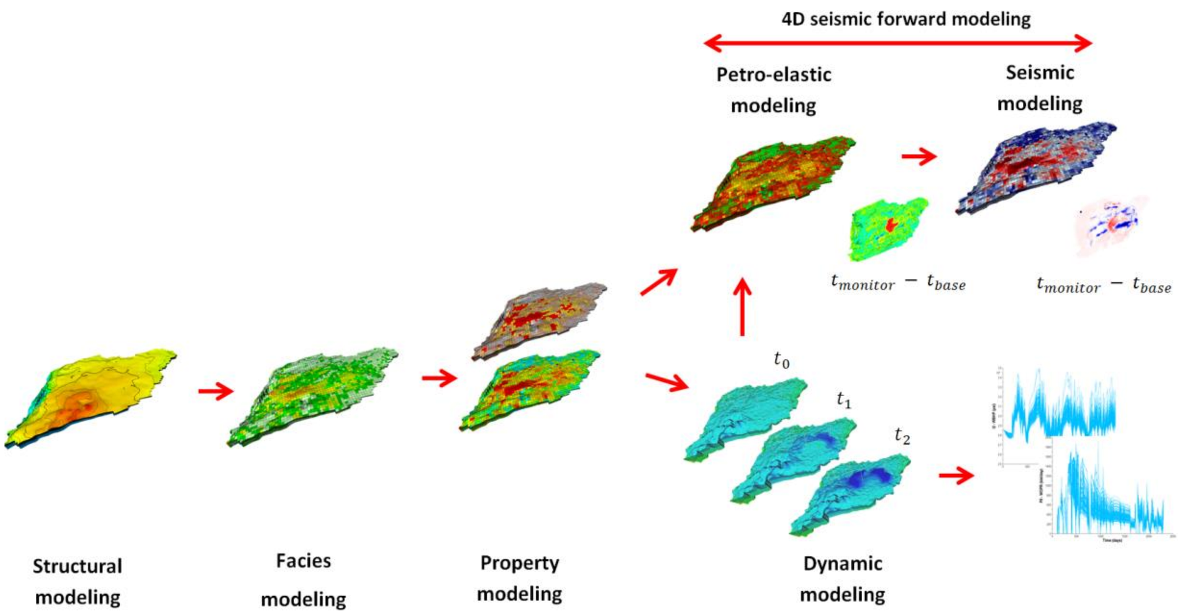

Figure 1-1: 4D seismic forward modeling in the joint assimilation of production data and 4D seismic data

One main difficulty with the PEM is its uncertainty in both the input variables and the rock and fluid models (Danaei et al., 2022). Moreover, the calibration of the PEM to the observed data might be difficult due to the errors in well-log data and laboratory measurements or lack of these measurements. Therefore, what we have as the outputs from the PEMs are wrapped in various uncertainties. In fact, it is difficult to develop a reliable PEM for some 4D seismic quantitative applications. In joint production and 4D seismic data assimilation, the problem with the PEMs is compounded by the fact that we need various grid variables to be extracted from the reservoir simulation models for the forward model calculations. This could be time-consuming for the simulation models of giant reservoirs. The combination of PEM and seismic model also brings problems in the quantitative applications of 4D seismic data. On top of the problems related to PEM, we have the traditional combination of PEM and the seismic model with its own main problem. It has time-consuming steps, such as scaling (from the simulation model grid to a regular seismic grid-SEGY) and depth-to-time conversion. These issues become a problem especially when they apply in 4D seismic history matching using several iterations to update simulation models. In these applications, PEM and seismic model are executed hundreds or, most likely, thousands of times to update simulation models. Furthermore, PEM and seismic modelling in 4D seismic history matching is a highly multidisciplinary task. Geophysicists and petroleum engineers are involved to develop and implement them in these algorithms. Based on the problems with PEM or the traditional PEM plus seismic model, the natural preference is to use a proxy to replace them in the 4D seismic quantitative applications. Previous studies showed wide choices of proxy models for 4D seismic data analysis.

1.1 Summary of previous research on a proxy for 4D seismic forward modeling

The previous research showed that there had been several attempts to replace the PEM or the traditional PEM plus seismic model with proxy models. Several proxy models are suggested to replace the 4D seismic forward model to estimate saturation-pressure changes. The first and the most important point in the literature is the lack of enough research to replace 4D seismic forward modelling with proxy models in the 4D seismic history matching procedure. It is worth noting that to be consistent in the entire text, we call the proxy for PEM in the 4D seismic applications, PEM-Proxy and the proxy for the combination of PEM and seismic model S4D-Proxy. A summary of previous research is presented here and a detailed literature review is presented in the research papers which followed this chapter.

1.1.1 Proxy models for PEM (PEM-Proxy)

Many existing studies have proposed the PEM-Proxy mainly to invert saturation-pressure changes from 4D seismic data. The first proxy model was reported in Landrø (2001) where the seismic parameters (P-wave, S-wave, and density) are related to the saturation change with a first order approximation and the seismic P, and S-waves are related with a second order approximation to the pressure change. The author used the PEM-Proxy for two main reasons. Firstly, the author performed 4D AVO inversion of saturation-pressure changes where 4D AVO intercept and gradient attributes are inverted to these changes. This inversion through a regular PEM could be costly and time-consuming; therefore, the author used the PEM-Proxy to relate 4D AVO parameters to saturation-pressure changes with coefficients. Secondly, using a proxy model was justified as the author mentioned the lack of reliable laboratory measurements to calibrate the PEM. Several modifications to the PEM-Proxy in Landrø (2001) are reported in the literature such as Meadows (2001), Trani et al. (2011), Bhakta and Landrø (2014), and Lang and Grana (2019). For instance, Lang and Grana (2019) included reservoir heterogeneity such as porosity, initial saturation, and initial pressure in the PEM-Proxy model. The authors performed 4D AVO saturation-pressure inversion using an ensemble-based method (Ensemble Smoother with Multiple Data Assimilation, ES-MDA). As we have used machine learning (ML) algorithms in our study, it is worth mentioning that these algorithms also could avoid PEM and invert saturation-pressure changes directly from 4D seismic data as shown in

Weinzierl and Wiese (2020) and Zhong et al. (2020). Previous studies have focused mainly on the PEM-Proxy applications in the 4D saturation-pressure changes inversion. To our knowledge, no study has examined the PEM-Proxy model in 4D seismic history matching which was our motivation and incentive to investigate and address this gap (Danaei et al., 2020).

1.1.2 Proxy models for PEM plus seismic model (S4D-Proxy)

Proxy models can also replace PEM plus seismic model in the 4D seismic quantitative applications. A map-based 4D saturation-pressure changes inversion is shown in Floricich et al. (2005) where the PEM plus seismic model was replaced with a proxy model. Here, the combination of PEM and seismic model is replaced with a linear summation of saturation-pressure changes with coefficients and is related directly to 4D seismic attribute (MacBeth et al., 2006). It must be pointed out that Alvarez and MacBeth (2014) comprehensively analysed how the PEM parameters impact and manifest themselves in the linear coefficients. They concluded that the reservoir porosity has an important role in proxy construction and they discussed how time-lapse seismic signature scales with this parameter. It is worth noting that they did not suggest an explicit proxy equation which contains reservoir porosity in the proxy formulation. Falahat et al. (2013) expanded the linear summation in Floricich et al. (2005) to include the gas saturation change. ML algorithms are soon intertwined to invert saturation-pressure changes from 4D seismic data. Corte et al. (2020), Dramsch et al. (2019b, 2019a), Maleki et al. (2022), and Xue et al. (2019) have used the ML models to directly invert saturation-pressure changes from 4D seismic data. It is interesting that the S4D-Proxy models also were proposed to jointly assimilate production and 4D seismic data to update reservoir simulation models. MacBeth et al. (2016) presented a proxy to replace the combination of PEM and seismic model in 4D seismic history matching and applied that in a synthetic case.

1.2 Motivation

Given the problems with the traditional 4D seismic forward modelling which includes PEM and a seismic model, we are interested in finding proxy models to replace them. In addition, few studies have investigated the proxy model (neither PEM-Proxy nor S4D-Proxy) applications for joint production and 4D seismic data assimilation. To shed light on this uncharted area, we were incentivised to address this gap in the literature and assess the impact of the PEM-Proxy and S4D-Proxy in 4D seismic history matching. As the oil and gas industry moves toward permanent reservoir monitoring settings (PRM), fast-track using of 4D seismic information is essential and could benefit model-based reservoir development and management. We believe that the PEM-Proxy and S4D-Proxy could reduce the cycle time in the 4D seismic data integration to update the reservoir simulation models. Future belongs to proxy model applications in 4D seismic quantitative data integration to help decision-makers to use 4D seismic data timely and properly.

1.3 Objectives

This work aims to find alternative proxy models to replace the traditional PEM and the combination of PEM and seismic model in 4D seismic quantitative applications. We use the proxy models in 4D seismic history matching, which makes it different from previous works reported in the literature. We believe that the traditional 4D seismic forward modelling can be replaced with faster, lighter, and more accessible proxy models without sacrificing the quality and accuracy of the traditional estimations. Figure 1-2 illustrates the overall objectives of the thesis schematically. In Figure 1-2a, proxy models are used to replace the traditional petro-elastic model and in Figure 1-2b, machine learning models are introduced to substitute PEM plus seismic forward modelling. The specific objectives of this work are as follows:

1- To develop the PEM-Proxy model and use it in ensemble-based data assimilation algorithms.

2- To improve the PEM-Proxy model and its applications and use the improved version in the ensemble-based data assimilation algorithms.

3- To use machine learning models as S4D-Proxy to replace the traditional PEM plus seismic model in the quantitative applications of 4D seismic data

4- To evaluate the impact of different training sets on deep neural network proxy models to replace 4D seismic forward modelling

It is worth noting that each objective is addressed as a research paper.

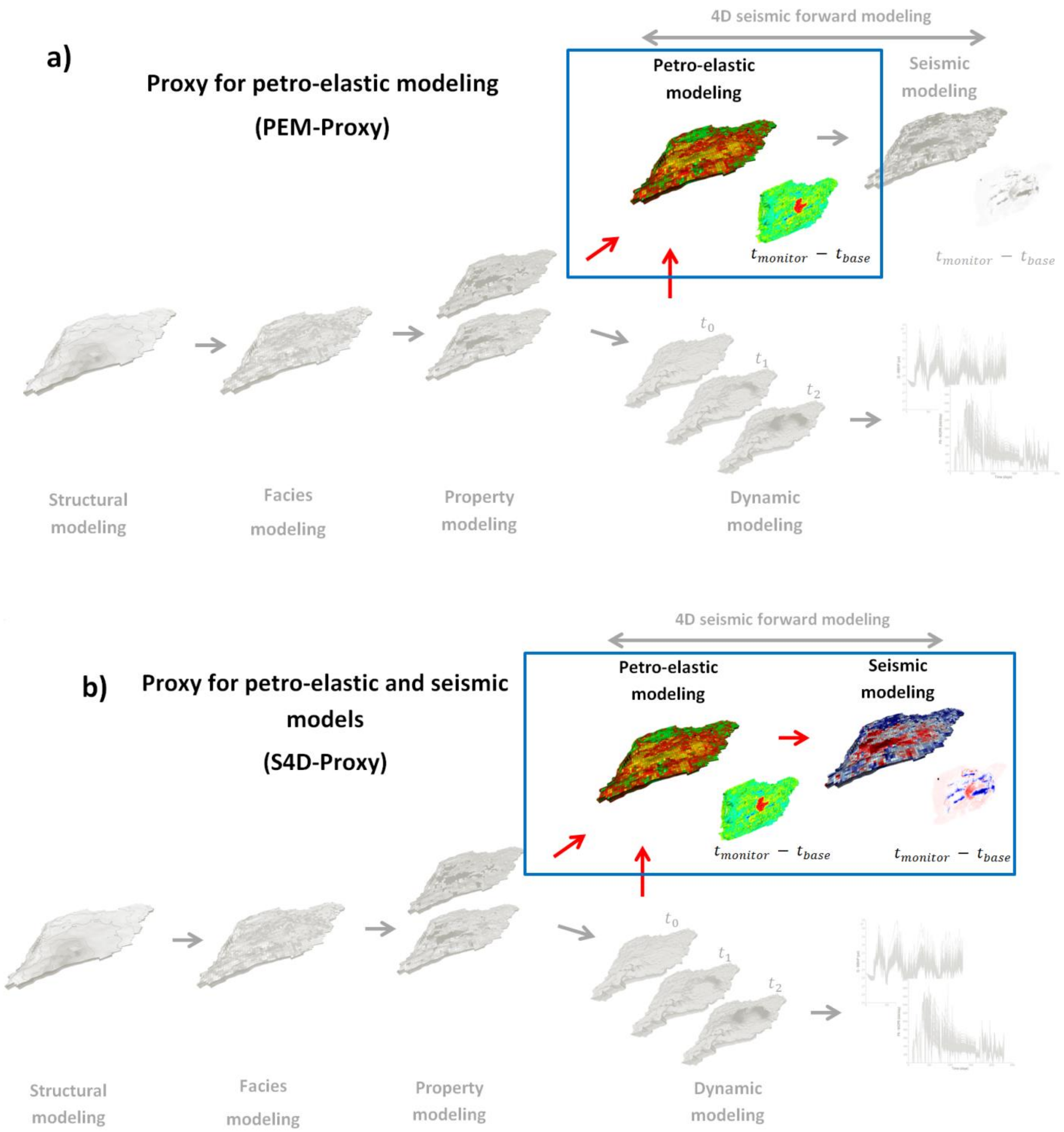

Figure 1-2: (a) proxy for petro-elastic modelling (PEM-Proxy) which is the focus of the first two chapters (chapters 2 and 3); (b) proxy for the combination of PEM and seismic model (S4D-Proxy) which is described in the last two chapters (chapters 4 and 5).

1.4 Structure of the work

This work is divided into four scientific research articles and has five appendixes. In this section, we present a summary of each article. The full manuscript of each article is presented in the following chapters. Appendix A presents the ensemble-base data assimilation algorithm we used for our research; Appendixes B describes in details the petro-elastic model for UNISIM-I case; and Appendix C presents the petro-elastic and the seismic models for the S-field. Two remaining appendixes present complimentary results for PEM-Proxy and S4D-Proxy models

1.4.1 First research paper

Title: Using petro-elastic proxy model to integrate 4D seismic in ensemeble-based data assimilation

Status of the paper: published (**https://doi.org/10.1016/j.petrol.2020.107457**)

Authors: Danaei, S.; Silva Neto, G. M.; Schiozer, D. J.; Davolio, A.

Published in: Journal of petroleum science and engineering, 2020

In general, this work proposes using the PEM-Proxy models to replace the traditional petro-elastic modelling in 4D seismic data assimilation algorithms. We develop a PEM-Proxy which relates time-lapse acoustic impedance change (4DAI) to a linear summation of saturation-pressure changes with two coefficients. The developed PEM-Proxy model is then applied to UNISIM-I-H case study for 4D seismic history matching. The main objectives of the work includes: (1) To develop a PEM-Proxy model to replace the PEM, (2) To use the PEM-Proxy model for 4D seismic history matching, and (3) To compare the data assimilation results from the PEM-Proxy applications and the PEM. This comparison shows how the proxy model behaves compared to the PEM application in the data assimilation process. Different data assimilation cases are developed using the proxy model and the PEM to compare their responses. The comparison is based on the data match quality for both production and 4D seismic data, uncertainty quantification for the grid properties and scalar uncertain model parameters and production forecast.

The results show that the traditional PEM could be replaced with simpler equations and a computationally less expensive or light model to integrate 4D seismic and production data. The comparison of the PEM-Proxy application results with those from the PEM shows that the data match quality is similar when using the proxy compared to the PEM case. In terms of uncertainty quantification, the PEM-Proxy has different responses compared to the PEM case. Mainly, the difference is observed in the grid parameter porosity when comparing the results of the PEM-Proxy case with those from the PEM case. The comparison of the results for production forecast reveals that the proxy model application overestimates or underestimates the reservoir's future behaviour compared to the PEM application. Based on these shortcomings of the PEM-Proxy, we decided to improve the proxy model and its application in the second scientific research paper.

This work presents key contributions when using 4D seismic and production data to update simulation models. Firstly, the work was the first to propose using a PEM-Proxy in 4D seismic history matching. The significant benefit of the PEM-Proxy is for the cases where a reliable PEM is hard to be developed (for example, carbonate reservoir) or challenging to calibrate the PEM with the observed data (for example, lack of the laboratory measured data). For these cases, using a PEM-Proxy could be beneficial. Moreover, the PEM-Proxy has few input variables compared to the rock and fluid models in the PEM. Therefore, a few grid variables must be extracted from the simulation models for the proxy calculations compared to the PEM. This fact is important, especially for large-scale simulation models where PEM-Proxy could save time and facilities the data handling of grid variable extraction. The PEM-Proxy is a lighter model than the PEM, making the data assimilation straightforward and could help petroleum engineers. Appendix D presents extra statistical analysis for PEM-Proxy model versus the PEM.

1.4.2 Second research paper

Title: Substituting petro-elastic model with a new proxy to assimilate time-lapse seismic data considering model errors

Status of the paper: published (**https://doi.org/10.1016/j.petrol.2021.109970**)

Authors: Danaei, S.; Silva Neto, G. M.; Schiozer, D. J.; Davolio, A.

Published in: Journal of petroleum science and engineering, 2021

This work is an extension of our previous published work. In the previous work, the importance of reservoir porosity was mentioned that could improve the results. Two main modifications are considered for this research. The first modification is related to adding reservoir porosity to the PEM-Proxy equation. Porosity is included as a function of the coefficients of the PEM-Proxy developed in the previous work. As the proxy model is different and also calculates 4DAI therefore, we call it “DAI-Proxy”. Adding porosity to the proxy model proved to be the right decision as the proxy models without porosity inclusion (proxy models in Landrø (2001) and MacBeth et al. (2006)) might yield biased estimation if the proxy was calibrated with high porosity samples and applied in low porosity sections of the reservoir. Adding porosity is the first main contribution of this work. Moreover, we propose including proxy model error in the ensemble-based data assimilation algorithm as the proper way of applying proxy models in 4D seismic history matching. Therefore, the second modification introduces different approaches to consider the proxy model errors in the data assimilation procedure. The objectives for this work are: (1) to develop the DAI-Proxy, (2) to consider the proxy model error with two different approaches, (3) to perform 4D seismic history matching with the DAI-Proxy, (4) to compare the proxy and the PEM applications in the data assimilation process based on different criteria.

We apply the 4D seismic history matching to UNISIM-I-H case considering different history matching cases. The behaviour of the proxy and the PEM is analysed based on the observed data match quality, uncertainty assessment for the uncertain model parameters, and the production forecast. Our results show that the DAI-Proxy model application with its model error treatment has similar responses to the PEM application not only for the observed data match quality but also for the uncertainty assessment and production forecast. Compared to our previous work, our current results show our desired improvements.

The DAI-Proxy model gives a significant advantage by including reservoir heterogeneity (porosity) in its formulation. The lack of porosity in the proxy model is mentioned in the previous works, including our previous research. The contribution of this work becomes more significant when we account for the proxy model error in the data assimilation algorithm. To our knowledge, no previous studies have considered the proxy model error for data assimilation. Overall, the DAI-Proxy is lighter than the PEM and has few input parameters. Similar to our previous work, using DAI-Proxy facilitates the joint production and 4D seismic data assimilation. As the results of the PEM and the DAI-Proxy and its model error treatment approach are similar, the proxy could be considered a reliable replacement for the PEM. For the reservoirs in which the PEM has a high level of uncertainty, then using the DAI-Proxy could be beneficial. Appendix D presents statistical analysis for DAT-Proxy and comparison between the proxy and the PEM model.

1.4.3 Third research paper

Title: All-in-one proxy to replace 4D seismic forward modeling with machine learning algorithms

Status of the paper: published (**https://doi.org/10.1016/j.geoen.2023.211460**)

Authors: Danaei, S.; Cirne, M.; Maleki, M.; Schiozer, D. J.; Rocha, A.; Davolio, A.

Published in: Journal of geoenergy science and engineering (formely known as the journal of petroleum science and engineering), 2023

This work goes beyond replacing the petro-elastic model, which was the focus of our previous papers. Here, we develop an alternative model to replace the combination of petro-elastic and seismic models (a complete 4D seismic forward modeling). Quantitative applications of 4D seismic data often require a 4D seismic forward modelling which relates the simulation model outputs to the synthetic seismic in the amplitude domain. Assimilation of observed seismic data in the amplitude domain has the benefits of being readily available after seismic processing (no seismic inversion is required), which makes it attractive for fast-track data assimilation procedures. However, the traditional seismic forward model has two connected forward models (PEM and seismic model) that pose some challenges for quantitative applications. The main problem with the PEM is uncertainty, and the seismic modelling is time-consuming as it requires depth-to-time conversions and scale transference to be applied to several simulation models and repeated in the data assimilation iterations. 4D seismic data is helpful in reservoir management and development activities, especially when integrated quantitatively to calibrate reservoir simulation models. To use 4D seismic information timely in the management and development phases, we need to develop fast-track 4D seismic quantitative application workflows. Using ML algorithms to replace the traditional 4D seismic forward modelling could accelerate the use of 4D seismic data in these applications, especially 4D seismic history matching. This work proposes replacing the traditional 4D seismic forward modelling with ML models. Basically, ML models are considered as a S4D-Proxy model. The proxy model could then be coupled with data assimilation algorithms for quantitative purposes. The objectives of this work are: (1) to develop S4D-Proxy models using ML models, (2) to compare the ML models' predictions with those from the traditional 4D seismic forward model. Note that the input features for the ML models are reservoir properties, and time-lapse saturation-pressure changes. The target for these models is the timely difference in seismic amplitude. We compare ML models' responses to those from the traditional approach based on the quantitative measure R-squared and a visual comparison.

In terms of the R-squared, our results indicate that the S4D-Proxy models could be considered as reliable proxy models to replace the traditional approach. The R-square of the proxy models are almost 0.68, which is an acceptable number considering the level of non-linearity in the PEM and seismic model. Moreover, the visual comparison also indicates that the S4D-Proxy models predict 4D seismic signals almost similar to the traditional approach without sacrificing the accuracy in the predictions. The main 4D signals of the reservoir are captured with the S4D-Proxy models. We also investigate the elapsed time of the machine learning predictions and those from the traditional approach. Our analysis indicates that the proxy models reduced the 4D seismic forward modelling cycle time from days to minutes, which could be helpful in 4D seismic history matching. In this application, reservoir models are updated iteratively, and using the S4D-Proxy models could save a huge amount of time in each history matching iteration.

The main benefit of the S4D-Proxy is its speed and the fact that it performs a 4D seismic forward model all at once, unlike the traditional stepwise approach. The S4D-Proxy models link the reservoir properties and dynamic changes directly to the time-lapse response of the desired seismic attribute. Therefore, the proxy models avert the step-by-step approach of the traditional 4D seismic forward modelling. Moreover, the developed proxy models avert the steps such as depth to time conversion and scale transference required by the traditional forward modelling. All these advantages make the machine learning proxy models practical and applicable for permanent reservoir monitoring (PRM) settings.

1.4.4 Fourth research paper

Title: Evaluation of a deep neural network algorithm as a proxy for 4D seismic forward modeling

Status of the paper: Submitted

Authors: Danaei, S.; Cirne, M.; Maleki, M.; Schiozer, D. J.; Rocha, A.; Davolio, A.

Submitted to: Journal of geoenergy science and engineering, 2022

In the previous work, we proposed the S4D-Proxy as an alternative to 4D seismic forward modelling. As shown in the previous work, Deep Neural Network (DNN) algorithms had very promising results, we want to evaluate this proxy for 4D seismic forward modelling and find out whether using the prior ensemble models are enough to train the algorithm and analyze it while using the posterior ensembles for the training phase. As we want to use the proxy in joint production and 4D seismic data assimilation, the analysis of the proxy when trained with the prior ensemble is important as it is faster to be used inside the joint assimilation procedure. It is worth noting that using the posterior models makes sense in a closed-loop set where we have posterior models to train the algorithm. The choice of reservoir models for the training varies greatly from the prior ensemble of reservoir models (before data assimilation) to the posterior ensemble (after data assimilation). In this work, we train the DNN algorithm with different ensembles of reservoir models (prior and posterior) and investigate the prediction capability of the trained models. Moreover, in map-based training, extracting information around a data point (neighbouring information) in input features for the training purpose might be helpful to develop the DNN model. We designed an experiment to investigate the impact of spatial information on DNN training. Here, the spatial information is gathered around a data point within regions of interest of sizes 3x3, 5x5, and 7x7. The objectives of this work are twofold: (1) to train the DNN algorithm with different ensembles of reservoir simulation models and compare the DNN prediction capability; (2) to train the DNN algorithm with different neighbourhood strategies to extract spatial information (3x3, 5x5, and 7x7).

Two experiments are designed to investigate the objectives of this work. In the first, the DNN algorithm is trained with three ensembles of reservoir simulation models: (1) prior ensemble, (2) posterior from production data assimilation, and (3) posterior ensemble from production plus 4D seismic data assimilation. In the second experiment, different strategies (3x3, 5x5, and 7x7) are used to extract spatial information from the input feature to relate them to the output. DNN models are developed to investigate the impact of spatial information on the prediction. The designed experiments are carried out on a Brazilian offshore field. The results show that the DNN model trained with the prior ensemble of reservoir models could generalize better compared to the DNN models trained with the posterior ensembles. This indicates that the variability in the prior ensemble plays an important role in the DNN predictions and yields better results than DNN models trained with the posterior ensembles. For example, the DNN model trained with the posterior ensemble from production plus 4D seismic data could not generalize well and the model has biases to predict one specific 4D seismic signals (for our case, softening 4D seismic signals). The results from the second experiment suggest two things. Firstly, in terms of elapsed time for the DNN training, the DNN model with 3x3 neighbourhood strategy in its training provides almost similar predictions compared to the DNN model with 5x5 and 7x7 strategies. The training elapsed time for the 3x3 strategy is 5 hours, while the 5x5 and 7x7 strategies use 8 and 12 hours, respectively. Secondly, for some reservoirs with complex geology, training the DNN with more spatial information (5x5 or 7x7) could help the model to predict more details. Appendix E shows information related to the machine learning algorithms and how the inputs are selected.

2 Using petro-elastic proxy model to integrate 4D seismic in ensemble-based data assimilation

Authors: Danaei, S.; Silva Neto, G. M.; Schiozer, D. J.; Davolio, A.

Published in: Journal of petroleum science and engineering, 2020
(**https://doi.org/10.1016/j.petrol.2020.107457**)

2.1 Abstract

4D seismic data provide valuable information for petroleum engineers to update simulation models using different data assimilation algorithms. To assimilate 4D seismic data, the conventional approach is to use a petro-elastic model (PEM) to bring simulation models to the same domain as the 4D seismic data, or vice-versa. PEMs are constructed using rock and fluid models with uncertainty in both input parameters and models. Apart from their uncertainty, PEMs' inclusion in data assimilation algorithms requires an interdisciplinary team of rock physicists and petroleum engineers to develop and implement them. A method was developed in this research to replace the PEM with petro-elastic proxy model (PEM-Proxy) for 4D seismic data assimilation in ensemble based algorithms. PEM-Proxy used here was a linear equation with two coefficients linking water saturation and pore pressure changes to the 4D signal, in our case 4D acoustic impedance (4DAI). Two versions of the PEM-Proxy were developed namely PFC and PUC with fixed and uncertain coefficients, respectively. Eventually, PEM was replaced by the PEM-Proxies in Ensemble Smoother with Multiple Data Assimilation (ES-MDA) algorithm to integrate 4D seismic data. Our method was applied to a benchmark case study, using various data assimilation cases to compare the PEM-Proxies application with the PEM. Results showed that the implementation of the PEM-Proxies did not change the behavior of well and 4D seismic objective functions through data assimilation iterations. Interestingly the PUC implementation was satisfactory in terms of well objective functions and even provided better data assimilation cases for 4D seismic objective function. Production forecast reliability for various cases were analyzed and wells forecast showed similar behavior comparing PEM and PEM-Proxies cases. Our method helps petroleum engineers avoid demanding rock and fluid physics equations and replace them with a straightforward and computationally less expensive model for 4D seismic data assimilation.

2.2 Introduction

The aim of data assimilation is to reduce uncertainty in reservoir simulation models to better represent the subsurface geology and pore fluid interactions, therefore improving production forecast and model-based decision analysis. Data assimilation algorithms update uncertain variables in the simulation models to reproduce available observed data (such as well production, 4D seismic, etc.) within a satisfactory tolerance (Alfonzo and Oliver, 2019; Oliver and Chen, 2011). These algorithms provide multiple reservoir models constrained by observed data and allow us to account for uncertainty in the production forecast. When 4D seismic data are used in assimilation algorithms, it offers a large number of observed data points and decelerates what is already known as a slow process, making it time-consuming to obtain acceptable models. In addition, 4D seismic data and simulation models are of different nature and it is necessary to bring them into a common domain and scale as discussed in Davolio et al. (2014), and Davolio and Schiozer (2019). However, using the 4D seismic data offers advantages as these provide spatial information over the reservoir and might offer a better calibration and forecast reliability for reservoir models (Mikkelsen et al., 2008).

4D seismic data are used qualitatively to infer dynamic reservoir changes (Danaei et al., 2018; Maleki et al., 2018a, 2018b) and these data are integrated quantitatively into data assimilation algorithms to update reservoir models. Quantitative use of the 4D seismic data are found for instances in Davolio and Schiozer (2018), Emerick (2016), and Luo et al. (2017, 2018). Conventionally, 4D seismic data assimilation is performed by comparison of the observed and model simulated 4D seismic signals in a common domain. Reservoir simulation outputs are forwarded (forward modelling) to seismic property domain or 4D seismic data are inverted (4D seismic inversion) to the pressure-saturation domain. Although, the most common domain is the elastic attributes, such as impedance, which can be considered as an intermediate domain between the forward modeling from simulation results and seismic inversion (Davolio and Schiozer, 2018). For comparison in all domains, a petro-elastic model (PEM) is needed as a hinge to establish an interdisciplinary connection between reservoir and seismic properties. The PEM is traditionally composed of the Gassmann fluid substitution to model fluid saturation changes in conjunction with pressure sensitivity modeling (empirical or theoretical).

Different uncertain parameters exist in the PEM in which their combinations yield possible true solutions. Despite the uncertainty, the calibration of the PEM is also challenging, especially for pore pressure changes. For some cases, the PEM could be a complex model such as in carbonate reservoirs (Xu and Payne, 2009), or when it has to be defined for different reservoir facies (Grana et al., 2017). Moreover, the PEM construction and implementation in data assimilation algorithms are interdisciplinary activities. PEMs are constructed by rock physicists and implemented by petroleum engineers. Demand for a simpler equation or model to replace the PEM has never been greater; therefore, these problems were the catalysts to consider alternative approaches to replace the PEM. One possible approach which is investigated in this research is a proxy for the PEM (PEM-Proxy).

Although, there are some studies to replace the PEM with a proxy in 4D seismic inversion (Alvarez and MacBeth, 2014; Floricich et al., 2005; Landrø, 2001; MacBeth et al., 2006; Salako et al., 2018; Xue et al., 2019) few studies have focused on the impact of PEM-Proxy in 4D seismic data assimilation. The following is a portrait of efforts which emerged since 2015 to use a proxy in 4D seismic data assimilation. MacBeth et al. (2016) and Geng et al. (2017) have shown proxy application for seismic history matching. However, the proposed proxy was never implemented for the ensemble based data assimilation algorithms. Obidegwu et al. (2015) presented binary image as a possible approach to avert the PEM for 4D seismic history matching, followed by Davolio and Schiozer (2018), who showed binary image application in one of the ensemble based data assimilation procedures. Yin et al. (2019) recently presented a new approach to circumvent the PEM in ensemble based data assimilation but their approach requires more than one monitor seismic survey (a minimum of four seismic surveys) which limits the application to any field with 4D surveys except when there is a permanent reservoir monitoring system.

Based on the PEM problems and literature review, the question is how to replace the PEM with a simpler model in ensemble based data assimilation algorithms. In this research, a method is developed to answer this question by using the PEM-Proxy. The proxy is a weighted linear relationship with two coefficients linking the water saturation and pore pressure changes to the 4D seismic signals (in our case 4DAI). The developed PEM-Proxy is then coupled with the ES-MDA to integrate both production and 4D seismic data. The method was applied to a benchmark case (UNISIM-I-M) based on a real field in the Campos Basin, Brazil (Avansi and Schiozer, 2015). Various data assimilation cases were considered and compared using the production data only, production and 4D seismic data with the PEM, and production and 4D seismic data with PEM-Proxies.

2.3 Objectives and scope

Three objectives have been considered in this work:

1- Develop the PEM-Proxy to replace the PEM in 4D seismic data assimilation procedures.

2- Couple the PEM-Proxies with the ES-MDA to assimilate production and 4D seismic data.

3- Compare the behavior of the PEM-Proxies with the PEM implementation in the data assimilation algorithm, considering two 4D seismic data (with high and low accuracy).

The developed method does not seek to improve the ES-MDA itself. Topics such as covariance localization, ensemble collapse issue, and model error are out of the scope aimed for this research.

2.4 Theoretical background

2.4.1 Ensemble Smoother with Multiple Data Assimilation (ES-MDA)

Reservoir models are built under various uncertainties in rock and pore fluid properties. Production forecast based on these uncertain models can be unreliable and inconsistent. There are different methods for conditioning the reservoir models to available observed data, including: local optimization methods (gradient methods), global optimization methods (for example evolutionary algorithms), and sampling method (Maschio and Schiozer, 2016). Ensemble based data assimilation algorithms (such as ES-MDA) are tools to reduce uncertainty in reservoir models and improve reliability of the models' forecast.

In 1994, Ensemble Kalman Filter (EnKF) was introduced to assimilate data using an ensemble of models (Evensen, 1994). The first application of the EnKF in petroleum engineering was presented in Lorentzen et al. (2001) and followed by Lorentzen et al. (2003). From then on, different applications of the EnKF to assimilate data in reservoir models are reported, for instance, in Emerick and Reynolds (2011), Naevdal et al. (2005), and Skjervheim et al. (2007). Based on the data assimilation terminology, the analysis is the process of updating model parameters and state variables (Emerick, 2016). While applying the EnKF, it updates a combined parameter-state vector, which includes the reservoir uncertain parameters (porosity and permeability, for example) and state of dynamical system (pressure, water saturation) (Emerick and Reynolds, 2013). It is also possible to assimilate measured data multiple times in the EnKF to improve data match quality as shown in Emerick and Reynolds (2012). There are two problems related to the EnKF: firstly, simulation restarts are required when a new measurement is assimilated which makes it time-consuming and computationally inconvenient for reservoir model applications. Secondly, parameter-state updates may provide inconsistent results, which leads to errors in the reservoir flow simulation numerical solution.

The ensemble smoother (ES) was proposed to simultaneously assimilate all available data (Van Leeuwen and Evensen, 1996). Elimination of simulation restarts is an advantage of the ES compared to the EnKF. Moreover, parameter estimation problem in the ES avoids inconsistencies in parameter-state estimation of the EnKF (Emerick and Reynolds, 2013). Although the ES solved the problems of the EnKF, single update scheme of the ES seems insufficient to properly condition reservoir models to dynamic data (Emerick, 2016; Emerick and Reynolds, 2013). Iterative ensemble smoother (iES) can improve the performance of the ES as discussed in Chen and Oliver (2013) and Luo et al. (2015) alongside, Emerick and Reynolds (2013) suggested assimilating data multiple times with the ES and introduced the ES-MDA. This algorithm is similar to the ES, with the main difference being the addition of an inflation factor which assigns a weight to the analysis equation in each iteration of data assimilation (Emerick, 2016). Further description related to the ES-MDA is available in the Appendix A or readers are referred to (Emerick, 2016; Emerick and Reynolds, 2013).

2.4.2 Data match quality

A normalized quadratic distance with sign ($NQDS$) is used here to assess the quality of the data assimilation for well and 4D seismic objective functions. It has been used in Davolio and Schiozer (2018, p. 263), Maschio and Schiozer (2016, p. 102), and Mesquita et al. (2015, p. 3-4) and calculates the misfit between the simulated model and observed data. For an objective function (well or 4D seismic) and each model in the ensemble, this measure computes the deviation of simulated values from the corresponding observed data. Together with deviation, $NQDS$ provides a sign (positive or negative) which indicates deviation direction. The positive sign shows that the simulated model exceeds the observed data for that objective function and vice versa.

N_{OF} is the number of objective functions in $\boldsymbol{d}_{obs}$ (equation A.1 presented in Appendix A) including well observations and 4D seismic data. The vector $\boldsymbol{d}_{obs_l}$ ($l = 1, 2, \cdots, N_{OF}$) is the observed data (for example, the observed oil rate or observed 4D seismic data) for objective function l in $\boldsymbol{d}_{obs}$ and for model j in the ensemble, $\boldsymbol{d}_{j_l}^{f}$ are its corresponding simulation results (for example, the simulated oil rate or simulated 4D seismic) in $\boldsymbol{d}_j^f$ (equation A.1 in Appendix A), then the $NQDS$ for objective function l is defined as:

$$\boldsymbol{NQDS} = \frac{\boldsymbol{LD_l}}{|\boldsymbol{LD_l}|}\boldsymbol{NQD_l} \qquad (\mathbf{1})$$

In this equation:

$$NQD_l = \frac{QD_l}{AQD_l} \qquad (2)$$

$$QD_l = \left(\boldsymbol{d}_l^f - \boldsymbol{d}_{obs_l}\right)^T * \left(\boldsymbol{d}_l^f - \boldsymbol{d}_{obs_l}\right) \qquad (3)$$

$$AQD_l = \left(Tol_l * \boldsymbol{d}_{obs_l} + \mathrm{C}_l * \mathbf{1}_{N_{obs_l}}\right)^T * \left(Tol_l * \boldsymbol{d}_{obs_l} + \mathrm{C}_l * \mathbf{1}_{N_{obs_l}}\right) \qquad (4)$$

$$LD_l = \left(\boldsymbol{d}_l^f - \boldsymbol{d}_{obs_l}\right)^T * \mathbf{1}_{N_{oobs_l}} \qquad (5)$$

For each objective function, N_{obs} is the number of observed data, $\mathbf{1}_{N_{obs}}$ is N_{obs}-long all-ones vector. The Tol is defined as a tolerance for example as a percentage of the observed data ($\boldsymbol{d}_{obs_l}$) and the $\mathrm{C_p}$ is a constant value to avoid division by zero (usually happens with the observed water rate or 4D seismic data). Values for tolerance and constant are chosen based on engineering judgment and they represent the uncertainty in the observed data. The term LD provides a sign (negative or positive) to the normalized quadratic distance (NQD) to show the deviation of the simulation model from the observed data. $NQDS$ result close to zero shows that the simulation model is mimicking the observed data behavior. This measure equals to unity shows that the mismatch is equal to the percentage of the observed data set as tolerance. $NQDS$ used in our research to assess the data assimilation quality as this measure is a powerful tool to visualize and plot the deviation of a model for each objective function.

2.4.3 Petro-elastic proxy model (PEM-Proxy)

Petro-elastic models make a connection between the reservoir properties and seismic attribute domains. This connection is needed both for the inversion of the pressure and saturation changes from the 4D seismic data and the forward modelling of simulation models for data assimilation or 4D feasibility studies. In the literature, a linear approximation between dynamic reservoir changes and 4D seismic attribute was proposed in Floricich et al. (2005) and MacBeth et al. (2006) for 4D seismic inversions. Reservoir oil saturation and pore pressure changes are related to the mapped 4D seismic attribute using:

$$\frac{\Delta A(x,y)}{\overline{A_b}} = C_s \frac{\Delta S_o(x,y)}{\overline{S_{oi}}} + C_p \frac{\Delta P(x,y)}{\overline{P_i}} \qquad (6)$$

In this equation, C_s and C_p are constants, $\overline{S_{oi}}$ is the average field oil saturation, $\overline{P_i}$ is the average field fluid pressure, and $\overline{A_b}$ is the pore-volume average weighted baseline seismic amplitude. A similar approach is taken by Alvarez and MacBeth (2014) relating weighted linear sum of water saturation and pore pressure changes to the mapped 4D seismic attribute. This linear relation of mapped 4D seismic attribute and reservoir dynamic changes is reliable, based on a comparison in Alvarez and MacBeth (2014). However, modeling has shown that the linearity does break down for reservoirs with thickness greater than 40m and, at this point, a nonlinear term for pressure is required (Falahat et al., 2013).

Using a simplified equation instead of a PEM is not limited to the 4D seismic inversion. It also can be used for 4D seismic data assimilation to update reservoir models. One approach to avoid the PEM implementation is to utilize an identical PEM-Proxy model which is a simple formulation representing the PEM. The general form of the proxy used for history matching in MacBeth et al. (2016) and Geng et al. (2017) is:

$$\Delta A(x,y) = \left(a_1\Delta P + a_2\Delta S_w + a_3\Delta S_g + a_4\Delta P^2 + a_5\Delta {S_w}^2 + a_6\Delta {S_g}^2 + a_7\Delta P\Delta S_w + a_8\Delta P\Delta S_g + a_9\Delta S_g\Delta S_w\right) * A_0(x,y) \qquad (7)$$

In this equation, ΔP, ΔS_w, and ΔS_g are pore pressure, water saturation, and gas saturation changes respectively. $\Delta A(x,y)$ is the 4D seismic signal and $A_0(x,y)$ is the baseline seismic attribute. a_{1-9} are the proxy coefficients. The proxy equation is applicable for thin reservoirs and also for 4D seismic difference maps where the vertical heterogeneity in the reservoir simulation and seismic domains are believed to have minimal influence on the proxy equation; therefore, all analysis should be performed on maps when dealing with the PEM-Proxy models. A good practical comparison exists between the proxy model elements and seismic attributes when working with map based analysis (MacBeth et al., 2016).

2.5 Methodology

The developed methodology comprises two parts, namely PEM-Proxy construction, and its implementation in ES-MDA algorithm. A description of each part is provided below:

Part 1: As simplicity is a central point in our approach to the PEM-Proxy construction, the first initiative is a weighted linear equation linking the saturation and pressure changes to the 4D seismic attribute. For our proxy formulation, we omitted the baseline seismic attribute term in equation (7) for two main reasons. Firstly, the linear regression could provide a good representation of the target 4D seismic attribute (4DAI in our case) as shown in the result section; secondly, to facilitate its use in data assimilation algorithms (note that if we add the baseline attribute term, we would have to estimate that for all the models during data assimilation which jeopardizes the concept of using a proxy). For a reservoir without free gas, the proxy model is written as:

$$\Delta A = a\Delta S_w + b\Delta P \qquad (8)$$

In this equation, ΔA is the time-lapse difference of the 4D seismic attribute, 4D acoustic impedance (4DAI) in our case, ΔS_w and ΔP are the water saturation and pore pressure changes respectively. Based on rock physics principles, two coefficients are defined as $a > 0$, and $b < 0$. The positive sign of coefficient a means that the substitution of oil by water has a hardening effect, which increases 4DAI. Moreover, the negative sign is preserved for coefficient b in the proxy equation to abide by the rock physics principles, in which a pore pressure increase ($\Delta P > 0$) leads to softening and a decrease in 4DAI. The following steps are taken to develop the PEM-Proxies (Figure 2-1):

Step 1: The initial set of models (prior models) before data assimilation is simulated to compute the water saturation and pressure changes between the baseline and monitor seismic times.

Step 2: 4DAIs are generated for the simulated prior models through petro-elastic modelling using the static and dynamic properties calculated in step 1. The petro-elastic modelling is done separately and only in this step to calibrate the proxy models. Once the PEM-Proxies models are developed, the entire data assimilation is performed by them.

Step 3: Linear regression is performed for each prior model to obtain the coefficients in PEM-Proxy (equation 8). In the regression, water saturation and pressure changes (calculated in step 1) acted as independent variables and 4DAI (calculated in step 2) is the dependent variable. Coefficients a, and b are calculated for each model in the initial ensemble.

Step 4: For the prior ensemble of models the distribution histogram of each coefficient is plotted and their mean, standard deviation, minimum, and maximum are calculated. Based on how the coefficients are treated, two distinct PEM-Proxy models are developed. The first PEM-Proxy model (PFC) considers fixed values for both a and b coefficients, which are the mean value calculated from the distribution histograms. The second PEM-Proxy considers a and b as uncertain coefficients (PUC), in this case each coefficient is parameterized based on its distribution histogram characteristics.

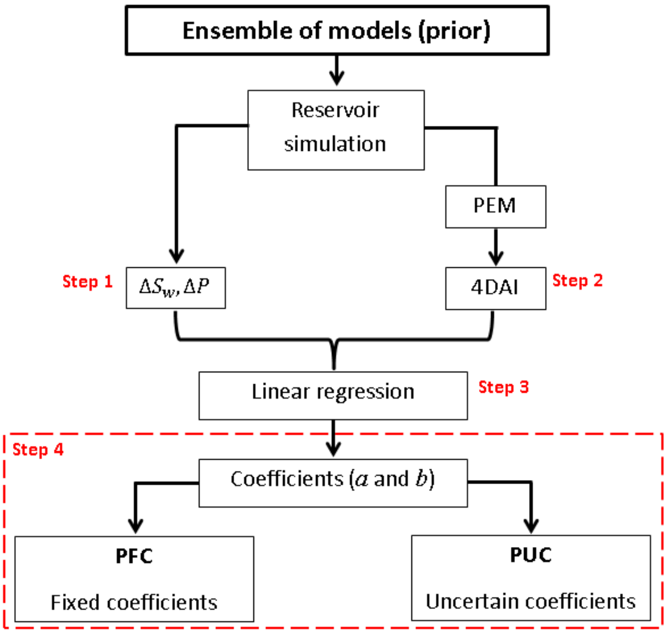

Figure 2-1: Diagram showing the process of PEM-Proxies development (part 1).

Part 2: The developed PEM-Proxies are coupled with the ES-MDA algorithm to assimilate both production and 4D seismic data (Figure 2-2).

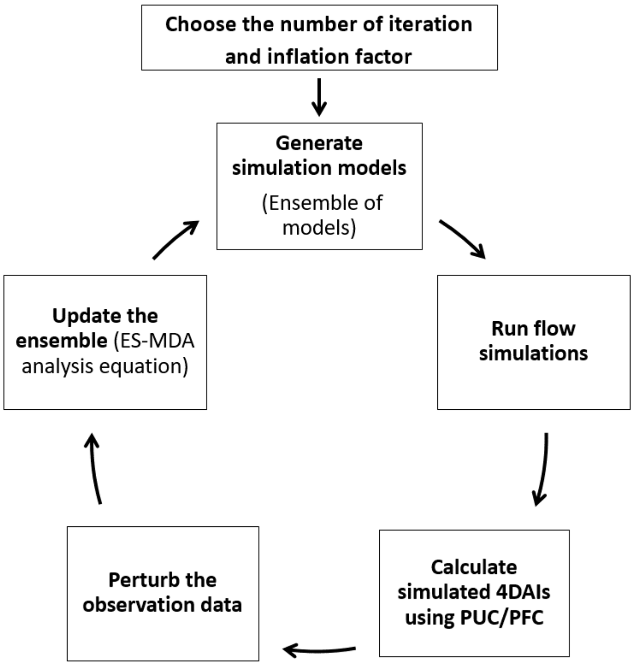

Figure 2-2: Coupling the PEM-Proxies with the ES-MDA algorithm (part 2).

It is worth mentioning that another data assimilation case is run in parallel using the PEM. The intention of this data assimilation case with PEM implementation is for comparison purposes in which the results from PEM-Proxies cases are analyzed and compared with the

PEM case. The comparison criteria are: well objective functions behavior, 4D seismic objective function behavior, uncertainty quantification, and production forecast.

2.6 Application

2.6.1 Dataset description

The developed method was applied to UNISIM-I-M which is a benchmark case developed from an actual field located in the Campos Basin, Brazil (Avansi and Schiozer, 2015). There is a reference model with 326*234*157 grid cells which is considered the true earth model. There is also a set of simulation models built through combination of uncertain properties containing 81*58*20 cells with 36739 active blocks. There are in total 25 wells (14 producers and 11 injectors) scattered over the reservoir. Figure 2-3a shows the location of producers and injectors projected on one porosity model in the ensemble.

The ensemble size considered for data assimilation is 500 models. Uncertain grid parameters include porosity, absolute permeability in each direction, and net-to-gross ratio, sampled using 500 petro-physical models. The uncertain global parameters, which indicate scalar quantities that affect all simulation model grids, are: rock compressibility, depth of the oil-water contact, Corey exponent for water relative permeability, and maximum water relative permeability. In addition, well indexes for both producers and injectors are the local uncertain parameters considered in the location of each well. Table 2-1 summarizes all the uncertain attributes with their parameterizations.

Table 2-1: Uncertain parameters with their parameterizations

Uncertainty	Mean	Minimum	Maximum	Distribution
Porosity	-	0.00	0.31	-
Permeability $(\boldsymbol{k_x})$ (mD)	-	1	5000	-
Permeability $(\boldsymbol{k_y})$ (mD)	-	1	5000	-
Permeability $(\boldsymbol{k_z})$ (mD)	-	1	500	-
Net-to-gross ratio	-	0	1	-
Oil-water contact depth (m)	3174	3169	3179	Triangular
Rock compressibility $(\boldsymbol{kgf/cm^2})^{-1}$	5.3×10^{-5}	1.0×10^{-5}	9.6×10^{-5}	Triangular
Corey exponent for water relative permeability	2.3	1.5	3.3	Triangular

Maximum water relative permeability	0.33	0.15	0.52	Triangular
Well index	-	0.7	1.4	Uniform

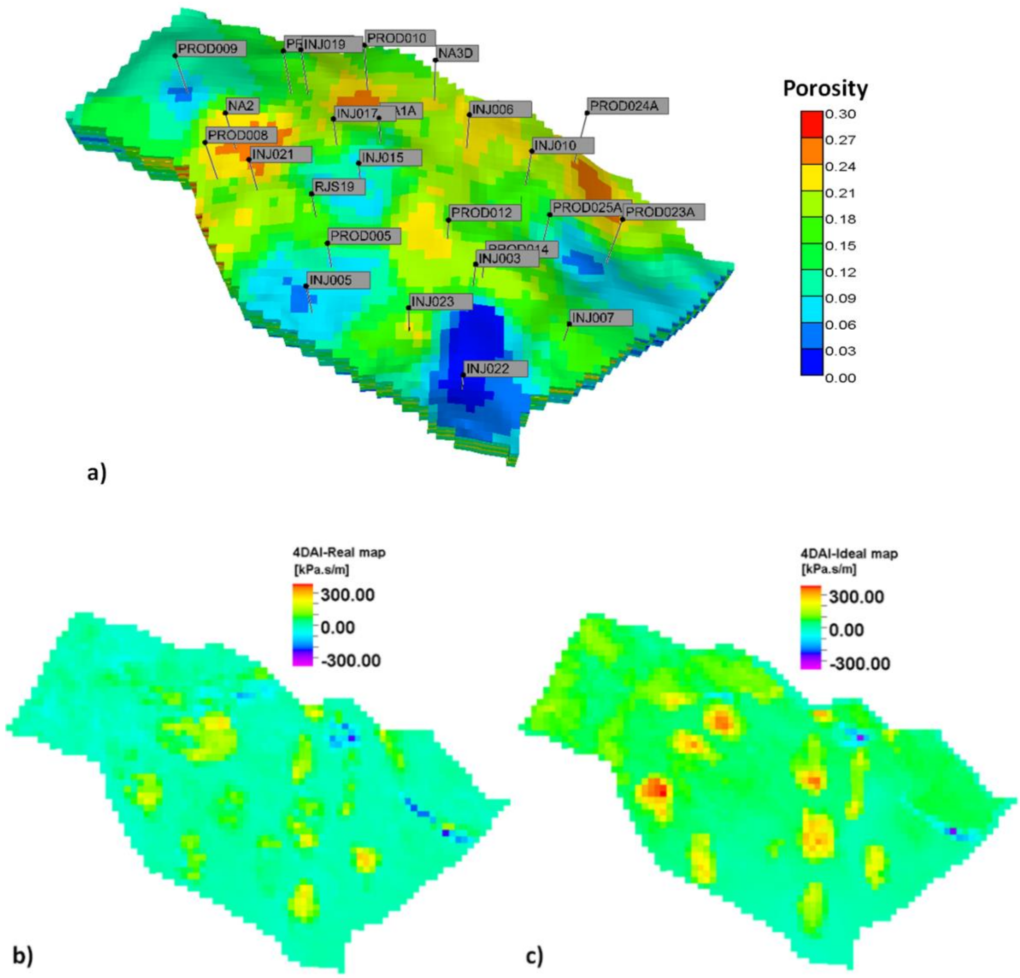

Figure 2-3: UNISIM-I benchmark case study. (a) 3D porosity for one model in the ensemble. (b) 4DAI-Real map for data assimilation, and (c) 4DAI-Ideal map.

2.6.2 Data assimilation conditions

Four iterations of ES-MDA algorithm were used to assimilate both production and 4D seismic data. Distance-based Kalman gain localization scheme was utilized for grid parameters in all data assimilation cases and for fair comparison, similar configurations were considered for different cases to start data assimilation, which include similar prior models and equal number of iterations. For production data, 2618 days of observations were provided including BHP measures for all producers and injectors, liquid, water, and oil rates for all producers, and injected water rates for all injectors. During the data assimilation process, the producer wells were controlled by liquid rates and the injector wells with injected water rates. Data assimilations were performed using BHPs (all producers and injectors), water and oil rates (all producers) and an observed 4D seismic map (4DAI) defined as the monitor (2618 days after production started) minus the baseline (pre-production, time=0).

2.6.3 Observed 4DAI maps (Real and Ideal)

For UNISIM-I-M benchmark case, synthetic baseline (time=0) and monitor (time= 2618 days after production started) acoustic impedance data generated using the reference model (Souza et al., 2018a, 2019). The steps to generate the 4DAI dataset are as follows:

Step 1: Elastic attributes (P and S wave velocities and density) estimated by applying petro-elastic modeling to the reference model's static and dynamic properties. The PEM model used here consists of the Gassmann fluid substitution equation (Gassmann, 1951) to calculate the effects of fluid saturation changes. Matrix moduli were calculated by Hashin-Shtrikman bounds (Hashin and Shtrikman, 1963) and fluid properties were obtained using the Batzle-Wang correlations (Batzle and Wang, 1992) and the Wood's formula (Mavko et al., 2009). Dry rock moduli were modeled by polynomial equations (Emerick et al., 2007), in which pressure and porosity dependencies are similar to Hertz-Mindlin contact theory model (Hertz, 1882; Mindlin, 1949). For interested readers, a detailed explanation of the PEM used here is presented in the Appendix B.

Step 2: The model with elastic properties was then converted from depth to time and convolved with a wavelet to generate 3D volume of seismic amplitudes.

Step 3: Colored inversion was used to create 3D inversion result. This inversion algorithm is a fast tool to invert seismic data to the relative impedance cube. The operator in colored inversion algorithm tries to match the seismic amplitude spectrum to the impedance spectrum from the well-log data (Lancaster and Whitcombe, 2000). As it is relatively easy to run, this inversion is applied to 4D studies such as Maleki et al. (2018a) and Stephen et al. (2006) to quickly access 4D impedances changes.

Step 4: Repeating steps 1 to 3 for the baseline and monitor times gave us two 3D acoustic impedance datasets and eventually the 4DAI map was obtained by subtracting the monitor from the baseline. Figure 2-4 summarizes all the steps to generate the observed 4D dataset.

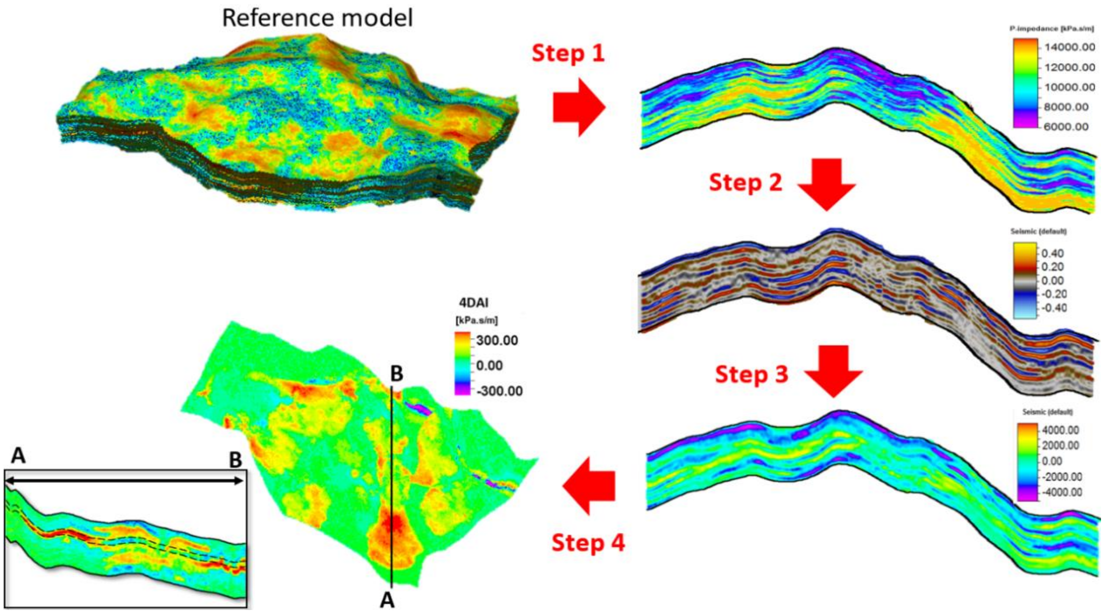

Figure 2-4: Steps to generate 4D seismic data for UNISIM-I benchmark.

Two 4D acoustic impedance (4DAI) maps were used separately in our research for data assimilation. The first 4DAI map was defined as monitor minus baseline of inversion results (Step 4). We call it 4DAI-Real map because it is a realistic representation of seismic impedances for this case which would be similar to the data available for data assimilation purpose in real cases (Figure 2-3b). The second 4DAI map was defined as monitor minus baseline from acoustic properties calculated in (Step 1). We call it 4DAI-Ideal map, as this is an ideal representation of seismic impedances without a proper loss of vertical resolution we know seismic data have (Figure 2-3c). These two 4D seismic maps were used separately for data assimilation in conjunction with the production data. The goal is to evaluate the impact of different quality of observed data into the process. Although the output in Step 2 is a noise-free seismic amplitude data, both 4DAI maps were perturbed by an uncorrelated Gaussian noise.

2.6.4 Design of data assimilation cases

Data assimilation cases were designed with ES-MDA algorithm considering:

- Different 4D seismic forward models: three forward models were considered to design the cases:

  1) Petro-elastic model: this forward model was acronymed PEM and it uses a complete set of equations described in the Appendix B.
  2) Petro-elastic proxy model with fixed coefficients: this forward model developed in section 4 and was abbreviated PFC.
  3) petro-elastic proxy model with uncertain coefficients: it was abbreviated PUC and it was described in section 4.

- Different observed data: Production data was used in conjunction with 4D seismic map leading to two sets of observed data:

  1) Production data with the realistic 4D difference of acoustic impedance: the 4D seismic map here was called 4DAI-Real in section 5.3. This set of observed data was abbreviated WSR.
  2) Production data with the ideal 4D difference of acoustic impedance: the 4D seismic map here was named 4DAI-Ideal map in section 5.3. This set of observed data was abbreviated WSI.

Combination of different 4D seismic forward models and observed data sets resulted in six data assimilation cases. For example, PEM as a 4D seismic forward model was used to assimilate WSR observed data leading to WSR-PEM case, or a combination of PFC and WSI created WSI-PFC data assimilation case and so on. These six cases aside, a separate case was designed to assimilate only production data and abbreviated as OW. Table 2-2 summarizes all the data assimilation cases with different color codes, designed and performed.

Table 2-2: Various cases of data assimilation for our research

Case	Abbreviation	Observed data	Forward model	Color code
1	OW	Only production data	-	
2	WSR-PEM	Production and 4DAI real map data	PEM	
3	WSR-PUC	Production and 4DAI real map data	PUC	
4	WSR-PFC	Production and 4DAI real map data	PFC	
5	WSI-PEM	Production and 4DAI ideal map data	PEM	
6	WSI-PUC	Production and 4DAI ideal map data	PUC	
7	WSI-PFC	Production and 4DAI ideal map data	PFC	

2.7 Results

This section is divided into five parts. Firstly, we discuss the construction of the PEM-Proxies for UNISIM-I-M and, in sections 6.2 to 6.5, the results of data assimilation for different cases are presented, based on well and 4D seismic objective functions, uncertainty quantification, and production forecast.

2.7.1 PEM-Proxies construction for UNISIM-I-M

Two versions of the PEM-Proxies were developed for our case study. The workflow includes four steps based on the diagram presented in Figure 2-1. Water saturation and pore pressure changes were calculated by considering baseline (time=0) and monitor (time=2618) seismic times. Time-lapse differences of 4DAI were generated for each prior model, then coefficients a, and b were calculated. Figure 2-5 shows the distribution histograms and their characteristics obtained for two coefficients from prior models.

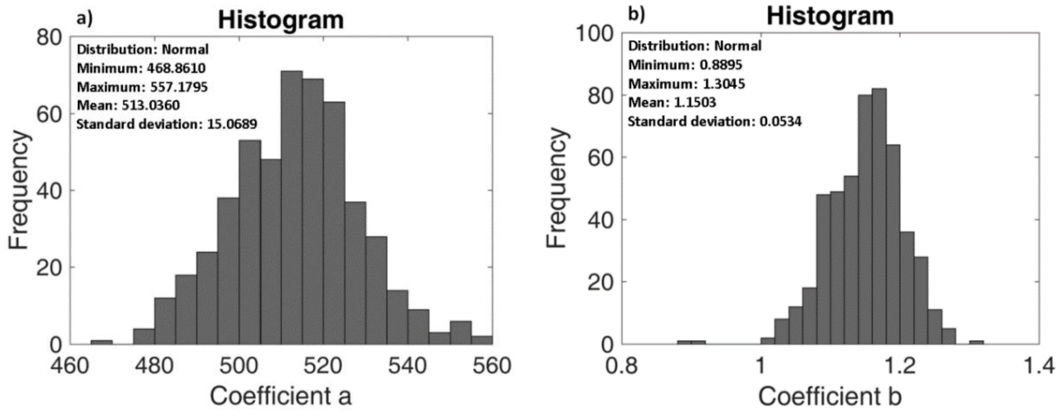

Figure 2-5: Distribution histogram for coefficients a, and b. (a) Histogram for coefficient a. (b) Histogram for coefficient b.

The PEM-Proxy with fixed coefficients (PFC) was developed using the mean values of coefficients a, and b. On the other hand, coefficients a, and b for PEM-Proxy with uncertain coefficients (PUC) were parameterized based on their distribution characteristics which, in our case, were defined by normal distribution. As the PEM-Proxy was proposed to replace the PEM implementation in data assimilation; therefore, the accuracy of the PEM-Proxy model was evaluated based on the coefficient of determination (R^2) of the linear regression. For our research, the average value of R^2 is 0.88, which shows that the PEM-Proxies correctly represent the actual PEM. Figure 2-6 shows three estimations of 4DAIs: using the PEM and the two PEM-Proxies. Comparison of Figure 2-6a with Figures 2-6b and c shows that the main 4D signals located around injectors are captured with the PEM-Proxies models. 4DAIs map generated with proxies (Figures 2-6b and c) show a smooth distribution of 4D signals without having the heterogeneities captured by the PEM model (Figure 2-6a). This comes from the equation of the PEM-Proxies which is a linear regression of main dynamic reservoir changes.

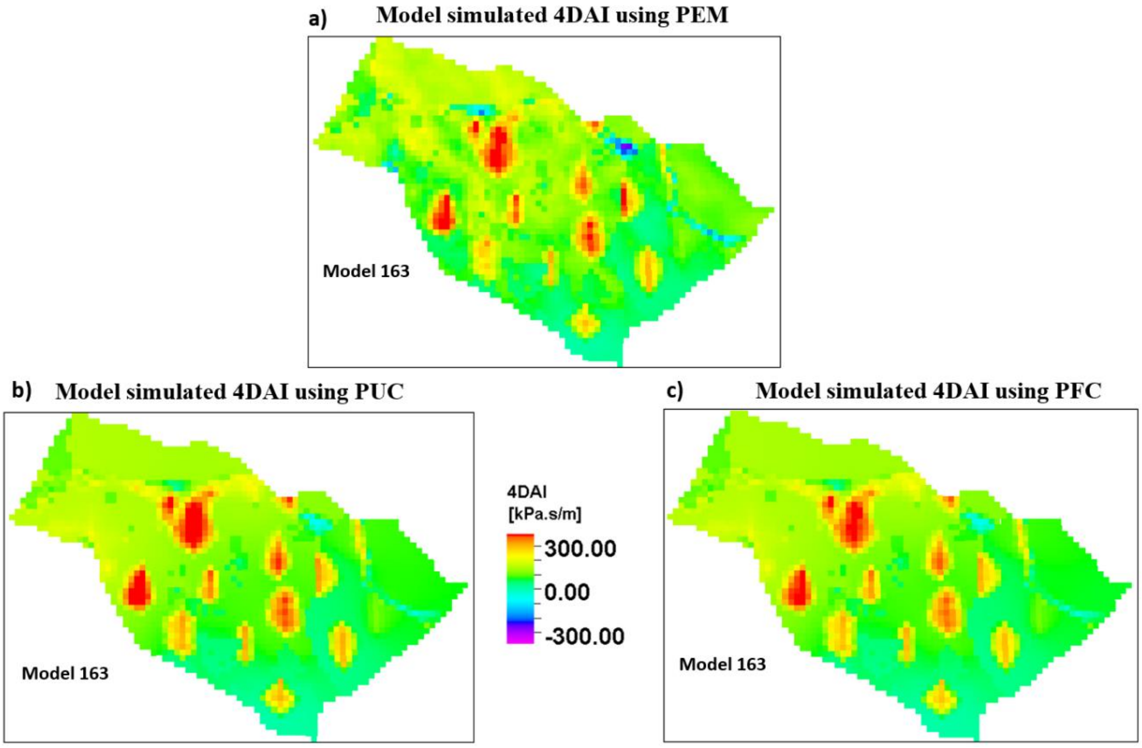

Figure 2-6: synthetic 4DAIs generated using the PEM and PEM-Proxies for a randomly selected model (model 163).

2.7.2 Data assimilation quality for well objective functions

In terms of data match quality, Figure 2-7 shows the boxplot presentation of the NQDS values for BHP of producer wells for all the data assimilation cases. In NQDS measure (equation 1), the Tol was considered 5% for BHP objective functions and 10% for all other objective functions, and also C_p was assumed 50 $\frac{m^3}{day}$ only for produced water rate. In Figure 2-7, the light gray box represents the prior models which have the highest uncertainty and show high variability for all well objective functions. The final sets of models after data assimilation (posterior) for all cases are represented by their respective colors and the low variability in each set indicates uncertainty reduction after data assimilation. This reduction is more pronounced when 4D seismic maps were used for both real and ideal 4DAI maps as we used more observed data for these cases (for example, one must compare the OW case to the WSR-PEM case for PROD014 in Figure 2-7a).

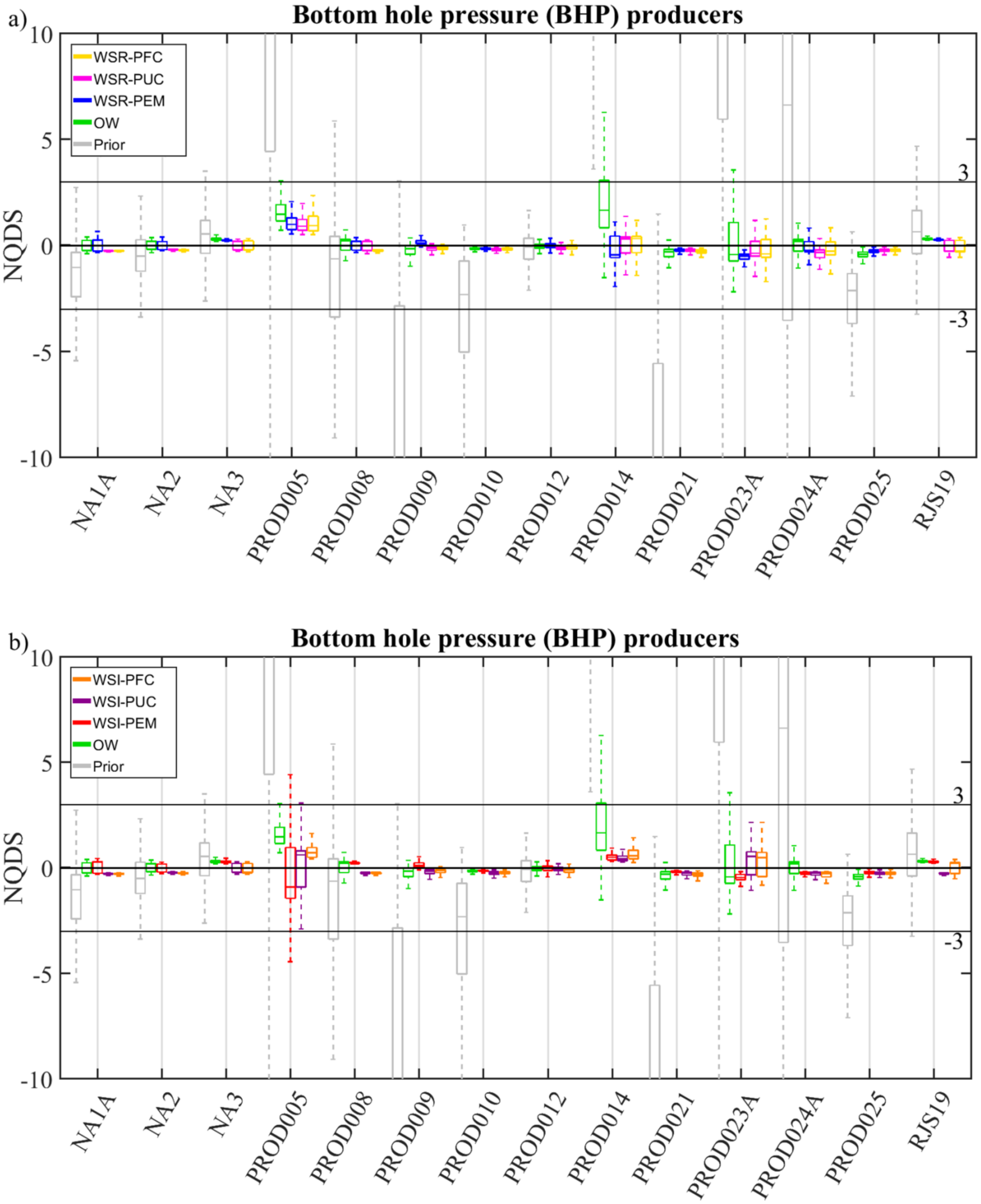

Figure 2-7: NQDS values for BHP of producer wells, light gray boxes show the prior models. (a) Using 4DAI-Real map with posterior models for different cases are indicated by their corresponding colors and (b) using 4DAI-Ideal map as observed data.

By comparing well objective functions in Figure 2-7, it is clear that PUC and PFC cases provided similar results compared to the PEM cases. The behavior of WSR-PEM case compared to WSR-PUC and WSR-PFC cases are identical for wells such as NA1A, NA2, and NA3D in Figure 2-7a, and even better results were achieved by the PEM-Proxies for some wells such as PROD009. In general, data assimilation was more efficient when 4DAI-Ideal map was used because the assimilated 4D seismic map was an ideal map (section 5.3) without a proper resolution loss. Other well objective functions provided similar results between the PEM and PEM-Proxies cases, which highlights that the PUC and PFC implementations did not change the production data assimilation behavior in terms of well objective functions. Figure 2-8 illustrates water rate curves for well (NA2) using PEM, PUC, and PFC for 4D seismic data assimilation. For Figure 2-8 the prior models are in light gray and only cases with 4D seismic data assimilation are shown to compare the results.

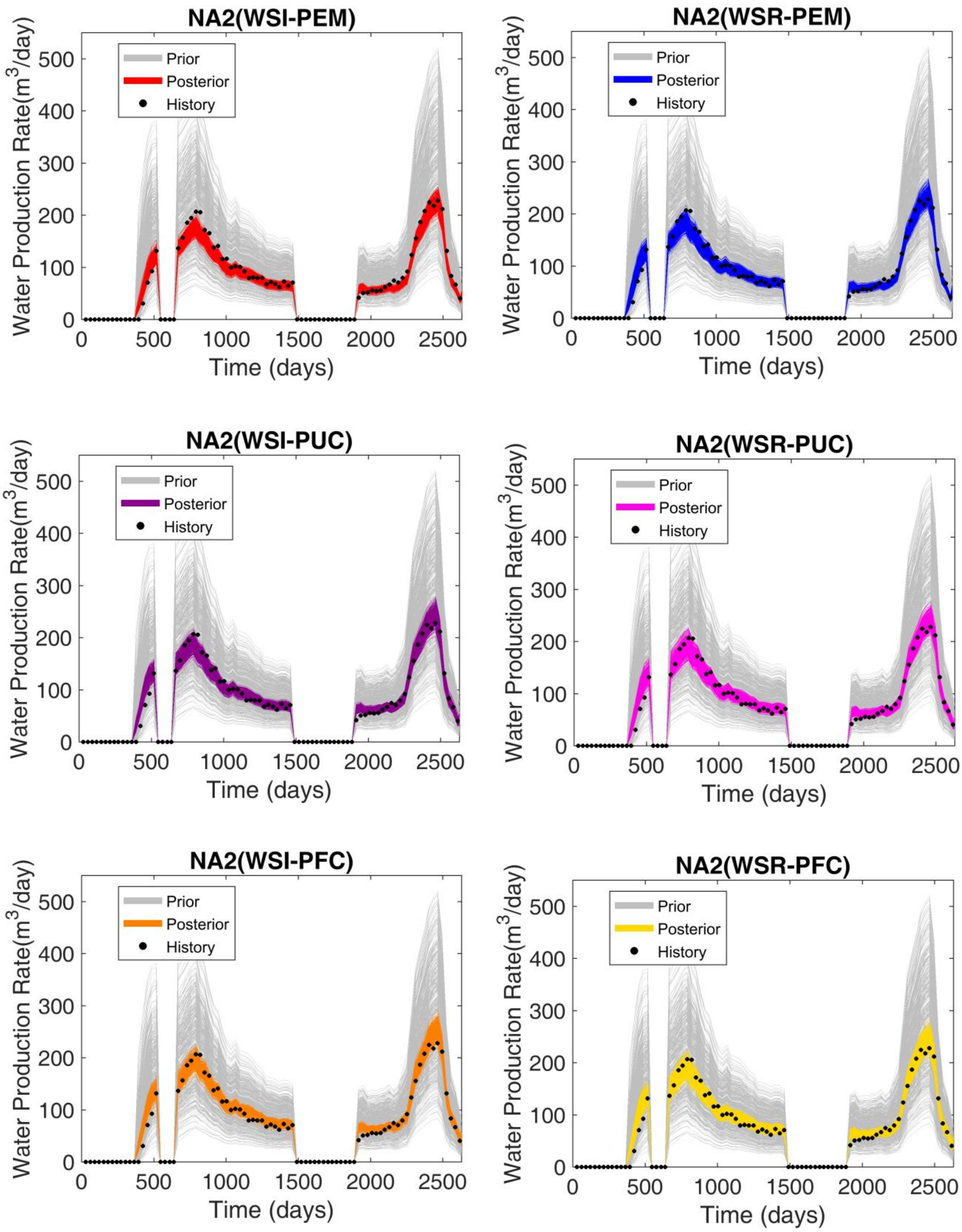

Figure 2-8: Water rate curves for prior models in gray and posterior models with each case color coded.

To analyze the behavior of each case for all the well objective functions as a whole, we used NQDS to rank the posterior models. Ranking assigns an overall matching quality to the posterior model, based on the behavior of all well objective functions. It means that if a posterior model is ranked with $-1 < NQDS < 1$ (an excellent match quality) or with $-5 < NQDS < 5$

(a moderate match quality), it means that all its well objective functions have $-1 < NQDS < 1$ or $-5 < NQDS < 5$, respectively. All posterior models for different cases were ranked and the number of models in each rank was counted. Figure 2-9 shows the ranking of posterior models for different cases using the 4DAI-Real map (Figure 2-9a) and the 4DAI-Ideal map (Figure 2-9b). The results in Figure 2-9 demonstrate the efficiency of data assimilation for PEM-Proxies cases when 4D seismic objective function was added to well objective functions.

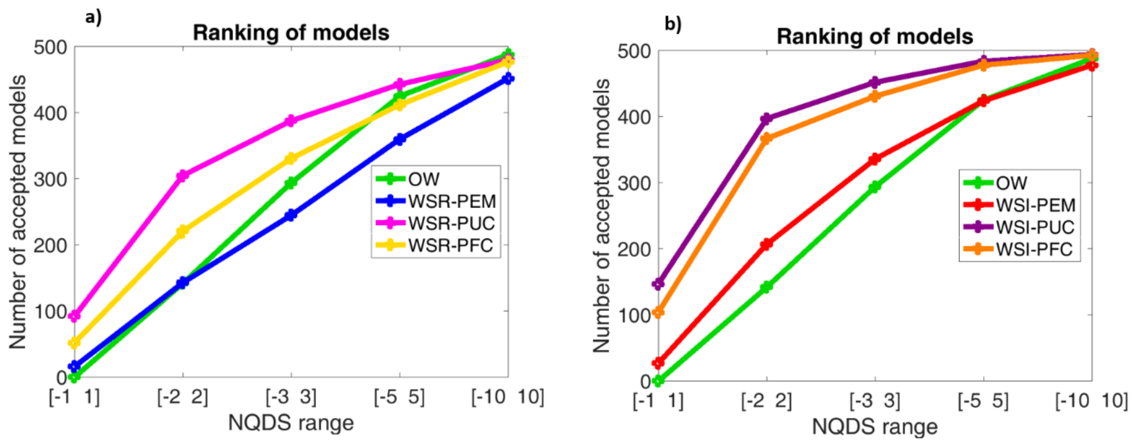

Figure 2-9: Ranking of posterior models for each case based on NQDS values of its well objective functions. In (a), the ranking result is shown for 4DAI real map assimilation and in (b), the ranking for 4DAI ideal is shown.

Our results showed that using PUC and PFC for 4D seismic data assimilation (for both seismic maps) yielded more models with low NQDS values (Figure 2-9) which means PEM-Proxies implementation performed efficiently in data assimilation, being the PUC implementation the best case.

2.7.3 Data assimilation quality for 4D seismic objective function

The qualities of 4D seismic data match (for both maps) were calculated based on NQDS measure for six cases which used both production and 4D seismic data. For NQDS calculation based on equation 1, the Tol was considered 10% with 30 $\frac{kPa.s}{m}$ used for C_p. NQDS was calculated based on the observed 4DAI maps to show an overall quality of 4D seismic match. We call it "overall" as it represents an overall match quality for the entire maps. In another investigation, both observed maps were divided into some areas to obtain a better understanding of match quality in these areas for different cases (Figure 2-10). These areas were defined in such a way to cover the entire map from east to west, and northward areas down to the southward locations.

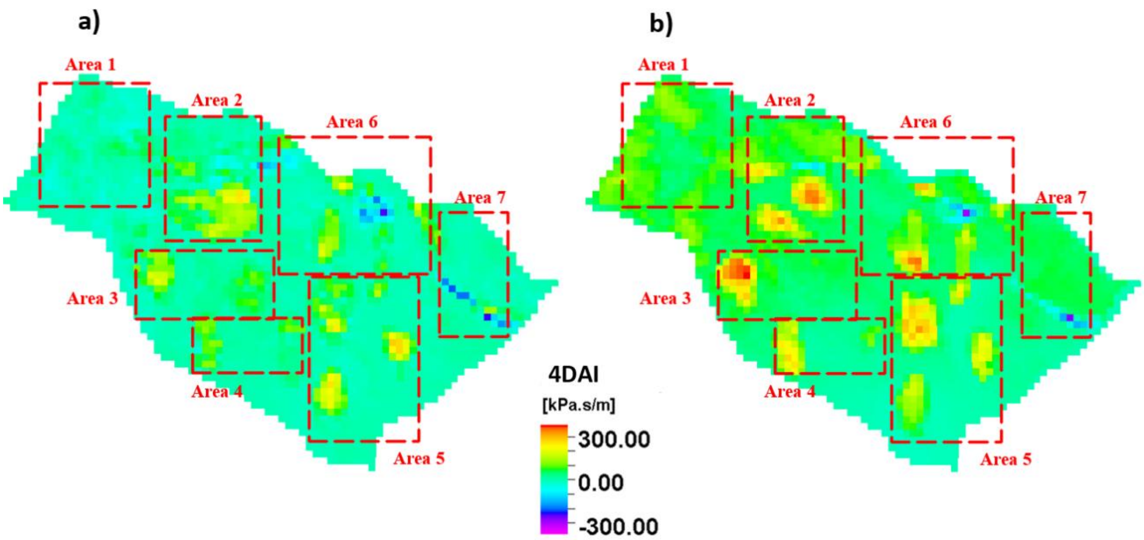

Figure 2-10: Division of observed 4D seismic maps into 7 areas. (a) 4DAI-Real map and (b) 4DAI-Ideal map

Figure 2-11 represents the 4D seismic match quality with boxplots for different cases calculated for the entire maps and also different areas. The light gray boxes represent the prior models and posterior models for each case are displayed in their respective colors. As shown in Figure 2-11a, PUC cases provided equal or even better results in some areas compared to the other cases. 4D seismic match quality for the ideal map lead to the similar superior cases for PUC implementation in data assimilation. The results for 4D seismic objective function (both maps) indicate an efficient data assimilation for PUC cases similar to the results for well objective functions. Comparison of the results between the 4DAI-Real and ideal maps implementations (Figures 2-11a and b respectively) indicates that the data assimilation for 4DAI-Ideal map was more efficient which are shown in low values of NQDS measure for all the areas. For example, area 1 in Figure 2-11b has lower NQDS values compared to the same area in Figure 2-11a. The comparison shows a good match quality for 4DAI-Ideal map. The reason might be related to the resolution loss through inversion algorithm.

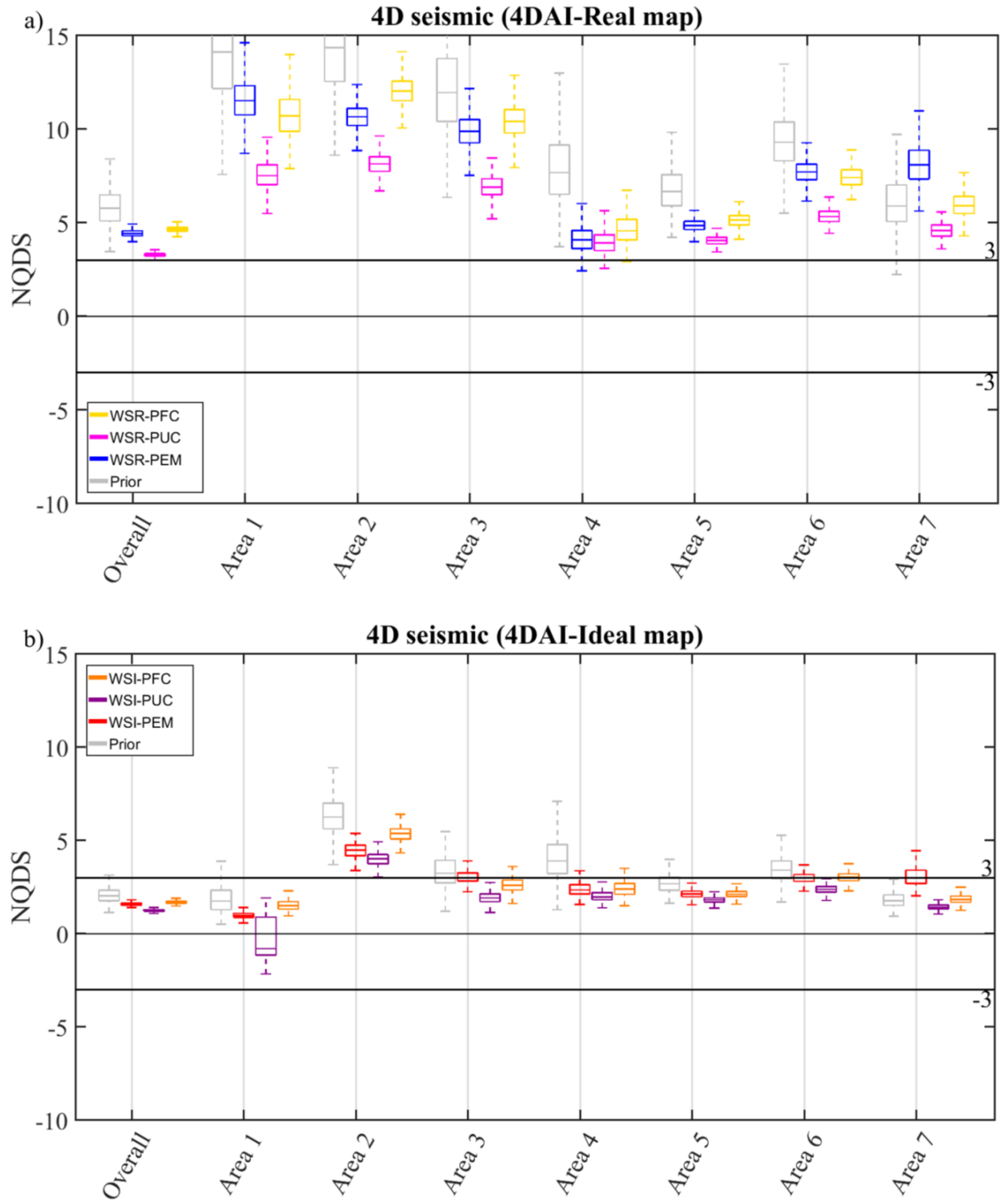

Figure 2-11: Quality of 4D seismic data assimilation based on NQDS measure for overall and different areas of the observed maps; The posterior models are shown in (a) when the 4DAI-Real map was used and in (b) for the 4DAI-Ideal map data assimilation.

Figure 2-12 shows the observed 4DAI-Real map (Figure 2-12a) and the mean of 4DAI for the prior (Figure 2-12b) and posterior (Figures 2-12c, d, and e) models for cases which used 4DAI-Real map in the data assimilation (WSR-PEM, WSR-PUC, and WSR-PFC). The hardening effects caused by injected water in observed data are captured by both PEM and PEM-Proxies cases. It shows that the PEM-Proxies do not change 4D seismic objective function and behaves similar to the PEM implementation in data assimilation. Mean 4DAI for prior models (Figure 2-12b) shows predominant hardening effects caused by water injection in the location of injector wells. After data assimilation, these effects were ameliorated and 4D signals around injector wells weakened, showing efficient data assimilation for all cases. Overall, the 4D seismic data match for the 4DAI-Ideal map also indicates that the PEM and PEM-Proxies cases are very similar (Figure 2-13).

There are some areas where the behavior of the PEM and PEM-Proxies cases are different. For example, a comparison of Figure 2-12c with Figures 2-12d and e indicates that the north-west area is different for WSR-PEM case with WSR-PUC and WSR-PFC cases (blue arrow). Different behavior in the north-west area is also seen in Figure 2-13 (compare Figure 2-13c with Figures 2-13d and e). This difference means that the responses of the PEM-Proxies model do not replicate the PEM model responses.

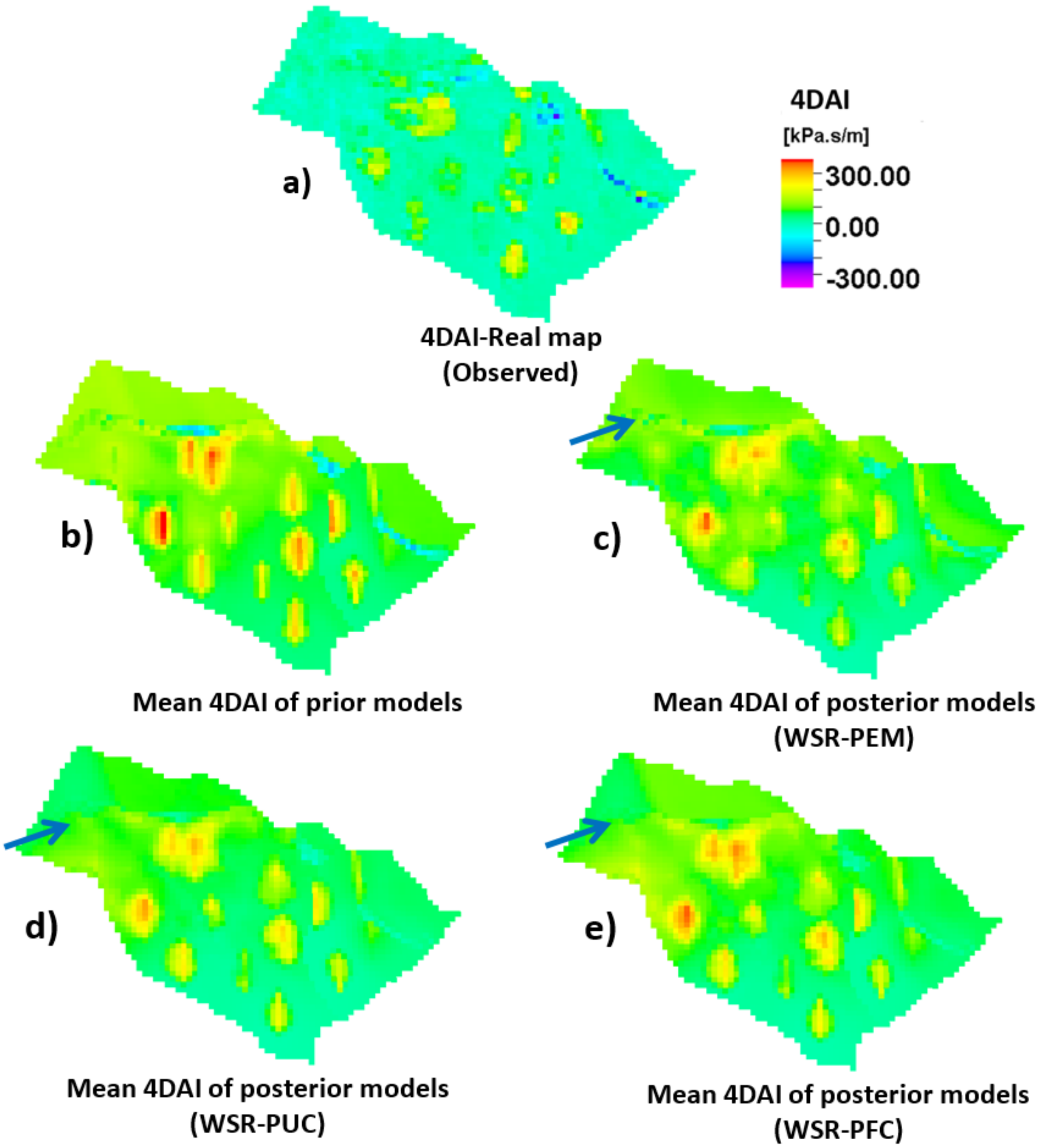

Figure 2-12: (a) observed data, (b) shows the mean 4DAI for prior models, (c), (d), and (e) indicate the mean posterior 4DAI with PEM, PUC, and PFC for data assimilation.

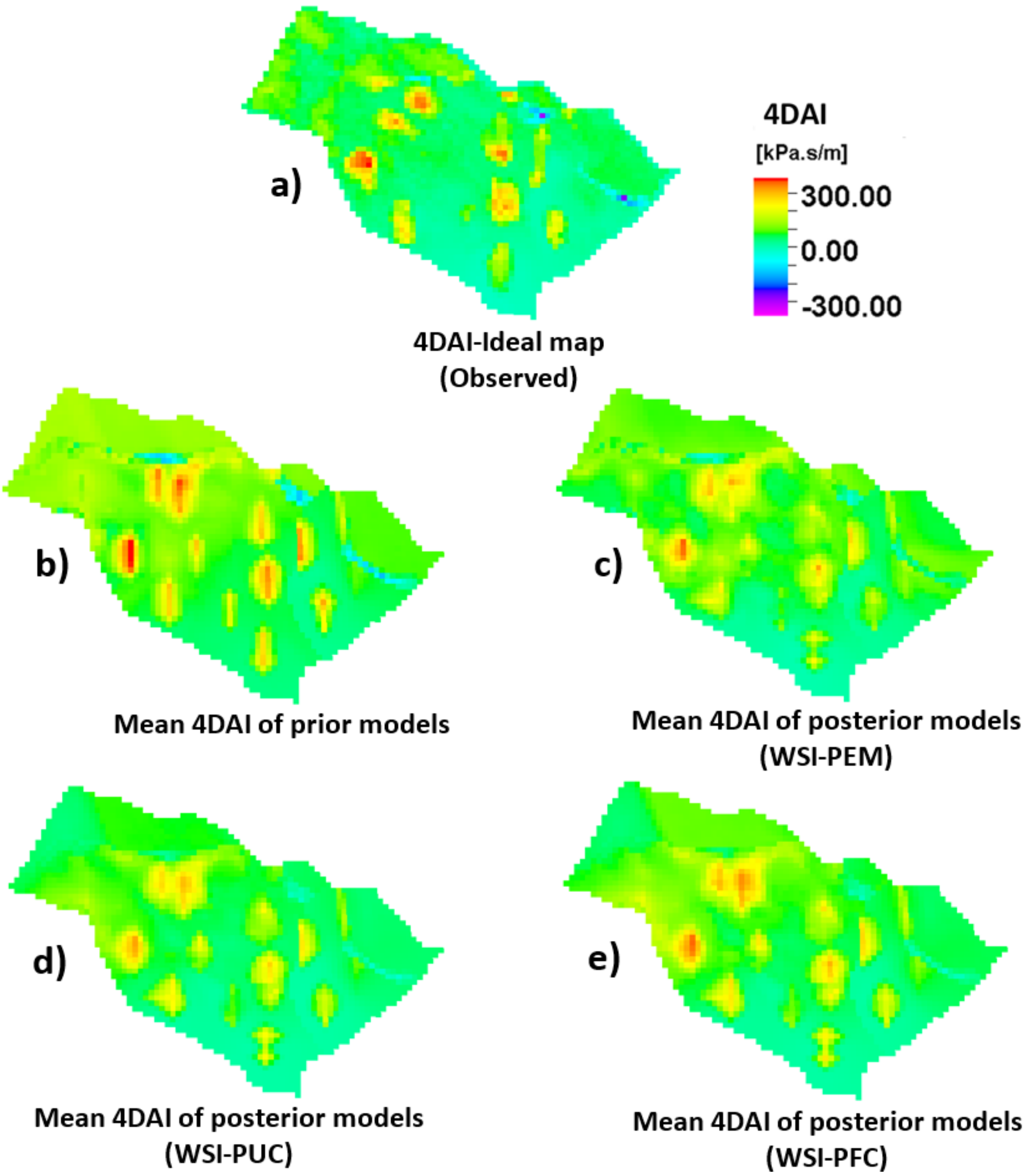

Figure 2-13: (a) observed data, (b) shows the mean 4DAI for prior models, (c), (d), and (e) indicate the mean posterior 4DAI with PEM, PUC, and PFC for data assimilation.

2.7.4 Uncertainty assessment

Matching qualities in terms of well and 4D seismic objective functions are important, but the data assimilation tries to reduce uncertainties in reservoir simulation models to have a better future forecast. Thus, uncertainty assessment is also essential for a successful data assimilation process. In terms of global uncertain parameters, Figure 2-14 shows the uncertainty reduction results after data assimilation for different cases. A noticeable uncertainty reduction occurred for all global uncertain parameters when 4DAI maps were assimilated. In fact, ensemble collapse for global uncertain parameters for 4D seismic data assimilation are reported in the literature (Chen and Oliver, 2014; da Nóbrega et al., 2018; Emerick, 2016).

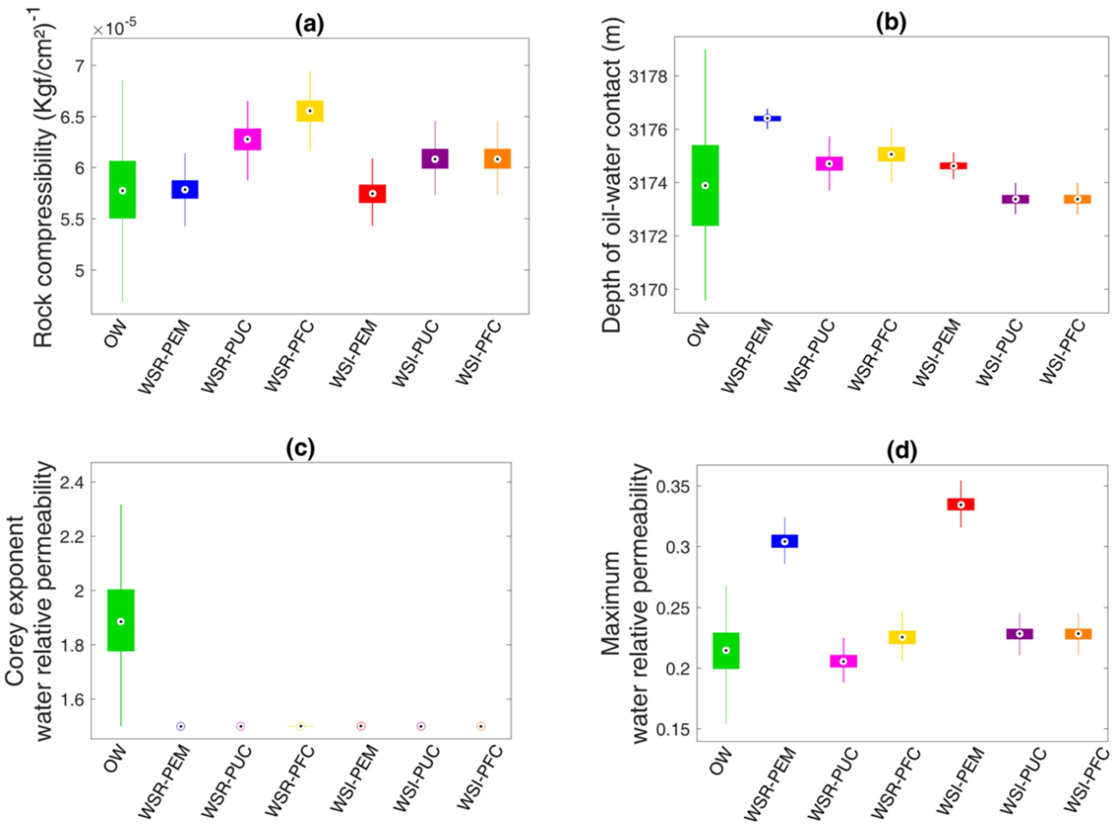

Figure 2-14: Posterior values for global uncertain parameters. In (a) shows the rock compressibility for posterior model, (b) shows depth of oil-water contact, (c) displays the Corey exponent, and (d) indicates the maximum water relative permeability.

According to Figure 2-14a, the uncertainty reduction for rock compressibility is different for the PEM and PEM-Proxies cases. A shift towards higher values in rock compressibility is detected when using the PUC and PFC models for 4DAI data assimilation. The pattern remains the same for both (Real and Ideal) 4DAI maps. For depth of oil-water contact, assimilation of data returned the same posterior values for different cases (Figure 2-14b). Although the behaviour of the PEM and PEM-Proxies cases were different in terms of maximum water relative permeability (Figure 2-14d), for Corey exponent of the water relative permeability, all the cases collapsed to a single value, which is the minimum value in its parameterization (Figure 2-14c).

In terms of grid parameters, Figures 2-15 and 16 show the mean porosity and standard deviation of porosity for the prior and posterior models for seven cases. Production data assimilation did not change the prior mean porosity significantly, but assimilating 4DAI maps resulted in changes in posterior porosity models, compared to the prior. The mean porosity for the WSR-PEM case is different from WSR-PUC and WSR-PFC (compare Figure 2-15c with Figures 2-15d and e), for 4DAI-Ideal map assimilation cases likewise. The different pattern in mean porosity between the PEM and PEM-Proxies cases is mostly seen in the north-west area of the reservoir (red arrows in Figure 2-15).

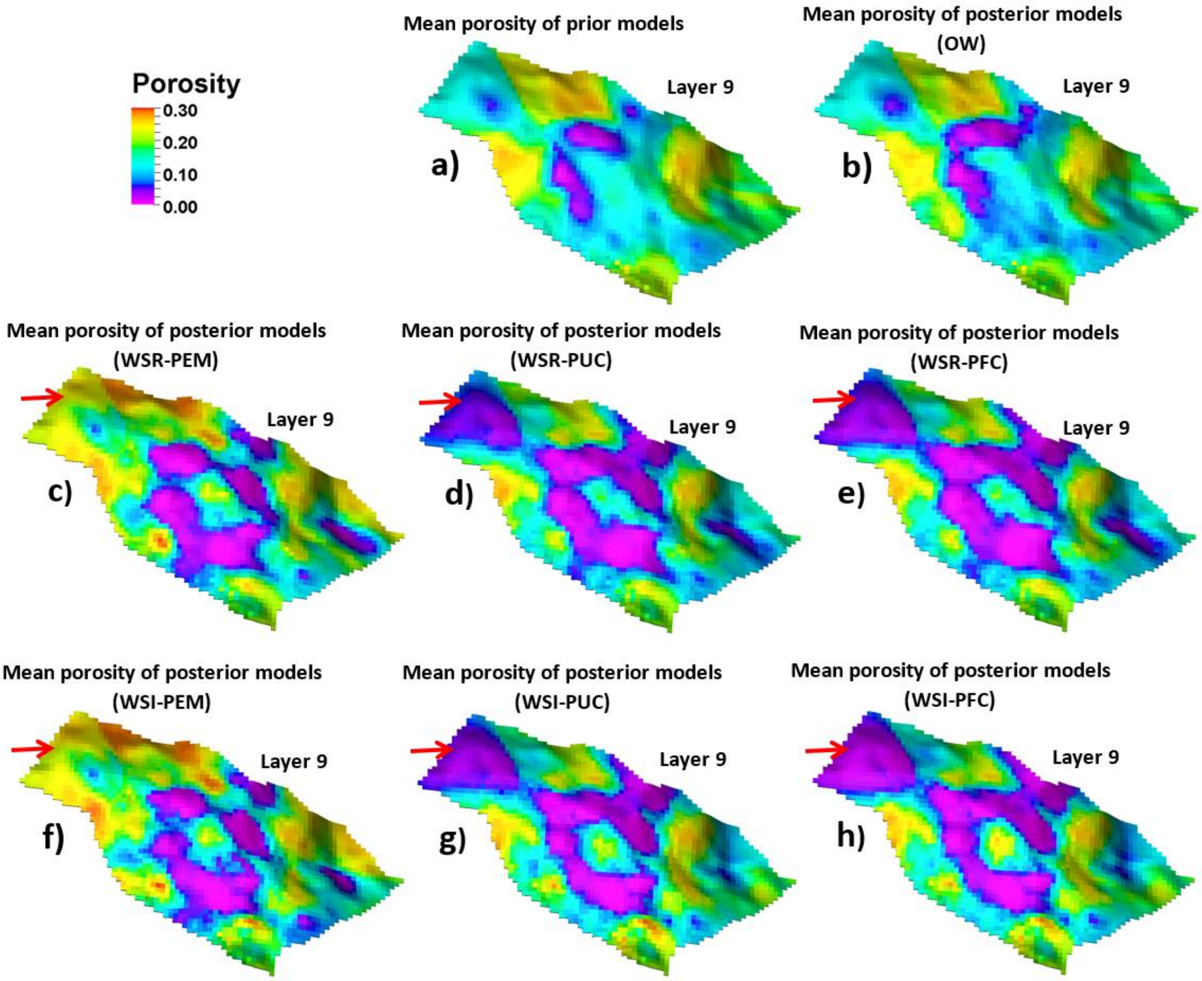

Figure 2-15: Mean porosity of prior and posterior models for different cases for layer 9.

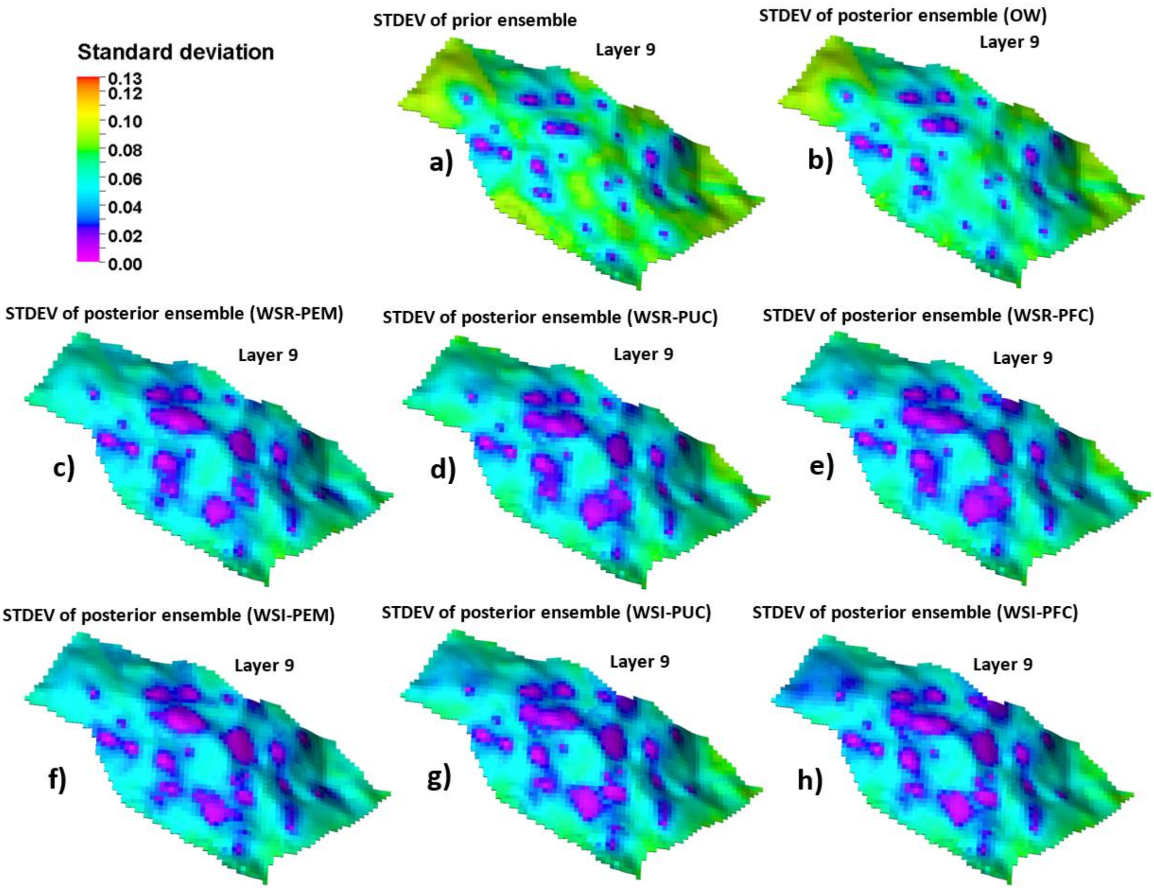

Figure 2-16: Standard deviation for porosity of prior and posterior models (layer 9).

2.7.5 Production forecast

Using a benchmark case study (controlled environment with known properties) gives us the ability to compare the production forecasts with the known future forecasts (after history data) for data assimilation cases. A total of 2618 days of production with a 4DAI map data were used for data assimilation (history data). For forecast, 3014 days from the end of history data were considered with forecast conditions and all the posterior models from different cases were run to analyze the production forecast. It is worth mentioning that adding 4DAI data to the assimilation provided better models for production forecast. Comparison of the results of Figure 2-18a with Figure 2-18b shows the impact of adding 4DAI information in cumulative field production. Figure 2-17 shows the oil rate forecast of producer (PROD005) for different cases. The PUC and PFC cases behave closely to the PEM cases for both 4DAI maps data assimilation. Although well-by-well analysis proved that the PEM-Proxies and PEM cases have similar behavior for production forecast, the cumulative field oil production showed that the PEM cases (Figures 2-18b, and e) provide more reliable models compared to PEM-Proxies cases (Figures

2-18c, d, f, and g). This difference is explained by the fact that PEM-Proxies models have utilized a straightforward equation and lack the heterogeneities of the PEM model; therefore, the overall cumulative field production shows different behaviours. Another explanation might be related to insufficient grid properties updates by the PEM-Proxies cases, which already are seen in uncertainty assessment in Figure 2-15 leading to differences in cumulative field production forecast.

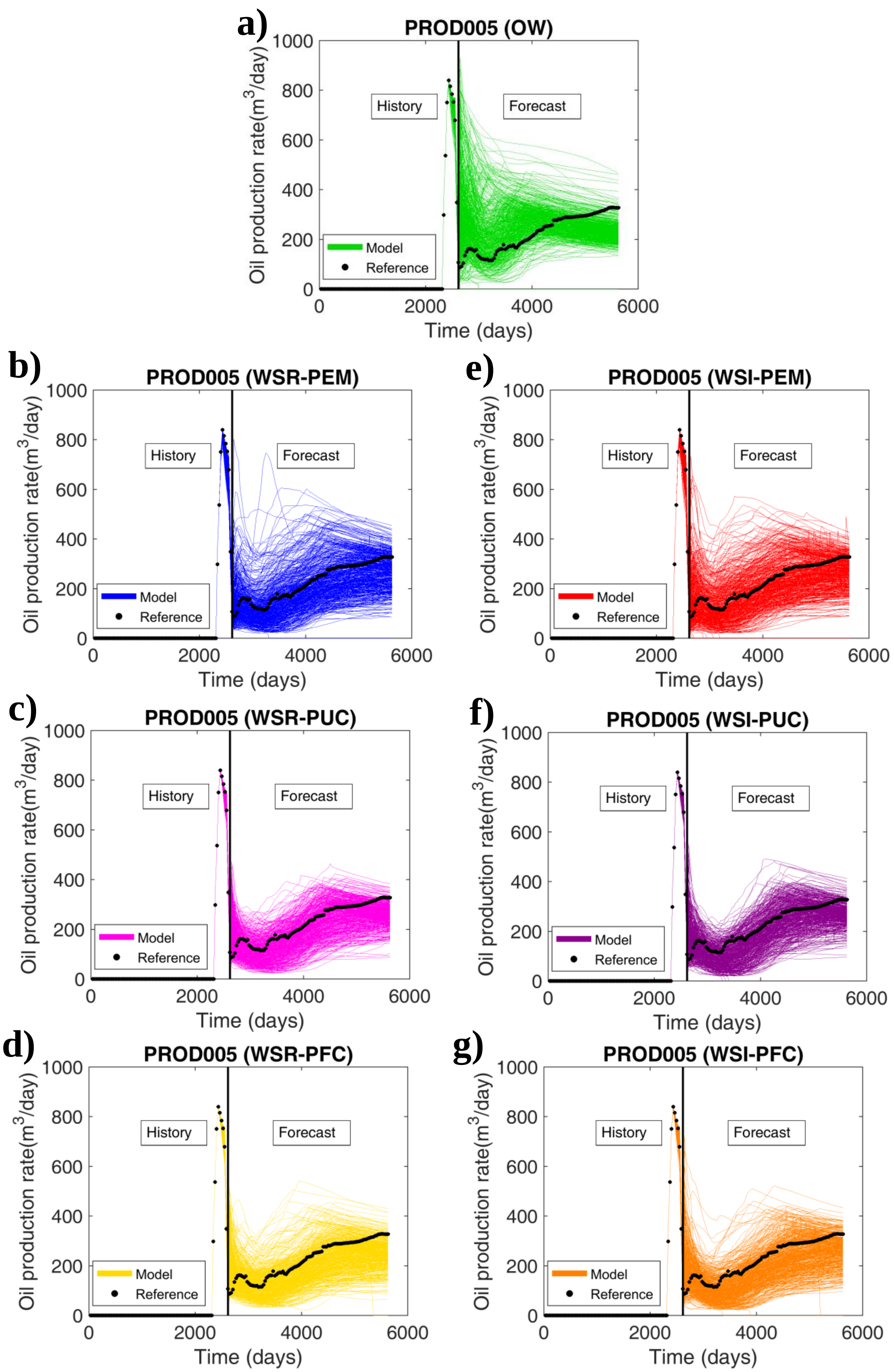

Figure 2-17: Production forecast of oil rates (PROD005). Black vertical line shows history-forecast transition and black dots indicate the actual responses from reference model.

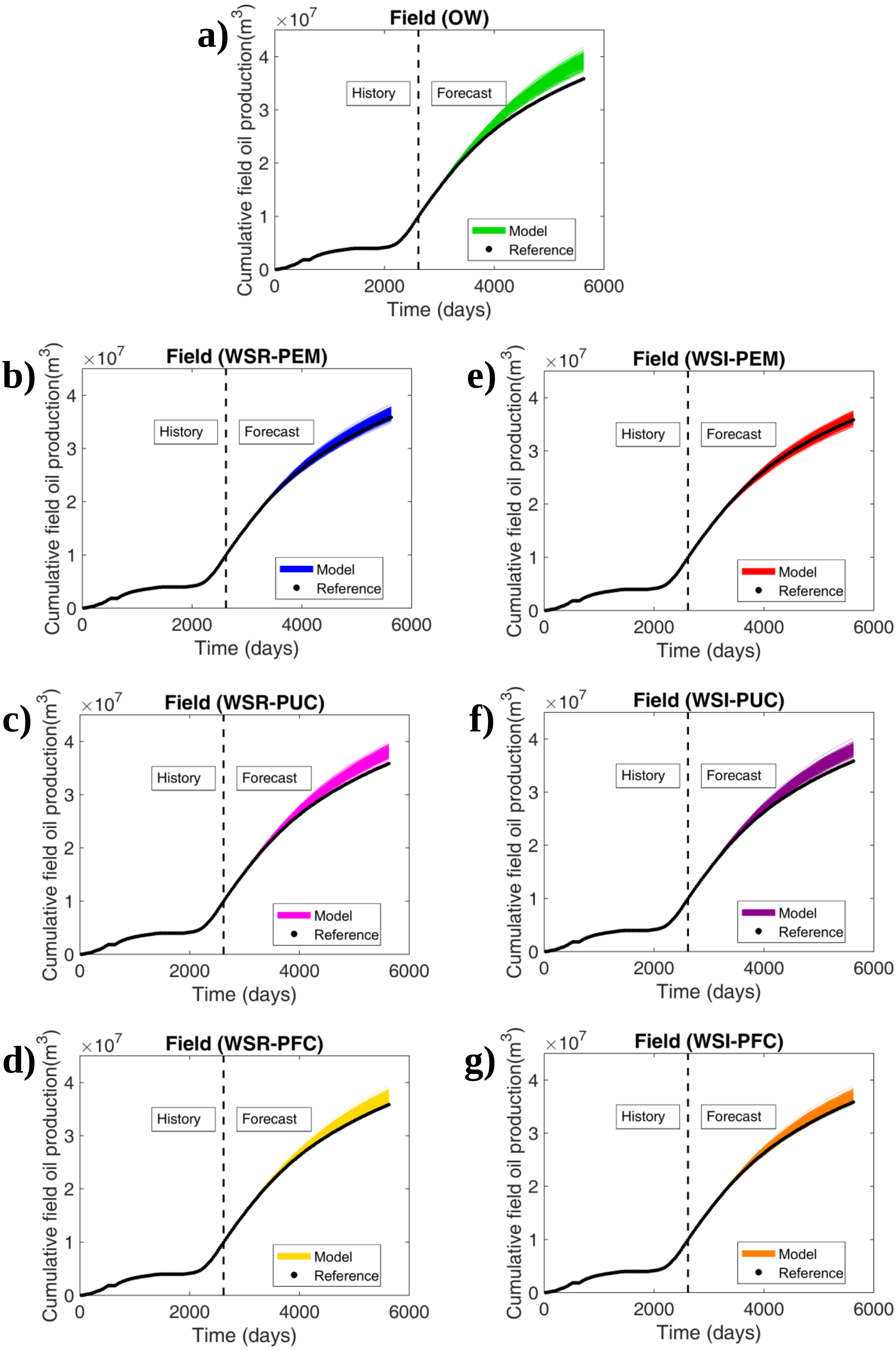

Figure 2-18: Cumulative field production forecast. The black dashed line represents the transition between history and forecast. Data assimilation cases are shown with their color codes while the actual responses from the reference model are given with black dots.

2.8 Discussion

Our research presents an alternative approach to replace the PEM implementation in data assimilation algorithms. PEM-Proxies are developed and coupled with the ES-MDA to assimilate both production and 4D seismic data. The results highlight that the PEM can be successfully replaced by a simpler rock/fluid model (PEM-Proxy model) for data assimilation in ensemble based algorithms. PEM-Proxy model is favored by petroleum engineers as it averts the interdisciplinary nature of the PEM construction using a computationally less expensive and a straightforward rock/fluid model. Given the uncomplicated nature of the PEM-Proxy equation, implementation of this approximation model proves to be efficient for data assimilation and satisfactory for production forecast.

It is important to analyze the efficiency of the 4D seismic forward modelling using the PEM-Proxies models in the context of the ES-MDA algorithm. The forward modelling is straightforward using the PUC and PFC models. A simulation model in the ensemble needs only water saturation and pressure changes to calculate the 4DAI. A similar forward modelling with the PEM, in addition to water saturation and pressure, needs porosity, fluid densities and their compressibility, the gas solubility ratio, and the oil formation volume for both times of baseline and monitor seismic surveys. Using the PEM-Proxy reduces the amount of data required to be extracted from simulation models, stored, and read to calculate the 4DAIs; therefore, it can have impact on the average turnaround time of the data assimilation especially when the PEM is an external program and the reservoir flow simulation is commercial software. For instance, in our application and for our reservoir, we needed 18 files to be extracted from every simulation model in the ensemble to generate 4DAI with the PEM. The number of files reduced to only 4 files using the PEM-Proxy models. Due to this reason and for our case, the data assimilation cycle time was 13 hours for PEM-Proxies implementations compared to 18 hours for the PEM application. The use of proxy reduced the data assimilation time in around 28% on average for our case study. However, this reduction is subjected to fluctuations in the network (cluster of computers) performance. It is also worth noting that the PEM implementation in the data assimilation could be optimized and performed faster, nonetheless this was not tried in our application.

In our study, 4D seismic data were assimilated using PEM-Proxies models and the results were compared with PEM implementation. 4D seismic data here helped us to have reliable models in terms of production forecast. Comparison of production forecast between OW case (Figure 2-18a) with WSR-PEM and WSI-PEM (Figures 2-18b and c respectively) highlights that those latter cases with 4D seismic data assimilation provide reliable models for production forecast. The implementation of PEM-Proxy models to assimilate both production and 4D seismic were analyzed based on different criteria.

The results showed that the PEM-Proxies implementation for data assimilation did not change the well objective functions behavior (Figure 2-7 and Figure 2-8) and even led to a higher number of matched models to the observed production data, which indicates efficient data assimilation (Figure 2-9). To explain this behavior, we should consider that the PEM-Proxy is a straightforward equation and does not consider uncertain parameters such as porosity; therefore, in data assimilation of both production and 4D seismic, production data in PEM-Proxy cases tends to update uncertain parameters in its favour. This matter is clear as we see lack of sufficient updates for porosity in PEM-Proxy cases (Figures 2-15d, e, g, and h) compared to the PEM cases (Figures 2-15c, and f). This tendency of production data to move updates to its favor is observed in production forecast and uncertainty quantification as well. In Figure 2-18, the forecast for PEM-Proxy cases (Figures 2-18c, d, f, and g) is relatively close to the OW forecast (Figure 2-18a). For uncertainty quantification, the pattern (not magnitude) of porosity updates in PEM-Proxy cases (Figures 2-15d, e, g, and h) resembles the OW case (Figure 2-15b) and also for uncertain global parameter in Figure 2-14d, the updates for the OW case is similar to WSR-PFC, WSR-PUC, WSI-PFC, and WSI-PUC cases. For the future research, we consider to put more weight on 4D seismic in data assimilation to ameliorate the effect caused by production data when PEM-Proxy models are implemented. The results also demonstrated that the PUC implementation in data assimilation led to better matched models for the 4D seismic data (Figure 2-11). This superiority is explained by degrees of freedom given to the uncertain coefficients in PUC model to minimize 4D seismic objective function. This suggests that PUC coefficients were updated alongside uncertain parameters in simulation model. It is unclear whether this behavior is suitable for data assimilation, since part of the updates is done on PEM-Proxy coefficients. It is important to note that, although the uncertainty quantification assessment was different for PEM and PEM-Proxies cases, proxy models describe uncertainties in rock/fluid modeling with only two coefficients. This advantage of using proxies is more noticeable when a certain PEM is hard to construct or not available (such as PEM in carbonate reservoirs); in these cases, PEM-Proxy implementation in data assimilation is more efficient compared to a PEM implementation.

Different behavior in uncertainty quantification was seen in grid parameter porosity and global uncertain parameter rock compressibility. For PEM-Proxies cases, unlike PEM, posterior values of rock compressibility shifted to higher values while the posterior mean porosity decreased, exhibiting inefficient updates in terms of porosity. This behavior in PEM-Proxies cases is explained by the pressure diffusivity equation, where the rock compressibility and the porosity render similar effects on the pressure disturbance caused by production and injection activities. For a pressure disturbance here, the decrease in porosity is compensated by the increase in rock compressibility values. The different behaviour compared to PEM cases is explained by PEM and PEM-Proxy equations. On the one hand, PEM equations depend on porosity, on the other PEM-Proxy linear equation disregards porosity influence on impedances calculated from water and pressure changes. The dependency to porosity in PEM implementation offers this uncertain parameter more chances to be updated through data assimilation iterations. Future work will consider a heterogeneity scaling factor for the proxies' equation. Adding a scaling factor to account for heterogeneity could help uncertainty quantification for the PEM-Proxy implementation in data assimilation and will possibly improve its forecast reliability. A lack of reservoir heterogeneity in the PEM-Proxy model may also be the reason why the PEM cases provided better cumulative field production forecast. Another reason might be related to the PEM model, as the petro-elastic model used here is ideal, with no uncertainty or error in its modelling (the same PEM used to generate the 4D seismic data, step 1 in Figure 2-4, was used in the data assimilation). PEM-Proxy models can also be calibrated directly to the well-log data and laboratory measurements as shown in Landrø (2001), and Salako et al. (2018) for the 4D seismic inversion. Lastly, the coefficient of determination of the linear regression for PEM-Proxy construction was high for our case study. For other cases where the linear fit is not good, attention should be given to the interpretation of the results.

2.9 Conclusions

Two versions of PEM-Proxies (PFC and PUC) were developed and coupled successfully with ES-MDA algorithm using different cases to assimilate production and 4D seismic data. Compared to the PEM, the PEM-Proxies are very straightforward models using linear regression of water saturation and pore pressure changes to calculate 4DAIs. We proposed a methodology to use the PEM-Proxy models in data assimilation ES-MDA algorithm. The methodology was applied to a synthetic case study and its robustness were analyzed based on past reservoir behaviour, uncertainty quantification, and reservoir production forecast. The results were promising and led to the following specific conclusions:

- The PEM-Proxies are successful in reproducing past reservoir behavior. Results showed that the PEM-Proxies cases provided similar conditioned models to reservoir history data, compared to the PEM cases.
- PUC and PFC models simplify the 4D seismic forward modeling in data assimilation algorithm. The results showed that a proper data assimilation was performed using PUC model in terms of history data match qualities. Being said that the suggestion is to use PUC model as an approximation for the PEM in 4D seismic data assimilation.
- In terms of reservoir future behavior (after history data), the PEM implementation in data assimilation provided more reliable forecast, compared to the PEM-Proxies cases. However, considering the straightforward equation of the PEM-Proxy (that has its own model error), the proxy behavior was satisfactory as the results were similar to the PEM cases.
- Unlike the PEM model, PEM-Proxy provides a straightforward and computationally less expensive model. Compared to the PEM, the PEM-Proxy models avoid demanding equations that require the definition/calibration of several rock and fluid parameters. Moreover, the PEM-Proxies require much less files to be exported from reservoir simulation models to compute the 4D seismic attributes to be matched during data assimilation. This strength of PEM-Proxy is very appealing for practical applications of data assimilation for petroleum engineers.

2.10 Acknowledgment

This work was carried out in association with the ongoing project registered under number 20372-9 ANP the "Development of integration between reservoir simulation and seismic 4D - Phase 2" (University of Campinas [UNICAMP]/Shell Brazil/ANP) funded by Shell Brasil Petróleo Ltda. under the ANP R&D levy the "Investment Commitment to Research and Development." The authors are grateful for the support of the Center of Petroleum Studies (CEPETRO-UNICAMP/Brazil), the Department of Energy (DE-FEM-UNICAMP/Brazil), the Research Group in Reservoir Simulation and Management (UNISIM-UNICAMP/Brazil) and the Energi Simulation. The authors also would like to thank Alexandre A. Emerick (from

Petrobras) for providing the EHM tool to UNISIM. In addition, special thanks to CGG, Schlumberger and CMG for software licenses.

3 Substituting petro-elastic model with a new proxy to assimilate time-lapse seismic data considering model errors

Authors: Danaei, S.; Silva Neto, G. M.; Schiozer, D. J.; Davolio, A.

Published in: Journal of petroleum science and engineering, 2021
(**https://doi.org/10.1016/j.petrol.2021.109970**)

3.1 Abstract

Dynamic data from oil and gas reservoirs (such as well-production or 4D seismic data) have been used often to reduce uncertainty in reservoir simulation models. These data are assimilated in the simulation models separately or jointly. Assimilation of 4D seismic data conventionally involves with a petro-elastic model (PEM) to transform outputs from the simulation models to elastic properties. The PEM is a set of different equations with uncertain parameters and its inclusion in assimilation algorithms calls on multidisciplinary teams of geoscientists and engineers. Moreover, PEM requires extraction of different outputs from the simulation models for the seismic forward model calculations. The extraction process can be costly for large-scale simulation models of giant reservoirs. This research presents a new petro-elastic proxy model (named DAI-Proxy) with a novel formulation to substitute the PEM and integrate 4D seismic data. DAI-Proxy relates time-lapse acoustic impedance to a summation of saturation and pressure changes with two coefficients which are functions of porosity. As the proxy is an approximation of the PEM, its application is affected by model error. We introduce two approaches to account for the proxy model error: (1) considering uncertain coefficients for the DAI-Proxy and (2) using fixed coefficients in the proxy while estimating model errors statistics from the prior ensemble of models. We incorporate these two approaches with a data assimilation algorithm to assimilate simultaneously 4D seismic and well-production data. A benchmark case is used with different cases of data assimilation to compare the DAI-Proxy and the PEM applications. Results show that data match quality for 4D seismic and well-production have similar responses for the PEM and DAI-Proxy implementations. In terms of production forecast, using fixed coefficients in the proxy with its model error treatment create a data assimilation framework comparable to the PEM case. Our results indicate that the traditional PEM application to integrate jointly 4D seismic and well-production data can be replaced with our new DAI-Proxy application. Given the degree of uncertainty in the PEM, related to the rock

and fluid models, our proxy provides similar results with fewer uncertain inputs. The proxy offers further advantage as it needs less outputs from the simulation models for seismic forward model calculations. In addition, it helps petroleum engineers to use a computationally less expensive model (light model) as a substitute for the PEM to assimilate 4D seismic data.

3.2 Introduction

Time-lapse seismic (4D seismic) is defined as seismic surveys repeated over a same reservoir in different time spans of its production history. 4D seismic data offer spatial information related to the dynamic reservoir changes, such as saturation, pore pressure, temperature, and compaction changes. Interpretation of these data is divided into two broad schemes of qualitative and quantitative interpretations. Qualitative interpretation seeks to display different dynamic changes and explain the causal effects of each 4D seismic signal (Danaei et al., 2018; Maleki et al., 2018a). Quantitative interpretation estimates production related changes such as saturation-pressure changes (Landrø, 2002; Lumley et al., 2003; MacBeth et al., 2006). Alongside interpretation, 4D seismic data could be used together with the well-production data to update reservoir simulation models and improve the reliability of model forecasts. In this scheme, 4D seismic and well-production data could be incorporated through data assimilation algorithms to constrain simulation models and allow better forecasts (Huang et al., 1997; Mikkelsen et al., 2008).

Simulation models have different uncertainties in subsurface rock properties and fluid characteristics. Available well-production data (scarce in space) and 3D or 4D seismic data (abundant in space) could be assimilated to update these models (Chassagne and Aranha, 2020). Using ensemble-based data assimilation algorithms, multiple simulation models are updated constantly and reservoir past behaviors are reproduced within a tolerance of field observed data (Alfonzo and Oliver, 2019). In these algorithms, 4D seismic data integration remains an open challenge due to the different nature of the seismic data and the simulation outputs (Davolio and Schiozer, 2019; Lorentzen et al., 2020; Luo et al., 2018). Firstly, 4D seismic data provide many observed data points to be assimilated and secondly, we should take the observed data and the simulation outputs to a common domain and scale for proper data assimilation. In terms of common scale, 4D seismic data are brought into the simulation model scale, or vice versa. There are three ways to make the simulation outputs and 4D seismic data be in a common domain. The first way is the time-lapse amplitude (or its attributes) domain. Here, the observed 4D seismic data is already in that domain and the simulation outputs are forward modeled to meet the seismic data. The second way is the time-lapse elastic attributes domain. Here, 4D seismic data are inverted to elastic properties to meet the simulation outputs which are forward modeled to those properties. The last way is the saturation-pressure changes domain. The simulation outputs are already in that domain while the observed seismic data are inverted to fluid saturations and pore-pressure changes to meet the simulation outputs. It is worth mentioning that we require a petro-elastic model (PEM) conventionally for each domain where 4D seismic data are assimilated.

PEMs are sets of different equations that relate reservoir static and dynamic properties to their corresponding elastic features. The main problem with the PEMs is uncertainty, both in the models (model uncertainty) and the input parameters (variable uncertainty). Limitations in the rock-physical models to represent the earth's actual elastic properties and variability in the input parameters render the PEMs uncertain with not unique responses. As a result, various combinations of input parameters yield possible true estimates of the elastic properties. In addition to the uncertainty, calibrating the rock and fluid models to the field data remains a challenge (Amini and Alvarez, 2014; Silva Neto et al., 2020). The PEMs likewise present problems in simultaneous assimilation of 4D seismic and well-production data. They call for an interdisciplinary teamwork of rock physicists and petroleum engineers to build and apply them in the data assimilation algorithms. Moreover, PEMs require a great variety of grid variables to be obtained from the simulation models for seismic forward model calculations. The extraction of the grid variables could be costly in some cases, especially for large-scale simulation models of giant reservoirs or when large sets of simulation models are chosen for the data assimilation algorithms. Based on these problems, there are growing appeals for methods to avert the PEMs (for example, binary image tools) or to replace them in 4D seismic applications with proxy models (PEM-Proxy). The emergence of the PEM-Proxy is a noteworthy event, much to the delight of the rock physicists and petroleum engineers in their applications of 4D seismic data. In general, the PEMs are different rock and fluid models with full mathematical equations and all aforementioned complexities while the PEM-Proxy models are computationally less expensive (light models), which represent the PEMs lightly in 4D seismic applications.

A closer look at the literature reveals that few studies have dispensed the PEMs for joint well-production and 4D seismic data assimilation. There are some alternative ways to avert PEMs or substitute them in the joint data assimilation scheme. One possible way is to use a proxy model in the form of an equation (linear or non-linear) that links dynamic changes in the reservoir (such as saturation-pressure changes) to time-lapse change in seismic attributes. In this context, MacBeth et al. (2016) proposed a formula (a proxy equation) to circumvent the PEM plus seismic modeling for the 4D seismic history matching. Geng et al. (2017) presented its application and discussed the importance of reservoir properties such as porosity for proxy construction. Danaei et al. (2020) showed the application of the PEM-Proxy for joint 4D seismic and well-production data assimilation in ensemble-based algorithms. In Danaei et al. (2020), they used a PEM-Proxy which linked time-lapse difference of acoustic impedance (4DAI) to a linear summation of saturation and pressure changes with two coefficients. Although they did not consider porosity in the linear formulation, its importance was mentioned, which may affect the assimilation results in terms of production forecast and uncertainty assessment. Moreover, the PEM-Proxy is an approximation of the PEM and its application is therefore affected by model error. To our knowledge, neither of the cited studies considered the impact of the proxy model error. Considering its effect in the data assimilation process could avoid unnecessary updates for the uncertain parameters and improve the production forecast, so we should tailor an approach to treat the impact of the proxy model error.

For this research, the question is twofold: how to formulate the PEM-Proxy in a way that includes porosity and how to address the proxy model error. Here, we propose a new PEM-Proxy (we call it DAI-Proxy) by considering porosity in its formulation. The DAI-Proxy relates 4DAI to a summation of saturation and pressure changes with two coefficients, which are functions of porosity; the proxy model is then coupled with the Ensemble Smoother with Multiple Data Assimilation (ES-MDA) algorithm to assimilate simultaneously well-production and 4DAI data. It is also of special interest to account for the proxy model error in the data assimilation; therefore, the model error is included in the ES-MDA algorithm using different approaches and its effect reduced during the assimilation procedure. To evaluate the DAI-Proxy implementation in the ES-MDA, different cases of data assimilation were organized and compared using the DAI-Proxy and the PEM implementations. A benchmark case (UNISIM-I-H) was used to apply different cases of data assimilation. The dataset of this controlled case study is driven from a real Brazilian offshore field and has all the complexities and characteristics of an actual field (Avansi and Schiozer, 2015). These comparative analyses on a controlled case study enabled us to assess the behavior of the proxy application not only for reservoir past behavior (observed data match quality) but also for its future behavior (forecast capability) and uncertainty reduction assessment.

3.3 Objectives and scope

Current research aims to substitute the PEM with a light model when 4D seismic and well-production data are used jointly in the data assimilation algorithms. The specific objectives are:

1- To formulate and develop the DAI-Proxy

2- To characterize the proxy model error to include it in the data assimilation procedure

3- To couple the DAI-Proxy with the ES-MDA while considering the proxy model error

Finally, a comparison is performed between the DAI-Proxy and the PEM implementations based on different criteria such as history data match quality, uncertainty reduction assessment, and production forecast capability.

3.4 Theoretical background and literature review

3.4.1 Assimilation of observed data with ensemble-based algorithms

Ensemble-based methods could be considered convenient alternatives to assimilate well-production and 4D seismic data (Emerick, 2016; Luo et al., 2015). These algorithms integrate available observed data to update reservoir models and offer an ensemble of posterior models. Within this framework, the Ensemble Smoother with MDA (Multiple Data Assimilation) or ES-MDA was suggested for data assimilation (Emerick and Reynolds, 2013). As it is self-evident from its name, the ES-MDA has two main characteristics: (1) it uses Ensemble Smoother (ES) algorithm (Van Leeuwen and Evensen, 1996) to assimilate observed data, and (2) it assimilates observed data through several iterations (multiple times). Using the ES algorithm enables simultaneous assimilation of all observed data while the iterative procedure improves data match quality. The main difference of the ES-MDA from the ES is an inflation factor in its analysis equation (Emerick and Reynolds, 2013). This inflation factor reduces model updates in each data assimilation iteration. In this research, ES-MDA is used to simultaneously assimilate 4D seismic and well-production data. Further information about the ES-MDA is in Appendix A. Danaei et al. (2020), Emerick (2016), and Silva Neto et al. (2020) present some examples of its applications.

3.4.2 Data match quality

There are various equations to assess the quality of simulation models and compare different models (Bertolini and Schiozer, 2011; Heidaryan, 2019). In this research, the model quality is measured based on a Normalized Quadratic Distance with Sign (NQDS) equation (Avansi et al., 2016; Danaei et al., 2020; Davolio and Schiozer, 2018). For each observed data (for example, water rate of a well or 4D seismic data), this equation shows the accuracy of the model's simulated outputs versus the observation. The NQDS equation has two main parts; the normalized quadratic deviation part and the sign part.

$$NQDS_l = \frac{LD_l}{|LD_l|} NQD_l \tag{1}$$

The normalized quadratic deviation (NQD_l) calculates the discrepancy between simulated values and the observed data that indicates the deviation of each model. The sign part comprises a linear deviation (LD_l) divided by its absolute value which shows the deviation direction with a positive or negative sign. If the model values exceed the observed data then the sign is positive and the negative sign is assigned when the model values fall short of reproducing the observation. It should be pointed out that Equation (1) and the following equations are valid for each simulation model (j) in the ensemble.

$$NQD_l = \frac{QD_l}{AQD_l} \tag{2}$$

$$QD_l = \left(\boldsymbol{d}_l^f - \boldsymbol{d}_{obs_l}\right)^T * \left(\boldsymbol{d}_l^f - \boldsymbol{d}_{obs_l}\right) \tag{3}$$

$$AQD_l = \left(Tol_l * \boldsymbol{d}_{obs_l} + \mathrm{C}_l * \mathbf{1}_{N_{obs_l}}\right)^T * \left(Tol_l * \boldsymbol{d}_{obs_l} + \mathrm{C}_l * \mathbf{1}_{N_{obs_l}}\right) \tag{4}$$

$$LD_l = \left(\boldsymbol{d}_l^f - \boldsymbol{d}_{obs_l}\right)^T * \mathbf{1}_{N_{oobs_l}} \tag{5}$$

In the above equations, l indexes each well or 4D seismic objective function. The vector of observed and simulated data are $\boldsymbol{d}_{obs_l}$ and $\boldsymbol{d}_l^f$ respectively. $\mathbf{1}_{N_{obs_l}}$ is a vector of all ones with N_{obs} size for each objective function (l), C_l is a constant to prevent division by zero (for example, zero can be a 4D seismic observed value), and Tol_l defines a tolerance which is a percentage of observed data. The tolerance value is chosen based on the uncertainty in the observed data. Its value is taken by an engineering judgment on the reliability of each observed data. The NQDS equals to zero shows that the observed data is reproduced exactly by the model's simulated values. The NQDS indicator grows in magnitude as the simulated data becomes distant from the observed data.

3.4.3 Proxy for petro-elastic model (PEM-Proxy)

This section is divided into two parts to first mention the PEM-Proxy models used in the literature, to invert for saturation-pressure change from 4D seismic data, and secondly the proxy models which are used as a seismic forward model for joint assimilation of well-production and 4D seismic data.

3.4.3.1 PEM-Proxy in 4D seismic inversion of saturation-pressure changes

The first application of the PEM-Proxy for 4D inversion of saturation-pressure changes was presented in Landrø (2001). Time lapse changes in reservoir velocities were considered as linear summation of saturation and pressure changes. Here, density change was approximated linearly only with saturation change. Since then, there have been modifications to the PEM-Proxy in Landrø (2001). Meadows (2001) modified it by considering second-order approximation for saturation change to relate it to the changes in velocities. Other modifications were reported in Trani et al. (2011) and Bhakta and Landrø (2014). In another attempt, Angelov et al. (2004) presented the PEM-Proxy where the time lapse changes in elastic impedances were related linearly to the saturation change and with logarithmic function to the pressure change. In all these studies, the regression coefficients of the linear equations in the PEM-Proxy were considered constant for the entire reservoir (Lang and Grana, 2019). To include reservoir heterogeneity, Lang and Grana (2019) presented the PEM-Proxy in which its coefficients were functions of porosity, initial water saturation, and initial pore pressure.

Using direct link between saturation-pressure change and 4D seismic attributes also averts the PEM plus seismic modeling in the 4D seismic inversion algorithms. This direct link was shown in Floricich et al. (2005) and a year later in MacBeth et al. (2006) to make a connection between 4D seismic attributes and saturation-pressure changes:

$$\frac{\Delta A(x,y)}{\overline{A_b}} = C_s \frac{\Delta S_o(x,y)}{\overline{S_{oi}}} + C_p \frac{\Delta P(x,y)}{\overline{P_i}} \qquad (6)$$

Where, C_s and C_p are constants, $\overline{S_{oi}}$, and $\overline{P_i}$ indicate the average field oil saturation and pressure respectively, and $\overline{A_b}$ is the pore-volume weighted average baseline seismic response. For interpretation of 4D seismic data, Alvarez and MacBeth (2014) used the same linear summation and also a similar equation was discussed in Falahat et al. (2013). In these studies, insightful investigations are provided on how the PEM parameters manifest themselves in the weights of the linear summation. More recently Corte et al. (2020), Weinzierl and Wiese (2020), and Xue et al. (2019) showed the application of machine learning algorithms for the 4D seismic inversion of dynamic reservoir changes. These algorithms are considered as a proxy for the PEM and seismic modeling, in which dynamic reservoir changes are linked directly to seismic properties. One must keep in mind that, in these studies, proxy models are used to invert saturation-pressure changes from 4D seismic data. Basically, their uncertain model parameters are saturation-pressure changes. Proxy models can also be used as seismic forward model to simultaneously assimilate 4D seismic and well-production data. This joint assimilation is used to invert uncertain model parameters, such as porosity, permeability, rock compressibility and related reservoir properties.

3.4.3.2 PEM-Proxy in joint assimilation of well-production and 4D seismic data

In this section, we consider the ways that the PEM-Proxy can be used beyond the 4D seismic inversion of saturation-pressure changes and interpretation. Proxy models can also be used to assimilate 4D seismic and available field data (such as well-production data) to update reservoir simulation models. A binary map of the 4D seismic signal is one way to circumvent the PEM plus seismic modeling in joint well-production and 4D seismic data assimilation (Davolio and Schiozer, 2018a; Jin et al., 2011; Obidegwu et al., 2017; Tillier et al., 2013). One must note that binary maps do not have information related to the couple (saturation-pressure changes) effects to update the simulation models. Geng et al. (2017) and MacBeth et al. (2016) proposed using a proxy to substitute the PEM and seismic modeling:

$$\Delta A(x,y) = \left(a_1\Delta P + a_2\Delta S_w + a_3\Delta S_g + a_4\Delta P^2 + a_5\Delta {S_w}^2 + a_6\Delta {S_g}^2 + a_7\Delta P\Delta S_w + a_8\Delta P\Delta S_g + a_9\Delta S_g\Delta S_w\right) * A_0(x,y) \quad (7)$$

Where, $\Delta A(x,y)$ stands for the time-lapse seismic data, and $A_0(x,y)$ is the baseline seismic response. ΔS_w, and ΔS_g represent changes in saturation for water and gas. ΔP defines pressure change while a_{1-9} are the proxy coefficients. Danaei et al. (2020) presented a PEM-Proxy to simultaneously assimilate 4D seismic and well-production data in impedance domain. The proxy they employed relates 4DAI to saturation-pressure changes (ΔS_w, ΔP) with two coefficients (a, and b) using:

$$4DAI = a\Delta S_w + b\Delta P \quad (8)$$

Porosity is considered constant throughout the reservoir in this equation. Although using this equation provided satisfactory data assimilation results, model parameters updating and production forecasts might benefit by adding porosity to this equation (Danaei et al., 2020a). This research is an extension of Danaei et al. (2020) where we propose DAI-Proxy to include porosity in Equation (8). We also offer a way to consider the proxy model error in the data assimilation procedure. We emphasize that, compared to Equation (7), which has the baseline seismic attribute, porosity is easier to be included in the data assimilation algorithm. Porosity can be extracted from the simulation outputs and with porosity inclusion, we avoid the forward model to calculate the baseline seismic attribute in Equation (7).

3.5 Methodology

The methodology is divided into three parts: The first describes the DAI-Proxy formulation, the second explains the proxy model error and approaches to treat it, and the third couples the DAI-Proxy and its model error with the ES-MDA algorithm.

3.5.1 How to formulate the DAI-Proxy

As one might expect, the PEM-Proxy should represent the rock/fluid models in the PEM. While Equation (8) is dominated by the dynamic changes of an oil-water system, the PEM has many other parameters, such as porosity. To include porosity in Equation (8), the 4DAI for an oil-water system is considered as two independent effects of saturation and pressure changes which are weighted by porosity functions. Note that the pressure here is the reservoir pressure and its time-lapse change. The DAI-Proxy is written as:

$$4DAI = 4DAI_{(\Delta S_w,0)} + 4DAI_{(0,\Delta P)} = f_s(\varphi)\Delta S_w + f_p(\varphi)\Delta P \qquad (9)$$

Here, $4DAI$ defines time-lapse acoustic impedance, $4DAI_{(\Delta S_w,0)}$, and $4DAI_{(0,\Delta P)}$ are the contributions of each individual term water saturation (ΔS_w) and pressure (ΔP) changes. The coefficients of the saturation-pressure change, $f_s(\varphi)$ and $f_p(\varphi)$ are functions of porosity. These coefficients should reflect the rock/fluid models which they represent therefore, the water saturation change coefficient ($f_s(\varphi)$) is positive. It means that the replacement of oil by water in the oil-water system increases the $4DAI$. The pressure change coefficient ($f_p(\varphi)$) is negative, which shows an increase in the pressure ($\Delta P > 0$) has a softening effect that decreases the $4DAI$. Equation (9) carries important quantities of each 4D seismic signal, which are the dynamic reservoir changes and porosity. The linear decomposition of 4D seismic attribute (e.g. $4DAI$) to the independent effects of saturation-pressure changes (e.g. $4DAI_{(\Delta S_w,0)}$, and $4DAI_{(0,\Delta P)}$) was proposed by Falahat et al. (2013) and also reported in Salako et al. (2018). It is important to mention that in Falahat et al. (2013), saturation-pressure changes were scaled by the thickness or pore-volume. However, our DAI-Proxy is explicitly designed to contain porosity in its coefficients with new formulations. In DAI-Proxy, the focus is primarily on porosity as this variable is an uncertain model parameter for history matching. There are four steps to estimate the coefficients and develop the DAI-Proxy, as shown in Figure 3-1.

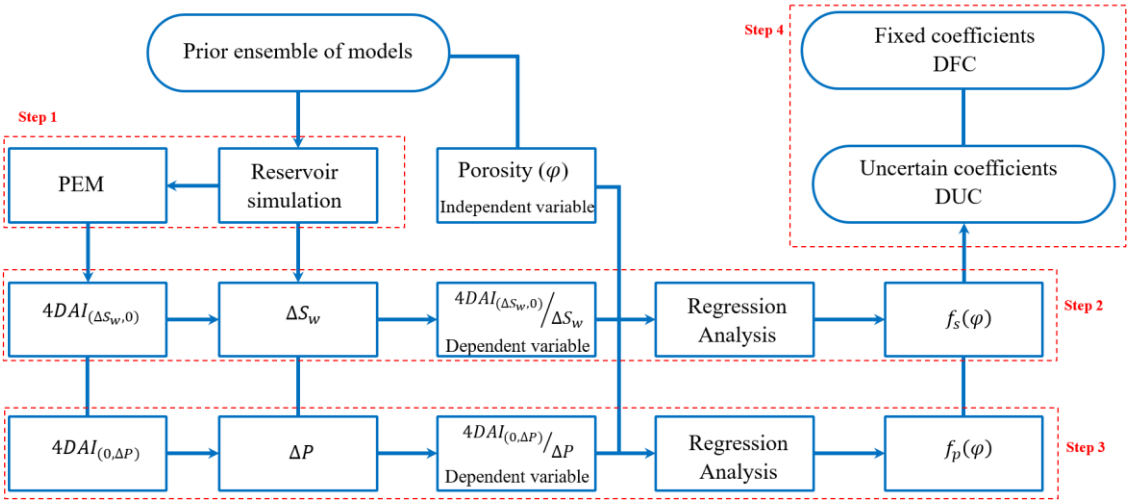

Figure 3-1: Steps to develop the DAI-Proxy model.

Step 1: Saturation-pressure changes (ΔS_w and ΔP) are calculated for the prior models in the ensemble through reservoir simulation. Considering constant pressure, the outputs of each simulation model are transformed to the $4DAI_{(\Delta S_w,0)}$ through petro-elastic modelling (more details about the PEM are provided in Appendix B). In the same way, $4DAI_{(0,\Delta P)}$ is calculated when water saturation is constant. This assumption is based on the total independent effects of pressure-saturation changes on the $4DAI$. However, the impact of pressure change on the water is different from oil. Therefore, saturation and pressure change terms are not completely independent. This difference causes uncertainty in our linear decomposition of saturation-pressure change terms. We could mitigate this uncertainty by adding a cross-term to the equation, thus increasing proxy complexity, or accounting for proxy model error (section 4.2). It is noteworthy that for proxy calibration, we use the petro-elastic model. Therefore, when the proxy is developed, the joint assimilation of well-production and 4D seismic data is done by the proxy model.

Step 2: This step aims to find the porosity function ($f_s(\varphi)$) for the water saturation change term (ΔS_w); therefore, Equation (9) is reduced to:

$$4DAI_{(\Delta S_w,0)} = f_s(\varphi)\Delta S_w \tag{10}$$

Regression analysis shows the relationships between the parameters in Equation (10). To make the regression analysis easier, $4DAI_{(\Delta S_w,0)}$ is divided by ΔS_w (both calculated in the previous step) to compute the dependent variable $4DAI_{(\Delta S_w,0)}/\Delta S_w$ while the porosity (φ) is the independent variable. The regression equation ($f_s(\varphi)$) is in terms of the porosity and its coefficients quantify the relationship between the dependent and independent variables. Based on our numerical experiments, the model which best explains this relationship is:

$$f_s(\varphi) = a_s\left(1 - \exp\left(-c_s(\varphi)\right)\right) \tag{11}$$

In this equation, $f_s(\varphi)$ is the porosity function for the saturation change term, φ is the porosity, and a_s, c_s are the coefficients. Note that this function is an empirical equation based on our numerical experiments. The equation properly fits rock physics models as shown in the result section. However, one can apply the same method with a different equation. For instance, Lang and Grana (2019) proposed a quadratic equation for porosity function in their analysis.

Step 3: The aim of this step is to find $f_p(\varphi)$, therefore, Equation (9) is reduced to:

$$4DAI_{(0,\Delta P)} = f_p(\varphi)\Delta P \tag{12}$$

Like the previous step, the regression analysis shows how the parameters in this equation are related. For the ease of regression analysis, $4DAI_{(0,\Delta P)}$ is divided to ΔP for each prior model to determine the dependent variable ${4DAI_{(0,\Delta P)}}/{\Delta P}$. The regression analysis is performed for each model considering porosity (φ) as an independent variable. The regression equation shows the relationship between the dependent and independent variables and generates $f_p(\varphi)$. The best fit model according to our numerical experiments is:

$$f_p(\varphi) = \left(a_p - b_p(\varphi)\right)\left(1 - \exp\left(-c_p(\varphi)\right)\right) \tag{13}$$

It is worth noting that the function (13) is an empirical function. The linear part in the equation is reported in the literature, which adds its own insights to the existing knowledge in Alvarez and MacBeth (2014), and Dvorkin et al. (1996) on how porosity affects the contribution of each dynamic change term in the linear summation.

Step 4: Two versions of the DAI-Proxy are developed considering fixed and uncertain coefficients in Equation (9). One, with the fixed coefficients, is named DFC and the other DUC with uncertain coefficients. For each coefficient in the DAI-Proxy, we estimate the mean, variance, minimum, maximum, and the standard deviation values. For the DUC model, uncertain coefficients are set based on their statistical parameters. In the DFC model, the coefficients are fixed with the mean values.

3.5.2 Proxy model error

The proxy model error occurs as the proxy equation approximates the PEM. The error is captured by the difference between the 4DAIs generated using the DAI-Proxy and the PEM models. The error treatment enables us to reduce its effects and improve the model updates in each iteration of the data assimilation. Two approaches are adopted for the proxy model error in this research. The first considers the uncertain coefficients in the DUC model as a way to treat the proxy model error. The uncertain coefficients increase the dimension of the problem and weaken the updates for the model parameters (Silva Neto et al., 2020a). The second uses the DFC model and estimates the model error statistics. For this approach, the model error is sampled using the prior ensemble of models:

$$\varepsilon_j^m = d_j^{DFC} - d_j^{PEM} \tag{14}$$

Where, j shows the model number in the prior ensemble, ε_j^m defines the proxy model error, d_j^{DFC} is the 4DAI results from the DFC model, and d_j^{PEM} represents the results from the PEM model. The statistics are generated from the samples including the mean model error and its covariance. The mean error removes bias and the covariance reduces the importance of data in which the variance of the model error is large (Stephen et al., 2009). This approach of the error treatment is fed into the data assimilation ES-MDA algorithm (Appendix A). To compensate for the bias, the mean model error is added to the observed data and the observed data error covariance matrix ($\boldsymbol{C}_D$ in Equation [A.1] in Appendix A) is inflated by the model error covariance matrix. A very similar approach to treat the model error is presented in Stephen (2007) and Stephen et al. (2009).

3.5.3 DAI-Proxies incorporation in the ES-MDA

The DFC and DUC models and their model error treatment approaches are incorporated into the data assimilation algorithm ES-MDA (Figure 3-2). The DFC model error statistics are calculated for the prior ensemble of models and the model error statistics are not updated through data assimilation iterations.

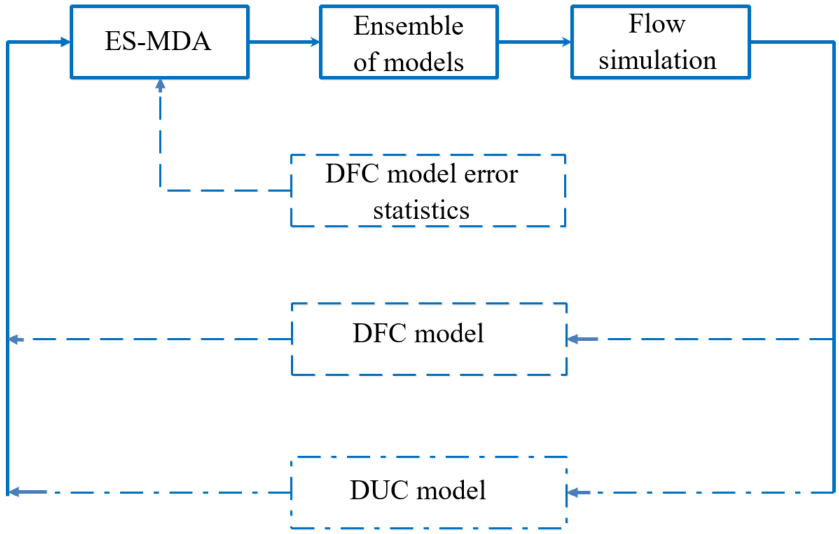

Figure 3-2: Assimilation of observed data using the ES-MDA with the DAI-Proxies and their model error treatment approaches.

Various assimilation cases are organized to integrate the observed data with the ES-MDA. We set side by side and analyze assimilation results with the DAI-Proxies and the PEM models. The criteria for the analysis are the past behavior of the reservoir (observed data match quality), its future behavior (forecast capability), and uncertainty assessment.

3.6 Application

We applied the proposed methodology to a synthetic dataset (UNISIM-I-H) to evaluate the performance of the DAI-Proxies. UNISIM-I-H is an open-access synthetic dataset as described in Avansi and Schiozer (2015) and Maschio et al. (2013). This dataset is well-suited for our study as it is driven from an offshore field in Brazil and has all the characteristics and complications of a real case. The dataset has a high resolution model with 3,408,633 active cells called UNISIM-I-R acts as a reference model. Having a reference case is beneficial as the DAI-Proxy application in the ES-MDA can be evaluated not only for the reservoir's past behavior but also for forecast capability. From the reference model, a set of simulation models was built at coarse scale with 81*58*20 grid cells and 36739 active cells. There are 25 wells, which include 14 producers and 11 injectors, as shown in Figure 3-3a.

Uncertain model parameters are divided into (1) grid parameter which has a value for each grid of the simulation model and include petrophysical properties such as porosity or absolute permeability and (2) scalar parameter which is defined as a particular value for all grids of the simulation model such as rock compressibility or relative permeability. Well indexes in the location of all wells are considered as local uncertain parameters. For our application, 500 petrophysical models in coarse scale were combined with scalar and local uncertain parameters to generate 500 simulation models (size of the ensemble).

A total of 2618 days of observed well-production data were used in the assimilation procedure. In addition to well-production data, an observed 4DAI map (Figure 3-3b) was used as 4D seismic observation. The 4DAI map was a time-lapse acoustic impedance of the monitor (post-production of 2618 days) minus the baseline (pre-production at time=0). This map was generated using the reference model (as mentioned UNISIM-I-R) through petro-elastic modeling. Firstly, the reference model was run at the fine scale to compute reservoir dynamic properties. Then, simulation outputs were transformed into acoustic impedance for the baseline and monitor times through petro-elastic modeling. Finally, the 4DAI map was obtained with the subtraction of the monitor acoustic impedance from the baseline impedance. A description of the petro-elastic model used here is provided in Appendix B and more information about 4D seismic data set can be found in Souza et al. (2018) and Davolio and Schiozer (2019). It is important to note that we considered an uncorrelated Gaussian noise to perturb the 4DAI map. Assimilation of observed data (well-production and 4DAI data) was done with the ES-MDA through four iterations. To have a fair comparison between different cases, all configurations in the data assimilation were set the same (for example, same prior models, number of iterations, and inflation factor).

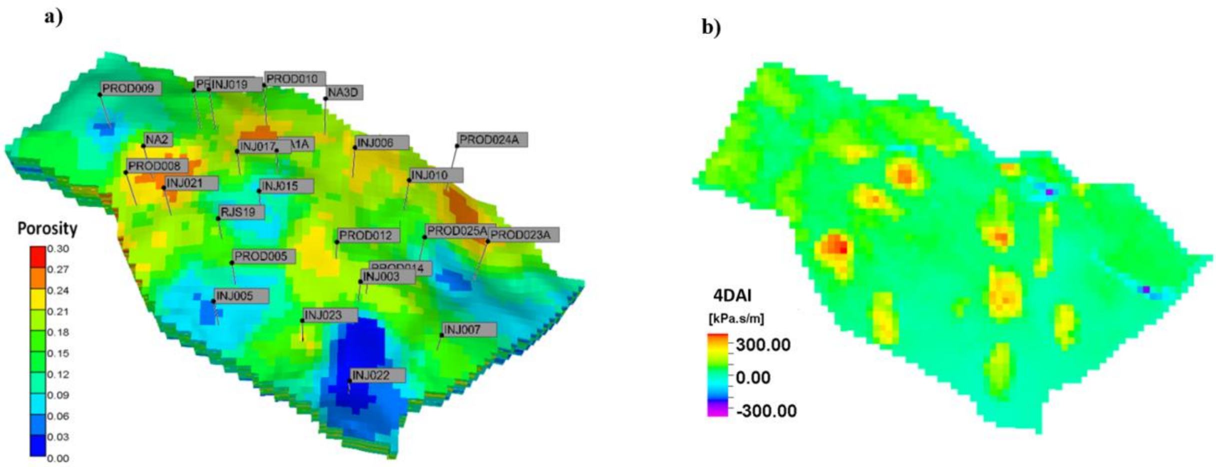

Figure 3-3: UNISIM-I-H which is a synthetic dataset. (a) petrophysical property porosity of a simulation model randomly selected from the ensemble and (b) map of 4D difference of acoustic impedance (4DAI) used in joint well-production and 4D seismic data assimilation

3.6.1 Different cases for assimilation of observed data

We organized five cases for assimilation of observed data to investigate the performance of the DAI-Proxies in the ES-MDA. In a comparative study, proxy performance was compared with the PEM application. There are three seismic forward models (PEM, DUC, and DFC) and two types of observed data (well-production and 4D seismic). Combinations of the seismic forward models and observed data generated these cases. Table 3-1 summarizes different data assimilation cases for this research. For instance, the WS-DFCE (case 4) means that the production data (W) and the 4DAI data (S) were used with the DFC model (DFC) considering its model error treatment approach (E) in the data assimilation process. A similar case without considering the model error treatment approach was named WS-DFC (case 5). The joint assimilation of production data (W) and the 4DAI data (S) with the PEM model (PEM) was named the WS-PEM case (case 2). This joint assimilation with the DUC model (DUC) generated the WS-DUC case (case 3). Finally, a case was organized to only assimilate well-production data and it was named the OW case (case 1).

It is worth noting that the cases 1, 2, 3, and 4 were compared based on different criteria to analyze their performance in the ES-MDA. The only purpose of the case 5 was to show the impacts of the proxy model error on the data assimilation using the DFC model. Therefore, this case was compared with the WS-DFCE case (case 4). By this comparison, we show how effective the model error treatment approach is for the WS-DFCE case (section 6-6).

Table 3-1: Different cases of data assimilation

Case	Name	Forward model	Proxy model error treatment approach	Observed data	Color code
1	OW	-	-	Only production data	
2	WS-PEM	PEM	-	Production and 4DAI data	
3	WS-DUC	DUC	Uncertain coefficients	Production and 4DAI data	
4	WS-DFCE	DFC	Model error statistics	Production and 4DAI data	
5	WS-DFC	DFC	-	Production and 4DAI data	

3.7 Results

This section summarizes the results in six parts. Firstly, we show the development of the DAI-Proxy for the UNISIM-I-H case. Then, we compare the results of proxy and PEM implementations in the ES-MDA algorithm. Lastly, we analyze the WS-DFCE and WS-DFC cases to highlight the role of the model error treatment approach in the ES-MDA algorithm.

3.7.1 DAI-Proxy model development

We used the steps shown in Figure 3-1 in the methodology section to calibrate the DAI-Proxy. Firstly, the prior models in the ensemble were simulated until the end of history time (2618 days). Using the simulation outputs, $4DAI_{(\Delta S_w,0)}$ was calculated for each prior model through petro-elastic modeling with constant pressure. With the same process, $4DAI_{(0,\Delta P)}$ was calculated for each prior model considering constant saturation. One must note that the 4DAIs were calculated for the base time (t = 0) and monitor time (t = 2618). For each model, regression analysis was performed between ${}^{4DAI_{(\Delta S_w,0)}}\!/_{\Delta S_w}$, and porosity to obtain $f_s(\varphi)$ in Equation (9) and coefficients a_s and c_s were determined (second step in Figure 3-1). The distribution histogram of each coefficient (a_s, and c_s) is shown in Figures 3-4a and b. The R^2 (R-squared) value for the fitted porosity function was calculated for all prior models with the mean value of 0.92. According to the third step in Figure 3-1, the coefficients for the pressure change term were estimated for each prior model by regression analysis between ${}^{4DAI_{(0,\Delta P)}}\!/_{\Delta P}$, and the porosity. Figures 3-4c, d, and e illustrate the distribution histogram for each coefficient. The mean value of the R^2 calculated for the fitted porosity function of all the models was 0.86. The DFC model was developed using the mean values in Figure 3-4 for the coefficients. The DUC model was likewise developed considering the characteristics and type of each histogram in Figure 3-4. For example, coefficient a_s was defined as a normal distribution with the mean and standard deviation equal to 676.67 and 37.59 respectively, and minimum and maximum values equal to 537.94 and 881.69, respectively.

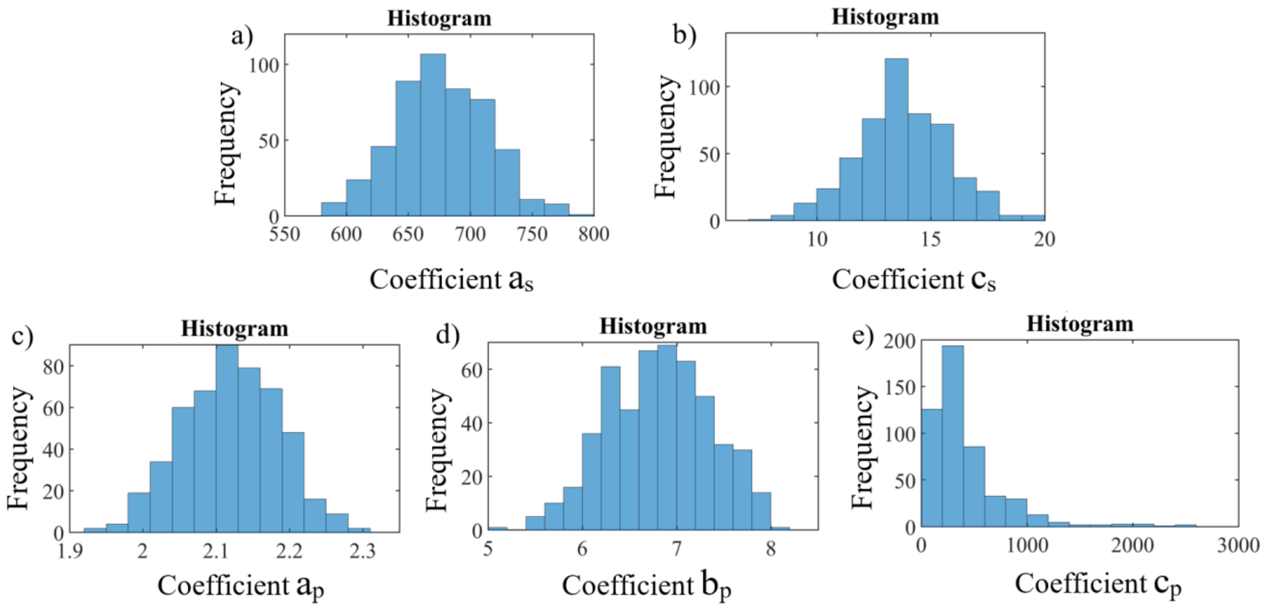

Figure 3-4: Histograms for the DAI-Proxy coefficients. (a), and (b) are the coefficients for the water saturation change term while (c), (d), and (e) are the coefficients for the pressure change term.

Figure 3-5 shows a comparison between the 4DAIs calculated using the DAI-Proxies and the ones with the PEM. The reservoir heterogeneity in terms of porosity is kept in the DAI-Proxy formulation with the porosity function. For each prior model in the ensemble, the DFC proxy model error was quantified using Equation (14). The DFC model error statistics (mean and standard deviation) were calculated and considered for the WS-DFCE case (Figure 3-2 in the methodology section). The mean model error was added to the observed data and the 4D seismic data error covariance matrix was inflated by increases in the standard deviation and the length of the horizontal correlation. In the following subsections, we show the assimilation results with the proxies and the PEM and analyze their differences and similarities. The criteria for the analysis are the past behavior of the reservoir (history data match quality), its future behavior (forecast capability), and uncertainty reduction assessment.

3.7.2 Match quality for well-production data

For prior and posterior models in the ensemble, the NQDS indicator of different cases was calculated. Figure 3-6 shows the NQDS measure for the BHP of producers (Figure 3-6a) and injectors (Figure 3-6b). The prior models were the same for different data assimilation cases. As a result of uncertain model parameters, the prior models for all cases showed a very high uncertainty and variability for all the wells' objective functions (light gray boxes in Figure 3-

6). Data assimilation reduced the uncertainty in posterior models for the OW, WS-PEM, WS-DUC, and WS-DFCE cases in Figures 3-6a and b.

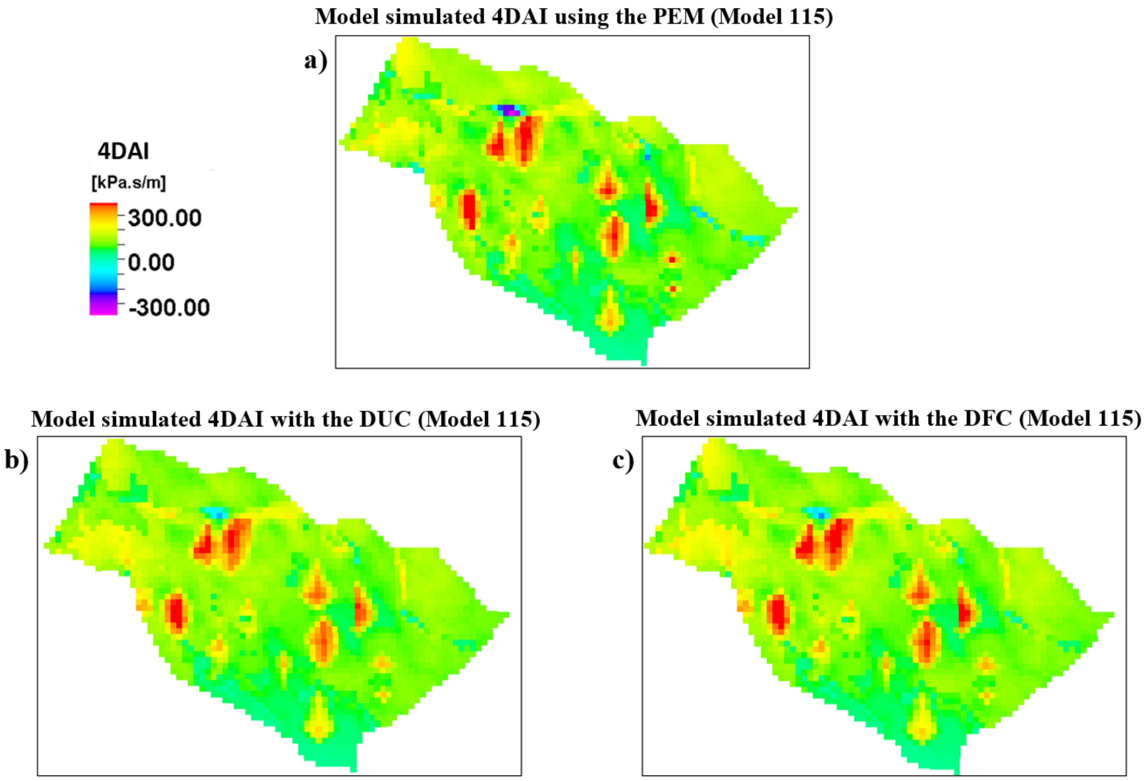

Figure 3-5: (a) 4DAI for randomly selected model in the ensemble (model 115) calculated using the PEM (b) 4DAI map through the DUC model and (c) 4DAI map using the DFC model.

When comparing the PEM and the DAI-Proxies cases, it is evident that match qualities did not alter when the proxy (DUC and DFC) models used in the data assimilation. The results of the WS-PEM case are similar to those with the DAI-Proxies (WS-DUC and WS-DFCE cases). For example, one can compare the data match quality for NA2, NA3, and PROD010 for the WS-PEM case and WS-DUC and WS-DFCE cases in Figure 3-6a. The pink and blue boxplots indicate the proxy responses, which are comparable to the PEM responses red boxplot. For the BHP injectors also the PEM case (WS-PEM) and proxy cases (WS-DUC and WS-DFCE) had similar responses (Figure 3-6b). In general, the results of the DAI-Proxies and the PEM cases were alike for other wells' objective functions (For example, oil rates for different wells also showed similar responses). The similarity of the proxy and PEM responses for all the wells' objective functions confirms that the PEM can be replaced with the DAI-Proxies.

In another investigation, the NQDS values of the posterior models were analyzed and ranked for assimilation cases. This is a good explanatory tool to show the data assimilation quality for different cases. If a model was ranked within the interval $[-1,1]$, it means that the NQDS value for all the wells' objective functions was in the range of $[-1,1]$. A model that ranked between $[-3,3]$ had all the wells' objective functions in that range. Unlike Figure 3-6, the ranking process gave us an overall match quality for all the well-productions' objective functions (Figure 3-7).

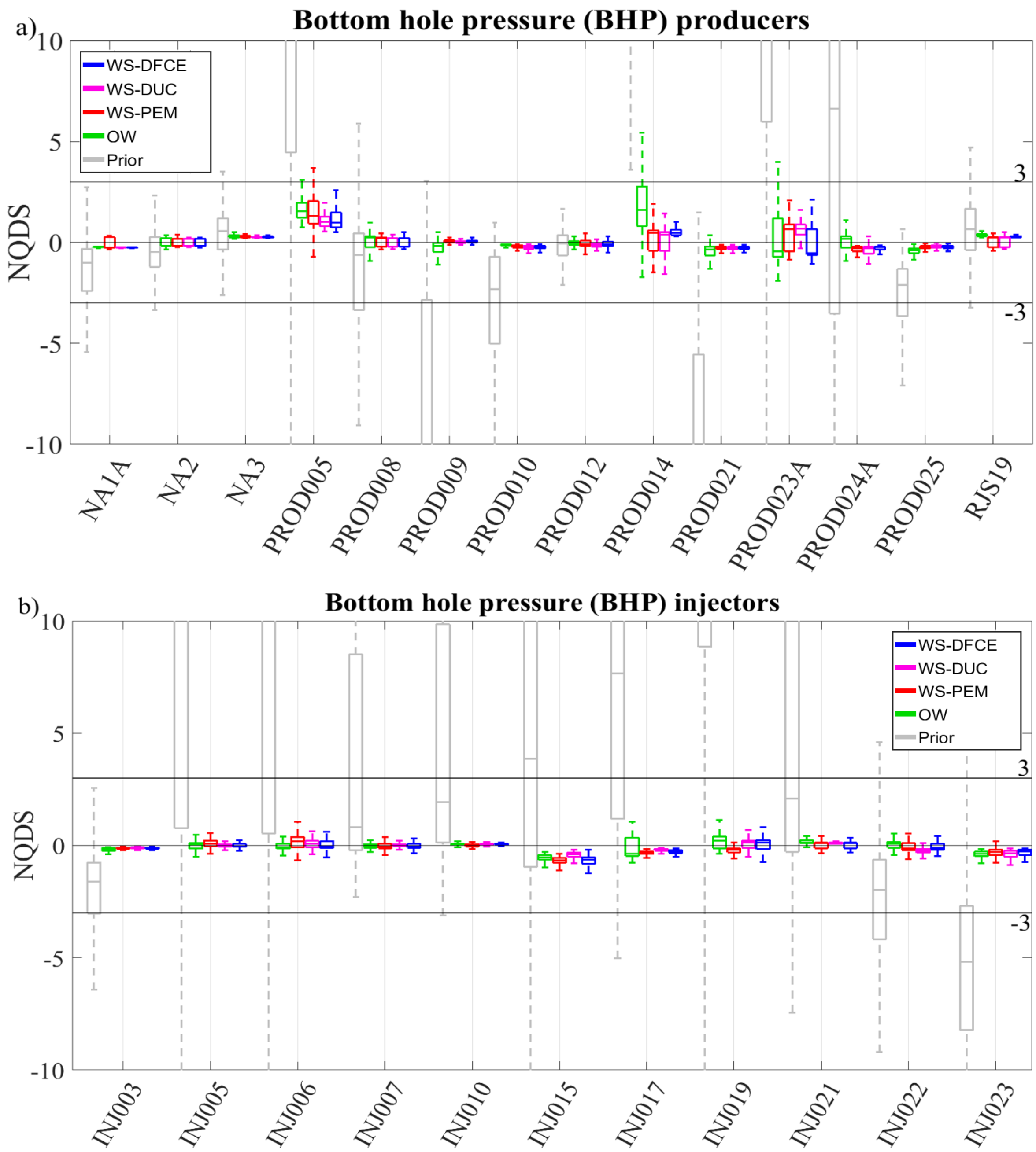

Figure 3-6: NDQS measure for different data assimilation cases. In (a), the NQDS values are shown for the BHP producers with different data assimilation cases and in (b), the NQDS values for the BHP injectors.

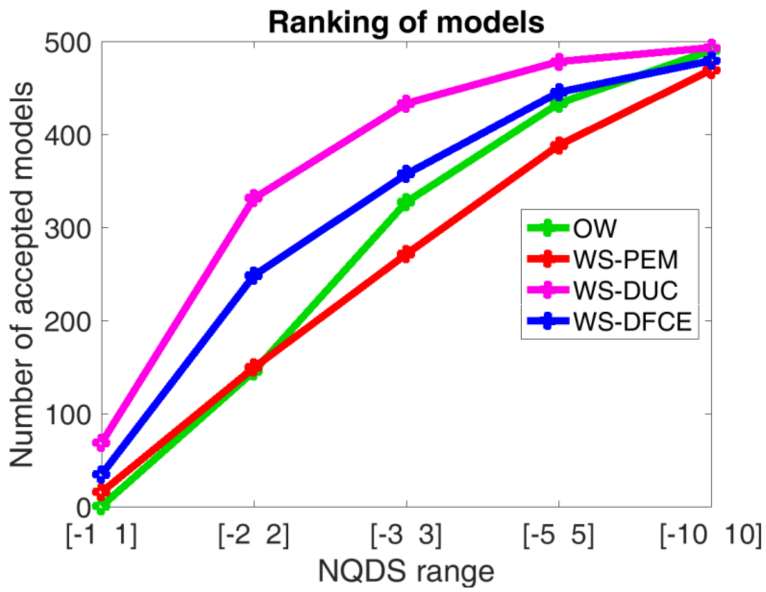

Figure 3-7: Number of accepted models in each NQDS range for different cases.

DAI-Proxies (DFC and DUC models) are approximations of the rock and fluid models. Using the DAI-Proxy instead of the PEM reduces the effects of the 4D seismic data and, therefore, production data shifts the joint assimilation to its favor. This is evident as slightly superior results were obtained using the proxy models in the data assimilation algorithm (pink and blue lines in Figure 3-7). This effect of the proxy is more pronounced for the WS-DUC case (pink line in Figure 3-7) as the DUC model has uncertain coefficients and the production data overshadow the 4D seismic data in the joint assimilation.

3.7.3 Match quality for 4D seismic data

NQDS indicator was calculated for the posterior models of WS-PEM, WS-DFCE, and WS-DUC cases. These cases used well-production and 4D seismic data simultaneously in the ES-MDA algorithm. The observed map was divided into seven areas (Figure 3-8a) and the NQDS indicator computed in each specific area (Figure 3-8b). An overall NQDS was also measured for the entire map and is shown in the Figure 3-8b. The prior models with high variability are shown with light gray boxes and posterior models for various cases with their respective colors (Figure 3-8b).

From the comparison of the results in Figure 3-8b, the WS-PEM and WS-DFCE cases (red and blue boxes, respectively) show similar responses. These results highlight that the DFC model and its model error treatment approach in the data assimilation procedure did not alter the match quality of 4D seismic data compared to the WS-PEM case. Similar observation was seen for well-production match qualities where the proxy cases did not change quality of match compared to the PEM case. The results for the WS-DUC case are slightly better than two other cases. To clarify this behavior, we highlight that the WS-DUC case has more degrees of freedom within the data assimilation as the proxy coefficients are uncertain. During the data assimilation procedure, the uncertain coefficients were updated to reduce the objective function of 4DAI data. However, uncertain coefficients in the DUC model weakened updates for other uncertain model parameters, which might cause adverse effects on posterior models. Alongside the NQDS measure, the mean 4DAI map of posterior models can help us to compare different data assimilation cases. Figure 3-9 shows the observed 4DAI and the mean maps of the posterior models in the ensemble for different cases of data assimilation. In general, the mean 4DAI map for the WS-PEM case (Figure 3-9c) shows that the data assimilation algorithm was effective to diminish the predominant hardening 4D signals around the injectors in prior models (Figure 3-9b).

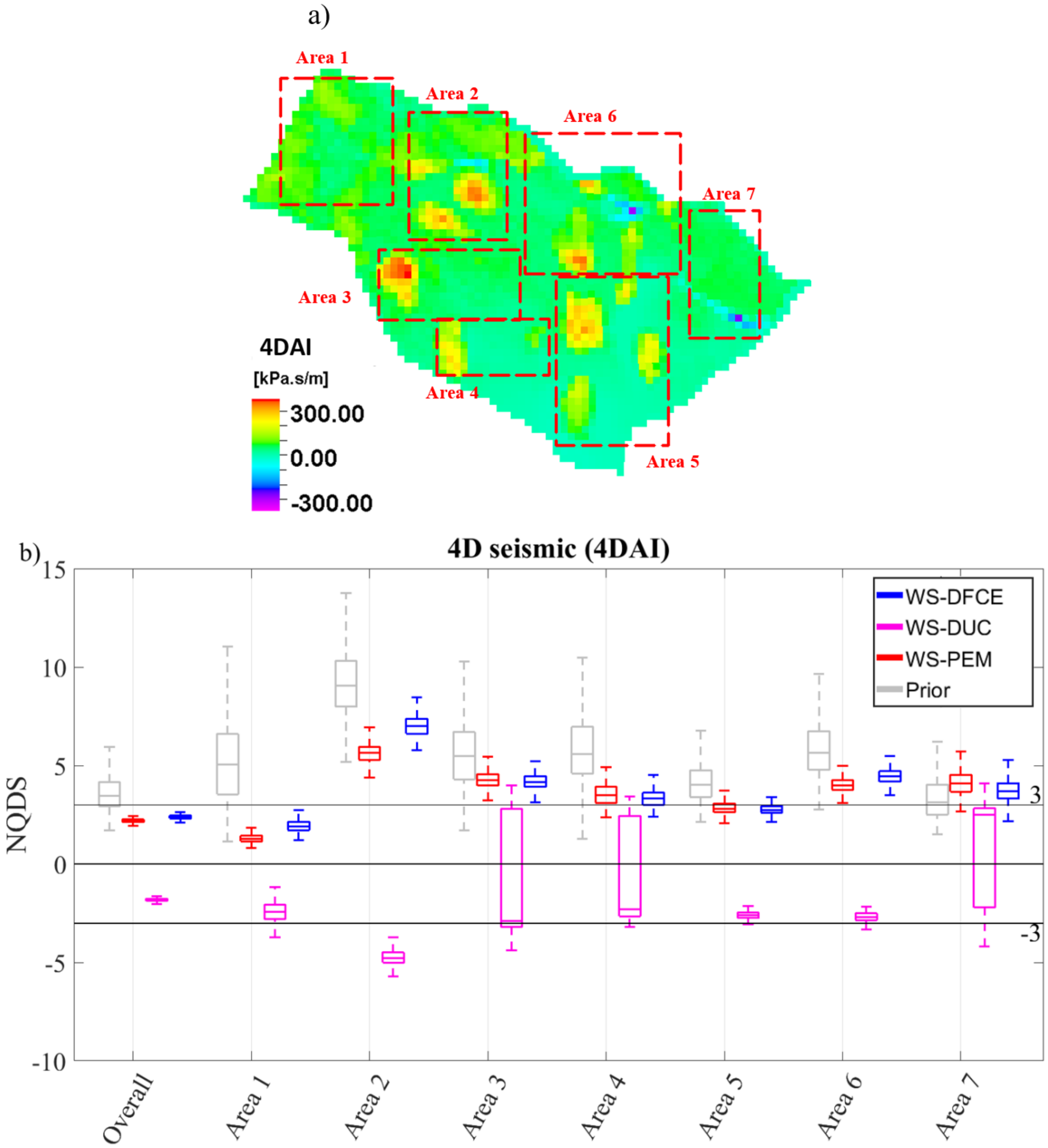

Figure 3-8: Match quality for the 4D seismic data, (a) fragments of the 4DAI observed map and (b) shows the NQDS indicator of different cases for each fragment of the 4DAI and also the entire map.

To have a sense of how effective the joint assimilation was for the DAI-Proxy cases, it is worth comparing Figures 3-9b, d, and e. Like the PEM case, in the proxy cases, the prior hardening 4D signals in the location of injectors were reduced in intensity. The comparison of the WS-PEM and WS-DFCE cases (Figures 3-9c and e) shows that the prior 4D signals around injector wells (Figure 3-9b) were ameliorated to the same degree by these two cases. This indicates that the DFC model and its model error treatment approach provided a data assimilation framework comparable to the WS-PEM case. It is worth discussing the results for the WS-DUC case (Figure 3-9d) as there are some areas indicated with red arrows. In those areas, the water saturation change signals are blurred compared to the observed 4DAI map (Figure 3-9a).

We performed additional calculations to analyze the performance of the WS-DUC case. The average 4DAI values for the observed (Figure 3-9a) and posterior maps (Figures 3-9c, d, and e) were calculated. This value for the observed map was 59.4 $\frac{kPa.s}{m}$ while for the WS-DUC, WS-DFCE, and WS-PEM cases the values were 49.4, 88.1, and 86.6 $\frac{kPa.s}{m}$ respectively. The average value is closer for the observed and the WS-DUC case. This indicates that this case tends to minimize the 4D seismic objective function in a way that the posterior 4DAI values are close to the average 4DAI value of the observed map. As the uncertain coefficients in the DUC model are scalar, they were updated to reproduce posterior 4DAIs close to the average value of the observed map. Thus, the WS-DUC case falls short of reproducing peak values of water saturation change signals around injectors (Figure 3-9d). By contrast, the WS-DFCE case was effective in those areas and diminished the prior hardening effects around the injectors.

3.7.4 Uncertainty assessment

Data assimilation algorithms update the prior models and reduce uncertainty in the model parameters. For our research, the model parameters were divided into grid and scalar parameters. Figure 3-10 shows the boxplots of the posterior values for the scalar uncertain parameters color coded by different cases. Production data assimilation reduced uncertainty in the scalar parameters, as shown by the green boxes in Figure 3-10. Joint assimilation with the 4D seismic data provided more observed data, which in turn led to a noticeable reduction of uncertainty for these parameters. The ensemble collapse for scalar parameters when using the 4D seismic data is reported in da Nóbrega et al. (2018), Danaei et al. (2020), and Emerick (2016).

From the results in Figure 3-10, it appears that both the WS-PEM and WS-DFCE cases provided similar uncertainty reduction for the scalar parameters. Both cases share a noticeable uncertainty reduction for the Corey exponent shown in Figure 3-10c. For other uncertain scalar parameters, both cases provided similar results. Perhaps the most different results for uncertainty assessment were seen in the WS-DUC case. A significant observation from Figure 3-10 is the close posterior values of the OW and WS-DUC cases. This indicates that the uncertain coefficients in the DUC model reduce the effects of the 4D seismic data and shift the joint assimilation to the well-production data. This observation is in line with the previous observation reported in the data match quality for well objective functions (Figure 3-7). To have uncertainty assessment for grid parameters such as porosity, mean of posterior models and its standard deviation are calculated for different cases of data assimilation (Figures 3-11 and 12). A comparison of the results in Figure 3-11 shows that the WS-PEM and WS-DFCE cases provided similar posterior models in terms of grid parameter porosity.

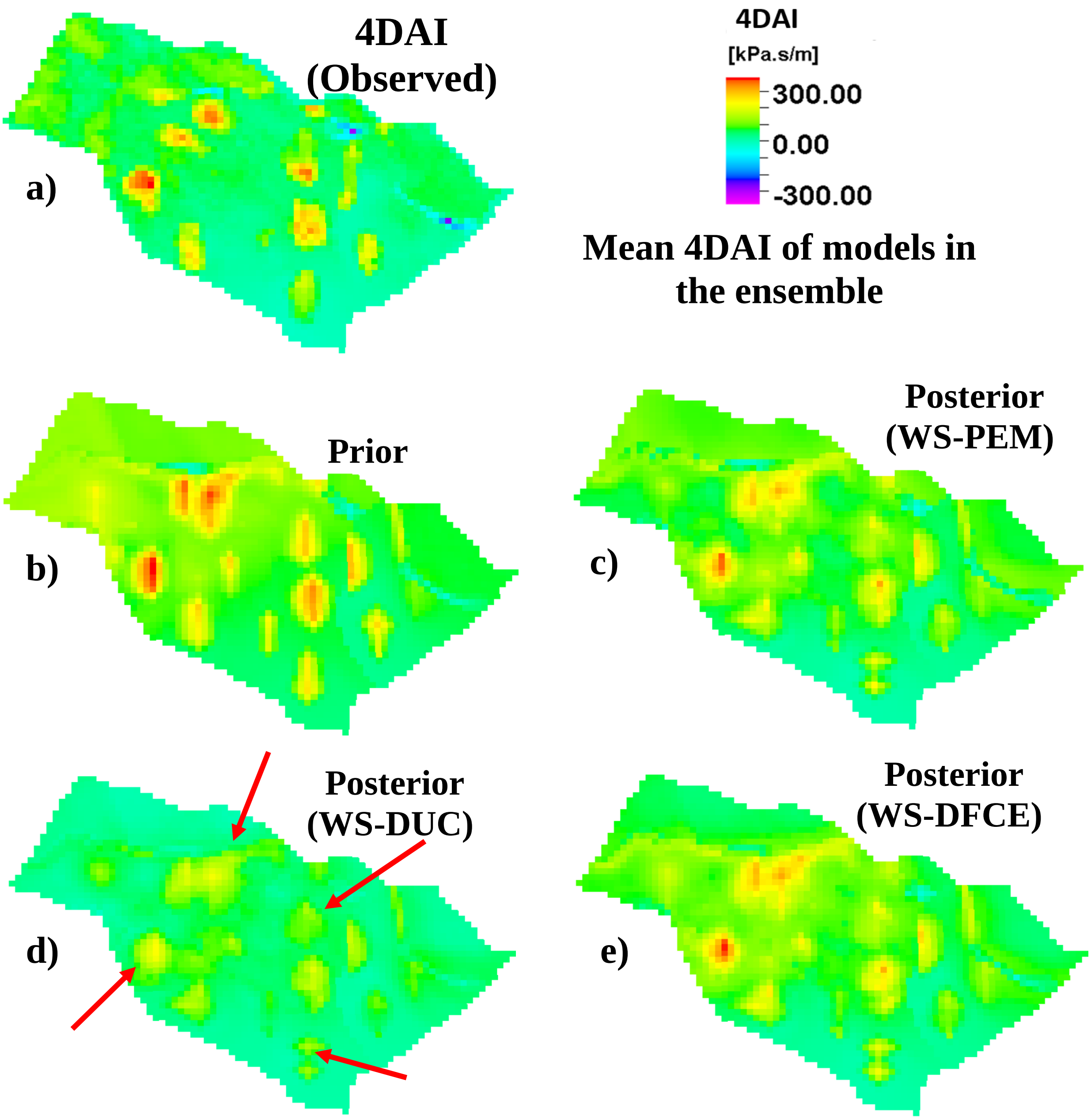

Figure 3-9: (a) the observed 4DAI map used for the data assimilation, (b) is the mean prior 4DAI map, and the mean posterior 4DAI maps are provided for the PEM case (c), WS-DUC case (d), and WS-DFCE case (e).

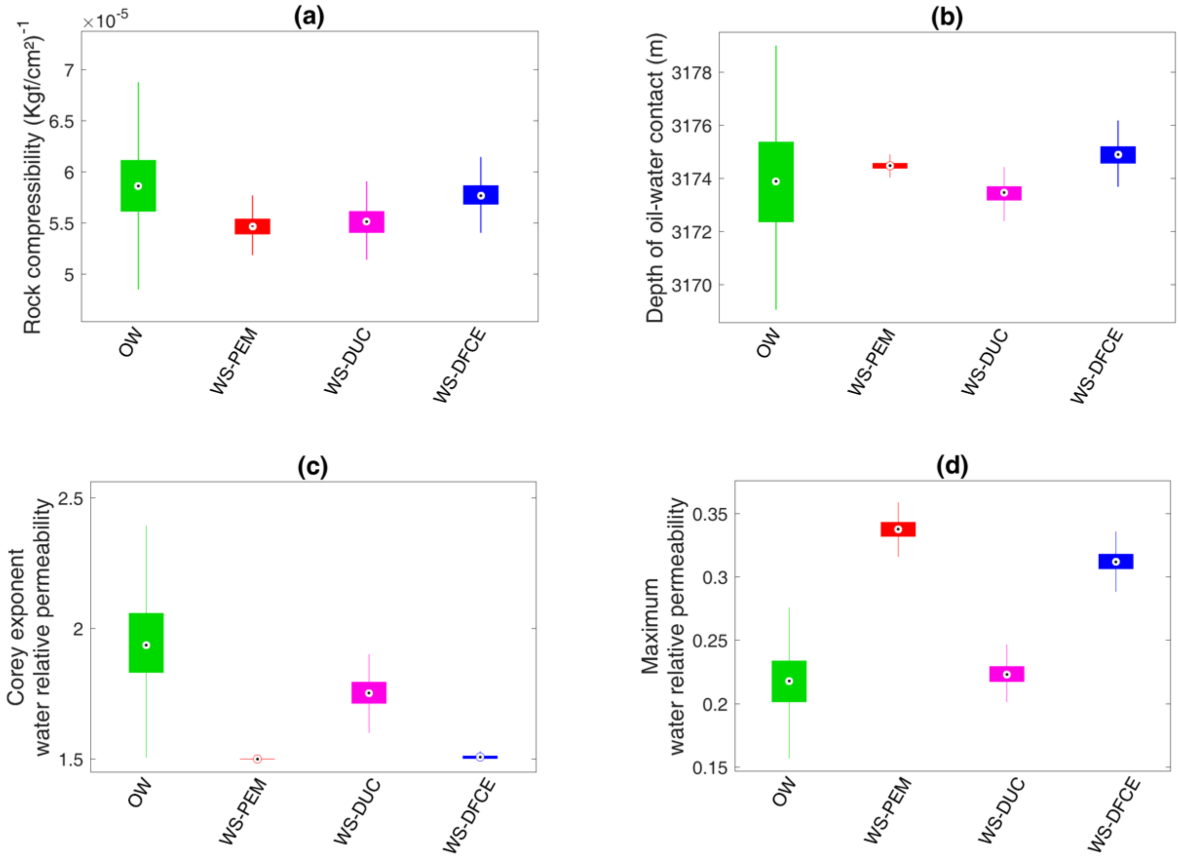

Figure 3-10: Uncertainty assessment for scalar uncertain parameters from different data assimilation cases

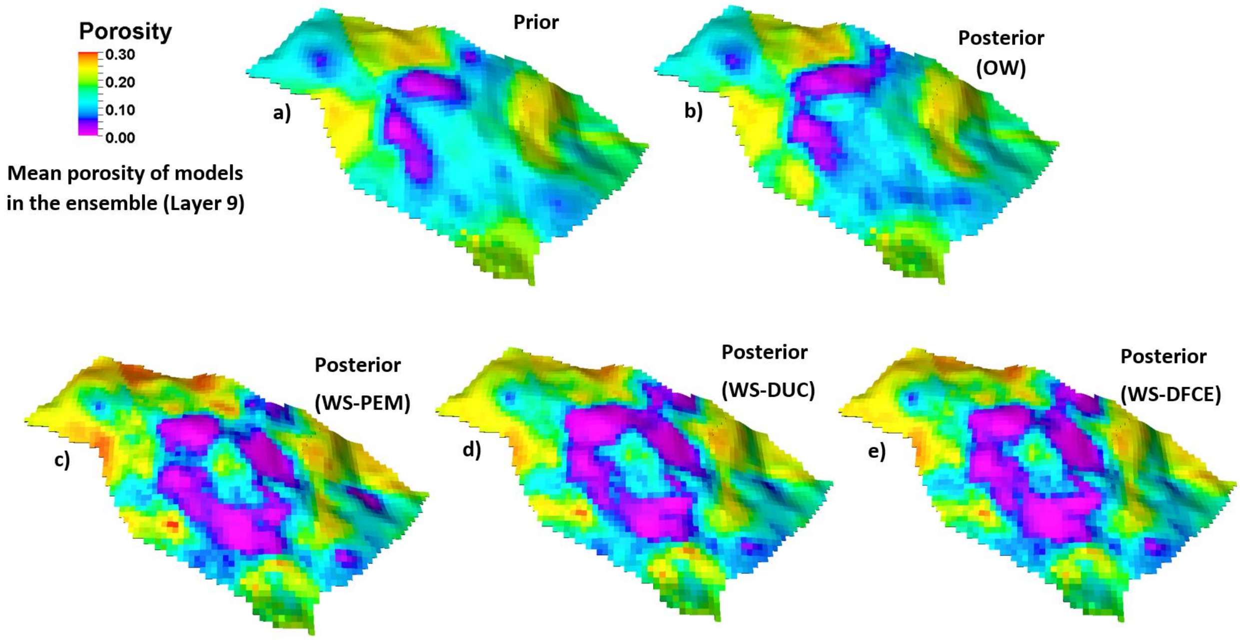

Figure 3-11: Prior models mean porosity (a), and posterior means for OW case (b), WS-PEM case (c), WS-DUC case (d), and WS-DFCE case (e).

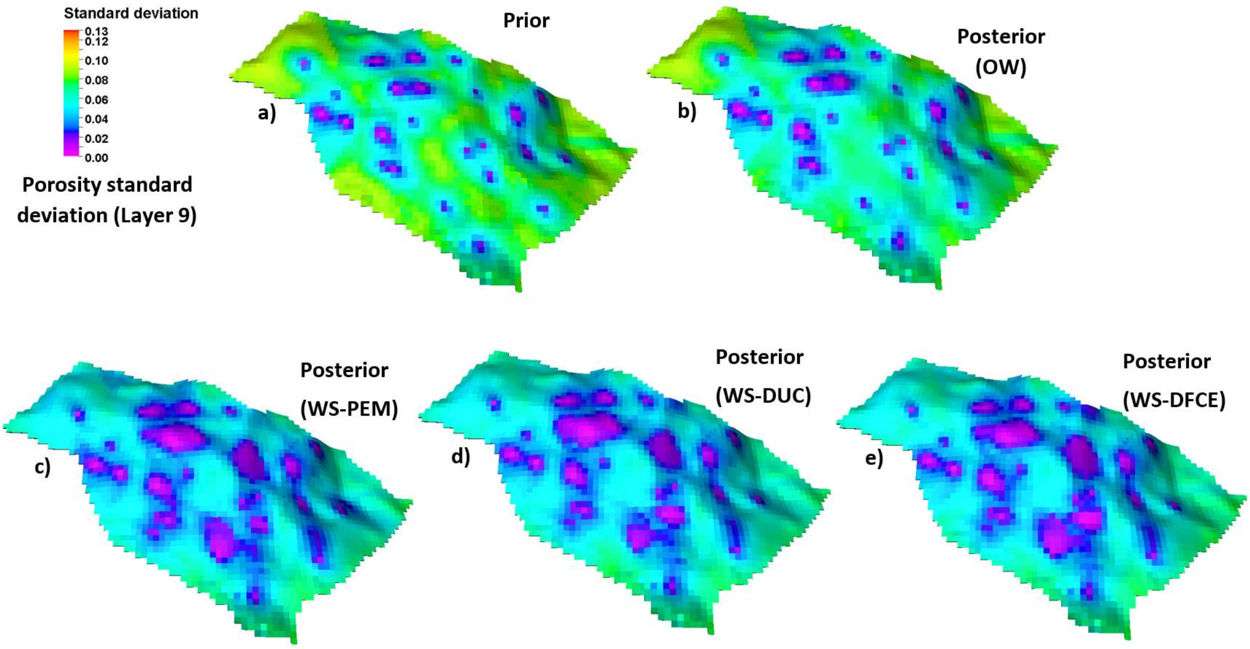

Figure 3-12: Standard deviation of porosity calculated for layer 9 of prior models (a), posterior models in the ensemble for the OW case (b), WS-PEM case (c), WS-DUC case (d), and WS-DFCE case (e).

3.7.5 Production forecast

The reference model (UNISIM-I-R) enables us to test the posterior models of different data assimilation cases in terms of production forecast. The reference model provides the future responses of the reservoir therefore; we evaluated the forecast capabilities of the posterior models. For the data assimilation, the ES-MDA used 2618 days of well-production data and a 4DAI map. We considered 3014 days after the history data (post history) for forecast evaluation. Figures 3-13 and 14 show the cumulative field oil production and oil production rate for a well (PROD005) color coded with different cases.

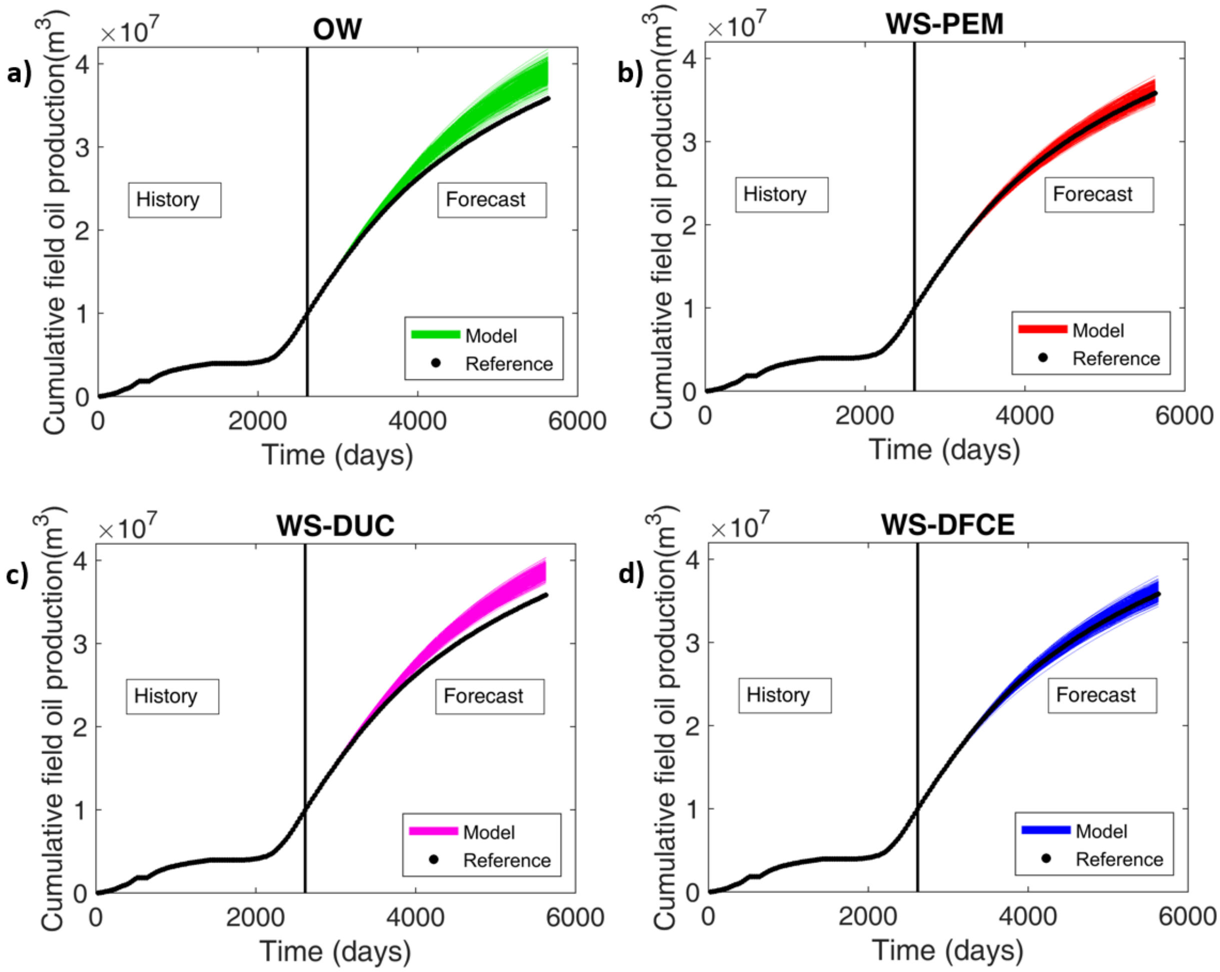

Figure 3-13: Cumulative field production forecast for different data assimilation cases. (a) OW case with posterior models in green; WS-PEM in (b), WS-DUC in (c), and WS-DFCE in (d).

For our case study, the 4D seismic data assimilation mainly impacted the production forecast. The WS-PEM case provided more reliable posterior models for production forecast compared to the OW case, as shown in Figures 3-13a and b. The production forecast of the WS-PEM case (red curves in Figure 3-13b) encompasses the reference data. The reliability of the production forecast for the WS-DFCE and WS-DUC cases are shown in Figures 3-13c and d, respectively. Although the WS-DUC case provided better posterior models for 4D seismic and well-production objective functions (Figures 3-7 and 8b), they were less able to provide reliable forecast in terms of cumulative field oil production (Figure 3-13c). The uncertain coefficients in the DUC model were updated during the data assimilation procedure, which weakened the updates for other uncertain parameters. The impact of uncertain coefficients in the DUC model for the WS-DUC case was especially severe on the production forecast. The comparison of the WS-PEM and WS-DFCE cases (Figures 3-13b and d) shows similar capability of posterior models for these cases throughout the forecast. The WS-DFCE case provided posterior models (blue curves in Figure 3-13d) that encompass the reference data. In Figure 3-14, the comparison of the results between the WS-PEM and WS-DFCE shows that the production forecast for the oil rate of PROD005 was similar.

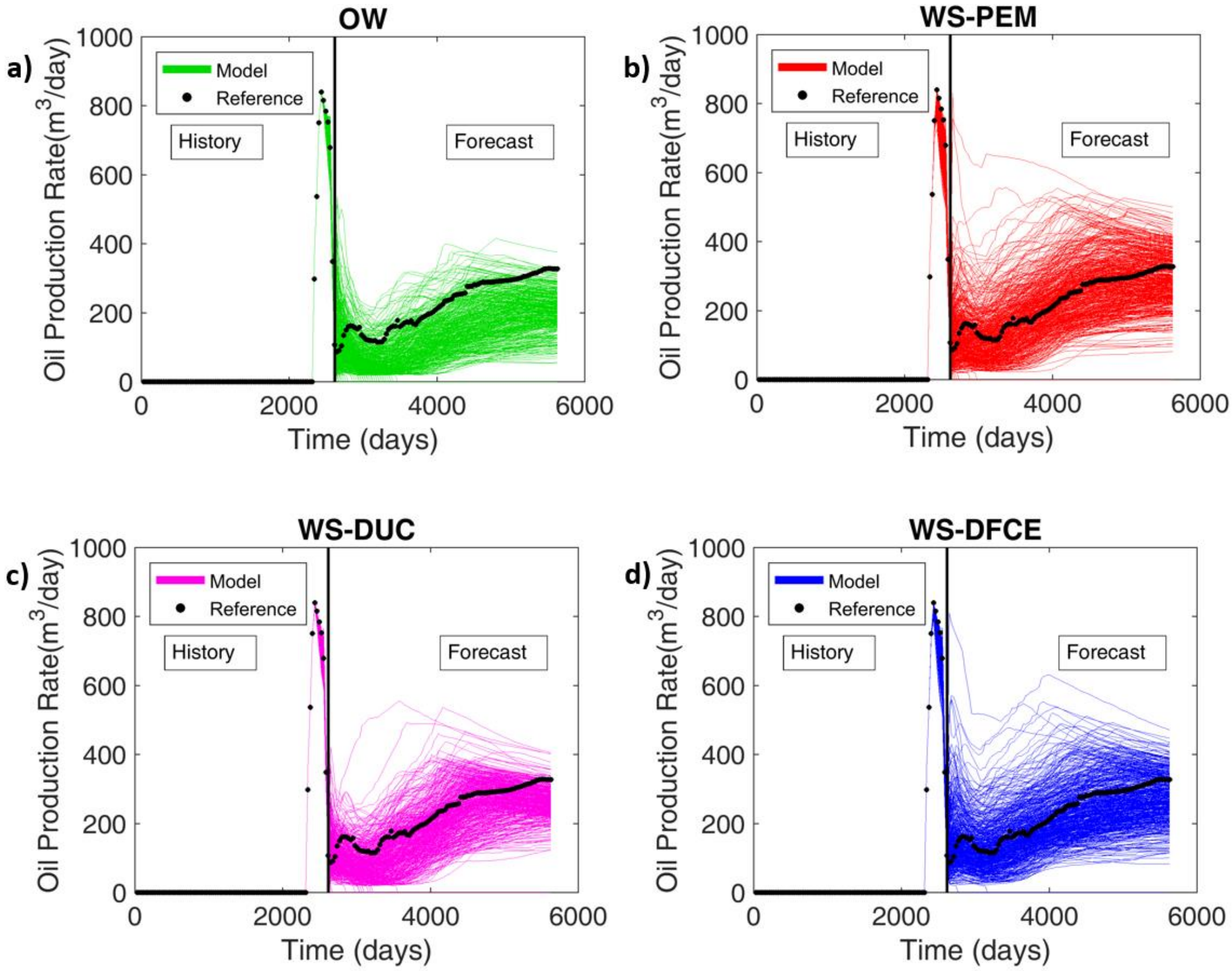

Figure 3-14: Oil production rate forecast (PROD005) for posterior models of different data assimilation cases.

3.7.6 The role of the proxy model error

We considered two cases to specifically analyze the role of the proxy model error in the data assimilation results and production forecast. Here, we performed the joint data assimilation considering the proxy with fixed coefficients without the model error treatment (WS-DFC) and with the same configurations used for the WS-DFCE case. We ranked the posterior models for these two cases using the NQDS indicator for all the well-production objective functions (Figure 3-15). This figure shows an overall match quality for the well-productions' objective functions likewise Figure 3-7 in section 6-2. From Figure 3-15, it is clear that the case with the proxy model error treatment (blue line) yielded better history matched models with lower NQDS values. For example, the WS-DFCE case had 35 models between [-1,1] and 249 models in the range of [-3,3], while the WS-DFC case had 20 models between [-1,1] and 202 models in the range of [-3,3].

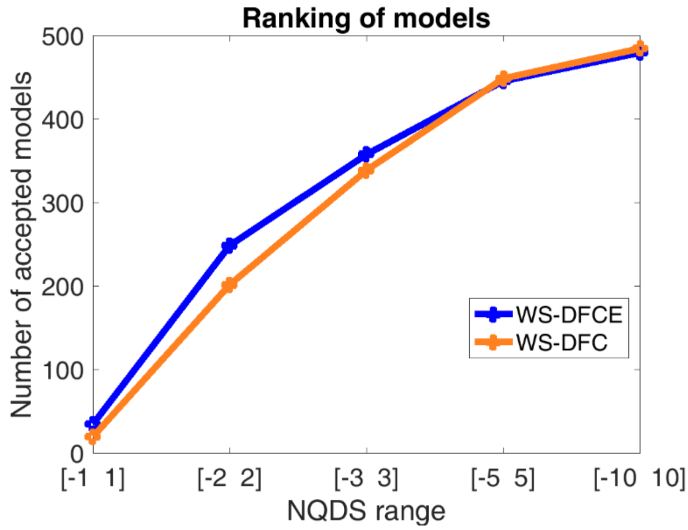

Figure 3-15: Comparison between the WS-DFCE with the proxy model error treatment and the WS-DFC without the treatment.

The analysis of the 4D seismic objective function and uncertainty assessment revealed two things. First, to account for the proxy model error in WS-DFCE case, the data error covariance matrix for the 4D seismic observed data was inflated. This generated lower values of 4D seismic objective function for the WS-DFC case, when compared to the WS-DFCE case. The second is related to the uncertainty assessment for these two cases. This analysis showed close responses for the WS-DFCE and WS-DFC cases, but the normalized variance of the model parameters was higher when we account for the proxy model error. This was expected as the proxy model error treatment in WS-DFCE weakened the updates for the uncertain model parameters through the data assimilation procedure.

We investigated further by comparing the production forecast reliability of the WS-DFCE and WS-DFC cases. Figure 3-16 shows the cumulative field oil production forecast for the WS-DFC case. Here we compared the result in Figure 3-16 with that of the WS-DFCE case in Figure 3-13d. The posterior models' forecasts highlight that accounting for the proxy model error led to more reliable production forecast for the WS-DFCE posterior models. The forecast obtained with this case encompasses the reference data compared to the optimistic forecast for the WS-DFC case (Figure 3-16).

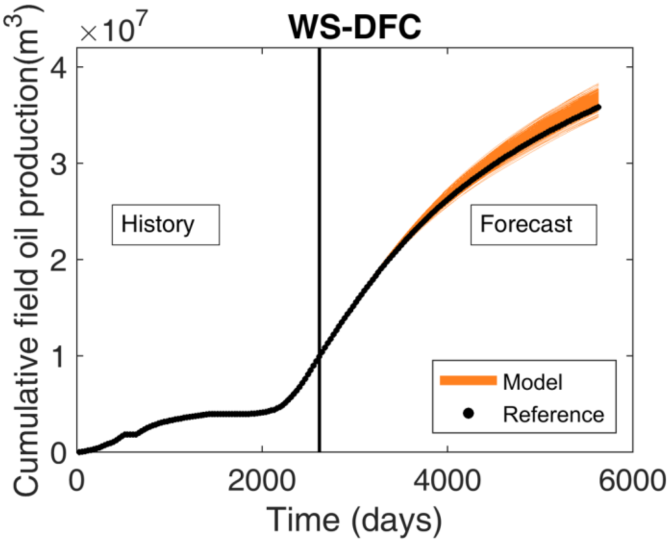

Figure 3-16: Cumulative field oil production forecast for the WS-DFC case posterior models.

For our case study, accounting for the proxy model error in the data assimilation improved the data match quality for the wells' objective functions. Although the treatment for the proxy model error in the WS-DFCE case did not improve the 4D seismic objective function, it weakened updates for uncertain model parameters and prevented inconsistent updates. By doing so, the production forecast improved when proxy model error was considered, a good indicator that this procedure generated more consistent models.

3.8 Discussion

The current research is based on the premise that we can substitute the traditional PEM with a lighter model in the simultaneous assimilation of 4D seismic and well-production data. Using these results, we can draw some comparative discussions with the previous research in Danaei et al. (2020). The argument here regarding the role of porosity in the DAI-Proxy and accounting for the proxy model error in data assimilation becomes more convincing by the results in Figures 3-10, 11, and 13. Here, the WS-DFCE and WS-PEM cases have similar uncertainty assessment for scalar and grid parameters. In Danaei et al. (2020), the cases with the proxy and PEM had different uncertainty assessment for scalar and grid parameters. Moreover, the WS-DFCE case shown here provides reliable production forecast, unlike the proxy case of Danaei et al. (2020), where the production forecast for posterior models were overestimated or underestimated. Overall, the inclusion of porosity in the DAI-Proxy models mainly assisted the inversion of uncertain model parameters from the 4D seismic data in the joint data assimilation scheme. A lack of porosity in the proxy formulation caused inconsistent updates for model parameters as argued in Danaei et al. 2020. Additionally, accounting for the proxy model error by estimation of the model error statistics mostly improved the production forecast as shown in section 6-6 when the WS-DFCE and WS-DFC cases were compared.

It is interesting to note that the DAI-Proxy (Equation 9) could be calibrated without using the prior models and a petro-elastic model. The water saturation change term ($f_s(\varphi)$ in Equation 9) can be calibrated with Gassmann fluid substitution on well-log information. It is well-known that the fluid substitution using the Gassmann equation is not a full rock physics modeling. Therefore, water saturation change term could be calibrated without a rock physics model. The pressure change term ($f_p(\varphi)$ in Equation 9) can be calibrated using a history-matched model and an interpreted 4D signal caused by pressure change in impedance domain. In this process, the pressure change (ΔP in Equation 12) is calculated with the history-matched model and by knowing the 4D signal caused by the pressure change, the coefficients of the pressure change term are evaluated. Note that adding other parameters (such as initial water saturation or initial pressure) to DAI-Proxy might seem to improve the proxy application, but by adding those, we may cast a shadow over the concept of using a simplified and straightforward proxy model like DAI-Proxy.

Unlike the PEM, the DFC model has fewer uncertain parameters and it is lighter. In addition, DFC model and its model error treatment approach provided similar results compared to the PEM application for 4D seismic data assimilation. This advantage of the DFC helps petroleum engineers to use a light model for 4D seismic data assimilation. Aside from being light, the DFC model is helpful for some applications with large-scale simulation models of giant reservoirs where extracting information from simulation models could be costly for seismic forward model calculations. The DFC model requires fewer outputs (only five grid variables) from simulation models to compute 4DAIs, whereas the same calculations are done with 18 grid variables using the PEM. Moreover, in some cases where PEMs could be uncertain (such as carbonate reservoirs) or challenging to be calibrated (for instance, due to the lack of laboratory measurements) then using an approximate model like DFC and its model error treatment approach for 4D seismic data assimilation could be beneficial and should be considered. However, DFC model considers fixed coefficients for all reservoir grids that could be a limitation in highly heterogeneous reservoirs. For these cases, a possible solution would be to consider the coefficients of the DFC as a fixed value for each reservoir grid in order to capture the reservoir heterogeneity. This seems to be a fair solution, although further analysis is needed.

It is noteworthy that the proxy with uncertain coefficients (the DUC model) also suffers from a limitation. Uncertain coefficients in this model are assumed as scalar uncertain parameters. This assumption simplifies the DUC application in the data assimilation algorithm. However, considering uncertain coefficients as grid properties can preserve the reservoir heterogeneity and might alter or improve the uncertainty assessment and production forecast for this case. Finally, we can extend the DAI-Proxy formulation (Equation 9) to three-phase flow and consider the gas saturation change term. However, two points should be noted and investigated here: (1) gas saturation change term should be inserted into the equation with its appropriate sign, for instance, an increase in gas saturation decreases the $4DAI$ and, (2) in three-phase flow, we might consider whether the gas replaces oil or the water. The porosity function and its non-linearity might be different when gas replaces water from the case that it replaces oil.

3.9 Conclusion

In this research, a method was presented to substitute the traditional PEM with a new proxy (named DAI-Proxy) for joint assimilation of well-production and 4D seismic data. The DAI-Proxy linked time-lapse acoustic impedance to a summation of saturation-pressure changes with two coefficients, which are functions of porosity. This proxy was then used with an ensemble-based algorithm to integrate the observed well-production and 4D seismic data. Alongside the DAI-Proxy, the novelty of the method was to account for the proxy model error in the data assimilation algorithm. Two approaches were taken to treat the proxy model error: the first approach considered the coefficients in the DAI-Proxy as uncertain variables and the second approach estimated the proxy model error statistics from the prior ensemble of models and used fixed coefficients. Different data assimilation cases were designed to compare the performance of the DAI-Proxy and its proxy model error treatment approaches with the PEM. The results broadly are concluded in three main points:

1- The proxy with fixed coefficient and its model error treatment approach provided a data assimilation case similar to the PEM case. Data match quality for both 4D seismic and well-production data of these two cases had similar responses. Here, the proxy and PEM cases were alike in terms of production forecast.

2- The data assimilation case for the proxy with uncertain coefficients successfully mimicked the reservoir's past behavior. However, this case fell short in the production forecast compared to the PEM case.

3- Based on the results, we recommend the DAI-Proxy with fixed coefficient and its proxy model error treatment approach as a substitute for PEM in the assimilation of observed 4D seismic data.

Future research on the DAI-Proxy could be devoted to the direct calibration of the proxy model with observed 4D seismic data, laboratory measurements, or well-log information. New approaches to account for the proxy model error in data assimilation are also desirable for the future research.

3.10 Acknowledgment

This work was carried out in association with the ongoing project registered under number 20372-9 ANP as the "Development of integration between reservoir simulation and 4D seismic - Phase 2" (University of Campinas [UNICAMP]/Shell Brazil/ANP) funded by Shell Brasil Petróleo Ltda. under the ANP R&D levy for "Investment Commitment to Research and Development." The authors are grateful for the support of the Center for Petroleum Studies (CEPETRO-UNICAMP/Brazil), the Department of Energy (DE-FEM-UNICAMP/Brazil), the Research Group in Reservoir Simulation and Management (UNISIM-UNICAMP/Brazil), Energi Simulation, and CNPq. The authors would also like to thank Alexandre A. Emerick (from Petrobras) for providing the EHM tool to UNISIM. In addition, a special thanks to CGG, Schlumberger and CMG for software licenses.

4 All-in-one proxy to replace 4D seismic forward modeling with machine learning algorithms

Authors: Danaei, S.; Cirne, M.; Maleki, M.; Schiozer, D. J.; Rocha, A.; Davolio, A.

Published in: Journal of Geoenergy science and engineering, 2023

(https://doi.org/10.1016/j.geoen.2023.211460)

4.1 Abstract

Time-lapse seismic data provides valuable information to assist reservoir monitoring, model-based reservoir management, and development activities. 4D seismic information can be used quantitatively to estimate saturation-pressure changes or update reservoir simulation models through a data assimilation process, which traditionally requires a 4D seismic forward model that includes two steps: (1) petro-elastic model to relate rock and fluid properties to elastic attributes and (2) seismic model to depict wave propagation in the reservoir. The traditional forward model brings some complications in quantitative applications, such as time-lapse seismic history matching. Its multidisciplinary nature is a significant bottleneck to update simulation models, once observed 4D seismic data is used with production data in the assimilation process. Furthermore, it is time-consuming, especially in three-dimensional simulation models within data assimilation with several iterations. Here, the traditional forward model needs to be run hundreds or even thousands of times. Aside from being time-consuming, it requires substantial computer memory for complex geology, where more sophisticated seismic models are needed. In 4D seismic quantitative applications, the timely use of the information and its full benefits fade away due to the computational cost and time of the 4D seismic forward model. This research proposes a proxy (we call it, S4D-Proxy) to replace the traditional approach. The S4D-Proxy leverages machine learning models to detect hidden patterns and learn relations between input features (e.g., porosity and saturation-pressure changes) and the target (time-lapse difference of seismic amplitude). Training data are prepared and fed to the machine learning algorithms to relate the inputs and the desired output. The performances of the machine learning models are evaluated based on a numerical measure (coefficient of determination) and visual comparison of the results with the traditional forward model. Our results show that the average coefficient of determination for the test dataset is in an acceptable range. Moreover, the visual comparison of the proxy predictions with those from

the traditional approach shows high similarity. Most hardening and softening 4D signals are reproduced with the proxy models. The main advantage of our approach is that it lowers the computational cost and time. The application of the proxy in data assimilation process could offer a significant speed advantage with faster 4D seismic forward modeling for data assimilation iterations. Unlike the traditional forward model, which is one step (petro-elastic model) then another (seismic model), our approach performs the forward modeling at once (all-in-one proxy model). It also offers an alternative 4D seismic forward model for time-lapse seismic feasibility study. All these advantages make the S4D-Proxy valuable and practical in permanent reservoir monitoring (PRM), where the reduced turnaround time in the forward model indicates the timely use of the 4D seismic information.

4.2 Introduction

Time-lapse (4D) seismic data typically comprises information related to changes in fluid saturations, pressure, compaction, and temperature. These changes affect reservoir density and stiffness, which eventually alter seismic responses and might be observed with repeated 3D seismic surveys or 4D seismic data. This data could assist reservoir monitoring, model-based reservoir management, and development activities. For example, Buksh et al. (2015) and Mateeva et al. (2015) discussed 4D seismic applications to optimize reservoir management. Also, Gee et al. (2017), and Pathak et al. (2018) used this information for reservoir future development strategies. A qualitative interpretation of these data could explain the causal effects of 4D signals and might help researchers and operators detect reservoir model deficiencies (Maleki et al., 2021). Apart from the qualitative applications, 4D seismic data is used quantitatively to estimate changes in reservoir property with time, like pressure and saturation changes. This estimation could prove helpful for reservoir management and well-planning decisions (Cao and Roy, 2017). Moreover, observed 4D seismic data might be assimilated quantitatively with production data (4D seismic history matching) to calibrate reservoir simulation models and update their model parameters. However, this joint assimilation of observed data is very time-consuming and usually involves several iterations. In iterative ensemble-based data assimilation methods, a set of prior simulation models is updated through several iterations and, therefore, hundreds or thousands of simulation runs are required. Examples of the observed data assimilation (4D seismic together with production data) that require multiple iterations are presented in Silva Neto et al. (2021) and also can be found in Danaei et al. (2022).

The quantitative applications of 4D seismic data traditionally need forward modeling to relate the simulated rock and fluid properties to the synthetic seismic responses. The traditional forward model has two connected steps performed in sequence. The first is a petro-elastic model (PEM), which relates the simulated rock and fluid properties to the synthetic elastic characteristics, and the second is a seismic model to simulate the wave propagation in the reservoir. Therefore, the traditional forward model is a combination of PEM and seismic model. This combination could be used with different data assimilation algorithms to quantitatively integrate 4D seismic information. For example, Amini et al. (2011), Bogan et al. (2003), and Tabatabaei et al. (2014) discussed the use of PEM and seismic model in the 4D seismic quantitative applications. Dadashpour et al. (2008) employed the combination of PEM and seismic model for inverse modeling of saturation-pressure changes, and Tolstukhin et al. (2012) used this combination in 4D seismic history matching to update reservoir simulation models.

One primary problem of the traditional forward model is its multidisciplinary nature. Rock-physicists are involved in developing the PEM, and geophysicists are responsible for simulating seismic wave propagation in the reservoir. This problem is more severe when petroleum engineers perform 4D seismic history matching to calibrate simulation models. In their applications, the traditional PEM and seismic model act as a tool that executes modeling in two consecutive steps. PEM is the first step and is then followed by the seismic model. This multidisciplinary nature of the traditional approach has resulted in complications and gaps being introduced to the joint data assimilation frameworks. However, some workarounds (such as proxy models) could make the traditional forward model more accessible to petroleum engineers. Another challenging problem of the traditional forward model is that it is a time-consuming task. For instance, there are different seismic modeling methods, finite- difference (FD) and finite-element (FE) methods, or ray-tracing methods. A common factor for all these methods is their high computational cost and time. Even a fast method like 1D convolutions could be time-consuming when applied to three-dimensional reservoir models or inside iterative ensemble-based data assimilation procedures, where PEM and seismic model are repeated several times to update simulation models. Moreover, each part of the traditional approach poses its own problems, which contribute to the overall complications. For instance, the main problem with the PEM is its uncertainty and, on occasion, it is challenging to develop a reliable model for the 4D seismic applications (Danaei et al., 2020). Based on these drawbacks and given the step-by-step process of the traditional forward model, our preference is to use a proxy model. It could be a partial replacement of the PEM with a proxy (PEM-Proxy) or a total replacement of the PEM and seismic model (we call it, S4D-Proxy).

For the partial replacement of PEM, there have been attempts to present proxy models. PEM-Proxy could be an alternative model where a reliable PEM is unavailable or difficult to develop (Danaei et al., 2020). Several authors have discussed and suggested different PEM-Proxy models to invert time-lapse saturation-pressure changes from 4D seismic data. Landrø (2001) presented a PEM-Proxy in which a first-order approximation is used to relate seismic parameters (P-wave velocity, S-wave velocity, and density) to saturation changes. P-wave and S-wave velocities are related to pressure change with a second-order approximation. Over time, several different studies have modified Landrø's proxy model (Bhakta and Landrø, 2014; Meadows, 2001; Trani et al., 2011). These modifications are mostly related to the order of approximation in how seismic parameters relate to the saturation-pressure changes. Lang and Grana (2019) proposed a second-order approximation to relate seismic parameters to saturation-pressure changes and porosity, initial saturation, and initial pressure. Perhaps PEM-Proxy models for 4D seismic applications have seen a constant evolution through decades. What began as a straightforward PEM-Proxy equation in Landrø (2001), has evolved to more sophisticated machine learning (ML) models to invert saturation-pressure changes directly from 4D elastic attributes. For example, Zhong et al. (2020) and also Weinzierl and Wiese (2020) presented inversion of saturation-pressure changes from 4D elastic attributes where the former used a deep learning approach with a cycle generative adversarial neural network (CycleGAN) model and the latter employed a deep neural network (DNN). Most of the aforementioned research discussed PEM-Proxy for the inverse modelling of saturation-pressure changes. Danaei et al. (2022, and 2020) have shown the application of the PEM-Proxy in 4D seismic history matching to constrain reservoir simulation models.

For the total replacement of the traditional PEM and seismic model (the combination), previous studies suggested proxy models. To estimate pressure-saturation changes, MacBeth et al. (2006) showed an inversion process where the combination of PEM and seismic model was replaced with a linear summation with two coefficients to relate saturation-pressure changes to the 4D seismic signals (inverse linear regression model). Therefore, this inverse model with coefficients to link time-lapse saturation-pressure changes to 4D signals could be an option to avert PEM and seismic modeling for the inversion process (Floricich et al., 2005). In fact, PEM and seismic model parameters are reflected in these coefficients (Alvarez and MacBeth, 2014). Further on, the linear summation was expanded to the three-phase flow in Falahat et al. (2013)

where the authors considered the gas saturation change term in the linear formulation. Recently, some authors have leveraged ML models for the inverse modeling of saturation-pressure changes (Cao and Roy, 2017a; Corte et al., 2020; Dramsch et al., 2019b, 2019a; Xue et al., 2019). For the total replacement of the traditional forward model in 4D seismic history matching to calibrate simulation models, one way is a binary map of 4D signals (Davolio and Schiozer, 2018). Alternatively, MacBeth et al. (2016) presented a proxy model as a replacement for the traditional forward model where the 4D seismic signal is related to saturations-pressure changes with a second-order Taylor series expansion scaled by the baseline seismic data (MacBeth et al., 2016; Oliver et al., 2021).

We must highlight that the ML models in the above applications are exclusively used to invert time-lapse property changes (such as saturation-pressure changes). Their main objectives are to propose an alternative inverse modeling method. To our knowledge, no study has focused on leveraging the ML algorithms as a proxy model for the combination of PEM and seismic model (as an alternative 4D seismic forward model). In this research, we address this gap in the literature and propose ML models to replace the traditional PEM and seismic model. As our new approach replaces the PEM and seismic model, we call it a proxy for the time-lapse seismic modeling or S4D-Proxy. The new approach was applied to a post-salt Brazilian offshore field. Three ML models were trained based on a training dataset prepared using an ensemble of reservoir models. Input features for the ML models were reservoir properties such as porosity, net-to-gross ratio (NTG), and time-lapse change in saturations and pressure. The target was a time-lapse difference of root-mean-square amplitude (dRMS). The ML models found hidden patterns between the input features and the desired output. Our proposed method could provide a better alternative approach to solve the problems when using the traditional forward model in the 4D seismic quantitative applications. Moreover, it is faster and provides an all-in-one model, unlike the traditional one, which comprises two steps.

4.3 Research objectives and scope

The specific objectives are twofold:

1) To estimate dRMS (target) from reservoir properties and their time-lapse changes (input features) using ML models
2) To compare the predicted dRMS from ML models with those from the traditional PEM and seismic model based on different criteria

The comparison criteria are based on a quantitative measure R-squared and a visual analysis of the predicted dRMS with those from the traditional PEM plus seismic model.

4.4 Theoretical background

This section has three separate parts. In the first, we briefly explain the ML algorithms that we used in our research. To train these algorithms, we employed two training strategies: (1) standard and (2) 3x3 neighborhood, which are provided in the second part. In the third part, the quantitative measure (coefficient of determination) is explained that we used it to assess the performance of different ML models to predict the dRMS.

4.4.1 Machine learning algorithms

Recently, there has been a sudden surge in the use of ML models in 4D seismic data analysis. The emergence of ML models could shape the future of the oil and gas industry to use 4D seismic data at a lower cost and time. The possibilities of using ML models in quantitative applications are vast, especially by knowing that these models automate time-consuming tasks and reduce computational storage and time. One possible use of the ML models in these applications could be as S4D-Proxy to replace the traditional forward model (PEM plus seismic model). For S4D-Proxy, two ML algorithms are considered: (1) Extreme Gradient Booster (XGBoost), and (2) Deep Neural Network (DNN).

The XGBoost algorithm is designed to be one of the most influential and fast machine learning algorithms (Chen and Guestrin, 2016). It combines the predictive power of multiple learning models (ensemble of weak learning models) to obtain a generalized and robust model. It uses decision tree models sequentially, one after another while starting from a base model. In the training phase, the base model prediction residual is calculated and trained with a new decision tree. Then, the residual of the new prediction is trained with another decision tree. In fact, each new model learns from the residual of the previous model. Sequentially, an ensemble of several decision tree models is formed, in which each model learns from its previous residual. The iterative process of tree building continues until the loss function (plus regularization term) does not minimize (improve) or converges to an expected value. Some advantages of the XGBoost algorithm are: (1) regularization term is included in the loss function, which averts overfitting; (2) the algorithm assigns weights to each leaf node of the decision tree which reduces the impacts of outliers in the input data; (3) parallel processing in the algorithm helps learning process and makes the algorithm fast. More details about the XGBoost algorithm are found in Chen and Guestrin (2016). Some applications of this algorithm in the reservoir engineering area are presented in Hadavimoghaddam et al. (2021), and Rostamian et al. (2022).

In addition to the XGBoost algorithm, a DNN structure is designed as the S4D-Proxy model. A typical structure for the DNN has three main parts. The first part is the input layer, the second is a sequence of hidden layers, and the last part is the output layer. The DNN architecture tailored for this research is based on the elements of the VGG architecture, which is an efficient structure, especially for image classification tasks (Simonyan and Zisserman, 2015). The structure is shown in Figure 4-1, where the input features run through a series of convolutional layers to capture the most relevant features from the inputs to predict the output. In the DNN structure, we start with two convolutional layers, followed by a rectified linear unit (ReLU) operator, a max-pooling layer, two other convolutional layers, and a max-pooling layer. Finally, we have two fully connected layers with the ReLU operator on top of them. All the convolutional layers use a kernel size of 3 with a stride equal to 1. The first two convolutional layers capture 32 feature maps and the last two output 64 feature maps. The fully connected layers have a size of 1024 each and, finally, the output layer predicts the labeled output of the network.

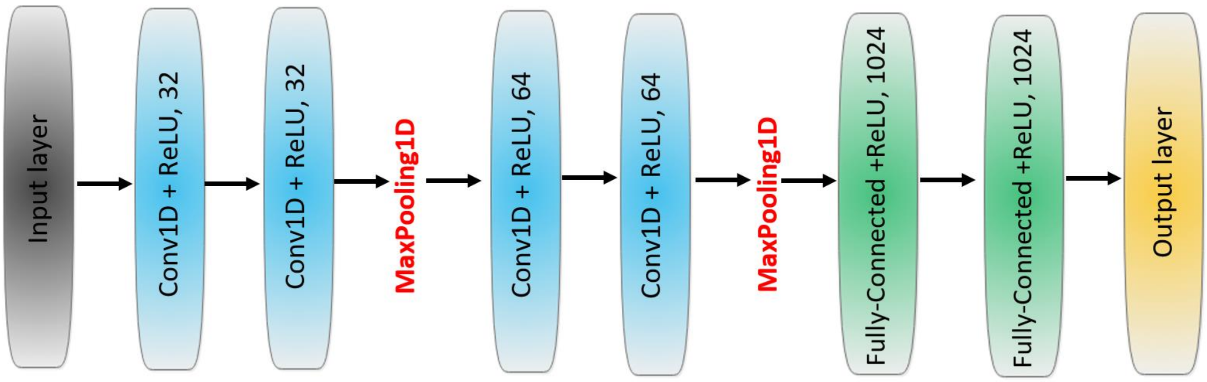

Figure 4-1: The DNN structure used as proxy to replace the traditional PEM plus seismic model in 4D seismic applications.

The training phase of the DNN algorithm is an optimization process where the optimum values for the DNN model parameters (weights and biases) are adjusted iteratively to minimize the loss function. The training phase stops when the loss function of the algorithm reaches an expected threshold value. It is worth noting that, as the DNN has more model parameters to be optimized, it is thus crucial to have a validation dataset to tune those parameters. Once the DNN architecture (as shown in Figure 4-1) is built, the training and validation datasets are fed to the DNN. After the training phase, the DNN model performance is evaluated using a test dataset.

4.4.2 Training strategies

A supervised learning approach is used to train the ML algorithms. The training dataset is labeled to assign the input features to the target with two strategies: (1) standard strategy: in this approach, the input features are labeled pointwise to a specific target. As shown in Figure 4-2a, each point (in the reservoir model, a grid) is assigned to one specific target. For example, the black point in Figure 4-2a for every input feature is labeled according to the target. (2) 3x3 neighborhood strategy: each point (or grid) and the spatial information around its neighbors are considered for the training phase. Therefore, the grid is represented by itself and its 3x3 neighbors as shown in Figure 4-2b. The black point and its 3x3 neighbors are assumed to train the ML algorithms in this figure. An obvious benefit of this strategy is that it provides more training data for the ML algorithms.

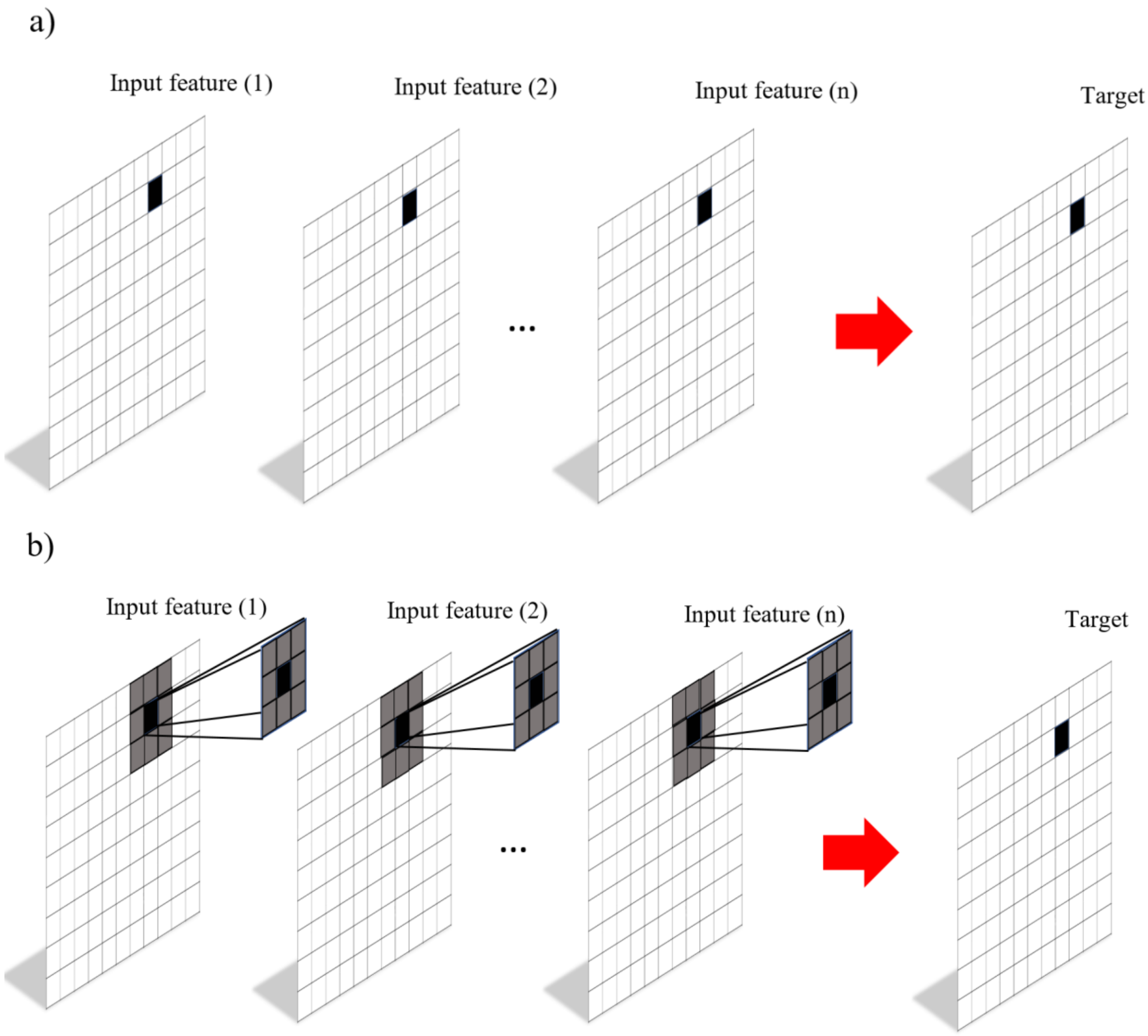

Figure 4-2: (a) standard strategy to train the ML algorithms where each black point in the input features is assigned to one specific target. (b) 3x3 neighbourhood strategy to train the ML algorithms where each black point is represented with itself and its 3x3 neighbours and are related to the target.

In the training phase, ML algorithms find hidden patterns between the input features and the target. After the training phase, the ML models are fed with the input features to predict the desired output (for our application, dRMS).

4.4.3 Quantitative measure for ML model evaluation

The coefficient of determination (R-squared) is used to evaluate the performance of each ML model. If we consider the vector of ML prediction ($\boldsymbol{d}_{pred}$) and the vector of true value ($\boldsymbol{d}_{true}$) then:

$$D = (\boldsymbol{d}_{true})^{T} * \mathbf{1}_{N_{true}} \tag{1}$$

$$R - squared = 1 - \frac{\left(\boldsymbol{d}_{true} - \boldsymbol{d}_{pred}\right)^{\boldsymbol{T}} * \left(\boldsymbol{d}_{true} - \boldsymbol{d}_{pred}\right)}{(\boldsymbol{d}_{true} - D)^{\boldsymbol{T}} * (\boldsymbol{d}_{true} - D)} \tag{2}$$

Where, $\mathbf{1}_{N_{true}}$ is a vector of all ones and its size (N_{true}) is equal to the size of $\boldsymbol{d}_{true}$. This measure is used to evaluate each ML model as shown in the result section.

4.5 Methodology

The XGBoost and DNN algorithms are trained to predict the desired output dRMS. Input features show the input variables for the training process, and the target denotes the output of the process. ML models learn to build a relationship between the input features and the target in the training process. For our application, the most common input features are reservoir properties such as porosity, net-to-gross ratio (NTG), initial fluid saturations, and initial pressure. The other input features include the time-lapse changes in the saturations and pressure. The input features are chosen based on two criteria: (1) features that are the main components of 4D sseismic signals (such as saturation-presuure changes), (2) those features that affect 4D signals and exist in petro-elastic modeling (such as porosity, and initial conditionas). For the application in this study, the target is dRMS. An ensemble of 3D reservoir simulation models is used to collect data and prepare datasets for the training and the evaluation phases. It is worth mentioning that the method is designed so that the map-based properties are extracted from the reservoir simulation models. The method to develop the ML models is divided into three main steps. Firstly, datasets are prepared for our application. The second step is to train the algorithms based on two training strategies mentioned in the previous section. The last step is to test the trained models using a portion of the prepared dataset that was not included in the training phase and is unseen for the ML models.

4.5.1 First step (dataset preparation)

The first common step in each machine learning approach is data preparation. This is important as the ML algorithms learn from the data and find hidden patterns between the input features and the target. Therefore, a good quality dataset is tantamount to being an excellent teacher to guide and correct the ML algorithms to the right answer. We use an ensemble of 3D reservoir models to prepare the dataset. The ensemble size (number of reservoir models) could have impacts on the training phase. Increasing the ensemble size provides more training samples and could capture more scenarios between the input features and the desired output. The training dataset must have variability which could provide better generalization (model ability to predict the output on unseen dataset) for the ML models. One must consider that the ensemble of 3D reservoir models could be either the prior ensemble (before data assimilation) or the posterior one (after data assimilation).

We consider $M = \{m_1, m_2, m_3, m_4, \dots, m_n\}$ as an ensemble of 3D reservoir models with the size n. Each 3D model has grid parameters (e.g., porosity and NTG) which are defined for each grid of the 3D reservoir model. For example, m_1 in the ensemble has porosity (φ_1), and net-to-gross (NTG_1) or m_2 has φ_2, and NTG_2. To follow standards and best practices to train the ML algorithms, we divide empirically the reservoir models in M to training, validation, and test models. The training models form a dataset to teach the ML algorithms; the validation models are used to calibrate the ML parameters and hyper-parameters; and the test models form a dataset to evaluate the trained ML models on unseen data. Each 3D reservoir model appears only once in the prepared dataset. We choose x models from the ensemble M as the training subset (T). In the same way, y and z are chosen from the ensemble for the validation (V), and the test (E) subsets:

Training subset: $T \subset M \quad card(T) = x$ (3)

Validation subset: $V \subset M \quad card(V) = y$ (4)

Test subset: $E \subset M \quad card(E) = z$ (5)

In these equations, T, V, and E are the training, validation, and the test subsets with sizes x, y, and z respectively. ($\subset$) denotes a proper subset from the ensemble of reservoir models (M), $card$ is cardinality and shows the number of elements in the subset. We describe the steps (A, B, C, and D) to build a dataset for the models in the ensemble (M) as shown in Figure 4-3. These steps should be repeated for all the models in the ensemble. After dataset preparation, x, and y number of models are used as training and validation datasets. The remaining z models form a dataset to test the predictions of the ML models.

4.5.1.1 Step A

Figure 4-3 provides an example of the 3D reservoir model in the ensemble. The model is simulated to generate the saturation and pressure fields. This includes 3D water and gas saturation and reservoir pressure. The input features for the training phase require the time-lapse difference of saturation and pressure changes. By knowing the baseline seismic survey time (mostly pre-production) and the monitor time (post-production), saturation and pressure changes are calculated.

4.5.1.2 Step B

Using the simulation outputs from the previous step, synthetic elastic attributes (such as acoustic impedance) are calculated through petro-elastic modeling. Input parameters of the petro-elastic model are the 3D saturation and pressure models together with the rock and fluid properties. Note that the synthetic elastic responses are generated for the monitor time as well the baseline. The petro-elastic model used in our research is described briefly in Appendix A.

4.5.1.3 Step C

1D convolutional seismic model is used to generate model simulated 3D seismic data. Subsequently, the root-mean-square (RMS) attribute is applied to the synthetic 3D seismic model to obtain the RMS attribute for baseline and monitor times. Finally, the dRMS attribute is generated by subtraction of the RMS attributes.

4.5.1.4 Step D

The last step of the data preparation is to extract 2D maps from the simulated 3D reservoir properties such as porosity, NTG, initial saturations, and initial pressure. These 2D maps of the static properties are stored in the prepared dataset. 2D maps are extracted for the simulated saturation and pressure changes (the outputs of step A), and static properties such as porosity, NTG, initial saturations and also initial pressure. Moreover, a 2D map is extracted for the synthetic dRMS from step C. The 2D maps could be an average property map in a window from top to the base of the reservoir.

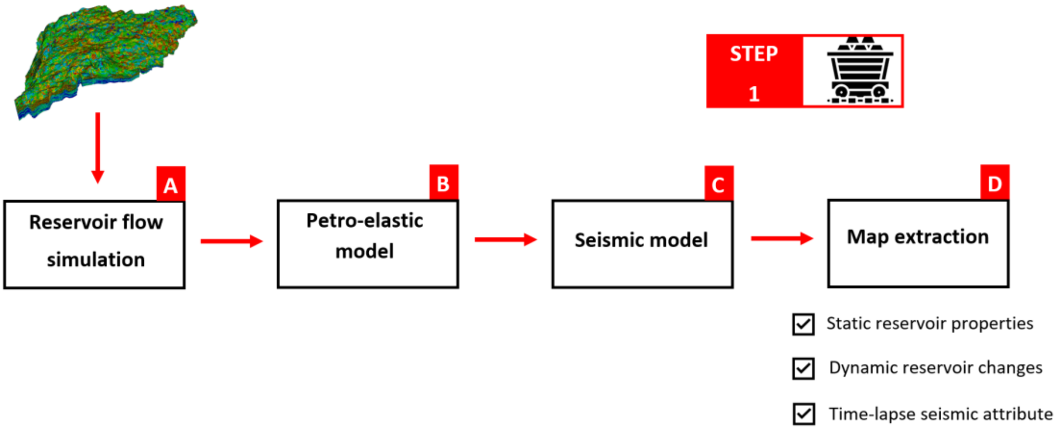

Figure 4-3: Steps for dataset preparation using an ensemble of 3D reservoir models.

The prepared dataset consists of the map-based properties for each model in the ensemble. These properties are reservoir properties, time-lapse changes, and the synthetic dRMS. It is worth noting that, when we mention a model in the prepared dataset, we mean its associated map-based properties. For instance, when we mention model n (m_n), we mean its associated map-based information including: porosity (φ_n), net-to-gross ratio (NTG_n), initial water and gas saturations ($S_{wi_{m_n}}$, $S_{gi_{m_n}}$), initial reservoir pressure ($P_{i_{m_n}}$), dynamic reservoir changes in saturations and pressure ($dS_{w_{m_n}}$, $dS_{g_{m_n}}$, dP_{m_n}), and synthetic timely difference in seismic attribute ($dRMS_{m_n}$). As mentioned, the prepared dataset is splitted into training, validation, and test datasets.

4.5.2 Second step (train the ML algorithms)

A supervised learning approach is used to train the ML algorithms, as shown in Figure 4-4. The training dataset is labeled, and the input data for the training process was paired to a particular output. The labeled training dataset helps the ML algorithms learn and correct by knowing the output. The goal is to develop an ML model that minimizes a loss function, the difference between model predictions, and the labeled outputs.

For the XGBoost algorithm, the training dataset is applied using two strategies: (1) standard training and (2) 3x3 neighborhood. These strategies are explained in the previous section and are shown in Figure 4-2. The algorithm was trained independently with these two strategies. The XGBoost learns from the labeled pairs of input and output to modify its weights. For the DNN, a 3x3 neighborhood strategy was used and the training dataset was applied to the DNN to adjust the appropriate weights of neurons. The validation dataset enables the algorithms to optimize and tune hyper-parameters. Tuning these parameters is crucial to develop efficient ML models.

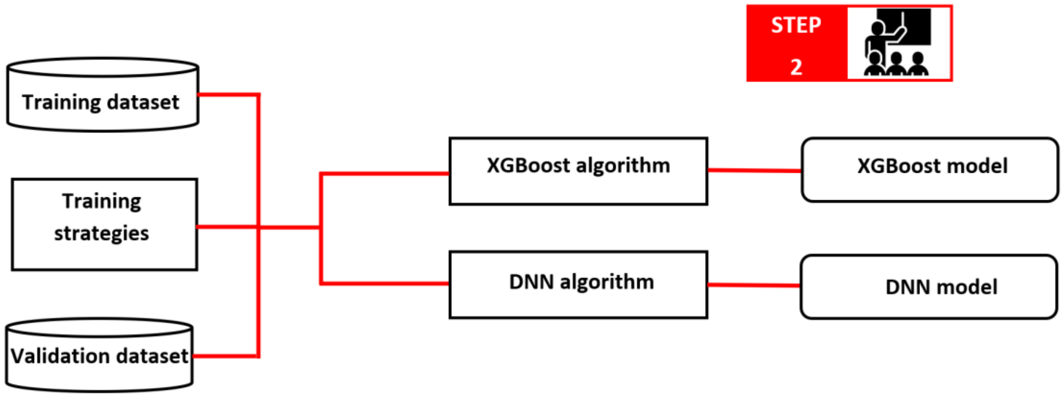

Figure 4-4: The second step in the proposed method where the ML algorithms are trained using the training and the validation datasets with the training strategies.

4.5.3 Third step (evaluate the ML models)

The performance of ML models is evaluated on the test models (Figure 4-5) based on two criteria. The first is the quantitative metric R-squared and the second is the visual comparison between the ML model predictions and the synthetic dRMS generated by the traditional PEM and seismic model. The test dataset is not used in the training phase (holdout dataset) and is unknown for the trained ML models.

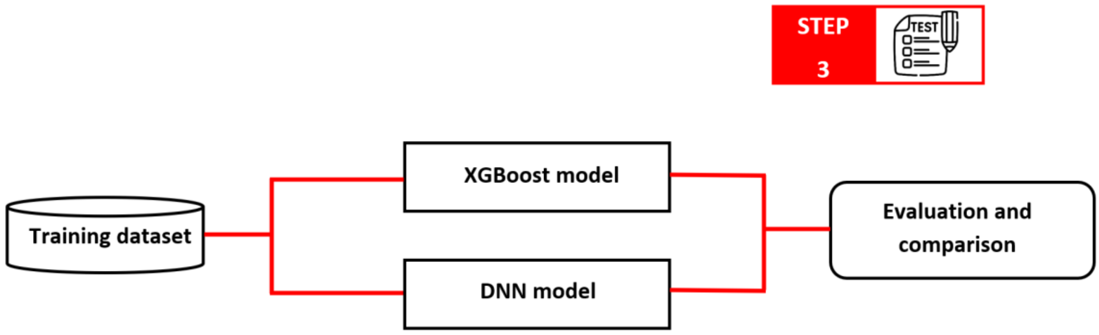

Figure 4-5: The last step in the proposed method. ML models are evaluated based on different criteria.

4.6 Application

The proposed methodology was applied to a post-salt Brazilian offshore field located in the Campos Basin. The field is composed of unconsolidated sandstone (soft sandstone) while the target reservoir is channelized and pinching out to the south and east (Maleki et al., 2019). There are 11 development wells, including seven producers and four injectors (Figure 4-6a). Production started in 2013 and injectors commenced water injection in 2014 mainly to maintain reservoir pressure. A Permanent Reservoir Monitoring (PRM) setting was installed in the field using Ocean-bottom Cable (OBC) technology which at the time of deployment was considered the deepest PRM setting in the world (Ebaid et al., 2017). The baseline (pre-production) seismic survey was acquired in 2013 and a monitor survey (post-production) in 2016. A comprehensive 4D seismic qualitative interpretation was performed for this field, as shown in Maleki et al. (2021). Main 4D signals were related to the hardening effects around the injectors (blue areas around I1, I2, I5, and I6 in Figure 4-6b) and softening effects due to gas out of the solution in the middle and the eastern parts of the reservoir (red areas in Figure 4-6b). These main 4D signals are based on the qualitative interpretation of observed 4D seismic data. In addition, there were small-scale 4D softening signals around injectors I1, I5, I6, and partially for the injector I2 (Figure 4-6b), which are likely related to pushed oil by these injectors. Moreover, small-scale 4D hardening signals in the western part of the reservoir which are likely related to aquifer water. For more detailed information, readers are referred to Maleki et al. (2021).

For this reservoir, an ensemble of 3D reservoir models was generated with the size of 200 models. Figure 4-6a shows a random reservoir model with the location of producers and injectors. This ensemble of 3D reservoir models was used to prepare the datasets (training, validation, and test) to train the ML algorithms and evaluate their performance. Each reservoir model had 218*113*58 grids with 364363 active cells and was bounded to three faults interpreted on the west flank. Model grid parameters included: porosity, net-to-gross ratio (NTG), absolute permeability in three main directions. These grid parameters were defined for each grid of the reservoir model. Apart from grid parameters, we also defined scalar parameters such as rock compressibility, oil, water, and gas relative permeabilities, and oil-water contact depth. These scalar parameters were a unique value for all the grids of the reservoir model. It is worth noting that the reservoir models in the ensemble are the prior models (before data assimilation), so the reservoir models neither match the production data nor the 4D seismic data.

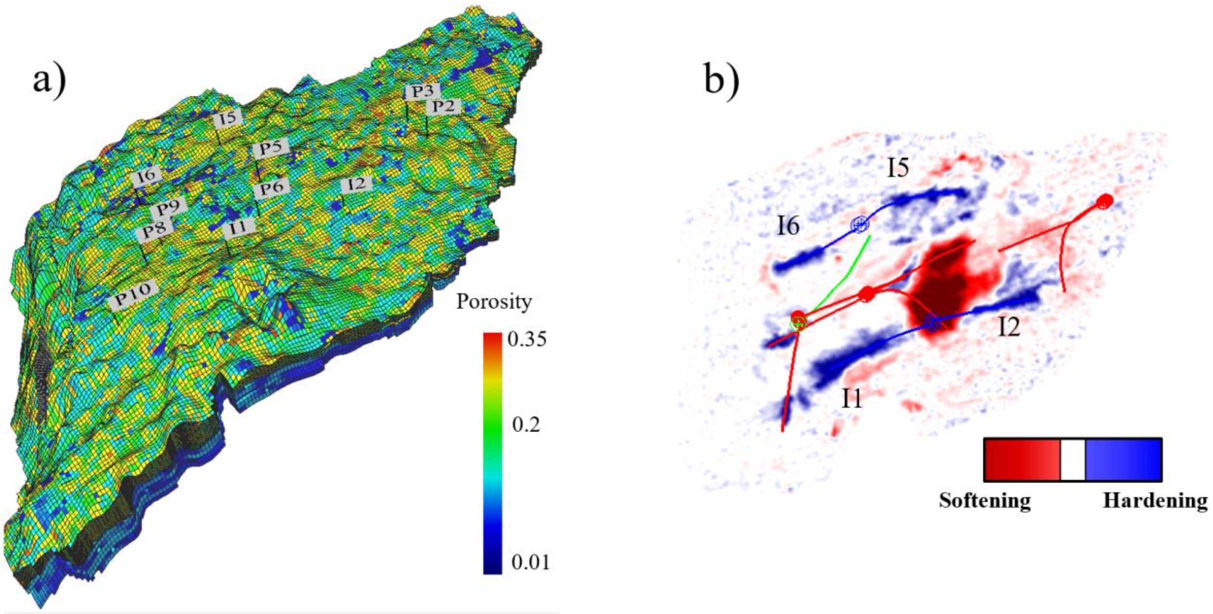

Figure 4-6: (a) a random simulation model in the ensemble showing the locations of producers and injectors; (b) 4D seismic signals showing the main softening (red) and hardening (blue) signals for the reservoir.

Three ML models (shown in Table 4-1) were developed under two setups: (1) different ML algorithms (XGBoost and DNN) and (2) different training strategies (standard and 3x3 neighborhood). The combination of different ML algorithms and training strategies developed three ML models. The first model used the XGBoost algorithm with a standard training strategy and was called XGB. The second was named XGB-3x3 and used the XGBoost algorithm and the 3x3 neighborhood as training strategy. The last model was labeled DNN-3x3 and used the DNN algorithm with the 3x3 neighborhood strategy for the training phase. For ease of analysis and comparison, a color-code was given to each ML model. The XGB model was given red, XGB-3x3 was coded green, and DNN-3x3 was given blue. Note that in the result section, we use “reference solution” to refer to the synthetic dRMS for test models in the test dataset which is generated with the traditional PEM plus seismic model.

Table 4-1: Three ML models to predict the desired output

ML model	Name	Machine learning algorithm	Training strategy	Color code
1	XGB	XGBoost	Standard	
2	XGB-3x3	XGBoost	3x3 neighbourhood	
3	DNN-3x3	Deep Neural Network	3x3 neighbourhood	

The prediction of each ML model is analyzed quantitatively with R-squared and a visual comparison is used to assess the prediction of the ML models qualitatively.

4.7 Results

The results of the ML experiments are presented in four parts. The first part explains the data preparation for our case study. The second evaluates quantitatively the ML models' predictions. Visual comparisons of the proxy predictions with those from the reference solution are presented in the third section. Finally, we discuss the elapsed time for the ML models predictions versus the traditional PEM and seismic model (reference solution).

4.7.1 Data preparation and training phase

Knowing the baseline (2013) and the monitor (2016) times, a dataset was prepared based on the steps described in the methodology section 4.1. The steps were repeated for all the models in the ensemble. Eventually, we divided the prepared dataset for our application into the training (70% of the models in the ensemble, or 140 models), the validation (10%, or 20 models), and the test dataset (20%, or 40 models). The performance of the three ML models (XGB, XGB-3x3, and DNN-3x3) was evaluated based on the quantitative measure R-squared and visual comparison of the predicted dRMS versus the reference solution (PEM plus seismic model which are described in Appendix C).

4.7.2 Quantitative measure R-squared

We analyzed and compared the responses of the three ML models on the test dataset. For each ML model result, a boxplot was drawn for the group of the R-squared in the test dataset (Figure 4-7a). Each ML model is shown in Figure 4-7 with its own color code. Aside from the boxplots, the group of the R-squared was represented with a histogram shown in Figure 4-7b. The results demonstrate that the DNN-3x3 had the best predictability when compared to the other two ML models. The mean R-squared of the DNN-3x3 on the test dataset was 0.64. However, the mean values for the XGB-3x3, and XGB models were 0.62, and 0.56 respectively.

Although both XGB-3x3 and DNN-3x3 had similar upper quartile values (0.72), the DNN-3x3 model had a maximum R-squared equals 0.8 while that value for the XGB-3x3 model was 0.78. An interesting observation in Figure 4-7a concerns the median value of these two ML models. The blue boxplot in the figure shows that the median value for the DNN-3x3 model was 0.67 and, for the XGB-3x3 (the green boxplot), the value was 0.64. This indicates that when, comparing the group of R-squared, the DNN-3x3 had more test models with R-squared higher than 0.67 compared to the XGB-3x3. In fact, a closer look at the results revealed that the DNN-3x3 had 20 test models with R-squared higher than 0.67, while the XGB-3x3 had only 14 test models. In line with our previous observation, Figure 4-7b also indicates that the DNN-3x3 had more test models with R-squared higher than 0.67 compared to the XGB-3x3 (One can compare the blue and red histograms in Figure 4-7b).

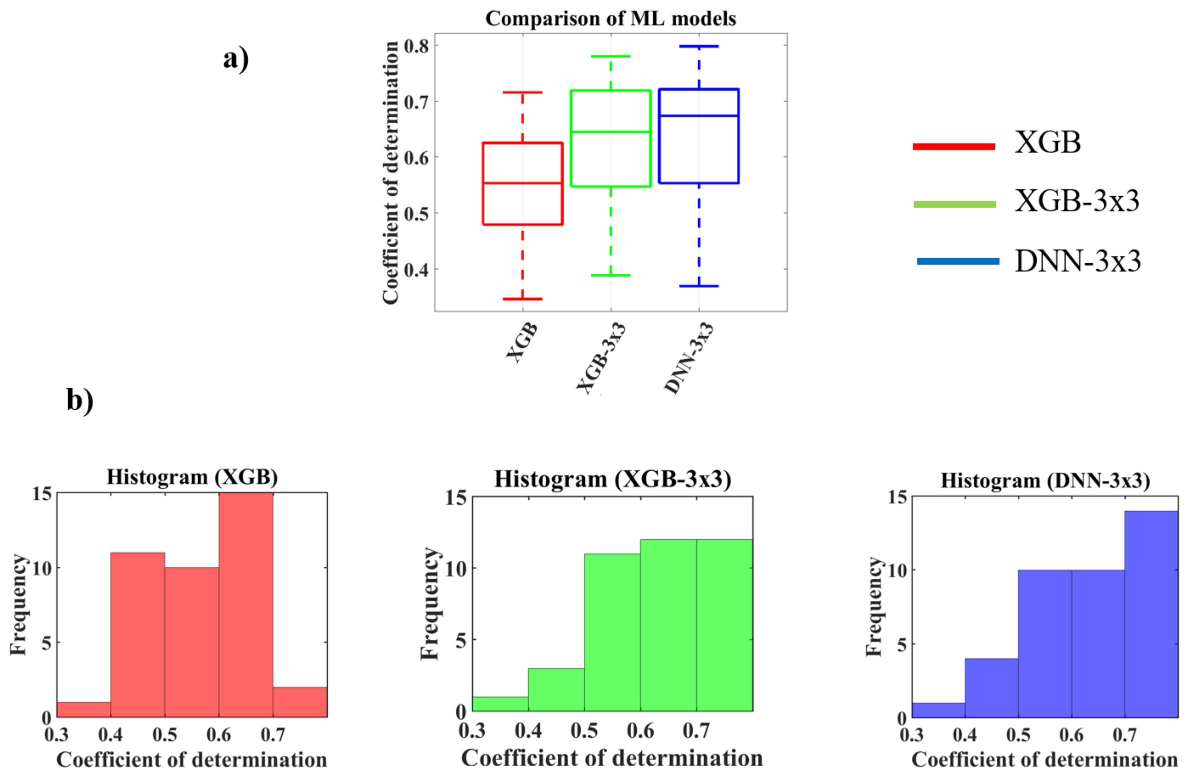

Figure 4-7: Boxplots for different ML models with their respective colours in (a); Histograms for the XGB, XGB-3x3, and DNN-3x3 with their colours.

The comparison of the XGB and the XGB-3x3 showed that the XGB-3x3 provided better predictability compared to the XGB. For example, comparing the red boxplot in Figure 4-7a with the green one indicates that all the five-number summaries (minimum, maximum, and quartiles) for the XGB-3x3 were better than the XGB model. The histograms in Figure 4-7b also indicate the same conclusion in much the same way. The XGB-3x3 model gave better results as in its training phase, the 3x3 neighborhood strategy was adopted. This shows the importance of including spatial information in the input features (information around a point paired to output) to train the ML algorithms.

The R-squared measure was used to analyze different ML models, but we also visually compared the proxy predictions with the reference solution (PEM plus seismic model). This comparison helped us observe the performance of each ML model to predict the main 4D signals of the reservoir.

4.7.3 Visual comparison of ML models predictions

For each ML model, the R-squared values in the test dataset were divided into four ranges. The first had an R-squared between [0.7, 1], which we called the "excellent" category. The second was between [0.5, 0.7] and called the "good" category. The third range had an R-squared between [0.3, 0.5], and the fourth was [0, 0.3], which were named "medium" and "low" categories, respectively. The four categories of R-squared (excellent, good, medium, and low) provided a suitable platform to compare different ML models visually. For each category, we selected a common model in the test dataset to compare the proxy predictions.

For a test model in the excellent category, all three ML models were able to predict the main 4D signals, as shown in Figure 4-8. Comparison between the reference solution and the proxy predictions showed that the hardening signals around the injectors were captured by the ML models (Figure 4-8 blue ovals). Though all three ML models predicted the hardening signals around the injectors, the DNN-3x3 model captured more details around the injectors. DNN-3x3 performed well, especially around injector I6, providing a good prediction for the softening red signal around that injector. Moreover, the DNN-3x3 predicted the hardening signal located in the eastern part of the reservoir (blue arrows in Figure 4-8). The XGB-3x3 model had not predicted that hardening signal. The results from the DNN-3x3 model demonstrated its ability to predict subtle changes in the reservoir. The reason could be in the DNN architecture used for our research, where different convolutional layers could be able to capture more features in the input data to train the DNN algorithm.

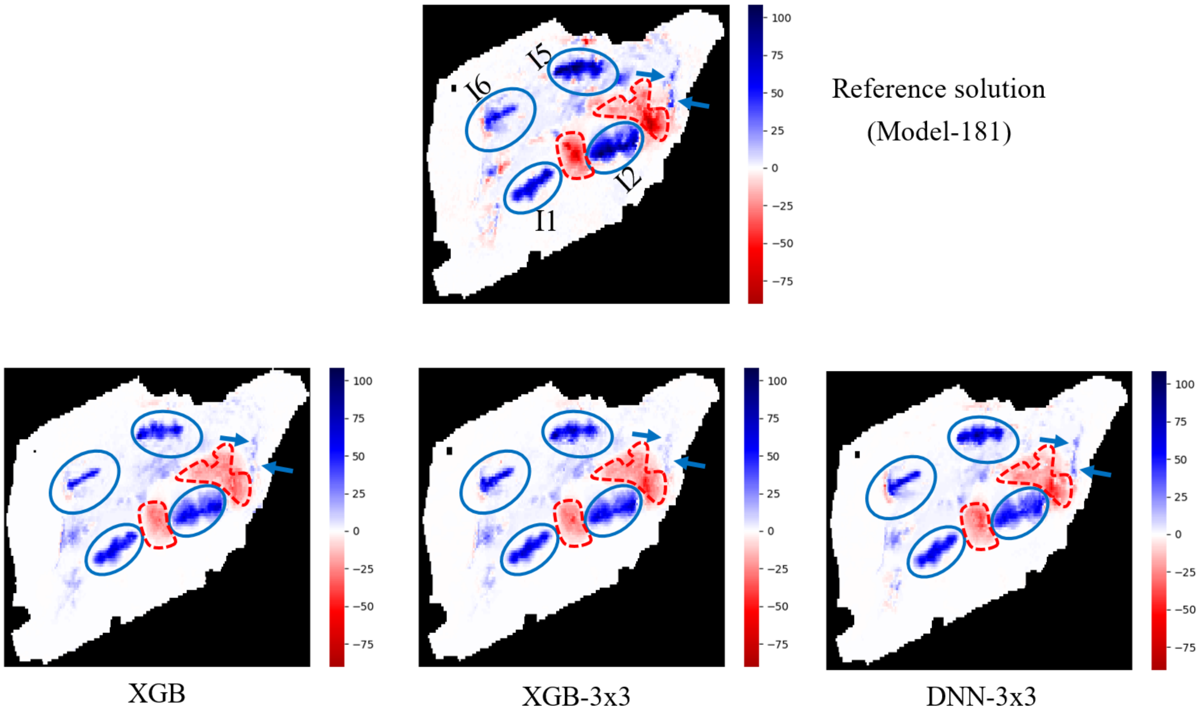

Figure 4-8: Visual comparison between the proxy dRMS predictions with those from the reference solution.

The softening signals due to the gas out of the solution in the center and the right flank of the reservoir were also predicted by all three ML models (red dashed areas in Figure 4-8). By comparing the results, we observed that the prediction of the softening signal in the right part of the reservoir was slightly better in the DNN-3x3 model. A further comparison between the XGB and XGB-3x3 models revealed comparable results, but the results of XGB-3x3 were better mainly in the locations of the softening signals. This underlines the effect of neighboring information to predict the output value by the XGB-3x3 model. A similar effect was observed in the analysis of the R-squared for these two ML models, where the XGB-3x3 model yielded a higher R-squared compared to the XGB model.

In much the same way, we analyzed the prediction results for a test model in the good category (R-squared from 0.5 to 0.7). The analysis tied well with our previous results for a test model in the excellent category. Here, the comparison of the predictions showed that the three ML models were nearly identically capable of predicting the hardening signals around the injectors (blue ovals in Figure 4-9). Additional observations revealed that the DNN-3x3 model had slightly superior predictions for the subtle 4D signals (small-scale 4D signals), as shown in Figures 4-10 and 11. For example, the DNN-3x3 model better predicted the softening signals around injectors I5, and I6 (a close-up view in Figure 4-10) and the DNN-3x3 model predicted the 4D signals located in the southern part of the injector I2, as shown in a close-up view in Figure 4-11. Contrary to the predictions of the hardening signals where all ML models were at the same level, the DNN-3x3 model had better predictions in terms of the softening signals than the XGB-3x3 and XGB models (red arrows in Figure 4-9). The DNN-3x3 model better captured the softening signal in the eastern part of the reservoir than the XGBoost models. This characteristic of the DNN model is almost in line with our previous observation for the test model in the excellent category. Comparison of predictions from the XGB-3x3 and XGB models showed that the 3x3 neighborhood strategy in the training phase helped the XGB-3x3 model predict better in some locations. For example, the prediction of the softening signal in the eastern part of the reservoir was better for the XGB-3x3 model compared to the XGB model.

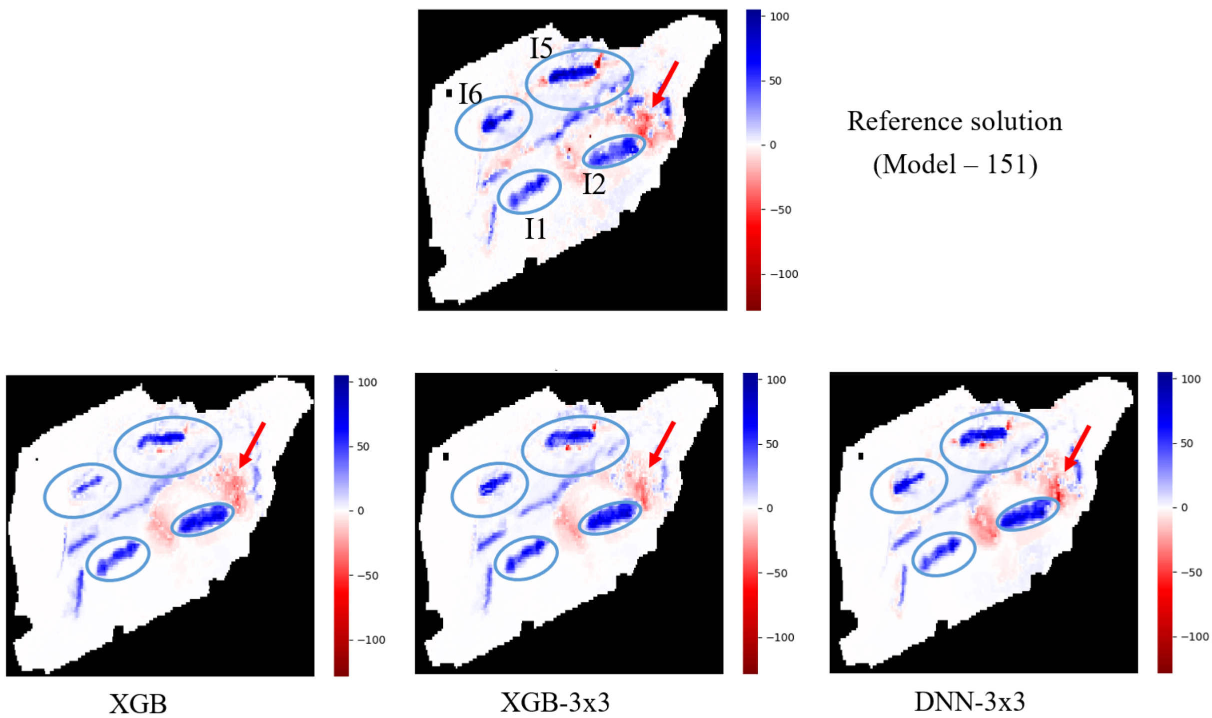

Figure 4-9: dRMS predictions with different ML models and the reference solution.

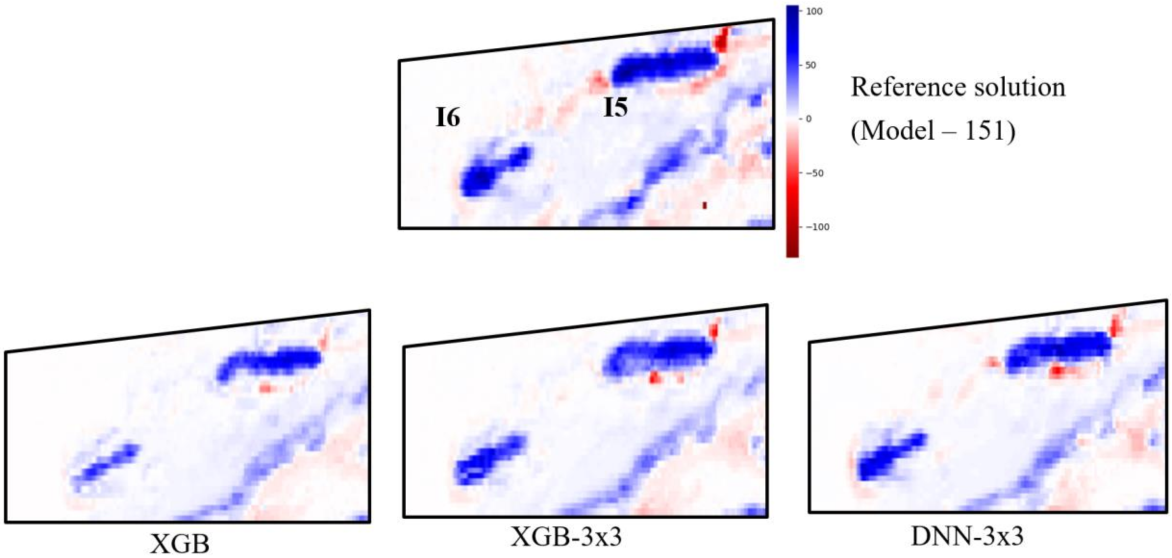

Figure 4-10: small-scale softening 4D signals around injectors I5 and I6. Here, proxy predictions are presented where the DNN-3x3 has more details compared to other two ML models.

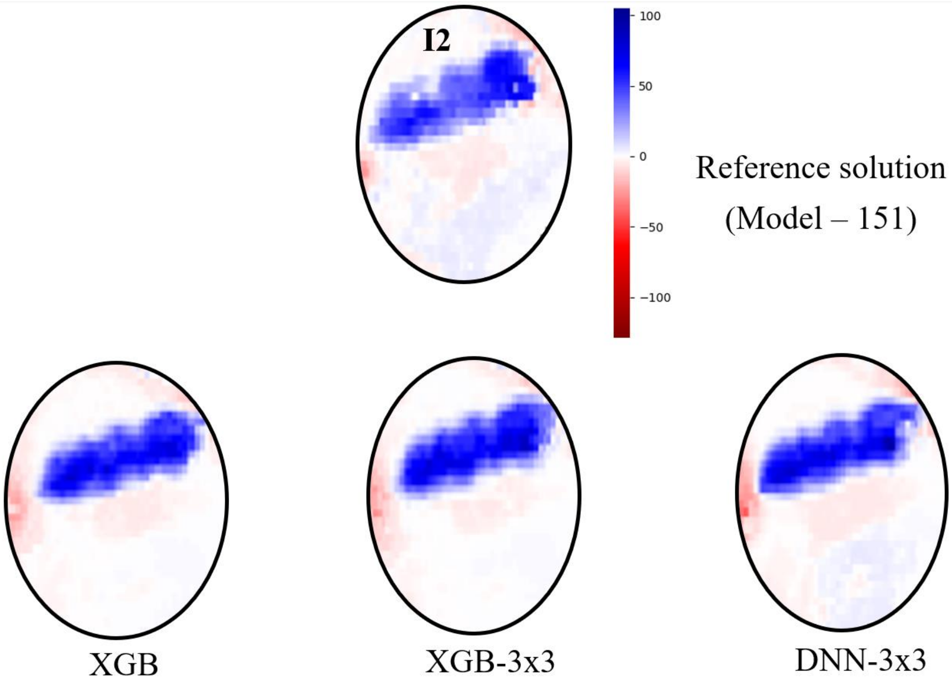

Figure 4-11: small-scale 4D softening signal around injector I2 which captured by the DNN-3x3 model.

To be consistent in our visual evaluation of the ML models, we compared a test model in the medium category for all three ML models. Figure 4-12 shows the reference solution and the ML models predictions. We observed that neither the DNN nor the XGBoost models could properly predict the hardening signals around injectors I5 and I6 (straight blue lines in Figure 4-12). One should note that the test model analyzed was in the medium R-squared category; therefore, the predictions of 4D signals are not as good as previous test models. The hardening signals for injectors I1 and I2 were captured by almost all ML models and a comparison of these signals showed that the predictions were equal and at the same level (blue ovals in Figure 4-12). Like the hardening signals, the prediction of the ML models for the softening signals was also comparable. However, some details were predicted by the DNN-3x3 model, while the XGB-3x3 and XGB models were not able to capture them. For example, Figure 4-13 shows the softening (red) signal near injector I2 in close-up. In this figure, the signal was predicted slightly better by the DNN-3x3 model compared to the XGB-3x3 and the XGB models.

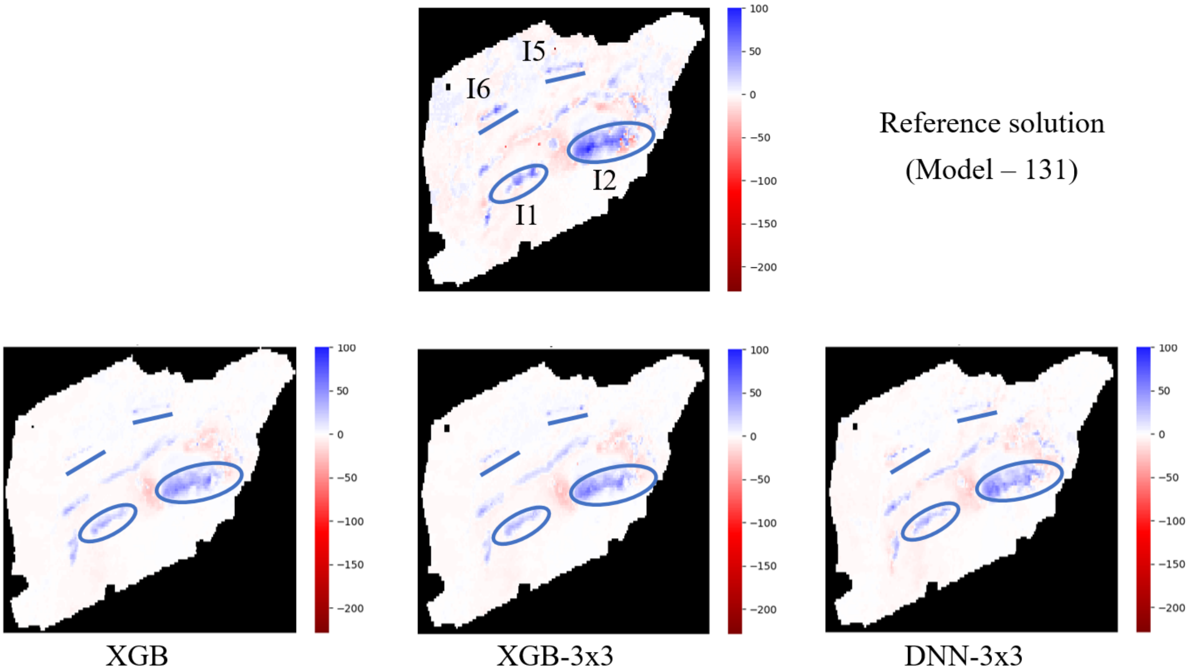

Figure 4-12: Performance of different ML models for a test model in the medium category.

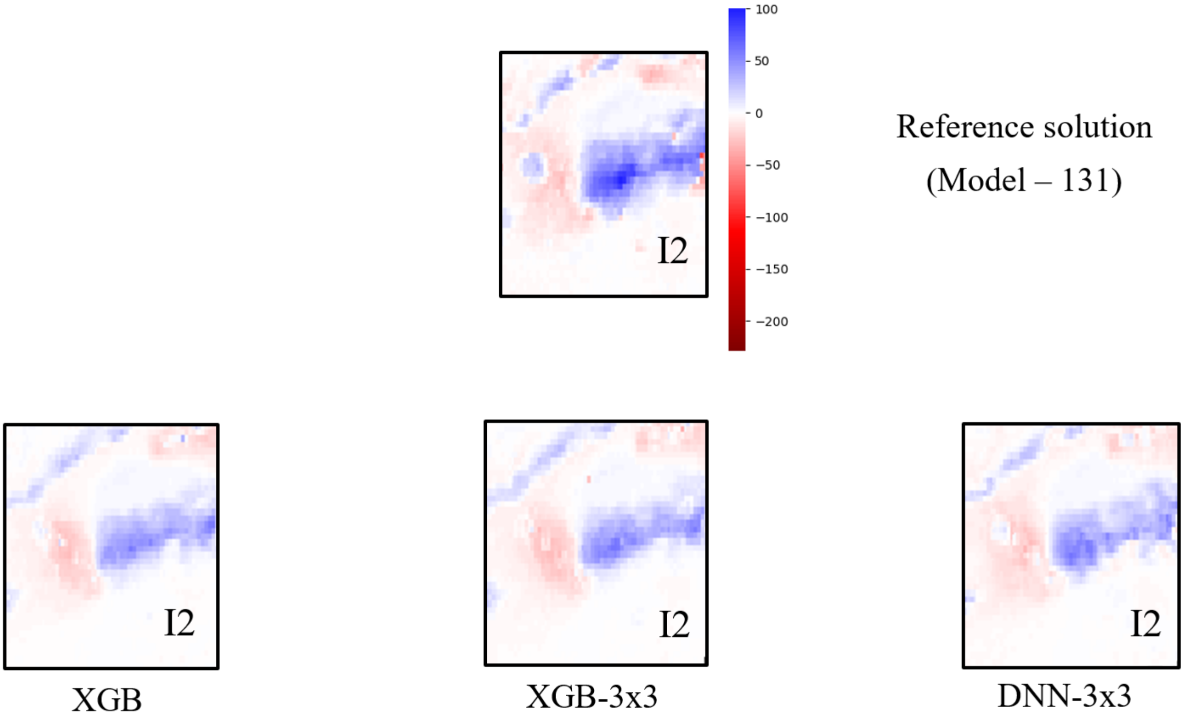

Figure 4-13: close-up of the softening (red) signal located in the centre of the reservoir near injector I2.

4.7.4 Computational time of the S4D-Proxy versus the traditional approach

The elapsed time for the S4D-Proxy predictions and the traditional PEM plus seismic model calculation were analyzed and compared. Using the ensemble of reservoir models (200 simulation models), the elapsed times to generate synthetic dRMS with the traditional approach and the ML models were computed. It is critical to understand how different the traditional and our new approaches are in terms of computational time. The traditional approach took 36 hours to generate dRMS for the ensemble of reservoir models. In contrast, the XGBoost models (XGB and XGB-3x3) took less than 30 minutes for training and some extra minutes to generate the synthetic dRMS for the ensemble of reservoir models. The same procedure for the DNN-3x3 model took about 4 hours for training and some minutes to compute the synthetic dRMS. This result demonstrates that the S4D-Proxy models reduce the computational cost of the traditional forward model. They also automate 4D seismic forward modeling, which is especially interesting for petroleum engineers performing 4D seismic history matching to calibrate reservoir simulation models. We used a multi-user cluster of computers to generate the synthetic dRMS for the ensemble of simulation models with the traditional approach. Therefore, the elapsed time was subjected to the task scheduling in the cluster and the node failure of the system. However, the mentioned times were the averaged elapsed times calculated from several attempts. Moreover, the ML models application also could be optimized to perform faster.

4.8 S4D-Proxy applications in 4D seismic data analysis

This section brings the most immediate applications of the new 4D seismic forward model S4D-Proxy. The proxy can be used in more diverse 4D seismic quantitative applications. Perhaps the two most prominent use cases of our new approach are: (1) as a forward model in the joint production and 4D seismic data assimilation to update simulation models, (2) as a 4D seismic forward model in the saturation-pressure changes inversion.

4.8.1 4D seismic forward model in the joint production and 4D seismic data assimilation

Production and 4D seismic data could be used to update reservoir simulation models. Joint assimilation of these data (or 4D seismic history matching) is performed in a common domain to compare the synthetic seismic data (forward modeled) with the observed one. 4D seismic data could be integrated in different domains, such as seismic amplitude, seismic impedance, or saturation-pressure changes domain. Each data integration domain has its pros and cons. For example, one practical advantage of the seismic amplitude domain is the prompt access to the observed data. 4D seismic data in the amplitude domain is readily available after the 4D seismic processing and there is no need to run 4D seismic inversion. Although the prompt availability of the observed data is highly appealing, generating the modeled 4D seismic data for seismic history matching process could be complicated and time-consuming. There is a primary problem related to the traditional 4D seismic forward modeling in these applications, which uses PEM (the first step) and the seismic model (the second step). This is further compounded when an ensemble of models is used for the joint data assimilation, where hundreds or thousands of simulation runs are performed. For the joint data assimilation, the S4D-Proxy perfectly fits as a 4D seismic forward model to accelerate the 4D seismic data integration. The proxy replaces the time-consuming task of the traditional 4D seismic forward modeling approach and could reduce the turnaround time of the joint data assimilation. For example, the proxy can be used especially with the iterative ensemble-based data assimilation algorithms such as Ensemble Smoother with Multiple Data Assimilation ES-MDA (Emerick and Reynolds, 2013) or iterative Ensemble Smoother iES (Chen and Oliver, 2013) to reduce turnaround time in simultaneous assimilation of production and observed 4D seismic data.

S4D-Proxy should be of broad interest to petroleum engineers. It provides an automated 4D seismic forward model tool to perform the joint data assimilation in the amplitude domain. This forward model tool averts the multidisciplinary nature of the traditional approach. It makes the 4D seismic forward model more accessible to petroleum engineers and reduces their dependency on geoscientists. As the S4D-Proxy is faster than the traditional approach, it could lead to a quick pace delivery of the data assimilation results (fast data assimilation). As shown in the results section (section 6.4), proxy application reduced the 4D seismic forward modeling time down to minutes. This is significant especially for the joint data assimilation with several iterations where the cycle time of the data assimilation could reduce considerably with the S4D-Proxy model. The S4D-Proxy model enables petroleum engineers to accelerate 4D seismic forward modelling in the joint data assimilation process (4D seismic history matching) and delivers assimilation results in hours unlike the traditional forward model in 4D seismic history matching, which is time-consuming and the results might take days or weeks. In addition, the proxy generates map-based dRMS. Therefore, it averts the depth to time conversion needed in some joint data assimilation projects.

4.8.2 4D seismic forward model in saturation-pressure changes inversion

For the inverse modelling of saturation-pressure changes, the proxy model can also be used as a 4D seismic forward model. In this inverse problem, the uncertain model parameters are saturation-pressure changes and the S4D-Proxy has both changes as input features and can be used with data assimilation algorithms (such as abovementioned iterative ensemble-based algorithms) for the inversion of saturation and pressure changes. One must consider that, naturally the preference of petroleum engineers is to perform the joint observed 4D seismic and production data assimilation in the saturation-pressure change domain. Therefore, our proxy offers a fast approach to invert saturation and pressure changes. These applications in sections 7.1 and 7.2 make the proxy model especially valuable in the permanent reservoir monitoring (PRM) settings.

4.8.3 S4D-Proxy model and permanent reservoir monitoring (PRM)

Quantitative applications of 4D seismic data in PRM settings require extreme speed to use the information in a timely manner. Therefore, the oil and gas industry turns to fast-track approaches to use 4D seismic information. Even as the methods for fast-track 4D seismic processing are quickly evolving, quantitative applications of these data in a fast way are lagging behind. This presents a challenge as timely use of the 4D seismic information could be helpful in model-based reservoir management and development activities. In this context, S4D-Proxy model could be calibrated once in the life cycle of a field as a 4D seismic forward model and can be used repeatedly in the PRM setting. It is a fast and on-hand tool which enables petroleum engineers to update subsurface model(s) rapidly when a monitor seismic survey is acquired. S4D-Proxy could facilitate the data assimilation procedure (model update) and makes it faster and more efficient in the PRM settings. This accelerated use of information could be essential for rapid model-based decision making. In general, fast subsurface model updating and rapid decision making are among important advantages of the PRM settings which lead to cost reduction and increase profitability in these projects. Our proxy model could be seen a good step forward (a fantastic initiative) to accelerate the use of 4D seismic data in the PRM settings and take full advantage of 4D seismic information in these setting. Combination of fast-track 4D seismic processing and S4D-Proxy model in the PRM settings could take 4D seismic quantitative applications to a level where rapid model-based decision making is not a subjective dream but an objective reality. In addition, the proxy could be helpful in the 4D seismic feasibility study to plan the appropriate time span to acquire the monitor seismic survey(s).

4.8.4 Limitations of the proxy model

Although S4D-Proxy model could be an alternative 4D seismic forward model, the proxy model might have shortcomings in accuracy for some complex cases (such as carbonate reservoir) or highly heterogeneous reservoir model. Moreover, the proxy model predictions could fall short when 4D signals are controlled with several competing effects. There could be two solutions to improve the proxy performance for these cases: (1) to increase training data samples, and (2) to increase neighboring information from 3x3 and extract more spatial information around a data point within regions of interest of sizes 5x5 or 7x7. Increasing neighboring information might reveal more heterogeneity and improve the proxy predictions. It is important to note that for our application, the S4D-Proxy model was developed using prior (before data assimilation or history matching) ensemble of reservoir models. Training the ML algorithms with posterior ensemble (after history matching) may alter or improve the proxy predictions as the history matching process might expose some hidden geological features and correct our prior reservoir models (especially for complex cases). However, two points should be considered here. Firstly, proxy replaces the traditional 4D seismic forward modelling which is time-consuming and provides a fast tool to save time. Using history matched models for training might overshadow this fact as history matching procedure could be time-consuming for some large-scale simulation models of giant reservoirs. Secondly, generalization is an important ability for ML models to fit and predict unseen data. History matching procedure reduces uncertainty and variability of reservoir models and might have adverse effect on training phase and hinder ML model generalization. It is worth noting that S4D-Proxy is an approximation of the 4D seismic forward modelling (PEM plus seismic model) which carries proxy model errors and should be treated when the proxy is implemented in 4D seismic quantitative applications. For more information about proxy model error treatment, readers are referred to Danaei et al. (2022). Finally, we could consider recalibrating the S4D-Proxy model in fields with intense production and/or injection activities. The recalibration process allows users to account for possible unmapped production scenarios.

4.9 Conclusions and future work

This paper proposed an alternative 4D seismic forward model to replace the traditional petro-elastic and seismic models. Quantitative applications of 4D seismic data such as 4D seismic history matching traditionally require a 4D seismic forward model with two sequential steps. The first is a petro-elastic model, followed by a seismic model. Aside from being a step-by-step process, the traditional approach is time-consuming and requires high computational cost within data assimilation frameworks. Moreover, an extra expense is its multidisciplinary nature to develop petro-elastic and seismic models and implement them in the data assimilation procedure. Therefore, we proposed a methodology to replace the traditional approach with machine learning models (S4D-Proxy). Our new approach provides an automated 4D seismic forward model and performs forward modeling all at once (an all-in-one model). We used machine learning models to identify hidden patterns between the input features (e.g., porosity, initial saturation, fluid saturation and pressure changes) and the desired output (time-lapse difference of root-mean-square amplitude). Two machine learning algorithms were used: (1) Extreme Gradient Boosting (XGBoost) and (2) Deep Neural Network (DNN). These algorithms were trained with two training strategies. The first strategy was the standard point-to-point to relate the input features to the target, and the second strategy considered the spatial information (3x3 neighbors) around each point of the input features to link them to the target. Eventually, three machine learning models were developed: XGBoost model with the standard training, XGBoost model with 3x3 neighbors training strategy, and a DNN model with 3x3 neighbors training strategy. Their performances were evaluated and compared with those from the traditional petro-elastic and seismic models based on the quantitative measure R-squared and the visual comparison of the machine learning models predictions. The specific conclusions are as follows:

1- The DNN model with a 3x3 neighbors training strategy performed better than the XGBoost models on the test dataset. Visual evaluation of the predicted dRMS from the DNN model showed that the model predicted the hardening and softening 4D signals and some minor details (small-scale 4D signals). The DNN model provided the best R-squared measures overall which further validate our findings.
2- The analysis of the XGBoost models with different training strategies showed that the model with a 3x3 neighbors training strategy offered better dRMS predictions in terms of the R-squared and the visual evaluation. Based on that, we recommend using a neighborhood strategy for the training phase, especially for map-based input features. The neighborhood strategy (for our application 3x3) uses spatial information and positively affects the machine learning model predictions.
3- The machine learning (XGBoost and DNN) models accelerate 4D seismic forward modeling and provide an all-in-one model while averting the multidisciplinary nature of the traditional 4D seismic forward model.
4- We recommend the DNN model with a 3x3 neighbors training strategy as a fast 4D seismic forward model to replace the traditional petro-elastic and seismic models in 4D seismic quantitative applications.

Future research could investigate the application of the S4D-Proxy in 4D seismic history matching. S4D-Proxy development in the presence of geomechanical effects could be desirable for future research and investigation. In addition, future work might also consider unsupervised machine learning algorithms for the proxy model development.

4.10 Acknowledgment

This work was carried out in association with the ongoing project registered under number 20372-9 ANP as the "Development of integration between reservoir simulation and 4D seismic - Phase 2" (University of Campinas [UNICAMP]/Shell Brazil/ANP) funded by Shell Brasil Petróleo Ltda. under the ANP R&D levy for "Investment Commitment to Research and Development." The authors are grateful for the support of the Center for Petroleum Studies (CEPETRO-UNICAMP/Brazil), the Department of Energy (DE-FEM-UNICAMP/Brazil), the Research Group in Reservoir Simulation and Management (UNISIM-UNICAMP/Brazil), Energi Simulation, and CNPq. In addition, a special thanks to CGG, Schlumberger and CMG for software licenses.

5 Evaluation of a deep neural network algorithm as a proxy for 4D seismic forward modeling

Authors: S. Danaei, M. Cirne, M. Maleki, D. J. Schiozer, A. Rocha, A. Davolio
Submited to: Journal of Geoenergy science and engineering (Minor revision)

5.1 Abstract

Time-varying 3D seismic (4D seismic) data might be used with production data to calibrate reservoir models through joint data assimilation, also known as 4D seismic history matching. This application traditionally requires a 4D seismic forward model with two back-to-back modeling steps (a petro-elastic model and a seismic model). The traditional seismic forward model is a time-consuming and complex process. Therefore, Deep Neural Network (DNN) algorithms could offer a proxy to replace it. To develop the proxy, the DNN is trained to discover patterns between the input features (such as porosity, and saturation-pressure changes) and the output (for our case, time-lapse change of root-mean-square amplitude, or dRMS). Reservoir models (especially an ensemble of models) provide sufficient training data points as each reservoir grid serves as a data point. However, the choice of the reservoir model for training could vary greatly. One could train the DNN with the prior ensemble of reservoir models before observed data assimilation or the posterior ensemble after data assimilation (also known as history-matched or calibrated models). The question here is to evaluate the DNN prediction when it is trained with various choices of reservoir models. In addition, extracting the spatial information around a data point in the input features and relating them to the output could be beneficial for developing the DNN model. The spatial information provides some spatial correlation to the DNN estimates. Another question is to evaluate the influence of spatial information in feature extraction on the DNN model prediction. In this research, two experiments are designed to address the above questions. In the first, a DNN is trained on three reservoir model ensembles: (1) prior, (2) posterior after production data assimilation, and (3) posterior from production plus 4D seismic data assimilation. For the second, neighboring information around a data point in the input features is extracted with different strategies. This includes strategies that extract information around a data point within regions of interest of sizes 3x3, 5x5, and 7x7. Two experiments were performed on reservoir models from a Brazilian offshore field. The first showed that the DNN trained on the prior ensemble had promising results on all the test models. This DNN model generalized better than the ones trained on the

posterior ensembles. The prior ensemble's variability could improve the DNN model's performance in predicting 4D signals. However, the lack of variability in the posterior ensembles was a limiting factor. For instance, the DNN from the posterior ensemble of production plus 4D seismic data assimilation showed a bias toward predicting 4D signals (in our case softening signals), which is not preferable. The results from the second experiment also showed that a 3x3 neighborhood strategy was enough to extract spatial information from the inputs to train the DNN. In terms of training elapsed time and visual comparisons between strategies, the 3x3 strategy yielded acceptable results.

5.2 Introduction

Information related to dynamic changes (such as saturation- pressure changes) from oil and gas reservoirs during production could help reservoir development and management activities (Buksh et al., 2015; Gee et al., 2017; Maleki et al., 2022). To capture this information, time-lapse seismic (4D seismic) data might sort out the production-induced changes in the reservoir and assist decision-makers in mitigating risks in the development strategies (Pathak et al., 2018). Qualitative analysis of the 4D seismic signals could explain the reasons which caused and controlled the 4D signals (Danaei et al., 2018, 2017; Maleki et al., 2021). Although this analysis is helpful, the quantitative use of 4D seismic data gives engineers a thorough understanding of the reservoir. The quantitative analysis uses a wealth of different data assimilation (inversion) algorithms to estimate dynamic changes from 4D seismic data or calibrate reservoir simulation models. A challenging problem in these applications is long turnaround time of using 4D seismic data, which might hamper the benefits of its timely use. Therefore, machine learning (ML) algorithms could accelerate the use of 4D seismic data in the quantitative applications (Maleki et al., 2022; Xue et al., 2019).

The possibilities for using ML algorithms in the oil and gas industry are endless. With these algorithms, the traditional methods and models (such as forward modeling, or inverse modeling) are changing slowly but surely. With an acceptable level of detail that is particularly matched with humans, ML models can replace tasks in 4D seismic processing and qualitative interpretation. Some applications of the ML models are discussed in the literature. Oldenziel et al. (2002) used multiple seismic attributes and a pattern recognition tool (neural network model) to detect 4D seismic signals. Matos et al. (2006) employed an unsupervised learning approach (self-organizing map (SOM)) to classify and detect time-lapse seismic changes. The application of machine learning models (such as neural networks) for 4D seismic data processing is reported in Alali et al. (2020) and Yuan et al. (2019).

At least two immediate ML applications could be considered for 4D seismic quantitative analysis. The first is to estimate dynamic reservoir changes from 4D seismic data. This application applies ML algorithms to invert time-lapse changes in reservoir properties, such as saturation-pressure changes. Basically, ML algorithms are used for inverse modeling of saturation-pressure changes (Cao and Roy, 2017; Côrte et al., 2020; Xue et al., 2019). The second is to use ML models as a proxy (we call it S4D-Proxy) to replace the traditional approach of 4D seismic forward modeling. In this application, ML algorithms could be used as a forward modeling tool to substitute the traditional approach of 4D seismic modeling, which has two sequential steps. Petro-elastic modeling (PEM) is the first step in which elastic properties (e.g. P and S wave velocities and density) are simulated, and the second step is to estimate seismic wave propagation in the reservoir. This application of ML as proxy model to substitute the traditional 4D seismic forward model is useful, especially in the context of 4D seismic history matching to accelerate the history matching process. The S4D-Proxy model makes 4D seismic forward modeling automated and faster in 4D seismic history matching frameworks. This ML proxy is the focus of this research to evaluate the proxy prediction while training with different datasets.

To develop the S4D-Proxy model, a dataset is prepared, and ML algorithms are trained to find hidden patterns between input features (e.g., porosity, saturation-pressure changes, initial saturation, and pressure) and the output (in our case, time-lapse change in root-mean-square amplitude, or dRMS). One way to generate the training samples in the dataset preparation for the training phase is to use reservoir simulation models. Each simulation grid contains simulated values of the input features and the desired output. Reservoir simulation models (especially an ensemble of reservoir models) provide sufficient training data samples with a good range of variability to train the ML algorithms. However, using reservoir simulation models seems to be a viable option for ML training, as suggested by Xue et al. (2019) and shown in Maleki et al. (2022). A further question is whether the models for the training should be a prior ensemble of reservoir models (before data assimilation or history matching) or a posterior ensemble (after data assimilation). Few studies in the literature analyzed the choice between different simulation models for the ML training phase. This research considers this question and evaluates S4D-Proxy performance when the proxy is trained with the prior and posterior reservoir models.

Moreover, using map-based 4D seismic data has become a norm in quantitative 4D seismic applications (Danaei et al., 2020). Lateral variations in reservoir saturation and pressure changes could be related pointwise to their corresponding 4D seismic signals (Landrø, 2001; MacBeth et al., 2006). Therefore, ML algorithms have leveraged this fact and many authors relate map-based input features to the map-based desired output (Côrte et al., 2020; Dramsch et al., 2019b; Xue et al., 2019). The common practice and standard of training the ML algorithms within map-based schemes are to relate the input features pointwise to their desired output (Xue et al., 2019). Maleki et al. (2022) have shown that, in map-based training alongside pointwise assignment, using information around each point (surrounding or neighborhood information) in the input features and relating them to the output could benefits the training phase. The question then becomes how much the surrounding information (around a point) is beneficial and positively impacts the training phase.

In this research, different experiments are designed to study these questions more deeply. A Deep Neural Network (DNN) algorithm is used as a proxy for the traditional 4D seismic forward modeling. Then, the DNN is trained with different ensemble of reservoir simulation models (prior and posteriors) from a Brazilian offshore field. The performance of the proxy models are evaluated based on the quantitative measure (coefficient of determination or R-squared) and a visual comparison of the S4D-Proxy predictions, and a complete 4D seismic forward model (PEM plus seismic model). In addition, the influence of neighborhood in the feature extraction is investigated by adding this information systematically to train the DNN algorithm. Here, the DNN is trained considering the surrounding information through three strategies; namely 3x3, 5x5, and 7x7 with increasing number of points added.

5.3 Objectives

The aim of this research is to evaluate the best strategies for the training phase of the ML model development. The specific objectives are:

1- To evaluate the S4D-Proxy model's performance when the DNN is trained on the prior and posterior ensembles of reservoir simulation models.
2- To assess the influence of neighborhood information in feature extraction to train the DNN algorithm

All the evaluations and assessments are based on the quantitative measure (R-squared) and the visual comparison between different ML models.

5.4 Deep neural network (DNN) architecture

DNNs are powerful algorithms to develop models of complex and non-linear systems with examples of their applications are in face recognition solutions (Zhao et al., 2020), virtual assistants (Campagna and Ramesh, 2017), and self-driving cars (Tian et al., 2018). A typical DNN algorithm consists of an input layer, multiple hidden layers, and an output layer. The DNN architecture used for this research was inspired by the VGG-16 architecture presented in Simonyan and Zisserman (2015) and custom-tailored for our research, as shown in Figure 5-1. The architecture starts with the convolutional and max-pooling layers to extract as much as features from the inputs. After extraction, the features are flattened and then run through fully connected layers to predict the desired output within a supervised training scheme. The main components of our DNN architecture are as follows:

1- Convolutional layer: The architecture contains four convolutional layers to capture the features from the inputs. The first two layers extract 32 feature maps and the last two obtain 64 feature maps. Each feature map passes through a rectified linear unit (ReLU) operator. The kernel size for all the convolutional layers is 3 with stride amounts to 1.

2- Pooling layer: This layer offers down-sampling feature maps with two common methods: (1) average pooling, and (2) max pooling. For our application, the feature maps run through two max pooling layers, as shown in Figure5-1.

3- Fully connected layer: These last layers are fully connected and relate the extracted features to the desired output. The size of the fully connected layers is 1024 and each is followed with the ReLU operator.

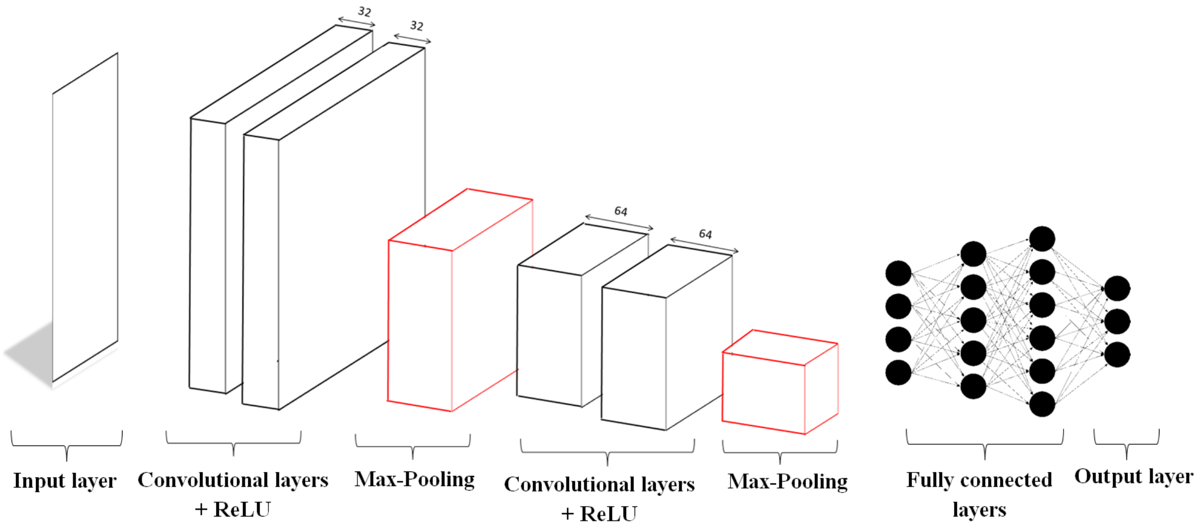

Figure 5-1: DNN architecture custom-tailored for our application.

Using the DNN architecture shown in Figure 5-1, two experiments are designed for our research. The evaluation of the DNN models from the experiments is done based on a visual comparison with the response from the traditional approach (ground truth, PEM and seismic model) and a quantitative measure (R-square) written as:

$$D = (\boldsymbol{d}_{true})^T * \mathbf{1}_{N_{true}} \quad (1)$$

$$R - squared = 1 - \frac{(\boldsymbol{d}_{true} - \boldsymbol{d}_{pred})^{\boldsymbol{T}} * (\boldsymbol{d}_{true} - \boldsymbol{d}_{pred})}{(\boldsymbol{d}_{true} - D)^{\boldsymbol{T}} * (\boldsymbol{d}_{true} - D)} \quad (\mathbf{2})$$

In these equations, $\boldsymbol{d}_{true}$ is the vector of true values (in our case, the dRMS from the traditional approach) and $\boldsymbol{d}_{pred}$ is the prediction from the DNN model. $\mathbf{1}_{N_{true}}$ is a vector of all ones with size (N_{true}) equals the vector of true values $\boldsymbol{d}_{true}$.

5.5 Methodology

The main steps to develop the S4D-Proxy are shown in Figure 5-2a. These steps are: datasets preparation for training and evaluation, training of the DNN algorithm, and evaluation of the trained model on the test dataset. In this research, two experiments are designed: (1) evaluate the DNN model prediction when it is trained on different ensembles of reservoir models (prior and posterior ensembles), and (2) investigate the influence of neighboring information extraction from the input features in the training of the DNN. Therefore, the focus of this research is on defining the best strategies for the training. However, the dataset preparation is an important phase as an efficient training requires a dataset with enough training samples. In this section, the data preparation phase is explained, then two experiments are described.

5.5.1 Dataset preparation

There are two characteristics in our approach to prepare the samples for the training phase. The first is the use of an ensemble of reservoir models to train the algorithm and the second is to convert the 3D reservoir models to maps (map-based training). If an ensemble of reservoir models is considered $\mathrm{E} = \{\mathrm{m}_1, \mathrm{m}_2, \mathrm{m}_3, \mathrm{m}_4, \dots, \mathrm{m}_\mathrm{n}\}$, then we choose x reservoir models for the training and y models for the evaluation. For each reservoir model, the map-based input features (such as porosity, saturation-pressure changes) and the desired output (time-lapse change in seismic amplitude or its attribute, dRMS for our case) are extracted using steps (Figure 5-2b) as follows:

Step 1 (reservoir simulation): 3D reservoir model is simulated to compute saturation and pressure fields at different times. It is important that we obtain these dynamic fields for the baseline time (baseline seismic survey time) and for the monitor time (monitor seismic survey time). 3D volumes of time-lapse saturation-pressure changes are calculated (for instance, water saturation or pressure change).

Step 2 (petro-elastic and seismic models): Using static properties from the 3D reservoir model (such as porosity and NTG) and dynamic properties (such as water saturation, pressure), 3D elastic properties such as P-wave velocity ($\mathrm{V_p}$), shear wave velocity ($\mathrm{V_s}$), and density (ρ) are calculated through petro-elastic modeling and synthetic seismic data is generated through seismic modeling (a description of petro-elastic and seismic models is provided in the application section). It is worth noting that the 3D synthetic seismic data is calculated for the baseline and monitor seismic surveys times and, finally, time-lapse seismic change is calculated (dRMS, for our case).

Step 3 (map extraction): As shown in Figure 5-2b, a map is provided for the input features (porosity (φ), net-to-gross (NTG), initial water and gas saturations, initial pressure, and time-lapse changes in saturation and pressure) and the desired output (dRMS). The map calculates the average of the reservoir property within a window.

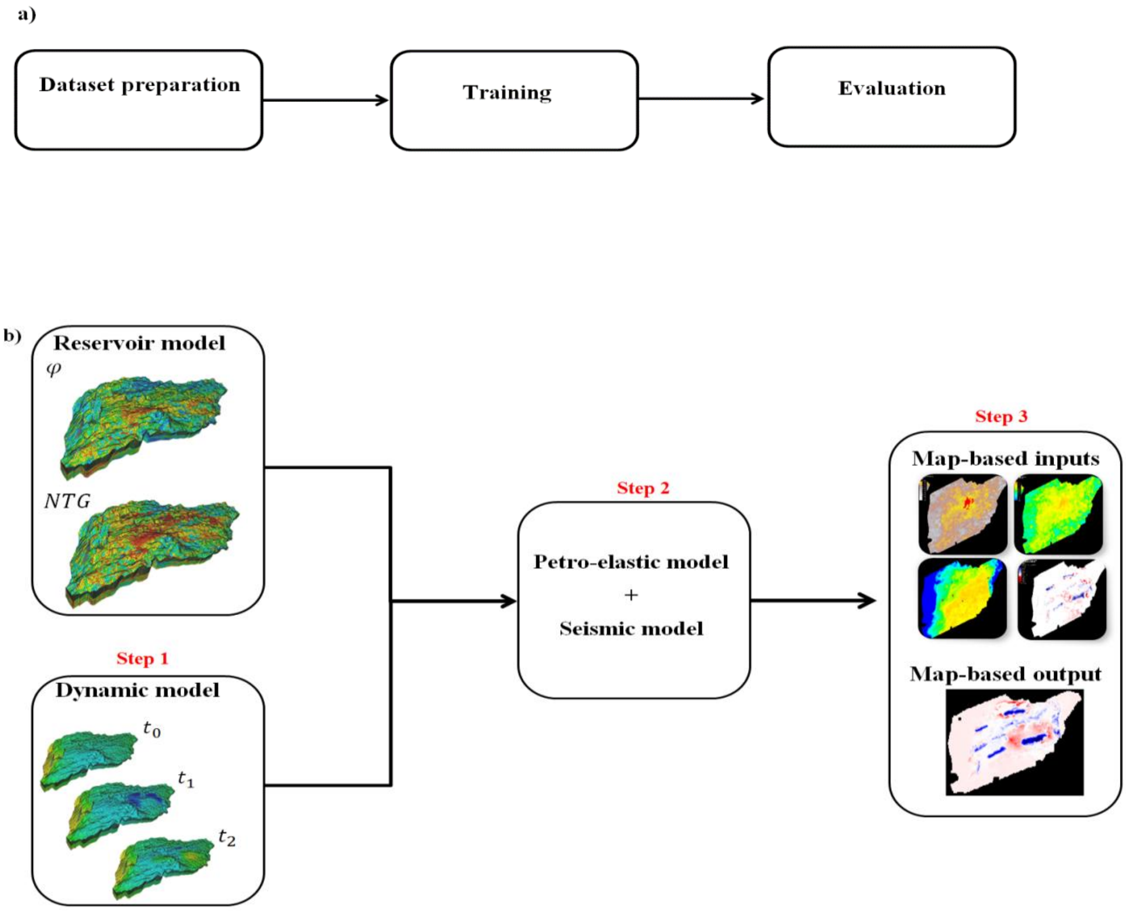

Figure 5-2: (a) steps to develop the proxy for the 4D seismic forward modeling (S4D-Proxy); (b) different steps to prepare training and test datasets using ensemble of reservoir models.

For each reservoir model in the ensembles, the data preparation steps are repeated to prepare the training dataset and the test dataset. After dataset preparation, two experiments are designed to analyze their impacts on the DNN training and its prediction.

5.5.2 First experiment

In this experiment, we train the DNN algorithm with three ensembles of reservoir models. The first consists of prior reservoir models before observed data assimilation. These models are mostly constrained with well-log information and 3D seismic data (static data) and they are not calibrated with the dynamic field data or 4D seismic data. The second ensemble has posterior models after production data assimilation. These models are calibrated with production data, such as bottom-hole-pressure (BHP) or production rate data, using a data assimilation algorithm. The calibration with production data makes the models totally different from the prior ensemble. The posterior models are supposed to be better since they have lower variability and uncertainty compared to the prior ensemble. The third ensemble contains reservoir models that are calibrated with production and 4D seismic data simultaneously. Using a data assimilation algorithm, observed 4D seismic and production data could be assimilated jointly to update reservoir models. As the models are calibrated jointly with production plus 4D seismic data, the models are different from the other two ensembles. It is to be noted that in the practical framework, training the S4D-Proxy model with this ensemble is useful when more than one monitor survey is available (mainly in permanent reservoir monitor settings).

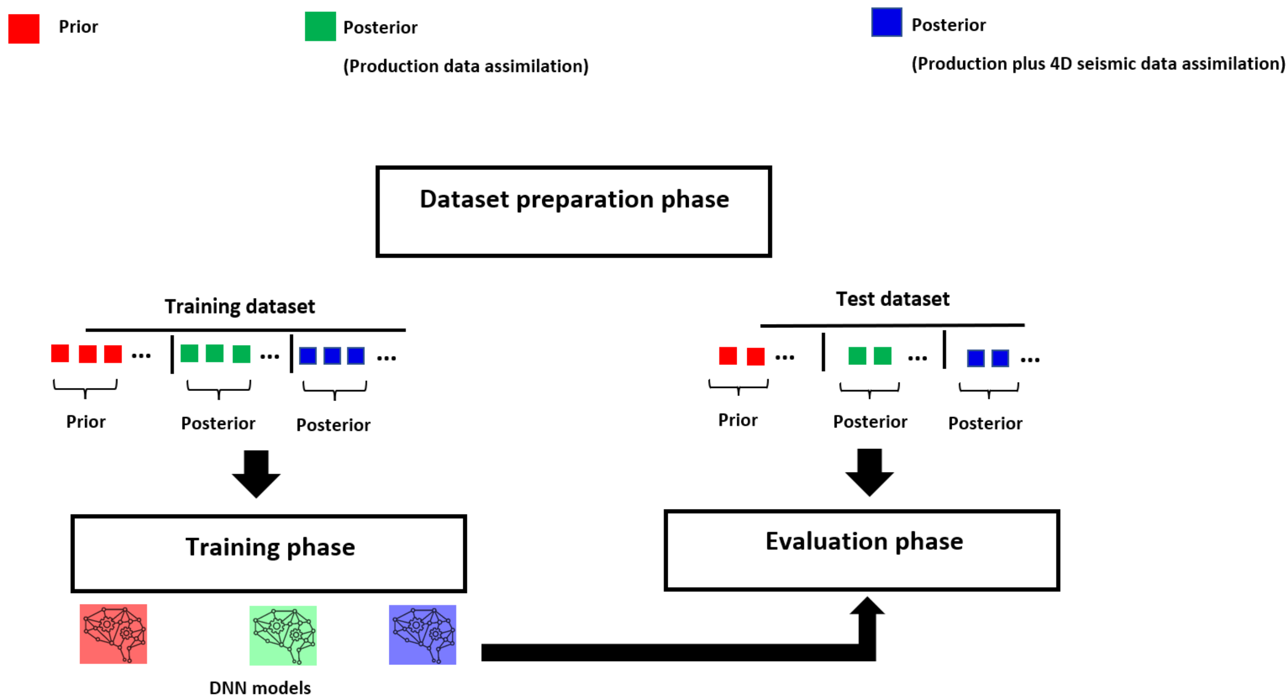

Figure 5-3: First experiment where the DNN algorithm is trained on the prior reservoir model ensemble, the posterior ensemble from the production data assimilation, and the posterior ensemble from the joint assimilation of 4D seismic and production data.

The first experiment (Figure 5-3) proceeds after the dataset preparation phase (section 4-1). The DNN algorithm is trained on three ensembles and, eventually, three DNN models are developed and their predictions are evaluated using the test dataset (as shown in Figure 5-3 in the evaluation phase). It is important to mention that the test dataset combines all three ensembles, so each DNN model is evaluated on all the test models.

5.5.3 Second experiment

This experiment attempts to investigate the influence of neighboring information on feature extraction. Therefore, the DNN algorithm is trained with three different strategies in feature extraction for the training phase. The standard approach for training machine learning algorithms is a pair-wise relation in which each point in the input features is related to the output in a pair-wise manner. For example, in Figure 5-4, the black squares in the center for the input features are related to the target pair-wised in a standard training. However, we extract neighboring information around a centered grid (for example, around black square in Figure 5-4a) and relate them to the output. As shown in Figure 5-4, we increase the window size to extract the neighboring information from 3x3 in Figure 5-4a to 5x5 and 7x7 in Figures 5-4b and c, respectively. Using different strategies (3x3, 5x5, and 7x7), three DNN models are developed and their performances are evaluated on the test models.

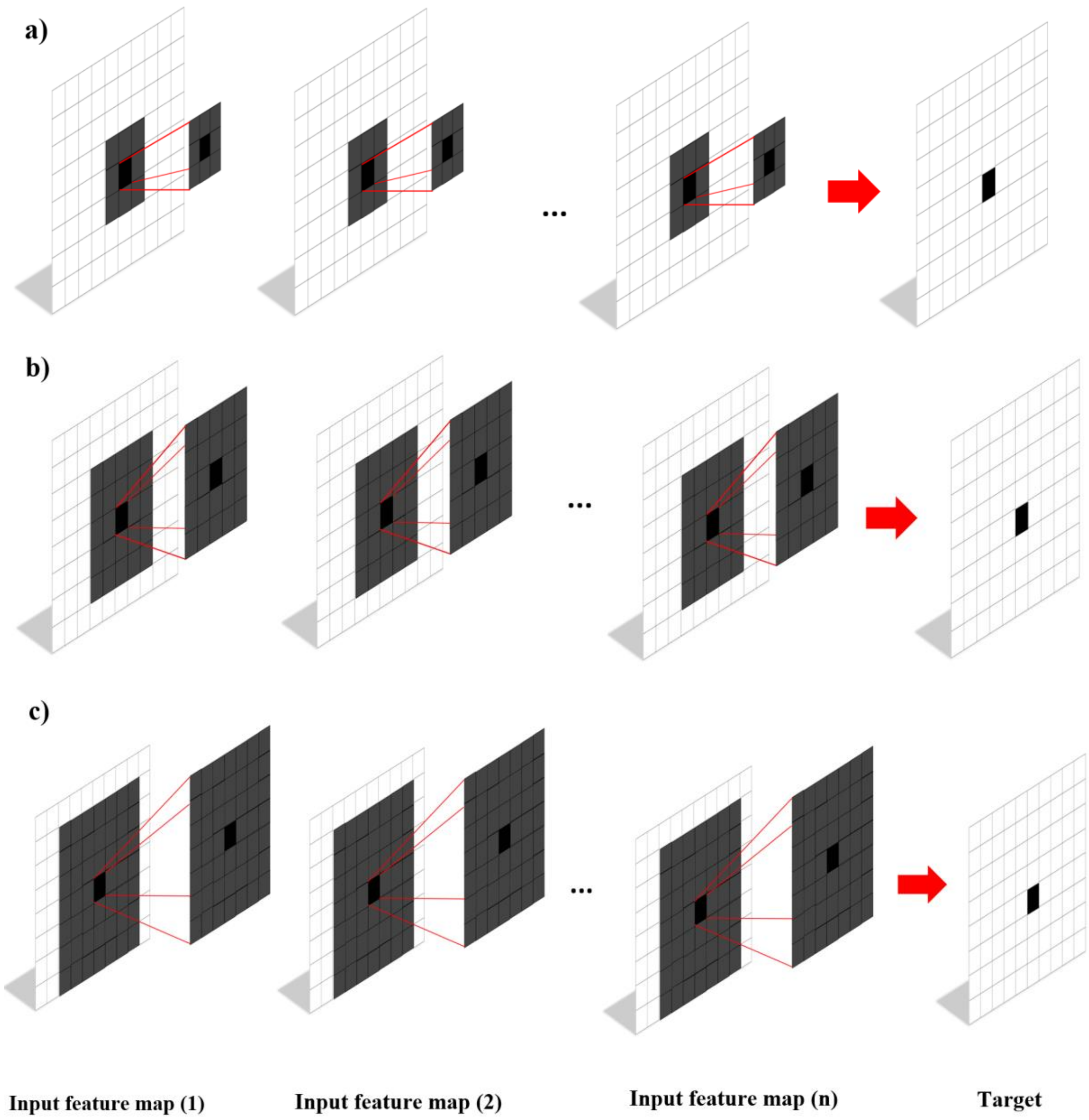

Figure 5-4: Strategies to capture neighboring information from a grid point. In (a) 3x3 strategy which captures neighboring information within a 3x3 square; (b) 5x5 strategy to capture information within a 5x5 square; and (c) 7x7 strategy to obtain spatial information in a 7x7 square.

5.6 Application

The designed experiments are performed on three ensembles of simulation models: namely, prior, posterior ensemble from production data assimilation, and posterior from production plus 4D seismic data assimilation. The ensembles were developed based on well-log, 3D seismic, and 4D seismic data for an offshore Brazilian field located in the Campos Basin. The target reservoir is composed of poorly consolidated sandstones with high porosity and permeability. There are three main faults and the reservoir is connected to an aquifer. As shown in Figure 5-5, there are eight producers and four water injectors to maintain reservoir pressure. These four injectors (I1, I2, I5, and I6) are scattered around the reservoir (Figures 5-5a and b). The production started in 2013 with the first seismic survey (baseline seismic survey) obtained in the same year. Water injection started four months later and the monitor seismic survey for our case was obtained three years from the baseline survey in 2016. Figure 5-5b shows the time-lapse difference of the root-mean-square amplitude attribute (dRMS) where the main hardening signals (blue) happened around the injectors and the softening effect was observed mainly in the middle of the reservoir due to the gas coming out of the solution. For more details on the qualitative interpretation of 4D seismic signals, readers are referred to Maleki et al. (2021) and Rosa et al. (2022). Some small-scale softening 4D signals are located around the injectors I1 and I5 as the result of pushed oil. Moreover, small-scaled hardening signals also are located in the western part of the reservoir (near injector I1), which might be related to the aquifer movement.

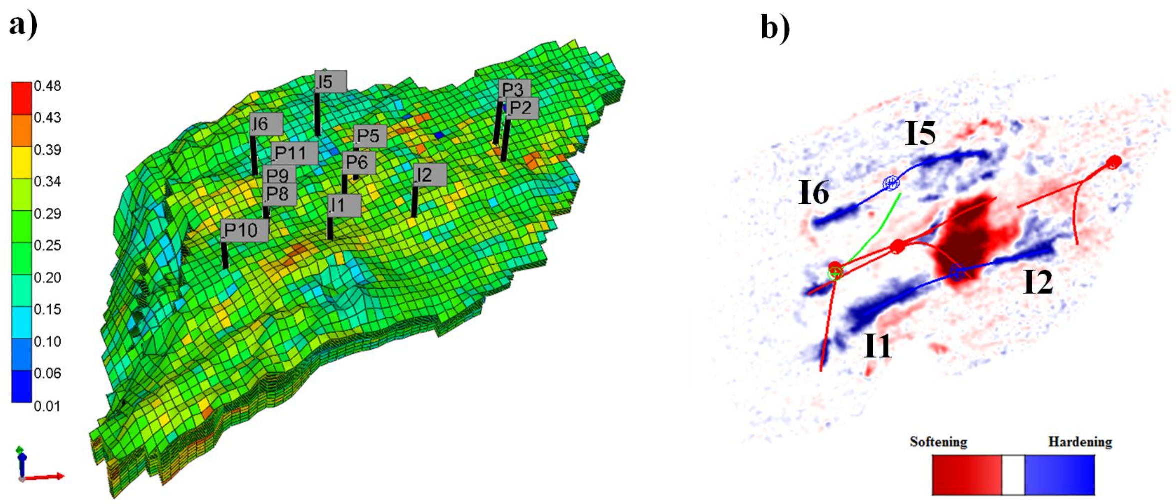

Figure 5-5: (a) a random 3D porosity model with all the producers and injectors around the reservoir; (b) 4D seismic amplitude map (dRMS) with the main 4D signals in the location of injectors and a main softening signal in the middle of the reservoir and around some injectors

It is worth mentioning that the PEM used for our application has four parts: (1) rock matrix, (2) dry rock, (3) fluid mixture, and (4) fluid-saturated rock. **First part (rock matrix):** we consider a rock with two mineral components; quartz and clay. The elastic moduli of the rock matrix are calculated using Voigt-Reuss-Hill average (Mavko et al., 2009). The rock matrix density is an arithmetic averaging of the densities of each mineral component. **Second part (dry rock):** the rock matrix moduli at zero porosity is considered one end member while the moduli at the critical porosity (calculated by Hertz-Mindlin model (Hertz, 1882; Mindlin, 1949)) is another end member. These two end members are interpolated by modified Hashin-Shtrikman lower bound (Mavko et al., 2009) to form the soft dry frame rock moduli within a range of porosities. **Third part (fluid mixture):** the fluid mixture bulk modulus is computed using an inverse averaging of water and oil bulk moduli (Mavko et al., 2009). Like the rock matrix density, the fluid mixture density is estimated using an arithmetic averaging of densities of each fluid phase. **Fourth part (fluid-saturated rock)**: Gassmann fluid substitution (Gassmann, 1951) is used to calculate the fluid-saturated rock elastic moduli. By knowing the percentage of the porosity, the fluid-saturated rock density is an average of the fluid mixture and rock matrix densities. Finally, the elastic properties are estimated. For the seismic modeling part, 1D convolutional method generates the synthetic seismic amplitude.

The size of each reservoir model ensemble is 200 and, for ease of use, each ensemble is abbreviated in that the prior ensemble is called “Prior”, the posterior ensemble from production data assimilation is named “Post-W”, and the posterior ensemble from production plus 4D seismic data assimilation is “Post-WS”. An explanation is provided for each ensemble as follows:

The prior ensemble (Prior): a full package of well logs, core descriptions, and 3D seismic data were used to build the prior ensemble of reservoir models (Rosa et al., 2022). The 3D seismic volume was mainly used for structural modeling (reservoir top, bottom, and fault picking) while the core and well log information were used for property (porosity, absolute permeability, and NTG) modeling. The reservoir was divided into four facies and the static properties were distributed in each facies. As the prior ensemble is before dynamic data assimilation (production and/or 4D seismic data) therefore, the uncertainty in the model parameters is high and the ensemble has wide variability and therefore covers a wider range of scenarios compared to the posterior ensembles, which are calibrated with the observed data. For example, standard deviation of the model parameter porosity is shown in Figure 5-7 where the prior ensemble has the highest standard deviation. Moreover, Figure 5-6a shows 3D porosity from a random model in the prior ensemble.

The posterior ensemble from production data assimilation (Post-W): Observed production data including bottom-hole pressure (BHP) for producers and injectors, water and gas rates for producers were assimilated to update the prior ensemble of models. The data assimilation used here was an ensemble-based algorithm ES-MDA (Emerick and Reynolds, 2013) with four iterations (Rosa et al., 2022). Observed data assimilation decreases model uncertainty and reduces variability compared to the prior ensemble as shown in Figure 5-7 for model parameter porosity. Figure 5-6b shows 3D porosity model after production data assimilation.

The posterior ensemble from production plus 4D seismic data assimilation (Post-WS): The third ensemble contains posterior models from simultaneous assimilation of production plus 4D seismic data. For the data assimilation, the ES-MDA algorithm was used with four iterations. Acoustic impedance was the level at which 4D seismic data was assimilated simultaneously with the observed production data. The simultaneous assimilation provides more observed data than the single production data assimilation, so the posterior ensemble has even less variability than the posterior ensemble from production data assimilation and the prior ensemble (Figure 5-7). Training the DNN algorithm with this ensemble is justified in permanent reservoir monitor settings where more than one monitor survey could be used for the quantitative applications. Figure 5-6c shows 3D porosity model from the joint data assimilation procedure.

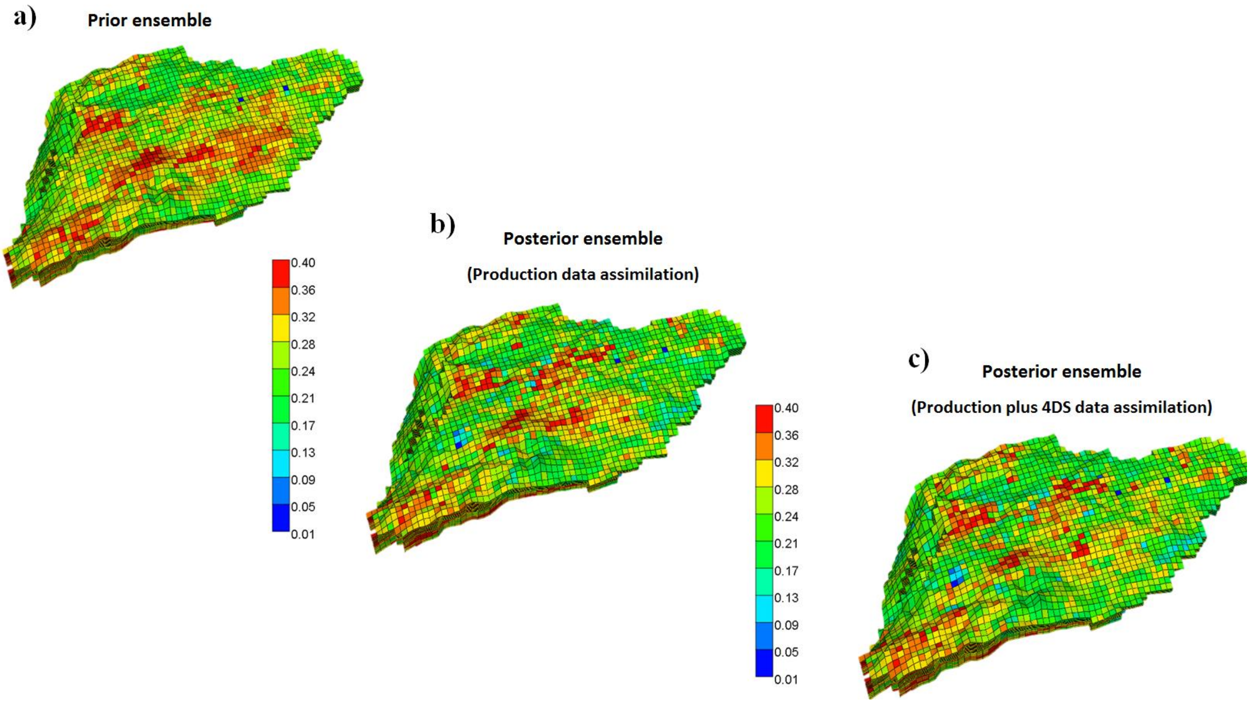

Figure 5-6: (a) 3D porosity model for a model in the prior ensemble; In (b), the 3D static model from posterior ensemble after production data assimilation; (c) 3D porosity model from the posterior ensemble of production plus 4D seismic data assimilation.

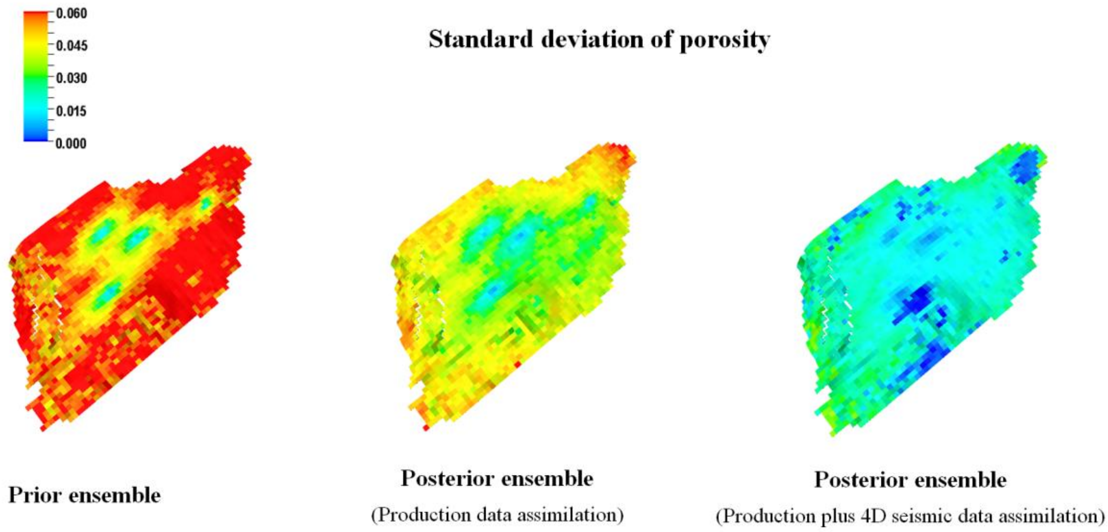

Figure 5-7: Standard deviation for porosity field for different ensemble of reservoir models.

5.6.1 Different deep neural network models

The DNN algorithm was trained separately on different ensembles of reservoir simulation models (prior and posteriors). For each ensemble, 160 models were used for the training phase and 40 models were set aside as test models. Table 5-1 shows different DNN models and the test set which includes all three prior and posteriors models. Each DNN model was evaluated on all prior and posterior test models.

Table 5-1: Different DNN models developed for our experiments.

Ensemble of reservoir models	DNN model	Test models
Prior (constraint with static data)	**DNN-Prior**	**Test-Prior** + **Test-Post-W** + **Test-Post-WS**
Posterior (Calibrated with production data)	**DNN-Post-W**	
Posterior (Calibrated with production & 4D seismic data)	**DNN-Post-WS**	

In table 5-1, the DNN algorithm was trained on the prior ensemble for the DNN-Prior model. The algorithm was trained on the posterior models from production data assimilation for the DNN-Post-W and, similarly, the training dataset for the DNN-Post-WS model was the posterior ensemble of production plus 4D seismic data assimilation. The test dataset is a combination of the test models from the prior and posterior ensembles.

5.7 Results and discussions

The results are presented in six parts. The first briefly reviews the process of generating training and test datasets for our application. Then, the performance of different DNN models is evaluated on the test dataset. A cross-comparison of the three DNN models is carried out to discuss several points in our evaluation. Finally, the DNN models trained with various neighboring strategies were compared and analyzed.

5.7.1 Dataset preparation

Three ensembles of models were used in our research: (1) prior, (2) posterior from production data assimilation, and (3) posterior from production plus 4D seismic data assimilation. The size of each ensemble was 200 reservoir models and for our application, 160 reservoir models were used and formed the training dataset and 40 reservoir models were used to test the developed DNN models. According to section 4-1 (dataset preparation), the steps to prepare training and test datasets were implemented for all three ensembles of reservoir models. Here, a brief description is provided to recap those steps of dataset preparation on the prior ensemble of models. The same steps were repeated to generate the datasets for the posterior ensembles. Firstly, the reservoir models in the ensemble were simulated to compute saturation and pressure fields, especially for the baseline seismic survey time and the monitor. Time-lapse changes of saturations and pressure were calculated with the dynamic properties in the baseline and monitor seismic survey times. In the second step according to section 4-1, by using static properties (such as porosity) from the reservoir models in the ensemble and dynamic properties (such as saturation fields), elastic properties (V_p, V_s, and ρ) are computed for the reservoir models through petro-elastic modeling and the synthetic seismic is generated through 1D convolution (seismic modeling). By repeating the petro-elastic and seismic models for the seismic baseline and monitor times, eventually, the synthetic dRMS is generated for each model in the ensemble. In the final step (step 3), maps are extracted from the input features (such as porosity and saturation-pressure changes) and the output dRMS. Figure 5-8 depicts the extracted maps from reservoir models in the prior ensemble.

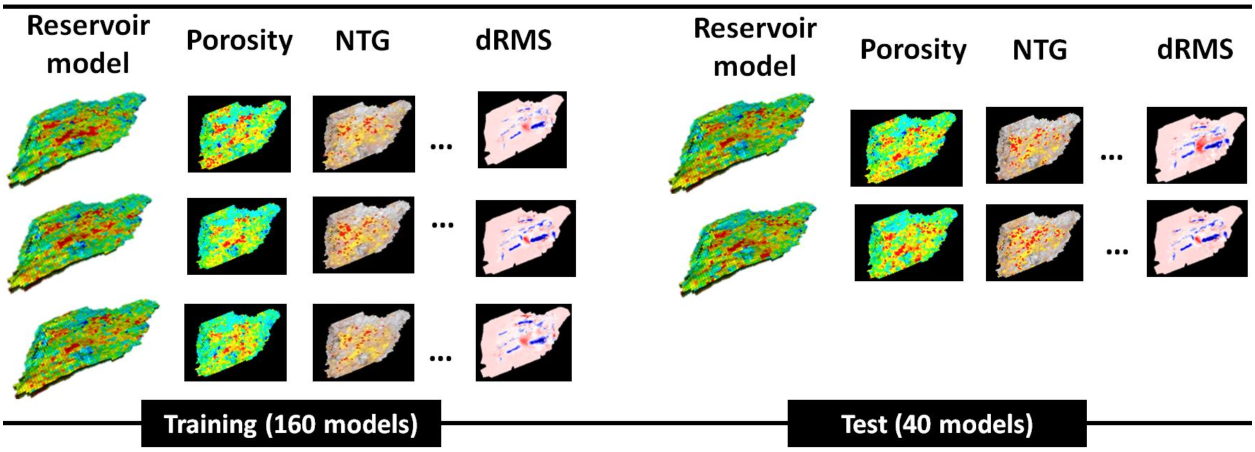

Figure 5-8: training and test datasets preparation from the prior ensemble of reservoir models.

After dataset preparation for three ensembles of reservoir models, the DNN algorithm was trained on each ensemble and the results were analyzed based on the R-squared and a visual comparison with the traditional approach. It is worth noting that we define R-squared values above 0.7 (R-squared>0.7) as “excellent”, the values between [0.5, 0.7] are “good”, the values between [0.3, 0.5] are considered “medium”, and the R-squared values between [0, 0.3] are “low”. This regulation helps us better evaluate different DNN models and have the same language when comparing the models.

5.7.2 Performance of the DNN-Prior model

The performance of the DNN-Prior model was evaluated on the test dataset. Figure 5-9 shows the boxplots of the R-squared values for each test model in the dataset. As mentioned, the test dataset is a combination of the prior and posterior models. For a better evaluation, the DNN-Prior performance is shown separately for different ensembles in the test dataset. The model performance on the Test-Prior yielded R-squared values in the good and excellent ranges. Likewise, its performance on the Test-Post-W provided the R-squared values within the excellent and good ranges. The average R-squared values of the DNN-Prior model were 0.78 and 0.74 for the Test-Prior and Test-Post-W, respectively. The DNN-Prior model performed well on the Test-Post-WS dataset with the average R-squared value equals 0.63 (in the good range). This is important for the DNN model to perform well on this test ensemble as the reservoir models for this ensemble are calibrated jointly with production and 4D seismic data, so they should represent the observed 4D seismic data better than the other test models. As the prior ensemble of models had the highest variability compared to the other two, this might be the reason that the DNN model predicted 4D signals for all the posterior test models. The high variability in the prior ensemble may have provided a wide range of different scenarios and helped the DNN-Prior better generalize and, as a consequence, contributed positively to its performance on the posterior test models.

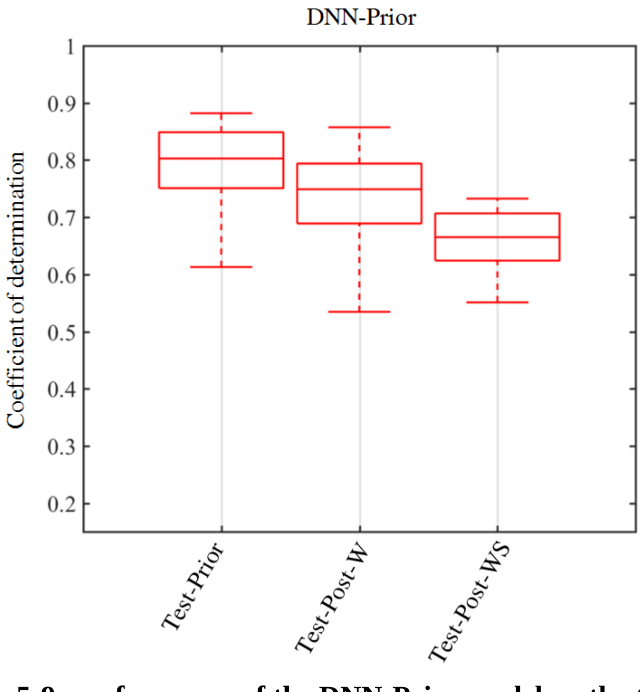

Figure 5-9: performance of the DNN-Prior model on the test dataset.

A visual comparison is provided in Figure 5-10 to evaluate the DNN-Prior performance on different test models. As shown in Figure 5-10 with red arrows, the small-scale softening 4D signal around injector I5 was predicted with the DNN-Prior model for all the test models. Moreover, the hardening signals in the location of injectors were captured with the DNN model. However, in some locations of the dRMS map (for example, the black square in Figure 5-10c), the DNN model could not to predict the 4D signal. In the location of competing hardening and softening effects, the DNN model might need more training samples to resolve this type of 4D signal effects.

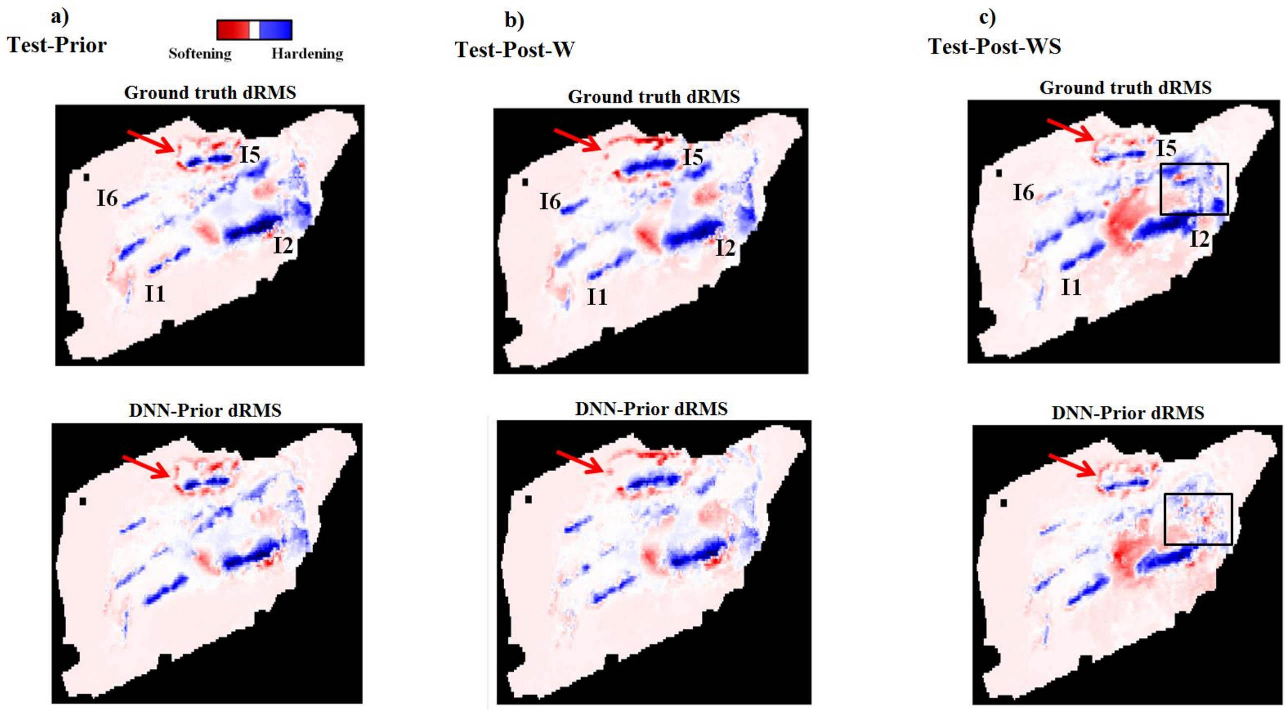

Figure 5-10: visual comparison of the DNN-Prior model performance on different test models. (a) on a test model in Test-Prior, (b) on a model in Test-Post-W, and (c) on a model in Test-Post-WS.

5.7.3 Performance of the DNN-Post-W model

Figure 5-11 shows the boxplot for the R-squared values evaluated on different test models for the DNN-Post-W model. As shown in the figure, the R-squared values for the Test-Prior and the Test-Post-W are within good range and relatively close. An explanation is that the mean of dRMS in the training dataset (Figure 5-12a) was close to the dRMS mean in the Test-Prior (Figure 5-12b) so the trained model could predict 4D signals in the Test-Prior. In contrast, the DNN-Post-W model did not successfully predict 4D signals in the Test-Post-WS, with the average R-squared equals to 0.42. This might be associated with two reasons: (1) dRMS mean for the DNN training (Figure 5-12a) was different from the mean map of the Test-Post-WS (Figure 5-12c) so the trained model could not predict 4D signals; (2) the DNN model was trained on the posterior set that was calibrated with the production data where the posterior models for training the DNN might not honor observed 4D seismic signals, which in turn might affect the DNN model's prediction.

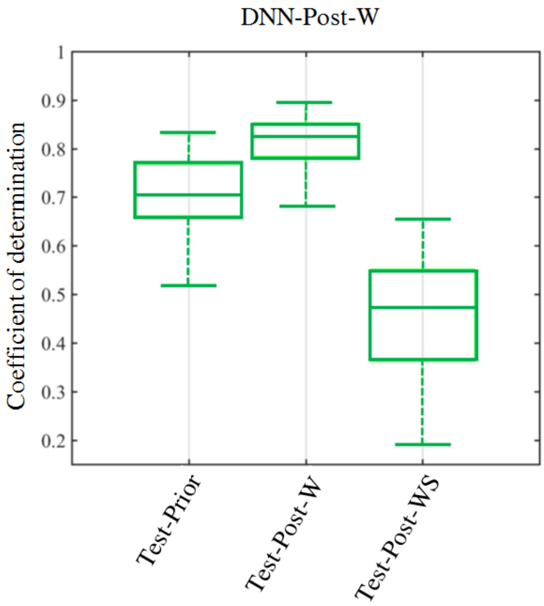

Figure 5-11: boxplots of the DNN-Post-W model performance on different test models.

It is worth noting that the DNN-Post-W was trained on the posterior ensemble, which has less variability compared to the prior ensemble. Two observations should be mentioned when the DNN-Post-W is compared with the DNN-Prior. These observations might affect the training phase and consequently the prediction capability of the DNN-Post-W model. The first is the lack of variability in the training to cover a wider range of reservoir scenarios compared to the training samples in the prior ensemble with higher variability. The second is that the posterior models for training the DNN-Post-W were calibrated to the production data. The posterior models mainly honor the production history data and not the 4D seismic data. Therefore, the DNN model trained on these posteriors was not successful to predict 4D seismic signals.

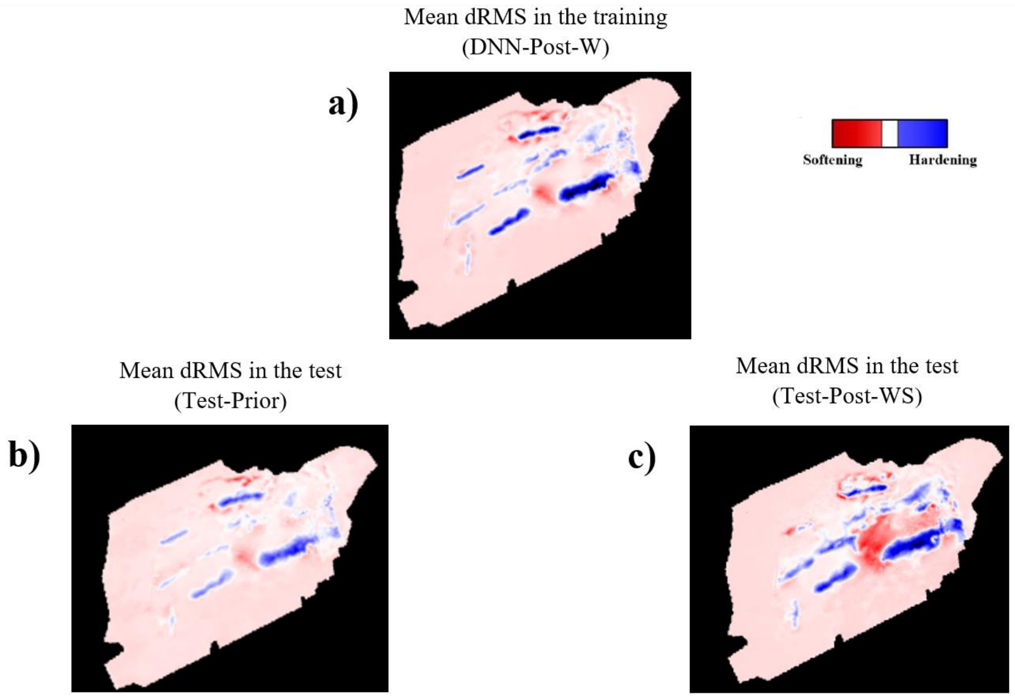

Figure 5-12: dRMS mean for the models in the training (a), mean dRMS for the test models in the Test-Prior (b) and, in (c), the mean map is provided for dRMS from models in the Test-Post-WS.

5.7.4 Performance of the DNN-Post-WS model

The DNN algorithm was trained on the posterior ensemble from production plus 4D seismic data assimilation. The developed DNN model was evaluated on all the test models, as shown in Figure 5-13. An interesting observation is the excellent performance of the DNN model on the Test-Post-WS with the average R-squared equals 0.90. However, the DNN model was weak on the Test-Prior as well as Test-Post-W, which proves that the DNN model could not generalize well and is biased.

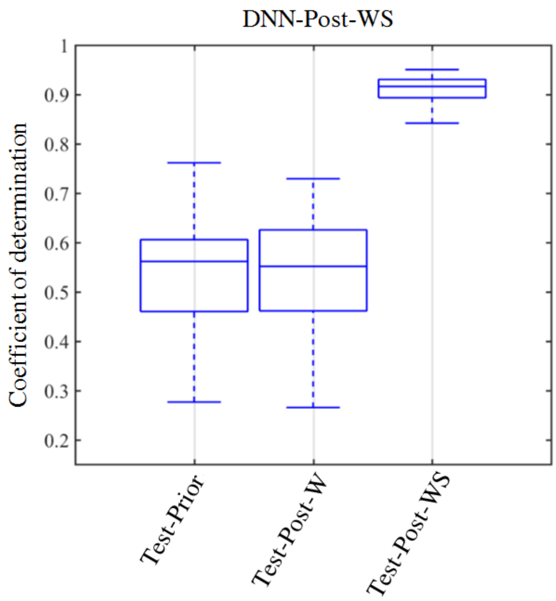

Figure 5-13: boxplots for the DNN-Post-WS performance on the test dataset.

The visual comparison of the DNN-Post-WS performance on different test models highlights the bias and lack of generalization for this DNN model, as shown in Figure 5-14. It became almost a characteristic of the DNN model to predict the softening signal for each model in the Test-Prior and Test-Post-W sets. For example, the test model in Figures 5-14a and b did not have the softening signal in the middle (red oval in the ground truth dRMS), but the DNN model predicted the softening signal by mistake. This result highlights that the DNN-Post-WS model is biased towards prediction of the softening signals in the middle of the reservoir. It could be explained as most of the training samples had the softening signal in the middle, so the DNN model learned that in the training and implemented it to the test. This also explains the very high R-squared on the Test-Post-WS, as the training set had low variability, the problem was easily solved by the DNN model (training and test models were very similar). This finding reveals that the DNN model is biased, which is not preferable as the model intends to replace forward modeling. A biased forward model would lead to biases in the data assimilation (inversion).

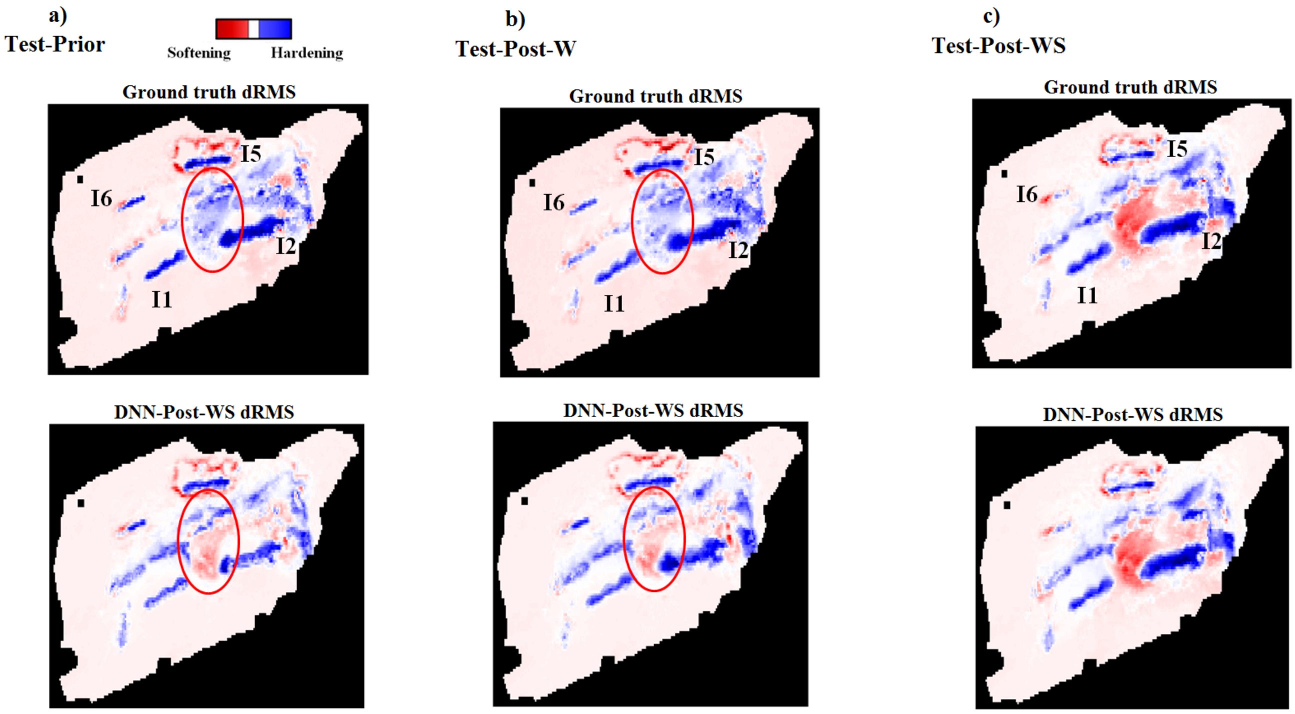

Figure 5-14: visual comparison of the DNN-Post-WS model on the test models in the Test-Prior (a), the Test-Post-W (b), and the Test-Post-WS (c).

5.7.5 Cross-comparison of different DNN models

A further analysis was done to perform a cross-comparison between different DNN models. By cross-comparison, we discussed how training on prior and posterior models might impact the DNN prediction. We put together all the DNN models in a plot with their respective color codes, as shown in Figure 5-15. This comparison showed that the DNN-Prior (red boxplots) not only performed well on the Test-Prior but also presented good results for the posterior model tests. However, when comparing the results of the DNN-Posts (DNN-Post-W in green and DNN-Post-WS in blue) with those from the DNN-Prior, the DNN-Posts could not generalize well. Lack of variability in posterior models (due to observed data assimilation) to train the DNN algorithm could be a reason that these models could not generalize. As the prior ensemble had considerable variability, the DNN-Prior was trained with a wider range of scenarios compared to the DNN models trained on the posterior ensembles. For instance, Figure 5-7 shows the standard deviation of the input variable porosity for the prior and posterior ensembles. The highest standard deviation of the input variable porosity for the prior set implies that the set has good variability for the DNN training. The standard deviation for all the other input variables was also the highest for the prior set compared to the posteriors.

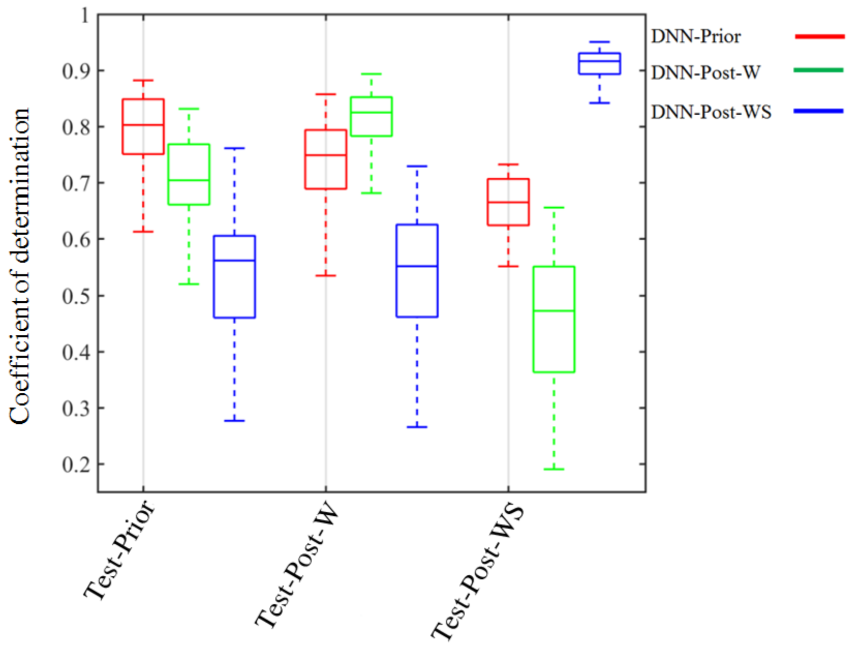

Figure 5-15: cross-comparison between different DNN models.

Although the DNN-Prior had acceptable performance on all the test models, we designed a training set in which reservoir models from prior and posterior ensembles were mixed. For this investigation, two mixtures for training were designed. If we consider a total of 160 reservoir models for the training, the first mixture consists of 50% training models from the prior ensemble (80 out of 160 from the prior ensemble), 25% training models from the posterior ensemble of production data assimilation (40 models out of 160), and 25% training models from the posterior ensemble of production plus 4D seismic data assimilation. The second mixture consists of 80% training models from the prior ensemble, 10% from the posterior of production data assimilation, and 10% training models from the posterior ensemble of the joint data assimilation.

The DNN algorithm was trained on two training mixtures and the trained DNN (DNN-Mix) was evaluated on all the test models. To analyze this result better, the DNN-Mix is color-coded pink. Figure 5-16 shows the performance of the DNN-Mix model, where the results from the DNN model with the first mixture (50%, 25%, and 25%) are shown in Figure 5-16a and the DNN model from the second mixture (80%, 10%, 10%) are evaluated in Figure 5-16b. The results from the DNN-Mix model on the Test-Post-WS demonstrated that this model clearly outperformed the DNN-Prior results (Figure 5-9). While the results from the DNN-Prior model were acceptable on all the test models, if we want to develop a DNN model with a better generalization, we might strike a balance between models in prior and posterior ensembles.

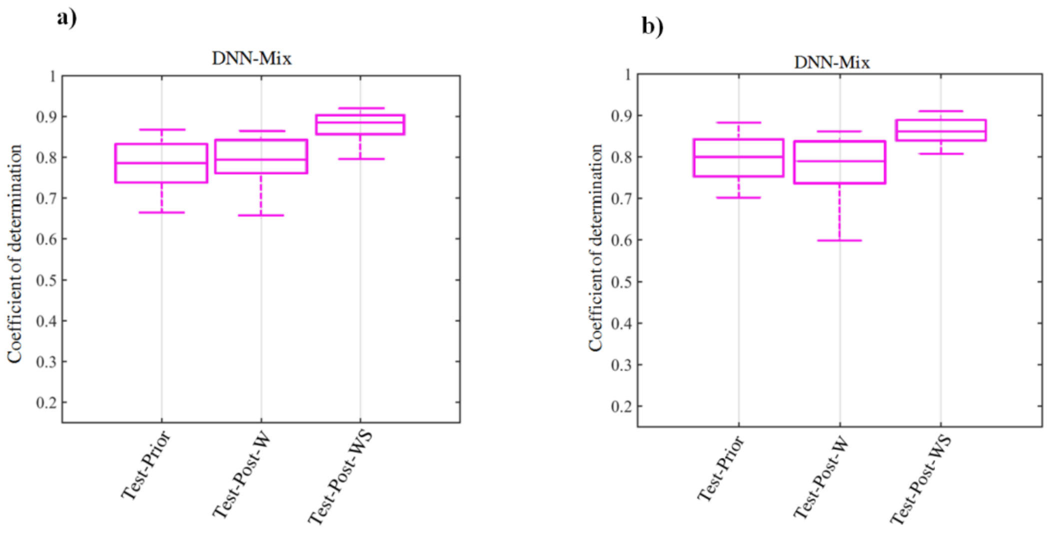

Figure 5-16: DNN-Mix performance on the test models.

5.7.6 Influence of spatial information in the feature extraction

As the DNN-Prior showed better results than the DNN-Posts, the second experiment was performed using the training set from the prior ensemble. Here, three strategies (3x3, 5x5, and 7x7) were tested to capture spatial information around a data point in the input features to relate them to the desired output. Figure 5-17 shows the R-squared boxplots when the DNN is trained with different strategies and evaluated on all the test models.

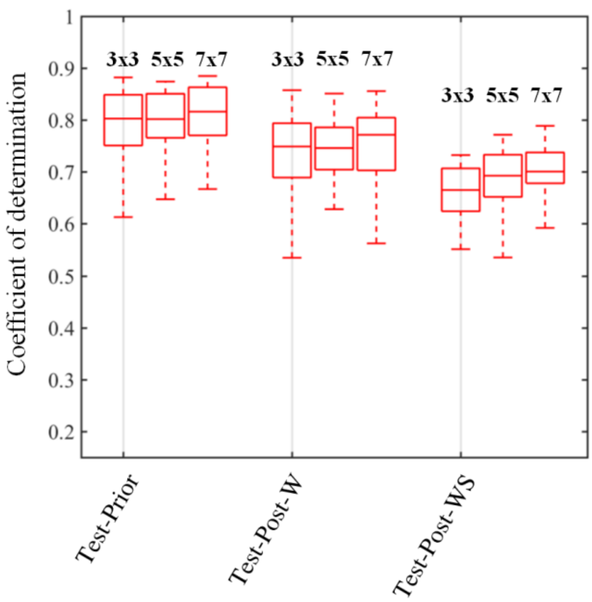

Figure 5-17: Different strategies (3x3, 5x5, and 7x7) to capture the spatial information in the input features and their respective DNN model performances (For the DNN-Prior model).

It is important to interpret the results in Figure 5-17, considering the DNN training elapsed time with different strategies. For the 3x3 strategy, the training phase took 5 hours. The training time for the 5x5 and 7x7 strategies was 8 hours and 12 hours, respectively. The elapsed time indicated that 3x3 training strategy took less time compared to the other two strategies. The analysis of the boxplots in Figure 5-17 indicates that the 7x7 strategy had slightly better results compared to the 5x5 and 3x3 strategies. For instance, one can compare the boxplots for the Test-Post-WS in Figure 5-17 where the 7x7 strategy performed better than the other strategies. The 7x7 strategy had more models in the excellent range compared to the 5x5 and 3x3 strategies. However, the visual comparison between different strategies (Figure 5-18) shows that the predictions for all the strategies are almost at the same level. The hardening signals in the location of injectors were captured by all the DNN models and the softening signals in the middle of the reservoir and around the injector I5 were predicted by the DNN models. Given the training elapsed time for different strategies and Figures 5-17 and 18, the 3x3 strategy could be sufficient to extract spatial information from the input features, especially for the cases where the reservoir simulation model has more active grids (models for giant oil and gas reservoirs). For these cases, the training of the DNN with the 5x5 or 7x7 strategies could take days compared to the 3x3 strategy. Though, for more complex geology, where more sophisticated seismic model is needed or in highly heterogeneous reservoirs (some carbonate reservoir cases), using 7x7 strategy to train the DNN algorithm could provide more details in the forward model, which might be beneficial for these cases.

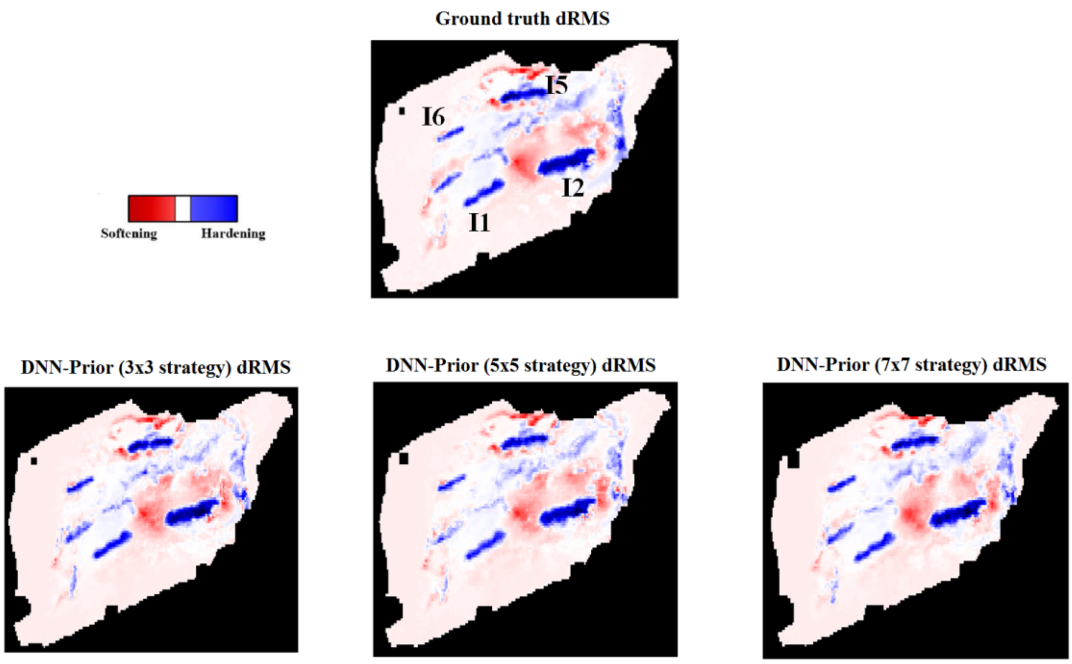

Figure 5-18: visual comparison of different DNN models trained on 3x3, 5x5, and 7x7 strategies. At the top, the ground truth from the traditional approach and, at the bottom, predictions of different DNN models

5.8 Conclusions

Deep neural network algorithms can be considered an alternative 4D seismic forward model to replace the traditional approach with two modeling steps (petro-elastic model plus seismic model). An ensemble of reservoir models could be seen as a viable option to train these algorithms. Nevertheless, model ensemble choice varies from prior ensemble (before observed data assimilation) to the posterior (after data assimilation). In this research, the DNN algorithm was trained on prior and posterior ensembles to evaluate its prediction capability. This experiment was performed on three reservoir model ensembles from a field located offshore Brazil. The three ensembles included: (1) prior ensemble, (2) posterior from production data assimilation, and (3) posterior ensemble from 4D seismic plus production data assimilation. Different DNN models were developed based on the training with different reservoir model ensembles. The results of this experiment helped us reach the following conclusions:

1- The DNN model trained on the prior ensemble had good predictions for all the test models. This DNN model could generalize better than the DNN trained on posterior ensembles. With this observation, we could suggest that variability in training plays an important role in developing proxy models for 4D seismic forward modeling. The performance of another DNN model, which was trained on a mixture training set (a mix of prior and posteriors) also confirmed the role of variability in the training phase to develop the proxy model.

2- The DNN model trained on the posterior ensemble from production data assimilation was generally weak in predicting 4D signals as the DNN model predictions were not promising on the test models with strong 4D signals. As the posterior models were calibrated with production data and not 4D seismic data, the DNN model could not perform well on the test models with strong 4D signals.

3- The DNN model trained on the posterior ensemble from production plus 4D seismic data was a biased DNN model toward the prediction of softening 4D signals. As this DNN model was trained on the posterior ensemble, which was jointly calibrated to production and 4D seismic data, the DNN model got used to predicting 4D signals for any test models in the test dataset, though the test model did not have that specific 4D signal. This bias is not preferable as the proxy is used as a 4D seismic forward model. Furthermore, the bias in the forward model might bring bias to the data assimilation (inversion).

The second experiment evaluated the influence of spatial information (around a data point) on the input features and their relation to the output. Spatial information was captured with three strategies: namely, 3x3 strategy that captured information around a data point within a square of 3x3, 5x5, and 7x7. These strategies were implemented to train the DNN algorithm and the results were compared. The 3x3 strategy successfully predicted 4D signals at the same level as other strategies with training elapsed time less than the 5x5 and 7x7 strategies. However, in a reservoir with complex geology, 5x5 and 7x7 strategies might capture more details in 4D seismic forward modeling. Future research might implement these strategies before extracting map and using spatial information of a data point in 3D reservoir model. This might improve the seismic modeling part as more features from the static properties (such as porosity) might improve the model of seismic wave propagation. In addition, future research might explore ways to treat the bias in the DNN-Post-WS model to make it generalize better. One solution could be optimizing the DNN loss function while adding some rock physics constraints. Therefore, the DNN model learns to consider these rock physics constraints in the training phase. Using Gassmann fluid substitution (Gassmann, 1951) could be an option to introduce rock physics constraints in the DNN algorithm training phase.

5.9 Acknowledgments

This work was carried out in association with the ongoing project registered under number 20372-9 ANP as the "Development of integration between reservoir simulation and 4D seismic - Phase 2" (University of Campinas [UNICAMP]/Shell Brazil/ANP) funded by Shell Brasil Petróleo Ltda. under the ANP R&D levy for "Investment Commitment to Research and Development." The authors are grateful for the support of the Center for Petroleum Studies (CEPETRO-UNICAMP/Brazil), the Department of Energy (DE-FEM-UNICAMP/Brazil), the Research Group in Reservoir Simulation and Management (UNISIM-UNICAMP/Brazil), Energi Simulation, and CNPq. In addition, a special thanks to CGG, Schlumberger and CMG for software licenses.

6 Conclusions

This chapter summarizes the key findings of our research and presents the main contributions of our study. This research aimed to find alternative proxy models to replace the traditional 4D seismic forward modeling in the data assimilation process. The added demand for fast-track 4D seismic data assimilation has created methods to accelerate the data assimilation procedure. One possible way to reduce turnaround time in 4D seismic data assimilation is to use a proxy model for the traditional 4D seismic forward modeling. The traditional approach requires two sequential modeling steps. The first is a petro-elastic model to transform the simulation model outputs to the synthetic elastic attributes, and the second is a seismic model to generate the synthetic amplitude (or its attributes) responses. The main problem with the petro-elastic model is its uncertainty and the combination of the petro-elastic and seismic models for 4D seismic forward modeling renders time-consuming. In this research, we developed two proxy models to replace the traditional petro-elastic modeling. In addition, machine learning algorithms were used to replace the combination of petro-elastic and seismic models.

The results indicate that the petro-elastic model could be replaced with a proxy model in the data assimilation frameworks to integrate jointly production and time-lapse seismic data. The first proxy for the petro-elastic model developed in our research was a linear summation of saturation-pressure changes to relate time-lapse acoustic impedance to these changes with coefficients. This proxy was used to jointly assimilate production and time-lapse seismic data with an ensemble-based data assimilation algorithm ES-MDA. The proxy implementation in the ES-MDA was compared to the petro-elastic model application. The comparison was based on various criteria to reveal the proxy performance and ways to improve the data assimilation results.

It can be concluded that the proxy for PEM was successfully reproduced the reservoir’s past behavior (history data). Both production and 4D seismic objective functions had similar results using proxy and the petro-elastic model in the joint data assimilation procedure. However, regarding uncertainty quantification and production forecast, the proxy failed to provide a reliable forecast and similar uncertainty assessment compared to the PEM case. Although the proxy application for PEM was promising, we discussed possible improvements for proxy development. For example, the proxy formulation could include the reervoir porosity as an uncertain variable. Based on the results and the analysis, we decided to improve the proxy formulation and its application in the data assimilation process. Overall, our research was the first initiative to use a proxy for the petro-elastic model in the joint production and 4D seismic data assimilation.

As we have argued, including the reservoir porosity in the proxy model might improve the data assimilation process in terms of model parameters update and posterior models production forecast. On this basis, the second proxy for the petro-elastic model was developed where the reservoir porosity was included in the proxy model coefficients. Moreover, the proxy approximates the rock/fluid models; therefore, its application contains forward model errors. In this research, the proxy model errors were accounted for in the data assimilation procedure ES-MDA using two different approaches. The first considered the proxy model coefficients as uncertain variables, and the second used fixed coefficients and computed the proxy model statistics from the prior ensemble of models. These model error treatment approaches were used with the ES-MDA to integrate production and 4D seismic data simultaneously. The application of the second proxy model in the data assimilation procedure was compared with the PEM application.

In summary, porosity inclusion in the proxy model and accounting for the proxy model error improves the data assimilation results. Comparisons of the proxy results with those from the petro-elastic model application indicated that the data match quality for the production and 4D seismic objective functions were similar. In addition, the proxy with fixed coefficients and its model error treatment had a similar response to the petro-elastic model application regarding the uncertainty quantification and the production forecast. We realized the importance of the uncertain model parameter porosity in the proxy formulation which mainly improved the uncertainty quantification. Moreover, we found out the role of the proxy model error and the proper approach (best practice) to consider the proxy models (to replace forward modeling) in the data assimilation algorithm. When used properly, the proxy for the petro-elastic model is considered reliable to produce reservoir past behavior (history data match quality) and the production forecast (future response).

Another aspect of our research (a new and different approach) was to use machine learning algorithms as a proxy model for the traditional 4D seismic forward modeling (a combination of petro-elastic and seismic models). Machine learning algorithms could cut the workload and automate the task of seismic forward modeling. In our research, we developed two machine learning models (proxy models) to replace the traditional 4D seismic forward model and generate synthetic dRMS maps. These proxy models aim to replace the combination of petro-elastic and seismic forward models in 4D seismic quantitative applications. The machine learning models are: (1) Extreme Gradient Boosting algorithm (XGBoost), and (2) Deep Neural Network algorithm (DNN). The algorithms were trained using an ensemble of reservoir models and the performance of the machine learning models was compared visually and quantitatively (with R-squared measure) with the performance of the petro-elastic and seismic models.

The analysis of the results indicates that the visual representation of the machine learning models' performance was close to the petro-elastic and seismic models performance. Main 4D seismic signals were reproduced by the machine learning models with little sacrifice in their quality. In addition, the quantitative measure R-squared also showed that the proxy performance was close to the combination of the petro-elastic and seismic models outputs. The main contributions of the machine learning proxy model to the 4D seismic quantitative applications involve: (1) automating the traditional 4D seismic forward modeling and avoiding scale transformation and depth-to-time conversion of the traditional forward model, (2) helping petroleum engineers to perform data assimilation in amplitude domain and reduce turnaround time of the 4D seismic forward modeling in iterative data assimilation process (fast-track 4D seismic data assimilation), and (3) accelerating the use of 4D seismic information in model-based reservoir management and development especially in permanent reservoir monitoring systems.

Finally, in an experiment, the performance of a deep neural network algorithm as a proxy for 4D seismic forward modeling was evaluated when the algorithm was trained with different reservoir simulation models. Three ensembles of reservoir simulation models were used, namely: (1) prior ensemble of the simulation model (before observed data assimilation), (2) posterior ensemble from observed production data assimilation, and (3) posterior ensemble from a joint production plus 4D seismic data assimilation. The deep neural network algorithm was trained separately with these ensembles. Its performance was analyzed based on a quantitative measure (coefficient of determination or R-squared) and a visual comparison between the predicted 4D signals and the results from the traditional petro-elastic and seismic models. In another experiment, the impact of spatial information extraction in input features for deep neural network training was investigated. Here, different strategies used to extract spatial (neighboring) information from the input features to relate them to the desired output. These strategies included extracting training samples from the input features within regions of interest of sizes 3x3, 5x5, and 7x7. These two experiments were carried out using a complete dataset of different ensembles of reservoir simulation models from a Brazilian offshore field (we call it S-Field).

For the first experiment, our results indicate that the deep neural network training with the prior ensemble provides acceptable results (high R-squared values) for almost all test models. In contrary, the training with the posterior ensembles developed deep neural network models incapable of predicting 4D seismic signals for some test models. For example, the deep neural network model trained with the posterior ensemble from production plus 4D seismic data assimilation gives a very biased 4D signal predictions. It has become, in many cases, a characteristic for this model to predict a specific 4D seismic signal (softening signal for our case). This bias in the forward model is undesirable as it affects the data assimilation results. Developing a generalized deep neural network model is a bedrock principle; training the algorithm with the prior ensemble with the highest variability and covering a wide range of reservoir scenarios would be beneficial. From the second experiment, we conclude that the 3x3 neighborhood strategy is sufficient to train the deep neural network algorithm. The developed model can predict 4D seismic signals almost closely to the models trained with the 5x5 and 7x7 neighboring strategies. Nevertheless, adding more spatial information from the input feature could help the deep neural network predictions for complex geology or highly heterogeneous reservoirs.

7 Future Studies

This chapter is designed to provide key components for future studies in the field of proxy development for 4D seismic forward modeling. The possibilities for the future studies are vast knowing the fact that the proxy models for seismic forward modeling is still in its infancy. More and more use cases of the proxy for the forward model is to be explored in the future. Future studies could explore the following items:

In chapters 2 and 3, adding gas saturation change to the proxy for petro-elastic model is an interesting issue for the future studies. Currently, the proxy model considers an oil-water system which could be expanded to three-phase flow. This could be an immediate line of research to study the impact of gas saturation on the proxy prediction. This term should be included in the proxy model considering that the gas saturation increase has softening effects. Moreover, adding initial saturation and pressure to the proxy for petro-elastic model could improve their prediction. Changes in effective pressure at low pressure conditions generate a more significant variation in elastic properties than changes at high pressure condition (Lang and Grana, 2019). We should treat the addition of initial conditions with caution as the core issue of the proxy modeling is to have a straightforward forward model and reduce complexities in the traditional modeling.

For chapters 2 and 3, future study could examine the use of proxy models for joint data assimilation in carbonate reservoirs. Uncertainty is the major issue to develop a petro-elastic model for carbonate reservoirs therefore; proxy models could be helpful as they have limited number of uncertain parameters while providing approximate results. Future studies are also needed to explore some alternative approaches to define proxy coefficients as grid variables instead of scalar variables. Defining these parameters as grid parameters might improve the performance of the proxy predictions especially for carbonate reservoirs. However, there should be a thorough evaluation on its costs.

As mentioned in chapter 3, the water saturation change part of the proxy for petro-elastic model could be calibrated with well-log information using Gassmann fluid substitution. It is widely accepted that the Gassmann equation is not a full rock physics modeling. However, a major source of information for this method is repeated Pulsed-neutron well logs (PNL) which could measure water saturation in the baseline and monitor times. By considering constant porosity and reservoir conditions, Gassmann fluid substitution could be used to calculate the reservoir stiffness in the monitor time with the repeated water saturation from PNL measurement. Monitor acoustic impedance is calculated with the reservoir stiffness and finally impedance change is measured between the monitor and baseline times. By having the impedance change and porosity, proxy model coefficients could be calculated. This method (or other alternative ways) for the calibration of the proxy model could be investigated in the future studies. There approaches would avoid the need of a full PEM to calibrate the proxy model.

Future studies could continue to use the proxy for petro-elastic plus seismic model in the joint assimilation of production and 4D seismic data. Using the proxy model developed in chapters 4 and 5 inside joint data assimilation scheme could accelerate the assimilation process and reduce its turnaround time. Future studies could certainly test the impact of the accelerated data assimilation on the model-based reservoir decision making process. In addition, using the proxy model error treatment (discussed in chapter 3) might improve the data assimilation results in terms of uncertainty quantification and production forecast. A combination of the proxy model and the proxy model error is a powerful package to use in joint data assimilation algorithms as shown in chapter 3. We might use the same methodology to utilize properly the proxy for PEM plus seismic model in joint data assimilation frameworks.

As shown in chapters 4 and 5, deep neural network algorithms could replace the traditional 4D seismic forward modeling. In addition, these algorithms could replace the traditional numerical reservoir simulation model using a physics-informed loss function to train the algorithm. The physics-informed soft constrains could speedup the learning process and reduce costs related to the training phase. The combination of deep neural network proxy models not only for the 4D seismic forward model but also for fluid flow modeling could reduce significantly elapsed time in 4D seismic history matching process. It is an interesting study to investigate the use of deep neural network algorithms for modeling of fluid flow in porous media. Future research should develop proxy forward models to emulate 4D seismic and numerical reservoir simulation and use them with different data assimilation or optimization algorithms. We might enhance this promising idea and use it in the future.

Finally, the proxy for 4D seismic forward modeling could be desirable for vast types of joint data assimilation schemes. For instance, the proxy model could be used in joint assimilation of 4D seismic and electromagnetic data. Using a proxy for 4D seismic forward could reduce the cycle time in this joint inversion. Moreover, future studies could investigate the use of the proxy model in a joint data assimilation of 4D seismic, electromagnetic, and production data. In addition, future studies should be devoted to examine the use of proxy model in 4D seismic feasibility studies especially in permanent reservoir monitoring settings. The proxy for 4D seismic forward modeling could provide information related to detectability of 4D seismic signals and could be helpful to reveal the best timing to acquire seismic survey in permanent reservoir monitoring settings.

References

Aki, K., Richard, P., 1980. Quantitative seismology: Theory and methods. la. ed. San Francisco (EEUU): Freeman and Company 1, 557.

Alfonzo, M., Oliver, D.S., 2020. Seismic data assimilation with an imperfect model. Comput Geosci 24, 889–905. https://doi.org/10.1007/s10596-019-09849-0

Alvarez, E., MacBeth, C., 2014. An insightful parametrization for the flatlander's interpretation of time-lapsed seismic data: Insightful parametrization for interpretation of time-lapsed seismic data. Geophysical Prospecting 62, 75–96. https://doi.org/10.1111/1365-2478.12071

Amini, H., Alvarez, E., 2014. Calibration of the Petro-elastic Model (PEM) for 4D Seismic Studies in Multimineral Rocks. Presented at the EAGE/FESM Joint Regional Conference Petrophysics Meets Geoscience, Kuala Lumpur, Malaysia. https://doi.org/10.3997/2214-4609.20132136

Angelov, P., Spetzler, J., Wapenaar, K., 2004. Pore pressure and water saturation variations; Modification of Landrø's AVO approach, in: SEG Technical Program Expanded Abstracts 2004. Presented at the SEG Technical Program Expanded Abstracts 2004, Society of Exploration Geophysicists, pp. 2279–2282. https://doi.org/10.1190/1.1851220

Avansi, G.D., Maschio, C., Schiozer, D.J., 2016. Simultaneous History-Matching Approach by Use of Reservoir-Characterization and Reservoir-Simulation Studies. SPE Reservoir Evaluation & Engineering 19, 694–712. https://doi.org/10.2118/179740-PA

Avansi, G.D., Schiozer, D.J., 2015. UNISIM-I: Synthetic model for reservoir development and management applications. International Journal of Modeling and Simulation for the Petroleum Industry 9, 21–30.

Batzle, M., Wang, Z., 1992. Seismic properties of pore fluids. GEOPHYSICS 57, 1396–1408. https://doi.org/10.1190/1.1443207

Bertolini, A.C., Schiozer, D.J., 2011. Influence of the objective function in the history matching process. Journal of Petroleum Science and Engineering 78, 32–41. https://doi.org/10.1016/j.petrol.2011.04.012

Bhakta, T., Landrø, M., 2014. Estimation of pressure-saturation changes for unconsolidated reservoir rocks with high V P / V S ratio. GEOPHYSICS 79, M35–M54. https://doi.org/10.1190/geo2013-0434.1

Bogan, C., Johnson, D., Litvak, M., Stauber, D., 2003. Building Reservoir Models Based on 4D Seismic & Well Data in Gulf of Mexico Oil Fields, in: All Days. Presented at the SPE Annual Technical Conference and Exhibition, SPE, Denver, Colorado, p. SPE-84370-MS. https://doi.org/10.2118/84370-MS

Buksh, G., Farmer, H.G., Galarraga, M.A., Lydon, M.T., Mautz, W.A., Norberg, D., 2015. Life Of Field Seismic In The Deepwater BC-10 Phase 2 Development, Brasil, in: All Days. Presented at the Offshore Technology Conference, OTC, Houston, Texas, USA, p. OTC-25803-MS. https://doi.org/10.4043/25803-MS

Cao, J., Roy, B., 2017. Time-lapse reservoir property change estimation from seismic using machine learning. The Leading Edge 36, 234–238. https://doi.org/10.1190/tle36030234.1

Chen, T., Guestrin, C., 2016. XGBoost: A Scalable Tree Boosting System, in: Proceedings of the 22nd ACM SIGKDD International Conference on Knowledge Discovery and Data Mining. Presented at the KDD '16: The 22nd ACM SIGKDD International Conference on Knowledge Discovery and Data Mining, ACM, San Francisco California USA, pp. 785–794. https://doi.org/10.1145/2939672.2939785

Chen, Y., Oliver, D.S., 2013. Levenberg–Marquardt forms of the iterative ensemble smoother for efficient history matching and uncertainty quantification. Comput Geosci 17, 689–703. https://doi.org/10.1007/s10596-013-9351-5

Chen, Y., Oliver, D.S., 2014. History Matching of the Norne Full-Field Model With an Iterative Ensemble Smoother. SPE Reserv. Eval. Eng. 17, 244–256. https://doi.org/10.2118/164902-PA

Chassagne, R., Aranha, C., 2020. A pragmatic investigation of the objective function for subsurface data assimilation problem. Operations Research Perspectives 7, 100143. https://doi.org/10.1016/j.orp.2020.100143s

Corte, G., Dramsch, J., Amini, H., MacBeth, C., 2020. Deep neural network application for 4D seismic inversion to changes in pressure and saturation: Optimising the use of synthetic training datasets. Geophysical Prospecting 1365-2478.12982. https://doi.org/10.1111/1365-2478.12982

Dadashpour, M., Landrø, M., Kleppe, J., 2008. Nonlinear inversion for estimating reservoir parameters from time-lapse seismic data. J. Geophys. Eng. 5, 54–66. https://doi.org/10.1088/1742-2132/5/1/006

da Nóbrega, D.V., de Moraes, F.S., Emerick, A.A., 2018. Data assimilation of a legacy 4D seismic in a brown field. Journal of Geophysics and Engineering 15, 2585–2601. https://doi.org/10.1088/1742-2140/aadd68

Danaei, S., Hermana, M., Ghosh, D.P., 2018. 4D Seismic Qualitative Interpretation for Water Injection Monitoring: Case Study in Southeast Asia, in: Offshore Technology Conference Asia. Presented at the Offshore Technology Conference Asia, Offshore Technology Conference, Kuala Lumpur, Malaysia. https://doi.org/10.4043/28505-MS

Danaei, S., Silva Neto, G.M., Schiozer, D.J., Davolio, A., 2020. Using petro-elastic proxy model to integrate 4D seismic in ensemble based data assimilation. Journal of Petroleum Science and Engineering 194, 107457. https://doi.org/10.1016/j.petrol.2020.107457

Davolio, A., Maschio, C., José Schiozer, D., 2014. A methodology to calibrate water saturation estimated from 4D seismic data. J. Geophys. Eng. 11, 055001. https://doi.org/10.1088/1742-2132/11/5/055001

Davolio, A., Schiozer, D.J., 2019. A Proper Data Comparison for Seismic History Matching Processes, in: SPE Europec Featured at 81st EAGE Conference and Exhibition. Presented at the SPE Europec featured at 81st EAGE Conference and Exhibition, Society of Petroleum Engineers, London, England, UK. https://doi.org/10.2118/195549-MS

Davolio, A., Schiozer, D.J., 2018. Probabilistic seismic history matching using binary images. J. Geophys. Eng. 15, 261–274. https://doi.org/10.1088/1742-2140/aa99f4

Dramsch, J.S., Corte, G., Amini, H., Lüthje, M., MacBeth, C., 2019a. Deep Learning Application for 4D Pressure Saturation Inversion Compared to Bayesian Inversion on North Sea Data, in: Second EAGE Workshop Practical Reservoir Monitoring 2019. Presented at the Second EAGE Workshop Practical Reservoir Monitoring 2019, European Association of Geoscientists & Engineers, Amsterdam, Netherlands, pp. 1–5. https://doi.org/10.3997/2214-4609.201900028

Dramsch, J.S., Corte, G., Amini, H., MacBeth, C., Lüthje, M., 2019b. Including Physics in Deep Learning – An Example from 4D Seismic Pressure Saturation Inversion, in: 81st EAGE Conference and Exhibition 2019 Workshop Programme. Presented at the 81st EAGE Conference and Exhibition 2019 Workshop Programme, European Association of Geoscientists & Engineers, London, UK, pp. 1–5. https://doi.org/10.3997/2214-4609.201901967

Dvorkin, J., Nur, A., Chaika, C., 1996. Stress sensitivity of sandstones. GEOPHYSICS 61, 444–455. https://doi.org/10.1190/1.1443972

Ebaid, H., Wang, K., Seixas, M., Kumar, G., Brew, G., Mashiotta, T., 2017. Practical example of data integration in a PRM environment, BC-10, Brazil. First Break 35. https://doi.org/10.3997/1365-2397.35.2.87479

Emerick, A.A., 2016. Analysis of the performance of ensemble-based assimilation of production and seismic data. J. Pet. Sci. Eng. 139, 219–239. https://doi.org/10.1016/j.petrol.2016.01.029

Emerick, A.A., Moraes, R., Rodrigues, J., 2007. Calculating Seismic Attributes Within a Reservoir Flow Simulator, in: Latin American & Caribbean Petroleum Engineering Conference. 15-18 April, Buenos Aires, Argentina. https://doi.org/10.2118/107001-MS

Emerick, A.A., Reynolds, A.C., 2013. Ensemble smoother with multiple data assimilation. Comput. Geosci. 55, 3–15. https://doi.org/10.1016/j.cageo.2012.03.011

Emerick, A.A., Reynolds, A.C., 2012. History matching time-lapse seismic data using the ensemble Kalman filter with multiple data assimilations. Comput. Geosci. 16, 639–659. https://doi.org/10.1007/s10596-012-9275-5

Emerick, A.A., Reynolds, A.C., 2011. History Matching a Field Case Using the Ensemble Kalman Filter With Covariance Localization. SPE Reserv. Eval. Eng. 14, 423–432. https://doi.org/10.2118/141216-PA

Evensen, G., 1994. Sequential data assimilation with a nonlinear quasi-geostrophic model using Monte Carlo methods to forecast error statistics. J. Geophys. Res. 99, 10143. https://doi.org/10.1029/94JC00572

Falahat, R., Shams, A., MacBeth, C., 2013. Adaptive scaling for an enhanced dynamic interpretation of 4D seismic data: Adaptive scaling for the interpretation of 4D seismic data. Geophysical Prospecting 61, 231–247. https://doi.org/10.1111/1365-2478.12005

Floricich, M., MacBeth, C., Staples, R., 2005. An engineering-driven approach for separating pressure and saturation using 4D seismic: application to a Jurassic reservoir in the UK North Sea, in: SEG Technical Program Expanded Abstracts 2005. Presented at the SEG Technical Program Expanded Abstracts 2005, Society of Exploration Geophysicists, pp. 2464–2467. https://doi.org/10.1190/1.2148221

Gassmann, F., 1951. Über die Elastizität poröser Medien. Vierteljahrsschrift der naturforschenden Gesellschaft in Zürich 1–23.

Gee, V., Stammeijer, J., Gomez-Alonso, H., Avila, R., Peppard, B., Tejera-Cuesta, P., 2017. 4D in a mature water-flood field: Shell Brazil, in: SEG Technical Program Expanded Abstracts 2017. Presented at the SEG Technical Program Expanded Abstracts 2017, Society of Exploration Geophysicists, Houston, Texas, pp. 5845–5849. https://doi.org/10.1190/segam2017-17623299.1

Geir, Æ., Mannseth, T., Vefring, E.H., 2002. Near-Well Reservoir Monitoring Through Ensemble Kalman Filter, in: SPE/DOE Improved Oil Recovery Symposium. 13-17 April, Tulsa, Oklahoma. https://doi.org/10.2118/75235-MS

Geng, C., MacBeth, C., Chassagne, R., 2017. Seismic History Matching Using a Fast-Track Simulator to Seismic Proxy, in: SPE Europec Featured at 79th EAGE Conference and Exhibition. Presented at the SPE Europec featured at 79th EAGE Conference and Exhibition, Society of Petroleum Engineers, Paris, France. https://doi.org/10.2118/185822-MS

Gosselin, O., Aanonsen, S.I., Aavatsmark, I., Cominelli, A., Gonard, R., Kolasinski, M., Ferdinandi, F., Kovacic, L., Neylon, K., 2003. History Matching Using Time-lapse Seismic (HUTS), in: SPE Annual Technical Conference and Exhibition. 5-8 October, Denver, Colorado. https://doi.org/10.2118/84464-MS

Grana, D., Verma, S., Pafeng, J., Lang, X., Sharma, H., Wu, W., McLaughlin, F., Campbell, E., Ng, K., Alvarado, V., Mallick, S., Kaszuba, J., 2017. A rock physics and seismic reservoir characterization study of the Rock Springs Uplift, a carbon dioxide sequestration site in Southwestern Wyoming. International Journal of Greenhouse Gas Control 63, 296–309. https://doi.org/10.1016/j.ijggc.2017.06.004

Hadavimoghaddam, F., Ostadhassan, M., Heidaryan, E., Sadri, M.A., Chapanova, I., Popov, E., Cheremisin, A., Rafieepour, S., 2021. Prediction of Dead Oil Viscosity: Machine Learning vs. Classical Correlations. Energies 14, 930. https://doi.org/10.3390/en14040930

Hashin, Z., Shtrikman, S., 1963. A variational approach to the theory of the elastic behaviour of multiphase materials. Journal of the Mechanics and Physics of Solids 11, 127–140.

Heidaryan, E., 2019. A Note on Model Selection Based on the Percentage of Accuracy-Precision. Journal of Energy Resources Technology 141, 045501. https://doi.org/10.1115/1.4041844

Hertz, H.R., 1882. Ueber die Berührung fester elastischer Körper. Journal für die reine und angewandte Mathematik (Crelles Journal) 1882, 156–171. https://doi.org/10.1515/crll.1882.92.156

Huang, X., Meister, L., Workman, R., 1997. Reservoir Characterization by Integration of Time-lapse Seismic and Production Data, in: SPE Annual Technical Conference and Exhibition. Presented at the SPE Annual Technical Conference and Exhibition, Society of Petroleum Engineers, San Antonio, Texas. https://doi.org/10.2118/38695-MS

Jin, L., Castineira, D., Fu, S., Van den Hoek, P., Pirmez, C., Fehintola, T., Tendo, F., Olaniyan, E., 2011. 4D Seismic History Matching Using Flood Front Information. Presented at the 73rd EAGE Conference and Exhibition incorporating SPE EUROPEC 2011, Vienna, Austria. https://doi.org/10.3997/2214-4609.20149333

Lancaster, S., Whitcombe, D., 2000. Fast-track 'coloured' inversion, in: SEG Technical Program Expanded Abstracts 2000. Presented at the SEG Technical Program Expanded Abstracts 2000, Society of Exploration Geophysicists, pp. 1572–1575. https://doi.org/10.1190/1.1815711

Landrø, M., 2002. Uncertainties in quantitative time-lapse seismic analysis. Geophys Prospect 50, 527–538. https://doi.org/10.1046/j.1365-2478.2002.00330.x

Landrø, M., 2001. Discrimination between pressure and fluid saturation changes from time-lapse seismic data. GEOPHYSICS 66, 836–844. https://doi.org/10.1190/1.1444973

Lang, X., Grana, D., 2019. Rock physics modelling and inversion for saturation-pressure changes in time-lapse seismic studies. Geophysical Prospecting 67, 1912–1928. https://doi.org/10.1111/1365-2478.12797

Le Ravalec, M., Tillier, E., Da Veiga, S., Enchery, G., Gervais, V., 2012. Advanced Integrated Workflows for Incorporating Both Production and 4D Seismic-Related Data into Reservoir Models. Oil Gas Sci. Technol. – Rev. IFP Energies nouvelles 67, 207–220. https://doi.org/10.2516/ogst/2011159

Lorentzen, R.J., Bhakta, T., Grana, D., Luo, X., Valestrand, R., Nævdal, G., 2020. Simultaneous assimilation of production and seismic data: application to the Norne field. Comput Geosci 24, 907–920. https://doi.org/10.1007/s10596-019-09900-0

Lumley, D., Meadows, M., Cole, S., Adams, D., 2003. Estimation of reservoir pressure and saturations by crossplot inversion of 4D seismic attributes, in: SEG Technical Program Expanded Abstracts 2003. Presented at the SEG Technical Program Expanded Abstracts 2003, Society of Exploration Geophysicists, pp. 1513–1516. https://doi.org/10.1190/1.1817582

Luo, X., Bhakta, T., Jakobsen, M., Naevdal, G., 2017. An Ensemble 4D-Seismic History-Matching Framework With Sparse Representation Based On Wavelet Multiresolution Analysis. SPE Journal 22, 0985–1010. https://doi.org/10.2118/180025-PA

Luo, X., Bhakta, T., Jakobsen, M., Nævdal, G., 2018. Efficient big data assimilation through sparse representation: A 3D benchmark case study in petroleum engineering. PLoS ONE 13, e0198586. https://doi.org/10.1371/journal.pone.0198586

Luo, X., Stordal, A.S., Lorentzen, R.J., Naevdal, G., 2015. Iterative Ensemble Smoother as an Approximate Solution to a Regularized Minimum-Average-Cost Problem: Theory and Applications. SPE Journal 20, 0962–0982. https://doi.org/10.2118/176023-PA

MacBeth, C., Floricich, M., Soldo, J., 2006. Going quantitative with 4D seismic analysis. Geophys Prospect 54, 303–317. https://doi.org/10.1111/j.1365-2478.2006.00536.x

MacBeth, C., Geng, C., Chassagne, R., 2016. A fast-track simulator to seismic proxy for quantitative 4D seismic analysis, in: SEG Technical Program Expanded Abstracts 2016. Presented at the SEG Technical Program Expanded Abstracts 2016, Society of Exploration Geophysicists, Dallas, Texas, pp. 5537–5541. https://doi.org/10.1190/segam2016-13818132.1

Maleki, M., Davolio, A., Schiozer, D.J., 2018a. Qualitative time-lapse seismic interpretation of Norne Field to assess challenges of 4D seismic attributes. The Leading Edge 37, 754–762. https://doi.org/10.1190/tle37100754.1

Maleki, M., Davolio, A., Schiozer, D.J., 2018b. Using simulation and production data to resolve ambiguity in interpreting 4D seismic inverted impedance in the Norne Field. Pet. Geosci. 24, 335–347. https://doi.org/10.1144/petgeo2017-032

Maleki, M., Danaei, S., Davolio, A., José Schiozer, D., 2019. Fast-Track Qualitative Interpretation of Seismic Data in a Permanent Reservoir Monitoring PRM Setting for a Brazilian Field, in: Day 2 Tue, October 01, 2019. Presented at the SPE Annual Technical Conference and Exhibition, SPE, Calgary, Alberta, Canada, p. D022S085R002. https://doi.org/10.2118/196185-MS

Maleki, M., Danaei, S., Mesquita da Silva, F.B., Davolio, A., Schiozer, D.J., 2021. Stepwise uncertainty reduction in time-lapse seismic interpretation using multi-attribute analysis. Petroleum Geoscience 27, petgeo2020-087. https://doi.org/10.1144/petgeo2020-087

Maschio, C., Schiozer, D.J., 2016. Probabilistic history matching using discrete Latin Hypercube sampling and nonparametric density estimation. J. Pet. Sci. Eng. 147, 98–115. https://doi.org/10.1016/j.petrol.2016.05.011

Maschio, C., Avansi, G., Santos, A.A., Schiozer, D.J., 2013. UNISIM-I-H: Case study for history matching [WWW Document]. UNISIM Website. URL: http://www.unisim.cepetro.unicamp.br/benchmarks/en/unisim-i/overview (accessed 3/5/2018)

Mateeva, A., Hornman, J.C., Hatchell, P., Potters, H., Lopez, J., 2015. Frequent Seismic Monitoring for Pro-Active Reservoir Management, in: SEG Technical Program Expanded Abstracts 2015. Presented at the SEG Technical Program Expanded Abstracts 2015, Society of Exploration Geophysicists, New Orleans, Louisiana, pp. 4817–4821. https://doi.org/10.1190/segam2015-5899850.1

Mavko, G., Mukerji, T., Dvorkin, J., 2019. The rock physics handbook, Third edition. ed. Cambridge University Press, Cambridge, United Kingdom.

Mesquita, F.B., Davolio, A., Schiozer, D.J., 2015. A Systematic Approach to Uncertainty Reduction with a Probabilistic and Multi-Objective History Matching, in: EUROPEC 2015. Presented at the EUROPEC 2015, Society of Petroleum Engineers, Madrid, Spain. https://doi.org/10.2118/174359-MS

Meadows, M.A., 2001. Enhancements to Landro’s method for separating time-lapse pressure and saturation changes, in: SEG Technical Program Expanded Abstracts 2001. Presented at the SEG Technical Program Expanded Abstracts 2001, Society of Exploration Geophysicists, pp. 1652–1655. https://doi.org/10.1190/1.1816433

Mikkelsen, P.L., Guderian, K., du Plessis, G., 2008. Improved Reservoir Management Through Integration of 4D-Seismic Interpretation, Draugen Field, Norway. SPE Reservoir Evaluation & Engineering 11, 9–17. https://doi.org/10.2118/96400-PA

Mindlin, R., 1949. Compliance of elastic bodies in contact. Journal of Applied Mechanics 16, 259–268.

Naevdal, G., Johnsen, L.M., Aanonsen, S.I., Vefring, E.H., 2005. Reservoir Monitoring and Continuous Model Updating Using Ensemble Kalman Filter. SPE J. 10, 66–74. https://doi.org/10.2118/84372-PA

Obidegwu, D., Chassagne, R., MacBeth, C., 2017. Seismic assisted history matching using binary maps. Journal of Natural Gas Science and Engineering 42, 69–84. https://doi.org/10.1016/j.jngse.2017.03.001

Oliver, D.S., Chen, Y., 2011. Recent progress on reservoir history matching: a review. Comput Geosci 15, 185–221. https://doi.org/10.1007/s10596-010-9194-2

Oliver, D.S., Fossum, K., Bhakta, T., Sandø, I., Nævdal, G., Lorentzen, R.J., 2021. 4D seismic history matching. Journal of Petroleum Science and Engineering 207, 109119. https://doi.org/10.1016/j.petrol.2021.109119

Pathak, R., Ranjan, R., Masoudi, R., 2018. Improved Understanding of Reservoir Performance Behaviors from 4D Seismic Data – A Case Study from Malaysian Basin, in: Day 4 Fri, March 23, 2018. Presented at the Offshore Technology Conference Asia, OTC, Kuala Lumpur, Malaysia, p. D041S035R002. https://doi.org/10.4043/28582-MS

Rostamian, A., Heidaryan, E., Ostadhassan, M., 2022. Evaluation of different machine learning frameworks to predict CNL-FDC-PEF logs via hyperparameters optimization and feature selection. Journal of Petroleum Science and Engineering 208, 109463. https://doi.org/10.1016/j.petrol.2021.109463

Salako, O., Jin, L., Barajas-Olalde, C., Hamling, J.A., Gorecki, C.D., 2018. Implementing adaptive scaling and dynamic well-tie for quantitative 4-D seismic evaluation of a reservoir subjected to CO2 enhanced oil recovery and associated storage. International Journal of Greenhouse Gas Control 78, 306–326. https://doi.org/10.1016/j.ijggc.2018.08.015

Silva Neto, G.M., Davolio, A., Schiozer, D.J., 2020a. 3D seismic data assimilation to reduce uncertainties in reservoir simulation considering model errors. Journal of Petroleum Science and Engineering 189, 106967. https://doi.org/10.1016/j.petrol.2020.106967

Silva Neto, G.M., Rios, V. de S., Davolio, A., Schiozer, D.J., 2020b. Improving fluid modeling representation for seismic data assimilation in compositional reservoir simulation. Journal of Petroleum Science and Engineering 107446. https://doi.org/10.1016/j.petrol.2020.107446

Simonyan, K., Zisserman, A., 2015. Very Deep Convolutional Networks for Large-Scale Image Recognition. arXiv:1409.1556 [cs].

Skjervheim, J.-A., Evensen, G., Aanonsen, S.I., Ruud, B.O., Johansen, T.-A., 2007. Incorporating 4D Seismic Data in Reservoir Simulation Models Using Ensemble Kalman Filter. SPE J. 12, 282–292. https://doi.org/10.2118/95789-PA

Souza, R., Lumley, D., Shragge, J., Davolio, A., Schiozer, D., 2019. 4D Seismic Bandwidth and Resolution Analysis for Reservoir Fluidflow Model Applications. ASEG Extended Abstracts 2019, 1–5. https://doi.org/10.1080/22020586.2019.12073147

Souza, R., Lumley, D., Shragge, J., Davolio, A., Schiozer, D.J., 2018. Analysis of time-lapse seismic and production data for reservoir model classification and assessment. Journal of Geophysics and Engineering 15, 1561–1587. https://doi.org/10.1088/1742-2140/aab287

Stephen, K.D., Soldo, J., Macbeth, C., Christie, M.A., 2006. Multiple Model Seismic and Production History Matching: A Case Study. SPE J. 11, 418–430. https://doi.org/10.2118/94173-PA

Stephen, K.D., 2007. Scale and Process Dependent Model Errors in Seismic History Matching. Oil & Gas Science and Technology - Rev. IFP 62, 123–135. https://doi.org/10.2516/ogst:2007011

Stephen, K.D., Shams, A., Macbeth, C., 2009. Faster Seismic History Matching in a United Kingdom Continental Shelf Reservoir. SPE Reservoir Evaluation & Engineering 12, 586–594. https://doi.org/10.2118/107147-PA

Tabatabaei, M.., Milovac, J.., Bastidas, R.., Lau, R.., Jameson, E.., 2014. North Sea Case Study of an Integrated Sim2Seis Workflow, in: All Days. Presented at the SPE Annual Technical

Conference and Exhibition, SPE, Amsterdam, The Netherlands, p. SPE-170710-MS. https://doi.org/10.2118/170710-MS

Tillier, E., Da Veiga, S., Derfoul, R., 2013. Appropriate formulation of the objective function for the history matching of seismic attributes. Computers & Geosciences 51, 64–73. https://doi.org/10.1016/j.cageo.2012.07.031

Tolstukhin, E., Lyngnes, B., Sudan, H.H., 2012. Ekofisk 4D Seismic - Seismic History Matching Workflow, in: All Days. Presented at the SPE Europec/EAGE Annual Conference, SPE, Copenhagen, Denmark, p. SPE-154347-MS. https://doi.org/10.2118/154347-MS

Trani, M., Arts, R., Leeuwenburgh, O., Brouwer, J., 2011. Estimation of changes in saturation and pressure from 4D seismic AVO and time-shift analysis. GEOPHYSICS 76, C1–C17. https://doi.org/10.1190/1.3549756

Van Leeuwen, P.J., Evensen, G., 1996. Data assimilation and inverse methods in terms of a probabilistic formulation. Monthly weather review 124, 2898–2913.

Weinzierl, W., Wiese, B., 2020. Deep Learning a Poro-Elastic Rock Physics Model for Pressure and Saturation Discrimination. GEOPHYSICS 1–55. https://doi.org/10.1190/geo2020-0049.1

Xu, S., Payne, M.A., 2009. Modeling elastic properties in carbonate rocks. The Leading Edge 28, 66–74. https://doi.org/10.1190/1.3064148

Xue, Y., Araujo, M., Lopez, J., Wang, K., Kumar, G., 2019. Machine learning to reduce cycle time for time-lapse seismic data assimilation into reservoir management. Interpretation 7, SE123–SE130. https://doi.org/10.1190/INT-2018-0206.1

Yin, Z., Feng, T., MacBeth, C., 2019. Fast assimilation of frequently acquired 4D seismic data for reservoir history matching. Comput. Geosci. 128, 30–40. https://doi.org/10.1016/j.cageo.2019.04.001

Zhong, Z., Sun, A.Y., Wu, X., 2020. Inversion of Time-Lapse Seismic Reservoir Monitoring Data Using CycleGAN: A Deep Learning-Based Approach for Estimating Dynamic Reservoir Property Changes. J. Geophys. Res. Solid Earth 125. https://doi.org/10.1029/2019JB018408

Zoeppritz, K., 1919. VII b. Über Reflexion und Durchgang seismischer Wellen durch Unstetigkeitsflächen. Nachrichten von der Gesellschaft der Wissenschaften zu Göttingen, Mathematisch-Physikalische Klasse 66–84.

Appendix A: ES-MDA algorithm

The analysis equation of the ES-MDA algorithm for a model parameter is:

$$\boldsymbol{m}_j^a = \boldsymbol{m}_j^f + \boldsymbol{R} \circ [\boldsymbol{C}_{MD}^f \left(\boldsymbol{C}_{DD}^f + \alpha_i \boldsymbol{C}_D\right)^{-1}]\left(\boldsymbol{d}_{obs,j} - \boldsymbol{d}_j^f\right) \qquad (A.1)$$

In this equation, $\boldsymbol{m}_j^a$ is the updated vector of the model parameter, $\boldsymbol{m}_j^f$ is the prior vector of the model parameter, and j is the model number in the ensemble. $\boldsymbol{R}$ is the localization matrix and $\circ$ denotes the Schur product. If N_a is the number of iterations for the ES-MDA algorithm and for each iteration (i), α_i is the inflation factor. In the ES-MDA algorithm, the inflation factor must satisfy $\sum_{i=1}^{N_a} \frac{1}{\alpha_i} = 1$. $\boldsymbol{C}_D$ is the observed data error covariance matrix, $\boldsymbol{d}_j^f$ is the vector of simulated data for model number j, the observed data vector is $\boldsymbol{d}_{obs}$, and a vector randomly chosen from $\mathcal{N}(\boldsymbol{d}_{obs}, \alpha_i \boldsymbol{C}_D)$ is $\boldsymbol{d}_{obs,j}$. In the ES-MDA algorithm, $\boldsymbol{C}_{MD}^f$ is the cross-covariance matrix between the prior vector of model parameter ($\boldsymbol{m}_j^f$) and the simulated data vector ($\boldsymbol{d}_j^f$). $\boldsymbol{C}_{DD}^f$ is the auto-covariance matrix of the simulated data. The matrices $\boldsymbol{C}_{MD}^f$, and $\boldsymbol{C}_{DD}^f$ are defined as follows:

$$\boldsymbol{C}_{MD}^f = \frac{1}{N_e - 1} \sum_{j=1}^{N_e} (\boldsymbol{m}_j^f - \overline{\boldsymbol{m}}^f)(\boldsymbol{d}_j^f - \overline{\boldsymbol{d}}^f)^T \qquad (A.2)$$

$$\boldsymbol{C}_{DD}^f = \frac{1}{N_e - 1} \sum_{j=1}^{N_e} (\boldsymbol{d}_j^f - \overline{\boldsymbol{d}}^f)(\boldsymbol{d}_j^f - \overline{\boldsymbol{d}}^f)^T \qquad (A.3)$$

In the above equations, N_e is the ensemble size, $\overline{\boldsymbol{m}}^f = \frac{1}{N_e} \sum_{j=1}^{N_e} \boldsymbol{m}_j^f$, and $\overline{\boldsymbol{d}}^f = \frac{1}{N_e} \sum_{j=1}^{N_e} \boldsymbol{d}_j^f$.

Appendix B: Petro-elastic model for UNISIM case

In this research, the petro-elastic model consists of four parts. Details of each part are presented:

Part 1 (Rock matrix model):

Two minerals are considered (namely quartz and clay) with bulk moduli (K_{qtz}, K_{cl}), shear moduli (μ_{qtz}, μ_{cl}), and densities (ρ_{qtz}, ρ_{cl}). The volume fraction of these minerals is assumed based on the net-to-gross ratio (NTG) where, the volume of quartz (f_{qtz}) is equal to NTG and $f_{cl} = 1 - NTG$ is the volume fraction of clay (f_{cl}). The matrix bulk and shear moduli (K_m, μ_m) are calculated using the avergae of Hashin-Shtrikman lower and upper bounds (Hashin and Shtrikman, 1963b):

$$K_m^{HS\pm} = K_1 + \frac{f_2}{(K_2 - K_1)^{-1} + f_1\left(K_1 + \frac{4}{3}\mu_1\right)^{-1}} \qquad (B.1)$$

$$\mu_m^{HS\pm} = \mu_1 + \frac{f_2}{(\mu_2 - \mu_1)^{-1} + \frac{2f_1(K_1 + 2\mu_1)}{5\mu_1\left(K_1 + \frac{4}{3}\mu_1\right)}} \qquad (B.2)$$

If we consider $K_1 = K_{qtz}$, $\mu_1 = \mu_{qtz}$, and $f_1 = f_{qtz}$ then the moduli of the matrix are Hashin-Shtrikman upper bound (K_m^{HS+}, μ_m^{HS+}). By considering K_1, μ_1, and f_1 for the clay mineral then we have Hashin-Shtrikman lower (K_m^{HS-}, μ_m^{HS-}) bound. In this research, the average of the upper and lower bounds is considered for the matrix moduli. The density of the mineral mixture is computed using:

$$\rho_m = f_{qtz}\rho_{qtz} + f_{cl}\rho_{cl} \qquad (B.3)$$

Part 2 (Rock frame model):

The dry rock moduli (K_{dry}, μ_{dry}) are calculated based on a polynomial equation presented in (Emerick et al., 2007b):

$$K_{dry} = f_K K_{dry,\varphi} \qquad (B.4)$$

$$f_K = C_{K_P,0} + C_{K_P,1}P_{eff} + C_{K_P,2}P_{eff}^2 + C_{K_P,3}P_{eff}^3 \qquad (B.5)$$

$$K_{dry,\varphi} = C_K K_m + C_{K_\varphi,0} + C_{K_\varphi,1}\varphi_{eff} + C_{K_\varphi,2}{\varphi_{eff}}^2 + C_{K_\varphi,3}{\varphi_{eff}}^3 \qquad (B.6)$$

$$\mu_{dry} = f_\mu \mu_{dry,\varphi} \qquad (B.7)$$

$$f_\mu = C_{\mu_P,0} + C_{\mu_P,1}P_{eff} + C_{\mu_P,2}P_{eff}^2 + C_{\mu_P,3}P_{eff}^3 \qquad (B.8)$$

$$\mu_{dry,\varphi} = C_\mu \mu_m + C_{\mu_\varphi,0} + C_{\mu_\varphi,1}\varphi_{eff} + C_{\mu_\varphi,2}{\varphi_{eff}}^2 + C_{\mu_\varphi,3}{\varphi_{eff}}^3 \qquad (B.9)$$

In equations $(B.8)$, and $(B.11)$, the dry rock bulk and shear moduli depend on effective pressure (P_{eff}) through f_K, and f_μ respectively. The dependency of these moduli on lithology and effective porosity (φ_{eff}) is expressed by $K_{dry,\varphi}$, and $\mu_{dry,\varphi}$. Constants $C_{K_P,i}$, C_K, $C_{K_\varphi,i}$, $C_{\mu_P,i}$, C_μ, and $C_{\mu_\varphi,i}$ are case dependent. It is worth noting that for our research, the responses for dry bulk and shear moduli calculated with above equations reflect the responses from Hertz-Mindlin dry rock modeling (Hertz, 1882b; Mindlin, 1949b).

Part 3 (Reservoir fluid model):

Batzle and Wang (Batzle and Wang, 1992b) correlations are used to compute water and oil bulk moduli (K_w, and K_o). The reservoir fluid bulk moduli (K_{fl}) is calculated based on the Wood's formula (Mavko et al., 2019):

$$\frac{1}{K_{fl}} = \frac{S_w}{K_w} + \frac{S_o}{K_0} \qquad (B.10)$$

$$\rho_{fl} = S_w \rho_w + S_o \rho_o \qquad (B.11)$$

Where, S_w, S_o are water and oil saturations, ρ_{fl} is the reservoir fluid density, and ρ_w, ρ_o are water and oil densities.

Part 4 (saturated rock model):

Saturated rock bulk modulus (K_{sat}) is modeled based on the Gassman fluid substitution (Gassmann, 1951b). If the effective porosity is φ_{eff} by knowing the matrix, rock frame, and reservoir fluid bulk moduli (K_m, K_{dry}, K_{fl}) from previous parts, K_{sat} is written as:

$$K_{sat} = K_{dry} + \frac{(1-\frac{K_{dry}}{K_m})^2}{\frac{\varphi_{eff}}{K_{fl}} + \frac{(1-\varphi_{eff})}{K_m} - \frac{K_{dry}}{K_m^2}} \qquad (B.12)$$

The saturated rock shear modulus is $\mu = \mu_{dry}$, and the density is calculated by knowing the matrix and reservoir fluid densities (ρ_m, ρ_{fl}):

$$\rho = \left(1 - \varphi_{eff}\right)\rho_m + \varphi_{eff}\rho_{fl} \qquad (B.13)$$

Based on our petro-elastic model, the compressional wave velocity (V_P) and shear wave velocity (V_S) are as follows:

$$V_P = \sqrt{\frac{K_{sat} + \frac{4}{3}\mu}{\rho}} \qquad (B.14)$$

$$V_S = \sqrt{\frac{\mu}{\rho}} \qquad (B.15)$$

And the elastic attributes compressional (I_P) and shear (I_S) impedances are:

$$I_P = V_P \rho \qquad (B.16)$$

$$I_S = V_S \rho \qquad (B.17)$$

Appendix C: Petro-elastic model and seismic model for S-Field

Seismic parameters such as P-wave and S-wave velocities (V_P, and V_S respectively) are related to the reservoir density and stiffness with two equations as follows:

$$V_P = \sqrt{\frac{K_{sat} + \frac{4}{3}\mu}{\rho}} \qquad (C.1)$$

$$V_S = \sqrt{\frac{\mu}{\rho}} \qquad (C.2)$$

In these equations, K_{sat}, μ, and ρ are the reservoir bulk modulus, shear modulus, and density. To compute seismic parameters (P-wave and S-wave) therefore, one should model the reservoir moduli and density. This modelling has three main parts, namely rock matrix model, dry rock model, and reservoir fluid model.

Part 1 (rock matrix model):

For our petro-elastic model, we consider a rock with two mineral components namely, quartz, and clay. Bulk moduli for quartz and clay are K_{qtz}, and K_{cl}, shear moduli are μ_{qtz}, and μ_{cl} while densities are ρ_{qtz}, and ρ_{cl}. Based on net-to-gross ratio (NTG), the volume fraction of each mineral component is calculated where, the volume fraction of quartz (f_{qtz}) is equal to NTG and the volume fraction of clay is considered $f_{cl} = 1 - NTG$. Knowing the mineral components moduli and their fractions, the rock matrix moduli are calculated with the average of Hashin-Shtrikman lower and upper bounds (Hashin and Shtrikman, 1963b):

$$K_m^{HS\pm} = K_1 + \frac{f_2}{(K_2 - K_1)^{-1} + f_1(K_1 + \frac{4}{3}\mu_1)^{-1}} \qquad (C.3)$$

$$\mu_m^{HS\pm} = \mu_1 + \frac{f_2}{(\mu_2 - \mu_1)^{-1} + \frac{2f_1(K_1 + 2\mu_1)}{5\mu_1(K_1 + \frac{4}{3}\mu_1)}} \qquad (C.4)$$

In these equations, when $K_1 = K_{qtz}$, $\mu_1 = \mu_{qtz}$, and $f_1 = f_{qtz}$ then the upper bound for the matrix moduli would be computed (K_m^{HS+}, μ_m^{HS+}). If we consider $K_1 = K_{cl}$, $\mu_1 = \mu_{cl}$, and $f_1 = f_{cl}$ then the matrix moduli are considered to be Hashin-Shtrikman lower bound (K_m^{HS-}, μ_m^{HS-}). It is worth noting that for our research, the matrix moduli are the average of upper and lower bounds using:

$$K_m = \frac{K_m^{HS+} + K_m^{HS-}}{2} \qquad (C.5)$$

$$\mu_m = \frac{\mu_m^{HS+} + \mu_m^{HS-}}{2} \qquad (C.6)$$

Using the volume fraction of each mineral component, the matrix density is:

$$\rho_m = f_{qtz}\rho_{qtz} + f_{cl}\rho_{cl} \qquad (C.7)$$

Part 2 (dry rock model):

Two end members are considered to model the dry rock moduli within a range of porosity. The first end member is at zero porosity which is rock matrix moduli and calculated in step 1. The second end member is at the critical porosity and its moduli (K_{HM}, and μ_{HM}) are calculated with Hertz-Mindlin model (Hertz, 1882b; Mindlin, 1949b):

$$K_{HM} = \sqrt[3]{\frac{C^2(1-\varphi_c)^2\mu_m{}^2}{18\pi^2(1-\nu_m)^2}P_{eff}} \qquad (C.8)$$

$$\mu_{HM} = \frac{5-4\nu_m}{5(2-\nu_m)}\sqrt[3]{\frac{3C^2(1-\varphi_c)^2\mu_m{}^2}{2\pi^2(1-\nu_m)^2}P_{eff}} \qquad (C.9)$$

$$\nu_m = \frac{3K_m - 2\mu_m}{2(3K_m + \mu_m)} \qquad (C.10)$$

In these equations, C is co-ordination number which shows the average number of contacts per grain. φ_c, and φ are the critical and total porosity respectively and effective pressure (P_{eff}) is equal to $P_{eff} = P_{over} - \eta P_{pore}$ where, P_{over} is the overburden pressure, P_{pore} is the pore pressure and η is the effective pressure coefficient which is equal to 1 in our petro-elastic model. K_m, and μ_m are the bulk and shear moduli of the rock matrix while ν_m is Poisson ratio. Rock matrix moduli (one end member) and the moduli at the critical porosity (another end member) are interpolated to calculate rock frame bulk K_{dry}, and shear μ_{dry} moduli within a range of porosity using modified Hashin-Shtrikman lower bound (Mavko et al., 2009b):

$$K_{dry} = [\frac{\varphi/\varphi_c}{K_{HM} + {4\mu_{HM}}/{3}} + \frac{1 - \varphi/\varphi_c}{K_m + {4\mu_{HM}}/{3}}]^{-1} - \frac{4}{3}\mu_{HM} \qquad (C.11)$$

$$\mu_{dry} = [\frac{\varphi/\varphi_c}{\mu_{HM} + z} + \frac{1 - \varphi/\varphi_c}{\mu_m + z}]^{-1} - z \qquad (C.12)$$

$$z = \frac{\mu_{HM}}{6}\left(\frac{9K_{HM} + 8\mu_{HM}}{K_{HM} + 2\mu_{HM}}\right) \qquad (C.13)$$

As a reminder, φ, and φ_c are porosity, and the critical porosity. K_{HM}, and μ_{HM} are the bulk and shear moduli calculated at the critical porosity with the Hertz-Mindlin theory model while K_m and μ_m are the rock matrix bulk and shear moduli.

Part 3 (reservoir fluid model):

The individual fluid bulk modulus is computed using Batzle-Wang correlations (Batzle and Wang, 1992b) and the mixture bulk modulus (K_{fl}) is calculated using Wood's law as (Mavko et al., 2009b):

$$K_{fl} = [\frac{S_w}{K_w} + \frac{S_o}{K_o} + \frac{S_g}{K_g}]^{-1} \quad (C.14)$$

Where, S_w, S_o, and S_g are the water, oil, and gas saturations. K_w, K_o, and K_g are the bulk modulus for water, oil, and gas respectively. In addition, by knowing the individual fluid density of water (ρ_w), oil (ρ_o), and gas (ρ_g) then, the reservoir fluid density (ρ_{fl}) is calculated based on:

$$\rho_{fl} = \rho_w S_w + \rho_o S_o + \rho_g S_g \quad (C.15)$$

All the parts mentioned before including the matrix, the dry frame, and the reservoir fluid moduli are assembled to compute the reservoir bulk modulus (K_{sat}) with the Gassmann fluid substitution equation (Gassmann, 1951b):

$$K_{sat} = K_{dry} + \frac{(1 - \frac{K_{dry}}{K_m})^2}{\frac{\varphi_{eff}}{K_{fl}} + \frac{(1 - \varphi_{eff})}{K_m} - \frac{K_{dry}}{K_m^2}} \quad (C.16)$$

Here, φ_{eff} is effective porosity and the reservoir shear modulus (μ) is equal to dry frame shear modulus (μ_{dry}). The reservoir density is estimated using the matrix density (ρ_m), the fluid density (ρ_{fl}), and porosity (φ) with:

$$\rho = (1 - \varphi)\rho_m + \varphi\rho_{fl} \quad (C.17)$$

After having calculated the elements of the equations (A.1) and (A.2), the seismic parameters including P-wave, S-wave, and density are computed. These parameters are used to simulate seismic wave propagation in the reservoir. There are different approaches to simulate seismic waves. In our research, 1D convolutional method is used for seismic modelling. Two components for this method include: (1) P-wave reflectivity (R_{PP}), and (2) wavelet. The P-wave reflectivity (R_{PP}) can be calculated using Aki and Richard (1980) which is an approximation of the Zoeppritz equations (Zoeppritz, 1919). The wavelet is chosen in such a way that the synthetic seismic trace has the highest correlation with the real seismic trace. These two components are convolved to generate the synthetic seismogram. It is worth mentioning two points here. Firstly, the root mean square (RMS) of the generated synthetic amplitude is used for our application. The second point is the fact that the PEM and the seismic model should be repeated for the baseline (pre-production) and the monitor time (post-production). Eventually, the time-lapse difference of the root mean square amplitude (dRMS) is calculated by subtraction of the monitor from the baseline.

Appendix D: Complementary results for petro-elastic proxy modeling

Petro-elastic proxy model (PEM-Proxy) tries to mimic a fullfledged petro-elastic model. However, as discussed in Danaei et al. (2022), the proxy is an approximation and its implementation involves with model error. A proper use of the proxy accounts for the model error and tries to alliviate it during data assimilation procedure. To compare the performance of the proxy and a fullfledge petro-elastic model, complementary statistical analysis are performed to to analyze the proxy predictions versus the results from a petro-elastic model. This analysis is performed for the proxy model developed in our first paper entitled “Using petro-elastic proxy model to integrate 4D seismic in ensemble-base data assimilation”. It is worth noting that this PEM-Proxy is a linear summation of saturation-pressure changes. In addition, we analyze the performance of the second version of the proxy model which developed in our paper entitled “Substituting petro-elastic model with a new proxy to assimilate time-lapse seismic considering model error”. In our second paper, the proxy model (we called it, DAI-Proxy) was a linear summation of saturation-pressure changes with two coeficients that are functions of porosity. The inclusion of porosity introduces heterogeniuty to the proxy model and make the proxy performs better in cases where heterogeniuty plays an important role to develop the eensemble of reservoir models.

The first version of the PEM-Proxy is abbreviated to the petro-elastic proxy model with fixed coefficients (PFC) and proxy model with uncertain coefficients (PUC). Figures D-1 and D-2 illustrate the crossplot between proxy predictions and the result from the petro-elastic model. Both PFC and PUC predictions are plotted against the actual petro-elastic model results. Models in these figures are randomnly selected and R-squared values are shown in the plots.

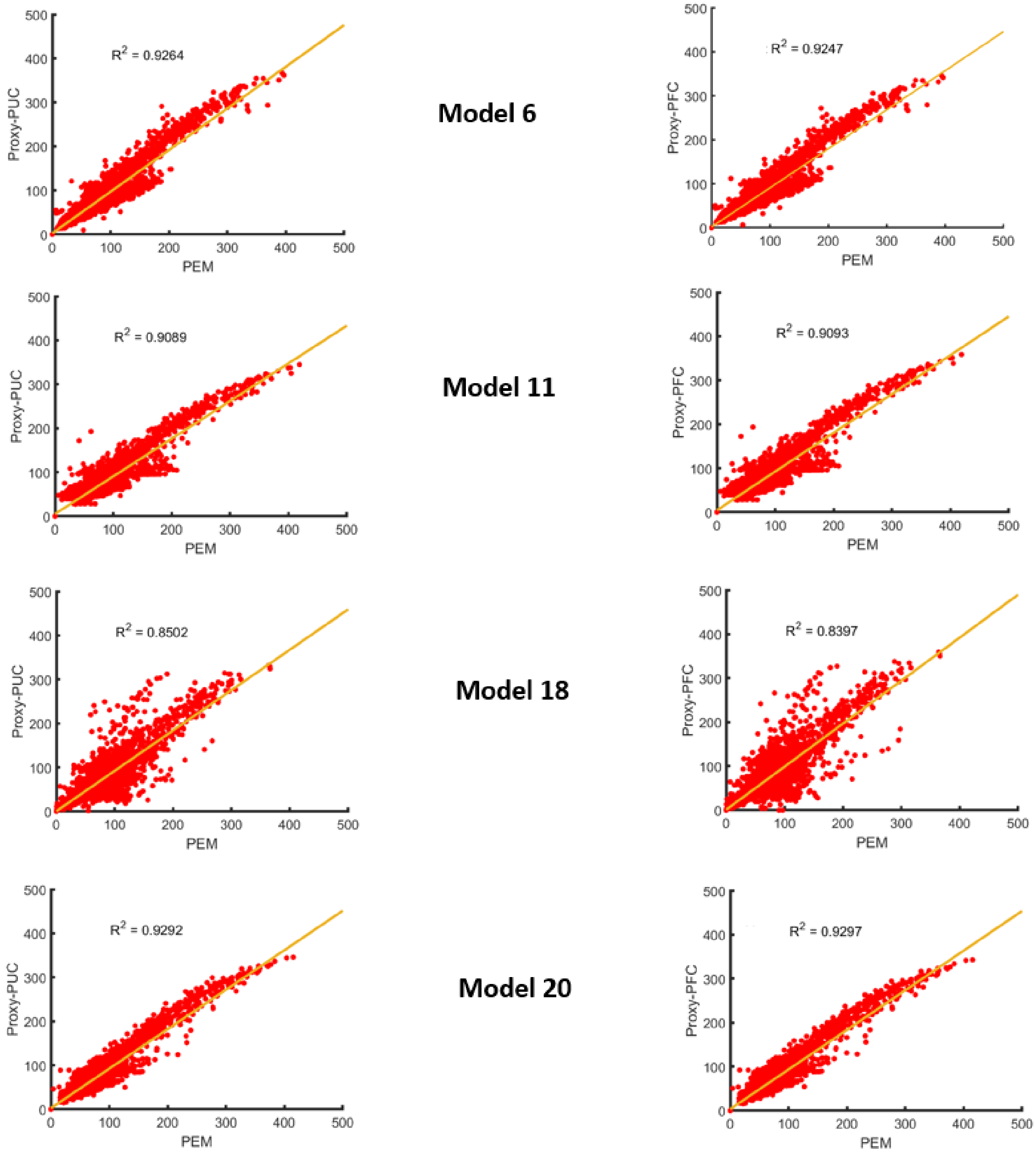

Figure D-1: Crossplots of the proxy and petro-elastic model results and their corresponding R-squared for four randomnly selected models in the ensemble

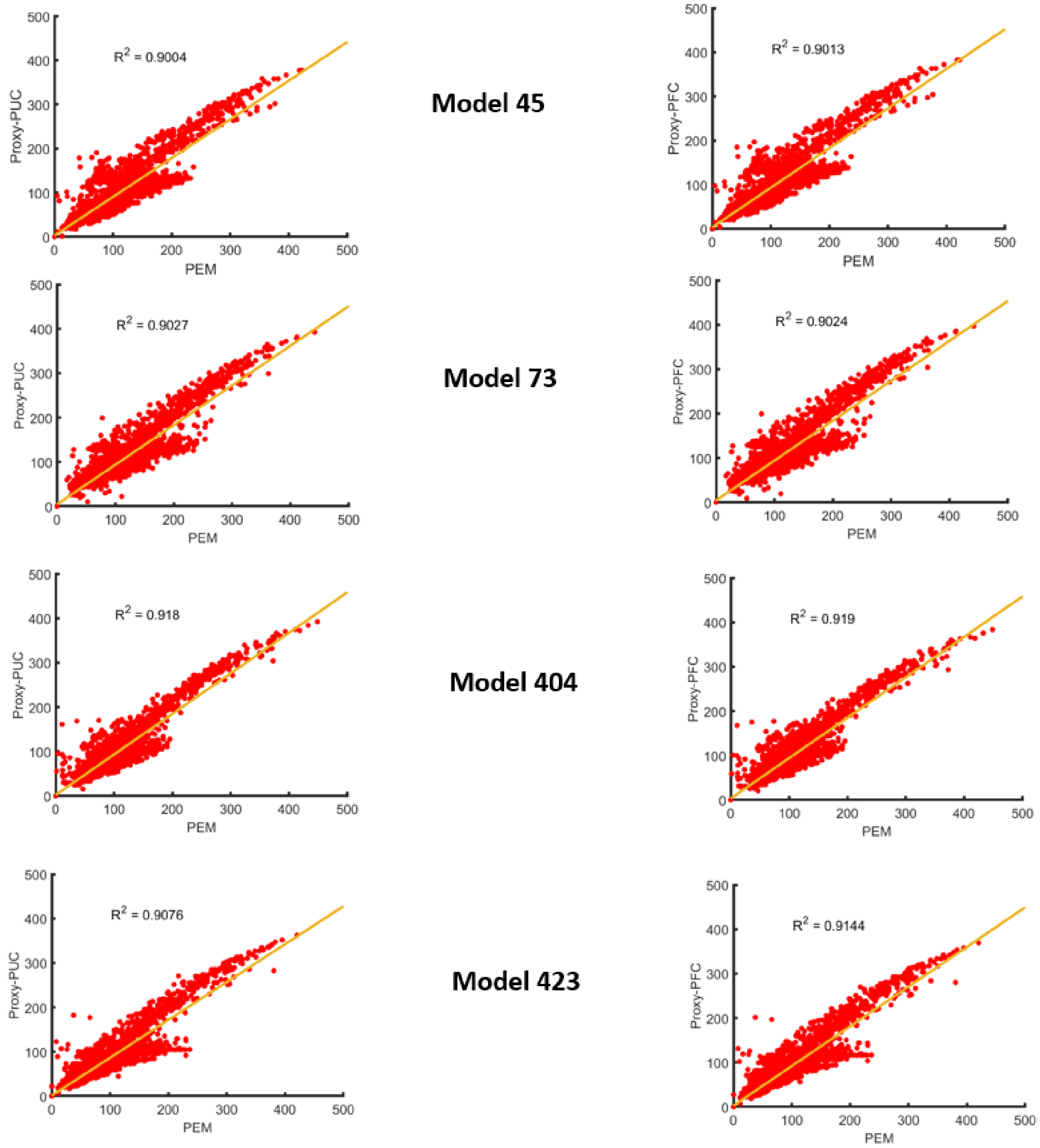

Figure D-2: PFC and PUC (proxy models) results versus the fullfledged petro-elastic model and their corresponding R-squared values.

The same analysis performed for the second version of the PEM-Proxy models. The main difference of this version with the previous one is the porosity inclusion. The second version has porosity as a function in its coefficients. This proxy model is abbreviated to the proxy model with fixed coefficients in the porosity function (DFC) and the proxy model with uncertain coefficients (DUC). Figures D-3 and D-4 show the crossplots of the proxy and petro-elastic model results for the same models of our first analysis.

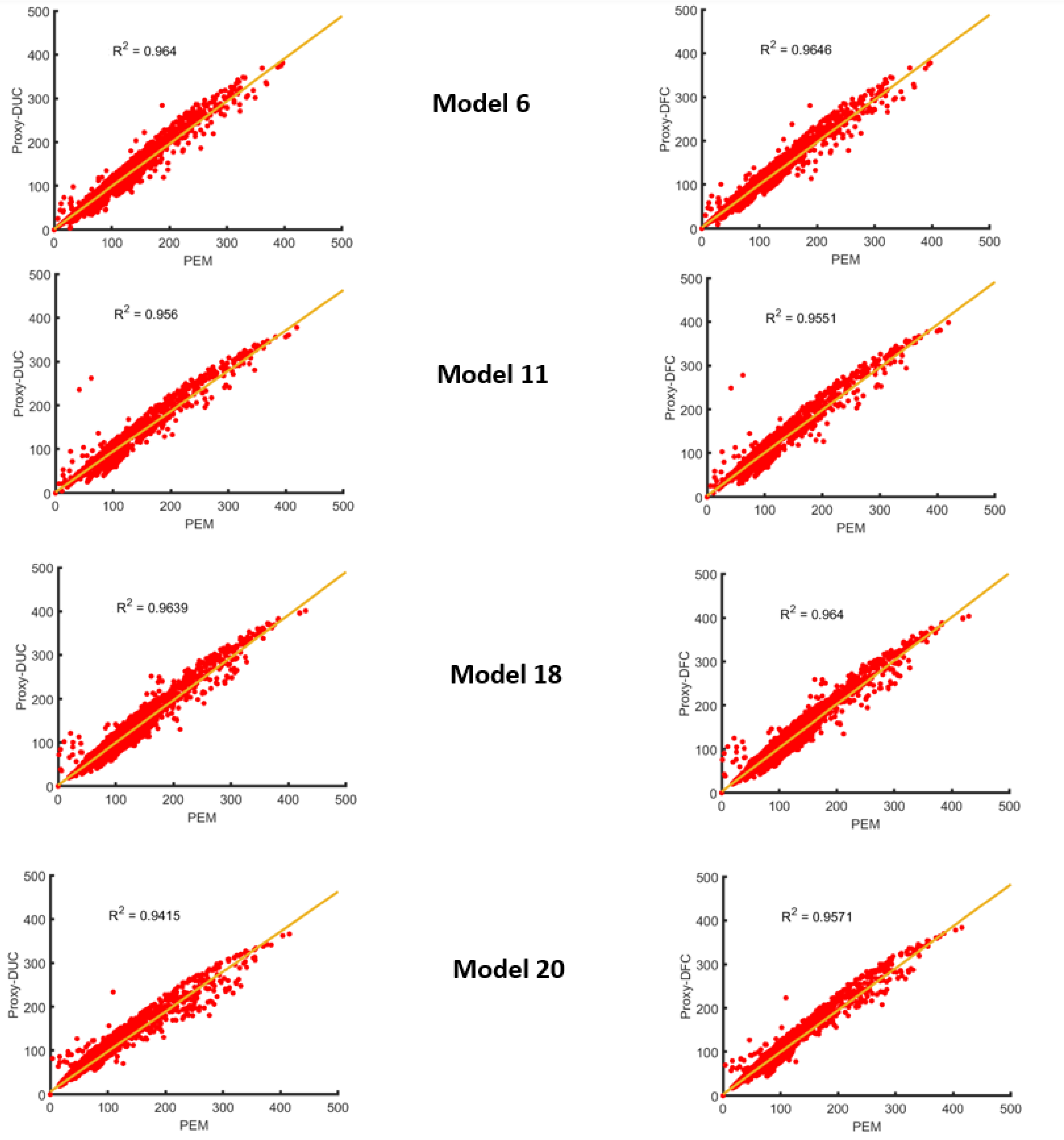

Figure D-3: Crossplots between proxy and the petro-elastic model results, alongside with the R-squared values.

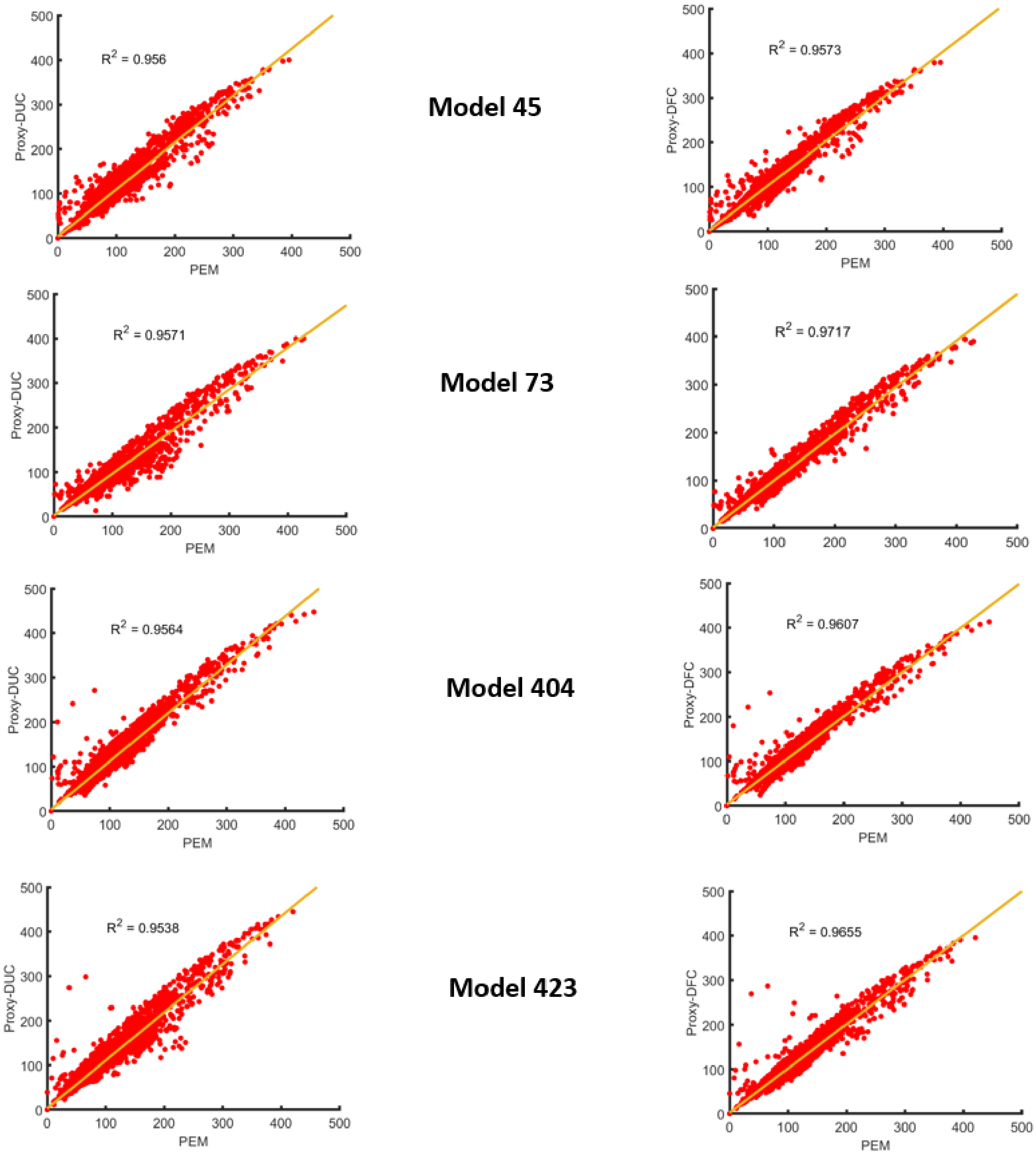

Figure D-4: Analysis of the proxy models (DFC and DUC) predictions with the results from the petro-elastic model.

An interesting observation when comparing the crossplots in figures D-1 and 2 with those in figure D-3 and 4 is the higher values of the R-sqauerd obtained with the second version of the proxy model. Porosity inclusion in the proxy equations could capture heterogenuity and resulted in higher R-squared and improved the proxy model predictions. In general, porosity has a significant role when decomposing 4D signals to saturation-pressure changes as shown in analysis in figures D-1 to 4. The importance of other parameters for proxy construction (such as initial saturations and initial pressure) should be considered for future invetigation. Including these parameters in the proxy might improve its implementation for reservoirs with more complex geology.

Appendix E: Complementary results for the proxy of 4D seismic forward modeling

In the quantitative applications of 4D seismic data, one needs a forward operator (simulation results) as an initial guess to start optmization or as prior information to perform data assimilation procedure. One alternative 4D seismic forward model is a machine learning proxy to replace the traditional forward model (a combination of petro-elastic and seismic models). For our application, two machine learning algorithms were chosen: (1) Extreme Gradient Boosting (XGBoost), and (2) a Deep Neural Networks (DNN). The XGBoost algorithm was choosen as this is a fast algorithm to train and the DNN was selected as the algorithm is powerfull to solve complex non-linear relations. Moreover, the importance of each input feature for the target (dRMS) prediction was measured using SHAP values. Figure E-1 illustrates SHAP values for all the input features of our algorithm.

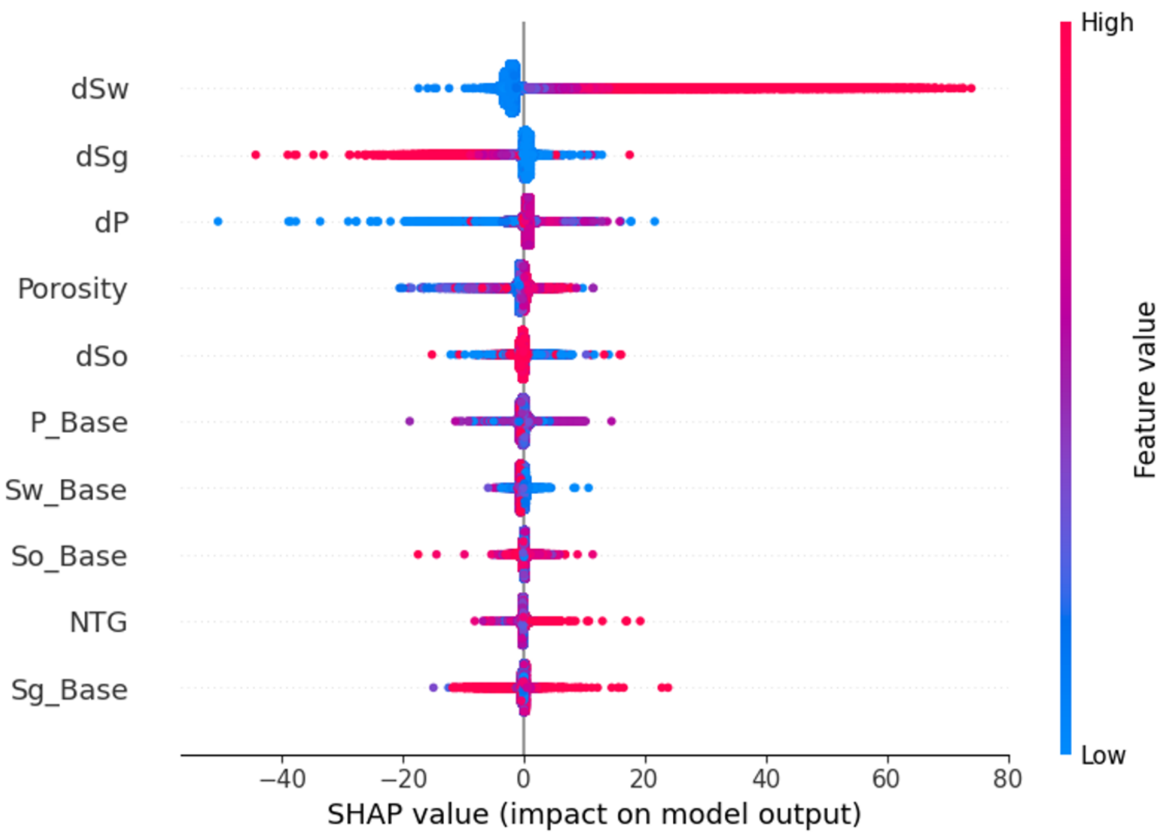

Figure. E-1: SHAP values for all the input features of our machine learning algorithms.

According the figure, saturation-pressure changes were the most significant contributers for dRMS prediction. It was expected as the 4D signals are generally composed of the dynamic changes such as saturation-pressure changes. In addition, the role of porosity also should be mentioned as this parameter indicates the influence and involvement of each dynamic change in the overal 4D seismic signal.